Numerical Investigations on the Function of Flush Waves in a Reservoir Sewer

Vom Fachbereich Bauingenieurwesen und Geodäsie
an der Technischen Universität Darmstadt

zur
Erlangung des Grades eines Doktor-Ingenieurs (Dr.-Ing.)
genehmigte

D i s s e r t a t i o n

vorgelegt von

Dipl.-Ing. Jörg Schaffner
aus Rüsselsheim

Referent:	Prof. Dr.-Ing. Martin Oberlack
Koreferent:	Prof. Dr. Jean-Luc Bertrand-Krajewski
Tag der Einreichung:	17.10.2007
Tag der mündlichen Prüfung:	25.01.2008

D17

Darmstadt, 2008

For my parents

Für meine Eltern

Des Menschen Seele gleicht dem Wasser:
Vom Himmel kommt es,
zum Himmel steigt es.
Und nieder zur Erde muss es.
Ewig wechselnd.
Seele des Menschen,
wie gleichst du dem Wasser!
Schicksal des Menschen,
wie gleichst du dem Wind!

Johann Wolfgang von Goethe
"Gesang der Geister über dem Wasser"

Eventually, all things merge into one, and a river runs through it. The river was cut by the worlds great flood and runs over rocks from the basement of time. On some of the rocks are timeless raindrops. Under the rocks are the words, and some of the words are theirs.

I am haunted by waters.

Norman Maclean
"A River Runs through It"

Abstract

The intention of this thesis was to apply the approach of three-dimensional numerical modeling to investigate the hydrodynamic principles of flush waves in a reservoir sewer in a high spatial and temporal resolution.
First, to give an overview on the topic of sewer sediments, the basics of sedimentation, content of deposits and remobilisation due to erosion are explained. In the following the basics of numerical modelling are given by the introduction of the three-dimensional Reynolds averaged Navier-Stokes equations and the turbulence modelling using the $k-\epsilon$ turbulence model to have a better understanding of the model StarCD, which was used for the following investigations. The discretisation in space and time with the Finite Volume Method is displayed as well as the determination of the free water surface with the Volume of Fluid method. The wall shear stress is the major parameter for the evaluation of the cleaning success of a flush wave. Therefore definition and calculation of the shear stress are explained in detail.
The analytical determination of the dam-break wave is derived from the three-dimensional Reynolds averaged Navier-Stokes equations over to the two-dimensional depth-averaged classical shallow water equations and then to the one-dimensional Saint-Venant equations. Two analytical solutions of Ritter and Dressler and their hydraulic basics are presented.
An overview on convenient one-, two- and three-dimensional simulation models to calculate flush waves is given followed by literature reviews on flushing devices and major investigations on flush waves and flush cleaning in sewers.
The investigated reservoir sewer August-Bebel Ring in Offenbach is described in its geometry and boundary conditions together with the location of the six ultrasonic probes and the used measurement approach. These probes recorded the data of six flush tests with different storage levels at the gate which was then used for the calibration and validation of the numerical model.

The investigations of the behaviour, development and effect of flush waves, carried out with the numerical model StarCD, were split up in eight different topics.
First the initial phase of the flushing wave was analyzed using the analytical Ritter and Dressler solutions and then compared to the results of a refined numerical model. The analysis of the bottom shear stress was the main investigation in this thesis. The effective flushing length for the dry-weather channel and the slopes against the storage level at the gate and the flushing volume were calculated and simple functions were developed. The influence of the flushing gate, the storage volume and the time step size on the bottom shear stress and the effective flushing distance were the next investigations which were carried out. A very detailed calculation of the bottom shear stresses determined the viscous boundary layer for the initial phase and for the longer running flush waves. The results of the modelling with very fine bottom cells were then compared with the common approach used in the before mentioned investigations.

The inclusion of the sunk wave into the cleaning approach of a sewer channel is a very important issue in practical applications. Therefore the development of the sunk wave and its cleaning efficiency were calculated in a refined numerical model. The last investigation regarded the exceeding duration of the critical shear stress along the sewer channel depending on the initial storage level and the flushing volume.

Kurzfassung

Die Intention dieser Arbeit war die Anwendung eines dreidimensionalen numerischen Modellansatzes zur Untersuchung der hydrodynamischen Grundlagen von Schwallwellen in einem Stauraumkanal mit einer hohen zeitlichen und räumlichen Auflösung.
Zunächst wird ein Überlick zum Thema Kanalablagerungen gegeben. Dabei werden die Grundlagen von Sedimentation, Inhalt von Ablagerungen und Remobilisation aufgrund von Erosion erläutert. Im folgenden werden die Grundlagen der numerischen Modellierung mit der Einführung der dreidimensionalen reynoldsgemittelten Navier-Stokes Gleichungen und der Turbulenzmodellierung mit dem $k-\epsilon$ Turbulenzmodel behandelt, um ein bessere Verständnis für das später verwendete Modell StarCD zu schaffen. Die räumliche und zeitliche Diskretisierung mit der Finiten Volumen Methode wird genauso aufgezeigt, wie die Bestimmung der freien Wasseroberfläche mit der Volume of Fluid Methode. Die Wandschubspannung als wichtigster Parameter zur Evaluierung der Reinigungsleistung einer Schwallwelle wird definiert und die Berechnung mittels des $k-\epsilon$ Modells wird erläutert.
Die analytische Berechung von Dammbruchwellen wird aus der dreidimensionalen reynoldsgemittelten Navier-Stokes Gleichungen über die zweidimensionalen tiefengemittelten klassischen Flachwassergleichung bis zu den eindimensionalen Saint-Venant Gleichungen abgeleitet. Zwei analytische Lösungen von Ritter und Dressler werden präsentiert und deren hydraulische Grundlagen erläutert.
Ein Überlick zu ein-, zwei- und dreidimensionalen numerischen Modellen, geeignet zur Berechnung von Schwallwellen, wird gefolgt von Literaturrecherchen zu Schwallspülorganen und den wichtigsten Untersuchungen zu Schwallwellen und Schwallspülungen in Abwasserkanälen.
Der untersuchte Stauraumkanal August-Bebel Ring in Offenbach wird in seiner Geometrie und Randbedingungen genauso beschrieben wie die Platzierung der fünf Ultraschallsonden und die verwendete Messmethode zur Visualisierung der Spülwellen. Bei sechs Spültests mit verschiedenen Einstauhöhen wurden mit Hilfe dieser Sonden die zur Kalibrierung und Validierung des numerischen Modells erforderlichen Messdaten ermittelt.

Die Untersuchungen zum Verhalten bzw. der Entwicklung der Spülwellen sowie deren Reinigungseffekt wurden mit dem numerischen Modell StarCD ausgeführt und in acht Teilanalysen aufgegliedert
Zuerst wurde die Initialphase einer Spülwelle mit der analytischen Lösung von Ritter und Dressler modelliert und mit den Resultaten einer verfeinerten numerischen Modellierung verglichen. Die darauf folgende Analyse der Bodenschubspannungen war die Hauptuntersuchung dieser Arbeit. Dabei wurden die effektive Spüllänge für die Trockenwetterrinne und Bermen in Abhängigkeit von der Einstauhöhe und dem Spülvolumen ermittelt und einfache funktionale Zusammenhänge definiert. Der Einfluss der Spülklappe, des Spülvolumens und der Zeitschrittgrösse während der numerischen Modellierung auf die Bodenschubspannung sowie die effektive Spüllänge wurde im folgenden untersucht. Eine

sehr detaillierte Modellierung der Bodenschubspannungen ermittelte das Verhalten der Welle in der viskosen Grenzschicht für die Initialphase und den weiteren Verlauf der Spülwelle. Die Resultate der Modellierung mit einer sehr fein aufgelösten Schicht von Bodenzellen wurde anschliessend mit den bisherigen Ergebnissen verglichen.
Die Betrachtung und Einbeziehung der Sunkwelle in die Reinigung von Abwasserkanälen spielt eine grosse Rolle in praktischen Anwendungen. Daher wurde das Verhalten der Sunkwelle und deren Reinigungsleistung in einem verfeinerten numerischen Modell untersucht. Die letzte Analyse galt der Schubspannungsdauer, die den Zeitraum beschreibt, während dem die Sohlschubspannung sich oberhalb der kritischen Marke befindet. Hierbei wurden die Abhängigkeiten von der Einstauhöhe und dem Spülvolumen betrachtet.

Acknowledgments

This work was mainly carried out during my occupation at the department of hydromechanics and hydraulics at the Technische Universität Darmstadt in the years 1999 - 2005. Most of the writing of this thesis was done in the following years 2006 and 2007.

I would like to thank my Ph.D. supervisor Prof. Dr.-Ing. habil M. Oberlack for giving me the possibility to receive a doctorate and for giving me the chance to work independently on a very special topic combining the fields of urban water and computational fluid dynamics. His precious and helpful suggestion enhanced my work invaluably.

I would like to thank Prof. Bertrand-Krajewski for the acceptance of the correferates and the valuable discussion on several conferences and workshops. Through this I had the chance to meet other specialists from all over Europe working on different aspects of flush waves.

Many thanks go to Prof. Dr.-Ing. M. Ostrowski, who encouraged me already as student and later as an research associate. Special thanks also to Dr.-Ing. D. Belke for his multidisciplinary discussions and good contact to the department of hydrology.

The project behind this thesis was founded by the Deutsche Bundesstiftung Umwelt who I would like to thank for their sponsorship.

Joerg Steinhardt and my colleagues at the Steinhardt company receive a special thank for giving me a large practical background on the topic of flush cleaning in all its variants. The daily fruitful discussion helped me a lot to see theoretical knowledge in practical applications. Thank you for your confidence in my competency.

A very special thank goes to my former colleague Norma Kirchheim. Her help, endless patience, ability to listen and ideas were giving me the best possible assistance. She made this thesis possible.
I also have to thank the other colleague at the department especially Tanja Weller and Ingmar Wendling.

The last and biggest thank go to my parents and my family for giving me the chance to study and to do this dissertation. Especially in hard times they listened to me and gave me energy to proceed and finish this work.

Contents

List of Figures

List of Tables

Nomenclature

Upper-case Roman

A	: Flow area
A	: Area
C	: Concentration - Volume of Fluid Method
$C_{\epsilon 1}$	: Constant of $k-\epsilon$ modell
$C_{\epsilon 2}$	: Constant of $k-\epsilon$ modell
C_j	: Konvective term
C_μ	: Constant of $k-\epsilon$ modell
C^+	: Constant of log-law
D	: Diameter
D	: Diffusion coefficient
$DGL(u)$	: Time independent ratios of the differential equation
$Diff1$	: Turbulent diffusion, reallocation of turbulenz
$Diff2$	: Turbulent diffusion, reallocation of turbulenz
$Diss$	: Dissipation, Destruction of turbulente energy
D_j	: Diffusive term
F_G	: Weight
F_j	: Mass flow
F_r	: Froude number
F_R	: Friction force
H_0	: Depth of runoff at time $t = 0$
I	: Transient term of k-equation
I	: Relative intensity of turbulence
I	: Mean bottom slope
I_E	: Energie slope
I_i	: Reynolds-averaged momentum equation
I_S	: Bottom slope
I_W	: Water level slope
I_0	: Bottom slope
I_i'	: Reynolds stress equation
$\bar{I}_i$	: Reynolds-averaged momentum equation of the Navier-Stokes equation
K	: Convection term of k-equation
L	: Length scale
L	: Hydraulic radius
L_{max}	: Effective flushing distance
L_s	: Flume length
$mol.Diff$	: Molecular diffusion
M	: Manning value

N : Node in the centre of two adjoining grid cells
P : Node in the centre of two adjoining grid cells
P : Production term k-equation
Pr_k : Modell constant $k-\epsilon$ modell
Pr_ϵ : Modell constant $k-\epsilon$ modell
Q : Flow rate
Re : Reynolds number
R_{hy} : Hydraulic radius
S : Bottom slope
S : Cell face
T_E : End of wave propagation
U : Flow velocity
U_τ : Friction velocity
$\hat{U}$: Uniform velocity
V : Volume
V : Dimension-less velocity
V_i : Volume
Vk : Variation
V_{Store} : Storage volume
$\hat{V}$: Scale of flow velocity
W : Dimension-less velocity

Lower-case Roman

a : Form factor front wave velocity
a : Opening distance of a valve
b : Channel width
c : Solid concentration
c_f : Friction coefficient
c_T : Volume-referred transport capacity
c_0 : Wave propagation velocity
d : Hydraulic diameter
d : Pipe diameter
d_{NP} : Geometrical factor
d_{90} : Diameter 90 % value of grading curve
d_{84} : Diameter 84 % value of grading curve
d_{65} : Diameter 65 % value of grading curve
d_{50} : Diameter 50 % value of grading curve
d_{35} : Diameter 30 % value of grading curve
d_{30} : Diameter 30 % value of grading curve
f : Functional term of time integration divergence form
f_j^l : Functional term of time integration divergence form
g : Acceleration of gravity
h : Water depth
h_{av} : Water level
h_F : Height of front head flush wave

h_{am} : Upstream water level
h_N : Water level
h_p : Sum of bottom height and water level
h_s : Storage level at flushing gate
h_{Store} : Storage level at flushing gate
h_v : Loss of energy head
h_0 : Depth of runoff at time $t = 0$
k : Turbulente kinetic energy
k : Absolute roughness
k/d : Relative roughness
k_s : Equivalent sand roughness
k_{st} : Strickler Value
l : Length
l_u : Wetted perimeter
l^+ : Mixing length
n : Manning coefficient
n : Number of flushes
n : Time step
n' : Grain fraction
p : Pressure
p_a : Atmospheric pressure
p_h : Free surface pressure
p' : Fluctuating value pressure
p^* : Pressure
$\bar{p}$: Mean value pressure
q : Width averaged runoff
q_f : Source term - divergence form
$\bar{q}$: Mean horizontal flow in x-direction
r_{hy} : Hydraulic radius
$r\bar{r}$: Mean horizontal flow in y-direction
s : Standard deviation
t : Time
t : Thickness of deposits
∂t : Iteration time step
Δt : Iteration time step
Δt : Time step
u : Flow velocity
u_b : Bottom velocity
u_{crit} : Critical flow velocity
u_F : Absolute flow velocity
u_h : Free surface velocity
u_i : Flow velocity
u_k : Flow velocity
u_r : Mean flow velocity over cell face S
u_s : Velocity surge wave
u_τ : Friction velocity
u_1 : Flow velocity - x_1 direction

u_2 : Flow velocity - x_2 direction
u_3 : Flow velocity - x_3 direction
u' : Fluctuating value flow velocity
u^+ : Dimensionless velocity - Log-law
$\bar{u}$: Mean flow velocity
$\tilde{u}$: Relative flow velocity
$\bar{u}_i$: Mean flow velocity
$\bar{u}^+$: Dimensionless flow velocity
v : Flow velocity - x_2 direction
v_b : Bottom velocity
v_F : Flow velocity front head of flush wave
v_h : Free surface velocity
v_m : Mean flow velocity
v_W : Motion speed of barrier
v_0 : Undisturbed flow velocity
w : Flow velocity - x_3 direction
w : Absolute surge velocity
w : Relative wave velocity
w_h : Free surface velocity
w_b : Bottom velocity
w_0 : Relative wave velocity in the undisturbed flow domain
x_F : Location front wave
x_i : Coordinate
x_k : Coordinate
x_s : Location surge wave
x_1 : Coordinate direction
x_2 : Coordinate direction
x_3 : Coordinate direction
x_2^+ : Dimensionless space coordinate
z : Height
z_b : Bottom boundary
z_h : Free surface height

Upper-case Greek

$\Gamma_{\Phi,j}$: Interpolated diffusion of face j
Φ : Flux term - Divergence form
Φ_f : Flux term
Φ_i : In- and outflow of control volume
Φ_{N+} : In- and outflow at node $N+$
Φ_P : In- and outflow at node P
Ω_i : Control volume

Lower-case Greek

α	: Angle of bottom slope
α'	: Correction factor
δ_{ij}	: Kroneker symbol
ϵ	: Turbulent kinematic dissipation
κ	: Karman constanteaus - Log-law
λ	: Friction factor
ℓ	: Mixing length
μ	: Discharge coefficient
μ	: Dynamic viscosity
ν	: Kinematic viscosity
ν_t	: Eddy viscosity
ρ	: Fluid density
ρ_b	: Bottom density
ρ_h	: Free surface density
ρ_L	: Air density
ρ_m	: Mean density
ρ_W	: Water density
$\bar{\rho}$	: Mean density
τ	: Bottom shear stress
τ_c	: Critical bottom shear stress
τ_{crit}	: Critical bottom shear stress
$\tau_{cE,t}$	: Erosion shear stress - Dry-weather
$\tau_{cE,r}$	: Erosion shear stress - Wet-weather
τ_{cS}	: Sedimentation shear stress
$\tau_{cS,t}$	: Sedimentation shear stress - Dry-weather
$\tau_{i,j}$	: Lateral stress
$\bar{\tau}_{i,j}$	: Lateral stress
$(\tau_{kin})_{tur}$	: Reynolds stress tensor
τ_{max}	: Maximum bottom shear stress
τ_{turb}	: Reynolds stress tensor
τ_W	: Wall shear stress
τ_0	: Wall shear stress

1 Introduction

1.1 Introduction to sewer deposits and flush cleaning

Deposits in sewer channels create several operational problems like the reduction of hydraulic capacity and the increasing number of polluted overflows into receiving waters. The low water level with its temporal changes and the slow flow velocity in partially-filled main collectors are responsible for the sedimentation of sewer solids. The dry-weather runoff has its minimum in the night hours. During this time deposits grow. Often they can not be remobilized and transported by the peak runoffs of the daytime. The remaining sewer deposits increase the roughness of the sewer and slow down the flow velocity which leads to a new sedimentation of particles. In the course of dry-weather periods the solids consolidate to a firm texture. The remobilisation of these consolidated sediments occurs only during strong rain events and leads to a substantional load of connected waters as well as of the sewage plant.
Stormwater holding tanks or reservoir sewers connected to a trunk sewer are elements of sewer systems which show similar problems. They are used to reduce the runoff peaks during storm events by accumulating large amounts of storm sewage. After the rain event the stored stormwater sewage is given back continuously to the sewer system. This prevents hydraulic shocks to the sewage plant and sewer overflows. The duration of the storm sewage storage is depending on the particular catchment and the location of the storage element within the sewer network. It can last from a several hours up to one week.
The long storage time of storm sewage together with a slow flow velocity and the common small slope in reservoir sewers lead to an increased sedimentation and formation of deposits on the bottom of the sewer. If a second rain event follows a first one soon these deposits can be washed away by the storm sewage. Otherwise the sediments will dry up and consolidate. Sometimes they can only be removed with a large mechanical effort.
Deposits in sewer systems cause several problems:

- Sewer deposits possess a larger roughness than the concrete bottom or the walls of a sewer channel. This fact leads to a decrease of the flow velocity which favors new deposits and reduces the hydraulic efficiency of the sewer channel.

- The reduction of the runoff cross-section lessens the hydraulic efficiency of the sewer channel. The result is a larger number of combined sewer overflows and a bigger hydraulic and substantional load to the connected waters. In individual cases it is possible that the cross-section of a sewer channel is blocked completely.

- Deposits can only be removed by a high flow velocity after a storm event. The remobilisation of the sediments leads to a bigger substantional load of the storm sewage. In case of a stormwater overflow the connected waters will be polluted

increasingly.

- Waste water treatment plants are strongly loaded by remobilised deposits from connected sewer systems. The contamination load reaches the sewage plant intermittently which cuts down its cleaning efficiency and causes operational problems.
- Deposits contain organic solids which are transformed biologically within the sewer. This process leads to a high consumption of oxygen. In anaerobic conditions hydrogen sulphide is set free to the sewage and the air of the sewer channel. An offensive smell can be the result.
- Corrosion of biogenic sulphuric acid can weaken materials containing cement and damage them with a long-term effect.
- Fouling water in the inlet leds to operation problems in sewage plants caused bulking sludge, smell or corrosion.

Planning-based measures can decrease deposit formations but it is not possible to avoid them completely. In order to reduce the negative effects of the deposits described earlier it is vital that sewers have to be cleaned at regular intervals. [Haumann, 1999]

The traditional way of cleaning sewer systems (95 %) in Germany is the use of a high-pressure water jets handheld by workers. [IKT, 2004] But this method has many drawbacks. High-pressure water jets have a high demand of energy and freshwater to clean the sewers which causes high costs. Their economical usage is limited to channels up to a size of DN 2000. Furthermore, they are no more reasonably usable.
The working conditions are unhygienic and the high-pressure water jets can damage the concrete surface of the sewer channels. The jets work with a water pressure of 80 -120 bar which harms the bottom and walls of the sewer long lasting. This creates long-term costs for the repairs of the sewers additionally to the freshwater and energy costs. [IKT, 2004] Because of these drawbacks the cleaning of sewer channels with the aid of flush waves is a sensible alternative, which was used before in previous ages. Tip-over cisterns or so-called flush-doors were used at the end of the 19th century in numerous big cities like Frankfurt a.M. in Germany. [Schuessler, 2002]

The flush cleaning method uses the available water which is dam up above the to be cleaned stretch of the sewer. This can be done with permanent installed slides, mobile flush gates or other flush devices. The dam up water will be released abruptly and creates a flush wave that runs along the sewer channels similar to a dam-break wave. The intense turbulence in the head of the flush wave generates the necessary shear stresses to remove the deposits from the bottom of the sewer. The water following the front wave then transports the deposits along the sewer. Excellent overviews regarding the available flush devices are given in Kirchheim (2003) and Oberlack et al. (2005).
The dimensioning of the respective flushing devices is the major problem when it comes to clean a certain sewer channel. The design rules for certain flushing devices depend mostly on the practical experience of the developer. Usually they are kept secret and are not available for scientific investigations.
Flow measurements of flush waves in sewer channels are one way to optimize particular flushing devices. Empirical relations derived from these investigations can lead to statements regarding the cleaning results. But this approach does not lead to general design rules. The hydraulic basics of individual flushing devices are very different so it is not

possible to compare them with each other. Individual sewers and their deposits may also vary which makes it difficult to transfer the results from one sewer to another.
The application of numerical modelling seems to be one appropriate method to develop general design rules for flushing devices and understand the hydraulic principles of flush waves. Numerical modelling is also, compared to expensive physical models, an economical alternative to investigate different scenarios of a flow domain with changing boundary conditions. Therefore it is necessary to calibrate the numerical model against reliable measured data. Afterwards it is possible to investigate, for example, the behaviour of the created flush wave and the cleaning effects of a certain flush device related to the flush volume to obtain general design rules. These design rules can be used later for new locations and further flush devices.

1.2 Motivation of the project and methodical approach

The intention of this thesis was to apply three-dimensional numerical modeling to investigate the hydrodynamic principles of flush waves in a reservoir sewer in a high spatial and temporal resolution. The project was carried out in the reservoir August-Bebel Ring in the city of Offenbach/Germany and was supported by the Deutsche Bundesstiftung Umwelt. Boundary conditions like the flushing gate, the storage volume or the time step size should be analyzed to understand their influence on the development and efficiency of the flush wave. A special focus had to be placed on the numerical modeling of the initial phase in contrast to historical analytical methods. The main investigation had to be focused on the cleaning efficiency of the flush wave. Therefore the calculation of the bottom shear stress under different boundary conditions had to be carried out to approximate the maximum flushing distance depending on the storage volume.

To give a basic understanding of the processes inside the sewer system a description of the solids in combined sewer systems, including their formation, content, influence on the sewer system and the remobilisation of deposits is carried out. Therewith the reasons for the cleaning demand in sewer systems are explained. Subsequently the basics of the numerical modelling, covering the major theoretical aspects for the following investigations, are given to introduce this complex subject. The following chapter shows the mathematical derivation of the one-dimensional Saint-Venant equation starting from the three-dimensional Navier-Stokes equation over to the two-dimensional Shallow Water equation. Then the derivation of the historical analytical approaches for the hydrodynamic description of dam-break waves is explained.
The first literature review presents several available numerical models, which are suitable for the simulation of flush waves. The benefits and drawbacks of one- and multi-dimensional models are given to understand the different approaches. Two following literature reviews give detailed overviews to the present flush devices and to the major scientific investigations on flush cleaning in recent years.
The description of the test site in Offenbach and its boundary condition is presented in the next chapter followed by the specification of the measurement of real flush waves in the reservoir sewer. These measurements were necessary to obtain data for the calibration and validation of the numerical model. The numerical model of the reservoirs sewer itself was set-up in the three-dimensional finite volume model StarCD. [StarCD, 2002]

This model allows the computation of turbulent flows with a free surface in complex geometries like changing bottom slopes, variable channel width and changing cross-sections. The three-dimensional nature of flush waves with steep gradients makes great demands on the accuracy of the solutions, which can only be fulfilled with a highly-developed numerical model.

After the set-up of the model according to the hydraulic conditions in the reservoir sewer in Offenbach, the calculated flush waves were calibrated and validated with the data of the measuring series for different boundary conditions. Therefore the bottom roughness was varied so that the modelled waves were matching the measured ones. Using the validated model, first the initial phase of the flush wave was investigated and compared to results with the already described analytical approaches. The determination of the bottom shear as the major value for the cleaning efficiency of the flush waves was the most important investigation. The maximum flushing distances for different storage levels and at the flushing gate were derived.
The following investigation analysed the influence of the flushing gate in the numerical model and the influence of the flushing volume on the cleaning efficiency of the flush waves. The analysis of the time step size and the log-region of the flush wave were carried out in the next chapter. The last chapters discuss the cleaning efficiency of the sunk wave upstream of the flushing gate and the duration of the critical shear stress on certain location in the sewer depending on the storage level and storage volume.
The described approach tries to cover a multitude of aspects concerning the flush cleaning of a reservoir sewer using the technique of advanced numerical modelling. The results of the numerical calculations specify the hydrodynamics and the important boundary conditions responsible for the cleaning success of a flushing device and the created flush wave.

2 Deposits in combined sewer systems

Deposits in sewers cause many problems like reduced runoff, smell or pollutant shock loads for receiving waters and treatment plants. The moving sediments are part of the transport cycle of a sewer system. Depending on their size and the flow conditions they can settle semi-permanently or consolidated at the bottom of the sewer. Fixed deposits and their remobilisation of deposits by the use of numerous cleaning devices was the subject of many investigations in the last twenty years. The following chapter will take a look at the formation of deposits, their content and influence on the combined sewer system and the mechanics of remobilisation. The last section will connect the sediment size to the bottom roughness, which is a very important parameter for the following numerical calculations in this thesis.

2.1 Formation of deposits

2.1.1 General movement

The investigation of the formation of sewer deposits starts with a general consideration of the sediment movement mechanisms. Figure 2.1 shows the different types of sediment movement in the flow of a sewer channel. Aggregation processes and the decomposition of conglomerates influence the complex system of advection, sedimentation and erosion.

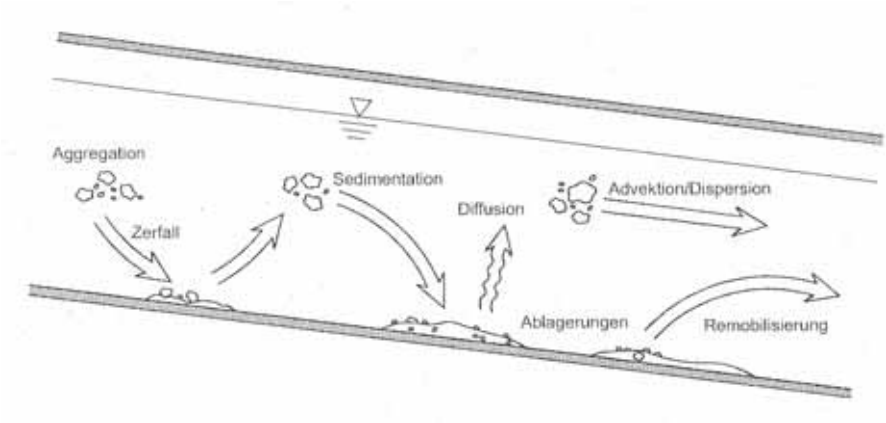

Figure 2.1: Movement mechanism of solids in sewer flow, [Frehmann, 2003]

Sperling (1984) describes the critical formations of deposits in a simplified manner depending on the flow conditions. For a flow velocity u smaller than 0.2 m/s stationary

deposits can be found and no transport takes place. The transport starts above 0.4 - 0.5 m/s when the upper layer of sediments is moved and small dunes are build. Flow velocities of 1 - 2 m/s show a strong transport of solids. All sediment layers are moved along the bottom in shape of dunes. More solids are jumping (saltation), rolling and sliding along the sewer bottom. The maximum transport rate is reached for flow velocities of 3 - 4 m/s when all solids are in suspension and no deposition is given. The concentration of solids in the flow is homogenous to a large extend. Despite the strong connection of moving and fixed deposits both categories will be described individually in the following sections.

Local deposits can be divided into long stretched bodies of solified sediments and sediments in front of obstacles or hydraulic unfavourable locations. Investigations of Ristenpart (1995) showed sediment levels of 5 - 20 cm in a sewer of 1500 mm diameter, which means 3.3 % to 13.3 % of the sewer diameter were affected by deposits. (Figure 2.2)

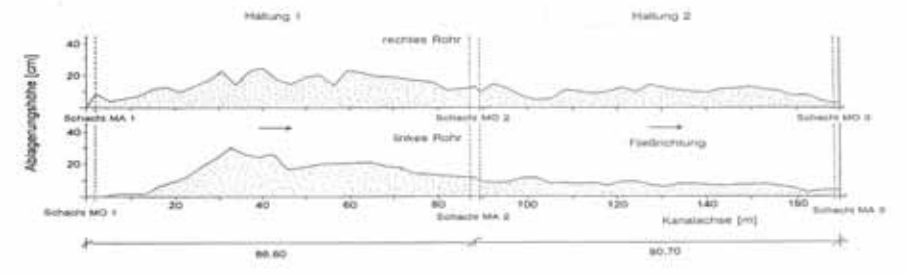

Figure 2.2: Longitudinal view of sewer deposits, [Ristenpart, 1995]

Two categories of local deposits can be classified. Blumberg & Bauer (1984) investigated an egg shaped sewer of 800/1200 mm diameter. They identified deposits with a high organic fraction and a spongy consistency. The content of the dry substance was measured with 10 - 40 %, the ignition loss was 25 - 60 %. Additionally deposits with a mainly mineral fraction (sand) and high compression strength were found. The content of the dry substance was higher with 50 - 80 % and the ignition loss was smaller with 5 - 20 %.
Perrusquia et al. (1995) found sediments consisting of coarse material at the sewer bottom as a first layer and a layer of fine material above (top organic layer). The characteristic and the movement of the found sediments seemed to be accidental and varied strongly.

2.1.2 Conditions for sedimentation

The reasons for the formation of sedimentations of sewer solids are the design of the sewer system, external factors of influence and the deposits itself. The parameters, which lead to sedimentation of deposits, will be shown in the following.
The hydraulic boundary conditions in a sewer system regulate the flow velocities and the bottom shear stresses, which are responsible for sedimentation and erosive processes. The slope of a sewer channel, the shape and diameter of the pipe, the roughness and

the line management of the channels influence the sedimentation as well as changes in profile, inlets, throttles and combined sewer overflows. The density, the size and the shape are also responsible for the sedimentation or the start of the movement due to changed flow conditions. [Schmitt, 1992]
During dry-weather periods the rate of sedimentation increases due the reduced flow velocity. Depending on the characteristics of the sewer this can lead to a reduced hydraulic radius and increased bottom roughness, which again slows down the flow velocity and favours the sedimentation. Seasonal changes in water consumption or the reduced inflow of industrial water at the weekends also influence the sedimentation processes. This applies for the connected catchment, which changes his entry of sediments into the sewer system during the year. In the wintertime more mineral sediments will enter the sewer channels while in the summer and spring the fraction of organic material will grow.

2.1.3 Areas of sedimentation

Based on the conditions of sedimentation as described in the prior section the typical areas of sewer solid sedimentation can be defined. Locations for the formations of deposits can be places with adverse hydraulic flow conditions like junctions, openings and strong bends in sewer channels where the flow velocity is reduced. Small sewers in the beginning of a system can be affected by small runoffs while the large sewers at the end of the system often have a low bed slope, which also favours the start of deposition. Siphons are sewer buildings, which usually show different slopes in their curvature and are strongly affected by sedimentation. [Westrich, 1984]

A good example for the deposition of sewer solids in a channel narrow gives the investigation of Brombach et al. (1993). The collector had an initial diameter of 1600 mm with a mean bottom slope of I=2.6 ‰. After 110 m length the sewer was reduced to a diameter of 0.8 m width and 1.8 m height. A backwater area is formed and the connected low flow velocities are responsible for the sedimentation. After a general cleaning during a period of six-month deposits with a thickness of 20 cm were built up. The content was predominately organic material with some mineral parts like sand or stones.

Settlements of sewer pipes or sewer buildings can also be responsible for the sedimentation of sewer solids. Beside the problem of infiltration water small steps are created along the sewer pipe, which create a hydraulic loss. The flow velocity and the shear stresses are reduced at these locations, while sedimentation can start then very easily under these conditions. Large steps may create a backwater with dead areas, which also helps the sewer solids to settle down. Brombach et al. (1992) found in his investigations sedimentations created by steps in sewer pipes.
A further example is the depositions investigated by Westrich (1984) in a reservoir sewer with an upstream combined sewer overflow (CSO). Sedimentation occurred especially at the end of a storm event when the runoff decreased and the critical flow velocity u_{crit} was approached. The areas 1 and 2 show an increase of sedimentation and the thickness of the deposit layer. At the CSO the flow velocity was increased and therefore the sedimentation was reduced. Further downstream at the end of the reservoirs the sewage was throttled to a constant runoff and the flow velocity was reduced again. Therefore the areas 3 and 4 acted like a sand trap. Figure 2.3 shows the flow condition in the reservoir

sewer.

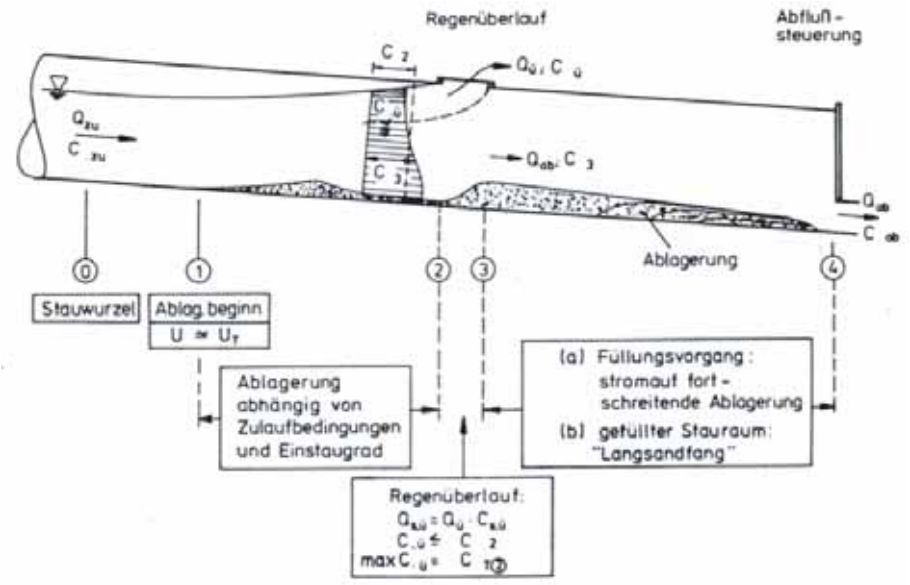

Figure 2.3: Longitudinal view of sewer deposits in reservoir sewer [Westrich, 1994]

2.1.4 Mobile deposits

Due to their physical properties sewer solids can be assigned to certain types of transport.

- Suspended particles move with the flow.
- Floating particles move ahead of the flow.
- Coarse suspended particles sail in the flow.
- Fine suspended particles settle down slow.
- Settleable particles can be transported by turbulent flows.
- Particles slide or bounce slowly along the sewer bottom.
- Sand particles wallow forward in dunes.
- Gravel and stones belong to fixed sediments.

Figure 2.4 displays the different ways of particle movements. The formation of conglomerates or flakes or adsorption of dissolved particles can lead to different forms of movement.

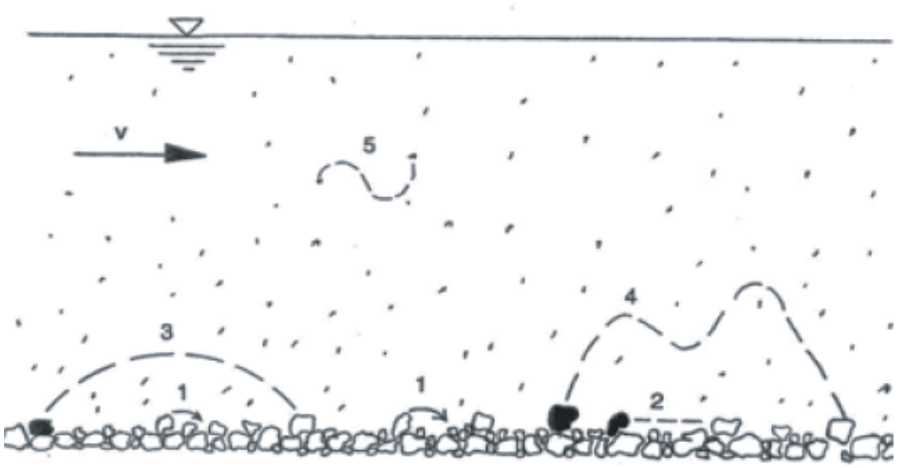

Figure 2.4: Particle movement, [Glazik, 1989]

The transport of sewer solids is composed of bed load and suspended transport. The bed load is the main source of sediments deposited on the sewer bottom and consists of highly concentrated organic material with fibres like toilet paper. [Ristenpart, 1995] The following figure 2.5 shows the bed load transport with the distribution of velocity and concentration of suspended solids during dry-weather runoff.

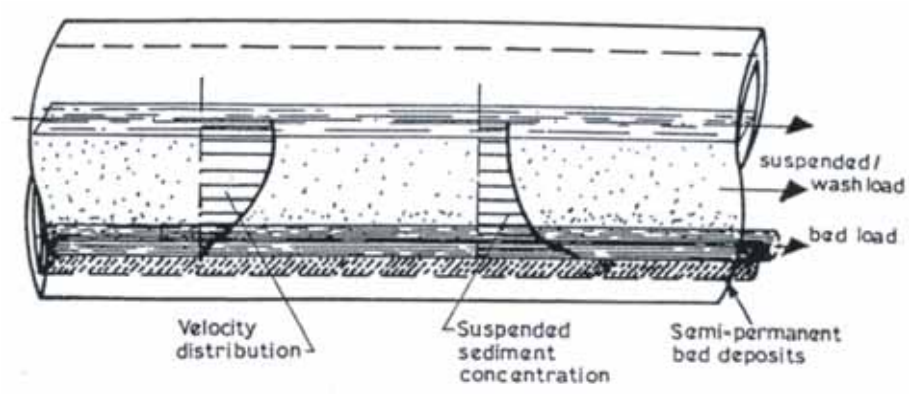

Figure 2.5: Bed load transport during dry-weather runoff, [Ashley et al., 1992]

Investigations on bed load transport divided the moved solids in two groups. First the small forms of deposition, which are ripples on the sewer, bottom and second the dunes or bars of sediments. Sander (1989) gives a good overview on the different shapes of mobile depositions.

2.2 Content of sewer deposits

2.2.1 Classification

Deposits or sewer sediments are difficult to define due to their strongly different appearances. Their classification is made complicated by the fact that sewer sediments can be

found in mobile form as well as deposited at the bottom the sewer. The transition from bed-load transport to deposition depending on the sewage runoff is very smooth. This transition is shown in figure 2.6.

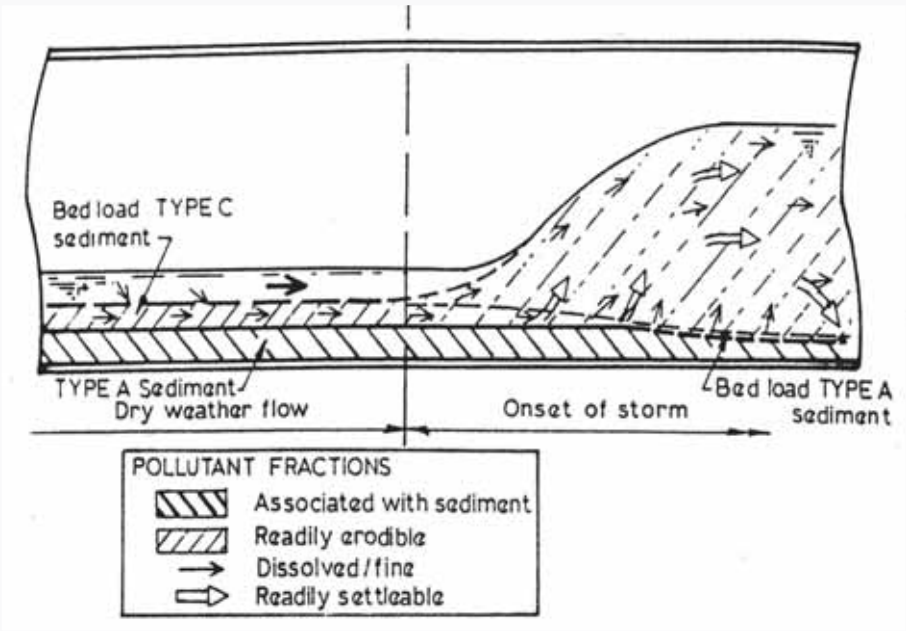

Figure 2.6: Erosion of sediments and start of bed-load transport [Menk, 1998]

A simplified classification of sewer solids was given by Lenz & Wielenberg (1997) and is shown in table 2.1.

Coarse classification	Fine classification
Visible fine sand	Organic elements, visible by black coloration
Sand with fine gravel, max. size of egg	Fibered elements, like textile or plant
Boulder, single large stones, size of fist	Consolidated sediments, difficult to extract by hand
Organic film	

Table 2.1: Classification of sewer sediments [Lenz & Wielenberg, 1997]

Crabtree (1988) recognised the different pollutant potentials and forms of erosion of sewer deposits as well as the need of a more specified classification. He defined a classification based on the physical and chemical sediment properties. Schmitt (1992) took up this classification and added further elements like suspended solids. (Table 2.2)
A more differentiated classification of sewer sediments can be done regarding the single layers of the deposits and their different properties. To avoid equivocalities Verbanck & Ashley (1992) used the definition of a heavy-fluid layer to describe the less mobile layers of deposits directly above the sewer bottom.

Class	Criteria	Visual	Runoff behaviour
A	Largest fraction of pollutants in storm sewage	Coarse, granulate of mineral matrix, incoherent at the sewer bottom	Erosion, fast and high loads at stormwater runoff
C	Largest fraction of pollutants in storm sewage	Mobile, fine-grained deposits of area with low flow velocity, isolated at the bottom or above material type A	Main source of bed-load at first flush
E		Fine-grained mineral and organic material, between type A and C	Deposits of storm tanks, manhole slopes, CSOs, sills above dry-weather runoff and areas of low flow velocity
B		Like type A, consolidated by biomass or fat	
D	Highest fraction of pollutant potential and largest dispersion	Organic film of channels with fluctuating water levels, predominantly organic material	

Table 2.2: Classification of sewer sediment [Schmitt, 1992]

Other authors like Ristenpart et al. (1995) and Verbanck (2000) use the term fluid-sediment to define the bed-load transport with an increased concentration of 300 mg/l - 4 g/l above the sewer bottom. The fluid-sediment is the layer, which is responsible for a bed-load transport of 12 % of the total solids. The fluid-sediment contributes also the pollution during first-flushes. The erosion of the fluid-sediment starts at a shear stress of 1 N/m^2.
Recent investigations of Ahyerre (1999) presented a further sediment layer which constitutes the transition between the sewage runoff and the coarse deposits. It is loaded with mainly organic material and paper. This layer has a thickness of 1.5 - 7 cm and is defined by the term organic layer. The organic layer is the main sources of the suspended pollution load of CSO's (40 - 70 %). Parts of the organic layer start to erode at shear stresses smaller 0.4 N/m^2, at shear stresses smaller than 0.1 N/m^2 the organic layer starts to grow like a bio-film. [Chebbo et al., 2003]
Arthur (1996) defined the term of near bed solids (NBS), which describes all substances that are transported near the sewer bottom. Chebbo et al. (2003) differentiated in three categories of near bed solids:

- Highly organic near bed solids. Accumulating in areas with low shear stresses. Affected by slow erosion processes during dry-weather periods.
- Near bed solids as a form of bed-load transport with a high organic pollution and coarse structure.
- Fluid sediments, moving in suspension above the sediment layer.

2.2.2 Composition

The sediments, introduced into the sewer system, are distributed unsteadily along the sewer system. Their characteristically properties are the subject of numerous investigations like the ones of Artieres (1988), Broeker (1983), Brombach (1995), Michelbach & Woehrle (1991) and Saul (1991).
These investigations showed a broad range of different results. The interaction of complex processes like the introduction of sediments, remobilisation of deposits, bio-film and the runoff conditions make it difficult to compare the results of different urban catchments. [Macke et al., 2002] [Seggelke & Rosenwinkel, 2004] One major problem is the different approach at collecting samples of deposits when describing the properties of deposits. The literature resources do often not explain the collection methods and the local conditions, which makes it difficult for the reader to compare the results. Therefore the results of the following investigations have to be treated with caution.
Results of the analysis of Ristenpart (1995) regarding sewer solids in Hildesheim, Germany showed strongly different values for the solid fraction, the organic fraction, the density and the particle size. Also the chemical and biological oxygen demand as well as the ammonium nitrate varied highly. Further investigations in Germany were carried out by Brombach et al. (1992), Schmitt (1992), Hahn and Xanthopoulos (1990), Seyfried and Schmitt (1985), Geiger (1984) and Xanthopoulos and Augustin (1991). International investigation were the ones of Arthur et al. (1999), Butler et al. (1995), Ashley and Dabrowski (1995), Ashley et al. (1994), Verbanck (1992), Crabtree (1988), Nalluri and Alvarez (1992) and Jefferies and Ashley (1994).

2.2.3 Properties

The properties of sewer solids or deposits can be demerged into physical, mechanical and chemical properties. In the following investigations by the author only the mechanical properties and here especially the cohesion and the critical flow conditions of sediments will be of interest. A very detailed description of sewer properties can be found in the works of Kirchheim (2003) and Ashely et al. (2004).

2.2.3.1 Cohesion

The cohesive properties of sewer sediments have a major influence on the start of the particle motion. The larger the content of cohesive material the longer the particle will resist the flow offence. Therefore the relation of the cohesion and the critical bottom shear stresses were subject of several investigations.

The term cohesion describes the inner coherence of molecules. This rheological property of sediments is based on electrochemical gravity forces between single particles also called van der Waals forces. Clay or clayey grain mixtures are soils with highly cohesive properties and because of its tetrahedron and octahedron structure clay has the ability to be very compressible. Investigations of sewer deposits of Mignot (1968) and Nalluri (1991) indicate that sewer deposits can be compared with clay soils.
In the case of sewer deposits the high stability is caused by the agglutination of the particles by fats, biomass and chemical cementation. The cementation of sewer solids by organic substances leads to an increased resistance against force effects. Even small additions of fine organic material closes cavities and therewith the permeability of the grain structure. The contact surfaces between the sediments increase the shear strength and reduce the affection to erosion. Investigations of Berlamont & Torfs (1996) proved that 10 - 20 percent of weight of fine cohesive material (≤ 63 μm) are necessary to turn ordinary sand into a cohesive matrix.

2.2.4 Height of deposits

The height of sewer sediments can be very different in dependence of the dominant flow conditions and the location inside the sewer system. It is possible that the deposits amount to only a few millimetres or to some decimetres. A large role plays the attached catchment, because of its responsibility for the introduced sediments, which form the deposits.
The long-term development of sediment heights in different sewer systems shows several parallels. After a rain period a tendency of increasing sediment heights is obvious and after a general cleaning of a sewer it is noticeable that the original sediment height is reached in short period of time. [Dette et al., 1996] Ristenpart (1995) called this a medium term development, which is described by the balance of the deposit slope and the existing hydraulic conditions. The characteristical sediment height is therefore the mean value of the sediment height. The height of sewer solids oscillates about this mean value, which will not change without external hazards.
During a rain period with increased runoff and shear stresses the sediment height is reduced and an unbalance is created. With the start of new period of dry-weather the sedimentation increases and the characteristical sediment height is reconditioned. Therefore it is very likely that a sewer pipe will not be blocked totally by regular deposits despite of large sized items introduced by accident. After a cleaning of the pipe the restoring of the previous sediment layer has a high probability.
An example for the characteristical sediment height is given by Ristenpart (1995) for the sewage system of the city of Hildesheim, Germany with 2.4 and 11.4 cm with a variation coefficient of 8 to 40.1 %. Similar results were stated by Verbanck et al. (1994) and Laplace et al. (1992). Dette et al. (1996) justified the fast regrow of sediments with an insufficient cleaning and a small transport capacity of the flow coming from the upstream sewers. He did not notice a continuous, long termed grow of sediments until the former height and the balanced was reached.

2.3 Influence of deposits on the sewer system

The influence of sewer deposits on the sewage system regarding the operation and the sewage quality can be noticed before the deposits may reach the sewage plant or receiving waters. This influence was investigated by Schmitt (1991) in his fundamental analysis where he divided the effects of sewer deposits in the following groups:

I. Reduction of the hydraulic efficiency

- Reduction of the available runoff diameter
- Increase of the bottom roughness
- Change of the water level near CSOs and an increase of overflows

II. Operational difficulties

- Increased cleaning effort
- Negative health effects for the operation personal due to gases under anaerobic conditions
- Sulphuric acid corrosion caused by the production of hydrogen sulphide

III. Influences on the environment

- Smell disturbance caused by hydrogen sulphide
- Increased pollution load in mixed sewer systems during storm events

Aside the reduction of the hydraulic effectiveness chemical and microbial activities of the introduced material lead to the formation of gases inside the sewer channel. These gases affect the stability and the impermeability of the concrete pipes and cause the start of corrosion. The formation of bad smelling gases which flow through the manhole into the outside environment also cause displeasure for the population. Furthermore the consistence of the sewage is changed by deposits and their chemical processes and this influences strongly the cleaning operations on the treatment plant. In the following some of the most important influences will be explained more detailed.

2.3.1 Hydraulic efficiency

The hydraulic efficiency of a sewer channel is depending on the geometry of the sewer diameter, the roughness of the pipe and the sewer slope. Due to the deposition of solids the sewer diameter is reduced and also the runoff. The flow velocity will be decreased and this all leads to a reduction of the hydraulic efficiency. The runoff capacity can be reduced by 20 % when 10 % of the diameter is affected by sewer solids. [Mark et al., 1996] Investigation on this subject and especially on the roughness of sewer pipes were carried out by Perrusquia et al. (1986, 1995).
The worst case of deposition can be the total blockage of a sewer pipe, which would cause a backwater in the upstream sewer system. (Figure 2.7)

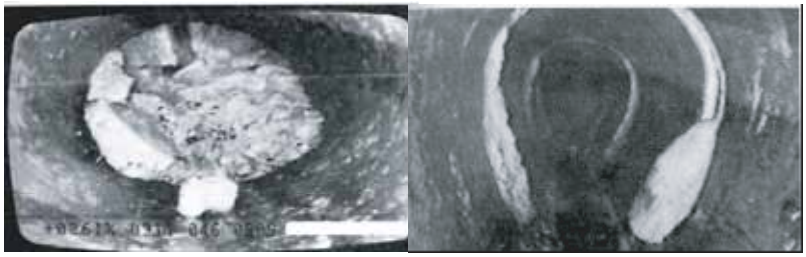

Figure 2.7: Blockage of sewer (left) and incrustation (right) [Stein, 1999]

Beside deposition incrustations and roots growing into the sewer are belonging to the group of flow barriers. Incrustation develops by the consolidation and long-term drying of deposits. They are a special form of sewer solids and can be removed only with a significant mechanical effort.
The reduction of the hydraulic efficiency and the connected consequences all lead to circle where the runoff is reduced furthermore and the deposits grow. This again leads to a reduction of the hydraulic efficiency, which favours a reduction of the bottom shear stresses.

2.3.2 Roughness and reduction of runoff

The change of roughness in sewer channels caused by the influence of bio-film is the subject of several investigations with different results. [Reiff, 1992] While Reid and Yang (1959) and Bland et al. (1975) noticed an increase of the hydraulic resistance, Picologlou et al. (1980) found a smoothening effect of the bio-film regarding the concrete walls of the channel. All these literature sources give no quantitve results of the influence of biofilm on the hydraulic performance of a sewer channel. In principle there is a common agreement that deposits, incrustations and abrasion lead to an increase of the sewer roughness.
Kirchheim (2003) shows an example on the influence of changing roughness for a sewer with a diameter of 2000 mm. The calculations are based on the well known Manning - Strickler equation without regarding the concentration of solids in the flow. The water level was varied for different fictive heights of deposits. Then the Strickler roughness k_{st} was calculated with the formula of Einstein and Horton. [Dauber & Novak, 1983] The results showed that there is a strong increase of roughness with increasing sediment height at smaller water levels. For larger water levels the influence of the sediment height deceased.

2.3.3 Reduction of storage volume

Deposits does not only lead to a reduction of the hydraulic capacity they also increase the amount of intermediate stored sewage in the sewer system during dry-weather. [Krauth, 1971] Borchardt (1992) showed that the sewage system and the stormwater tanks can store 2 mm of rain that falls on sealed surfaces. This means that small rain event could be retained completely but the grow of deposits reduces the available storage volume in

the sewer system and larger storm events will then result in early and stronger overflows into the receiving waters. These shock loads put hydraulic and pollutant stress on recieving waters and influence also the operation of the treatment plant.
Chemical and biological decomposition of the sewage takes place in backwater areas where the flow velocity is reduced and anoxic conditions can be built due to low ventilation of the sewer channels.

2.3.4 Biogenous sulphuric acid corrosion

Corrosion is the reaction of metal and non-metal materials due to chemical, electrochemical and microbiological procedures, which lead to a derogation of the material. Biogenous sulphuric acid corrosion is one form of corrosion which chemical and microbiological reactions take place in sewer deposits (50 %) and bio-film (50 %). The development of sulphuric acid is depending on the sewage consistence, content of deposits, appearance of bio-film, air- and sewage temperature and flow velocity. A low exchange rate of the air inside the sewer channel can lead to high humidity and this will increase the living conditions of microorganism and bacteria.
The formation of sulphuric acid corrosion can be described in four steps:

1. Sulphates and proteins are reduced to hydrosulphide and sulphide under anaerobic conditions inside the deposit layers.
2. Due to diffusion and turbulence the hydrosulphide enters the atmosphere above the deposit layers.
3. Elementary sulphur is generated from hydrosulphide by dissociation.
4. Theo-bacteria at the sewer sidewalls take off the sulphur from the atmosphere and oxidation leads then to sulphuric acid, which damages the walls.

Sulphate concentrations of 600 - 3000 mg/l in the sewage can create an effective attack to the concrete of sewer pipes. Sulphate concentrations above 3000 mg/l will lead to a serious damage of the pipe walls due to sulphuric acid corrosion. [Koppe & Stozek, 1999] The danger of sulphuric acid corrosion increases with a reduced sewage runoff, rising temperatures in the sewer system and a low bottom slope of the sewer channel.

Keding (1990) gives detailed statistics about damages in sewer systems and states that 7 % of all damages are due to corrosion. Figure 2.8 shows biogenous sulphuric acid corrosion in a typical manhole.

The damage symptoms of corrosion are listed below:

- Leakages in the sewer pipes (In- and exfiltration of groundwater)
- Influence of the loading capacity due to reduction of the pipe wall thickness
- Erosion of mortar by clinker constructions
- Increase of wall roughness and flow resistance

[Kirchheim, 2005]

Figure 2.8: Biogenous sulphuric acid corrosion in a manhole [Grube et al., 1990]

2.3.5 Emissions

Smell and corrosion effects appear more often due to the reduction of sewage caused by water saving in the industry and population. Krebs et al. (1999) state that deposits cause the major part of sewer emissions. These unpleasant odours, coming from the sewer system, can derogate the human well being to the loss of appetite and insomnia. Artieres (1988) refers in this context to health damages caused by the fouling of organic deposits.
The emission can be diverted into primary and secondary osmogenes. Primary osmogenes are caused by the direct discharges of industrial and commercial sewage. Secondary osmogenes are depended on the organic content in the sewage and on a lack of ventilation in a sewer channel.
One gas, which is build, is hydrosulphide. The decomposition of fat acids, alcohol and aldehydes will lead to a fouling under anaerobic conditions. [Ruettgers, 1987] The bacterial reduction on nitrogenous material without oxygen creates a fermentation process, which develops the biogas that consists of methane and carbon dioxide. Concentrations of 47 mg/l methane in an unventilated sewer as measured by Koppe and Stozek (1999) can create a dangerous environment for the operational personnel. Further emission can be butyric acid and trimethylamin. [Kirchheim, 2005]

2.4 Remobilisation of sewer deposits

2.4.1 Stability

To clean a sewer channel it is necessary to detach the deposits out of their compound and to transport them with the flow. This can take place during and after storm events, which create an increased runoff in the sewer. The critical flow condition for lifting the deposits and their retention forces will then be exceeded and the erosion of the sediment starts. Due to its capacity the flow in the sewer channel transports the solids. Depending on the turbulence, the form, size and weight of the particles they slide, roll and bounce along the bottom or they can be transported in suspension.
The bottom shear stress is the critical parameter, which is responsible for the start of

the sediment transport as well as temporal and local fluctuations of the flow conditions due to the turbulence.

It must apply

$$\tau_{crit} \leq \tau_0. \tag{2.1}$$

The critical wall shear stress τ_{crit} is a parameter, which was determined for many materials in hydraulic experiments and documented in extensive tables. [Bollrich, 2000]

2.4.2 Critical flow conditions

In chapter 2.4.1 the stability conditions and the beginning of the solid transport were already mentioned. The critical flow condition describes the transition with that erosion or sedimentation can take place. In the case of an excess of the critical wall shear stress, the channel deposits begin to erode. Falling below the critical flow velocity leads to a deposit of sediments, which were transported with the current.
The erosion of solids is an active procedure with energy input while the sedimentation represents a passive settling procedure induced by gravitation. The deposit-free flowing state is defined by the sedimentation shear stress τ_{cs}. Results of the measurements in Hildesheim and a literature search of Ristenpart (1995) are represented in the tables 2.3 and 2.4.

Statistical distribution	Dry-weather runoff
Mean value	$\tau_{cS,t} = 0.29\,\mathrm{N/m^2}$
Minim. value	$\min\,\tau_{cS,t} = 0.04\,\mathrm{N/m^2}$
Max. value	$\max\,\tau_{cS,t} = 0.67\,\mathrm{N/m^2}$
Standart deviation	$s = 0.19\,\mathrm{N/m^2}$
Variation	$Vk = 65.5\,\%$

Table 2.3: Critical flow condition, Values of the sedimentation shear stress [Ristenpart, 1995]

Regarding erosion two different reactions are shown depending on the material structure according to Nalluri and Alvarez (1992):

- Above the firm sediment layer a liquid mud layer is formed from predominantly organic components, which leads, due to turbulent flow, to a loosening and/or a liquefaction of the firm deposits. The erosion takes then place layer by layer.
- Collapse of the bed structure due to corresponding critical conditions. The material erodes in clumps of variable size, which behave afterwards like cohesive materials. The collapse occurs suddenly and a total break down of the bed will be the result.

$\tau_{cS,t}$ [N/m^2]	Author	Remarks
1 - 4	Nalluri und Ab-Ghani 1993	Calculation limit value for self-cleaning sewers
1.4 - 2.1	Gustafsson 1964*	
2 - 3	Schultz 1960*	
4	Lysne 1969* Paintal 1972* Yao 1974*	Calculation suggestion for large sewers
4	Ackers 1991	Limit value for cohesive sediments
6	Clark et al. 1993	Calculation rules for partly and completly filled pipes

Table 2.4: Sedimentation shear stress $\tau_{cs,t}$ for sedimentation free transport [Ristenpart, 1995], * in [Macke, 1982]

As already described the interparticular forces determine the beginning of erosion with cohesive materials considerably. The influence parameters for the beginning of transportation with no-cohesive materials e.g. sand or gravel can be summarized as follows [Nalluri & Alvarez, 1992]:

- Grain size, -volume, -shape, -density, surface finish
- Conditions of the bottom layer
- Flow conditions close to the grain
- Characteristics of liquid (Density, viscosity)

A comparison of the erosion behaviour of both materials groups shows clearly the differences at the beginning of transportation.
The extracting of individual particles from the grain collective is typical for the beginning of erosion with no-cohesive sediments. Subsequently, it comes to a bed load transport at the sole of the channel, which leads to formation of an alluvial bed (mobile unconsolidated sediment layer) on the surface of the sewer bottom.
In cohesive material whole particle clumps are solved from the grain matrix, which change then immediately into suspension. There is no bed load transport at the sole. Clearing away the soil takes place in layers or suddenly with very strong flow turbulences. Figure 2.9 shows a typical erosion procedure of a cohesive sediment bed.

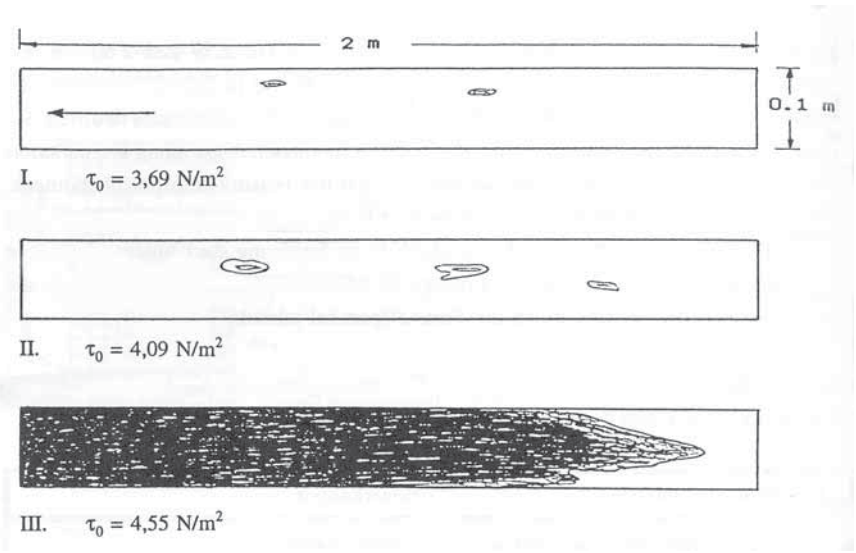

Figure 2.9: Erosion of a cohesive sediment bed [Nalluri & Alvarez, 1992]

Ristenpart (1995) came with his measurements of the critical erosion shear stresses to the following results (Table 2.5):

Statistical distribution	Dry-weather runoff	Storm runoff
Mean value	$\tau_{cE,t} = 0.7\,\mathrm{N/m^2}$	$\tau_{cE,r} = 2.3\,\mathrm{N/m^2}$
Minim. value	min $\tau_{cE,t} = 0.44\,\mathrm{N/m^2}$	min $\tau_{cE,r} = 0.98\,\mathrm{N/m^2}$
Max. value	max $\tau_{cE,t} = 1.02\,\mathrm{N/m^2}$	max $\tau_{cE,r} = 5.6\,\mathrm{N/m^2}$
Standard deviation	$s = 0.21\,\mathrm{N/m^2}$	$s = 1.02\,\mathrm{N/m^2}$
Variation	$Vk = 30\,\%$	$Vk = 30\,\%$

Table 2.5: Critical flow condition, values for the erosion shear stress [Ristenpart, 1995]

A composition of literature values in table 2.6 shows the different results of numerous investigations. A comparison or a transmission of critical wall shear stresses is possible with the restrictions specified before.

$\tau_{cE,t}$ [N/m^2]	Author	Remarks
1.5 - 2	Ashley et al. (1994)*	Field measurements
2 - 4	Stotz and Krauth (1986)*	Deposits of domestic waste water
1.3 20	Kamphuis (1990)* Ristenpart (1995)	Laboratory investigations: Flow with sand particles and clear water
1	Ashley et al. (1994)	Fluid sediment layer
1.1 - 1.2	Verbanck (1995)	Collapse of the under flow
1.8	Ashley et al. (1992)	Erosion in top layer
2.0	Berlamont and Torfs (1996)	
2.5	Nalluri and Alvarez (1992)	Sediment type C (Bed load)
2.5	Nalluri (1991)	Sedimented non-cohesive material
4 - 6	Wotherspoon (1994)	
6 - 7	Nalluri and Alvarez (1992)	Sediment type A (Deposits, lightly consolidated)
6 - 7	Williams et al. (1989)	Synthetic cohesive material

Table 2.6: Criticial values for the start of erosion: Erosion shear stress $\tau_{cE,t}$ *[Ristenpart, 1995] supplemented by Kirchheim (2003)

Despite the different results of the presented investigations the value $\tau_c = 5.6\,[\mathrm{N/m^2}]$ from the measurements of Ristenpart (1995) became generally accepted as the typical limit value for the start of erosion.

2.4.3 Modelling of sediment transport - approaches

In the literature many calculation approaches for the critical wall shear stress and/or the transport of channel deposits can be found, but most of these formulas were developed for unconsolidated sediments, like the ones to be found e.g. in rivers. The approach of Shields [Bollrich, 2000] is here the perhaps most well known example. Detailed descriptions of several approaches are given in the publications of Kirchheim (2003), Ristenpart (1995) and Macke (1980).
Sewer sediments are, as previously mentioned, mostly a mixture from cohesive and non-cohesive material. It is different with river sediments where the non-cohesive sediment portions outweigh. An extensive listing of the relevant differences between sewer deposits and river sediments are to be found in Kirchheim (2005).
For this reason the mentioned computational approaches are restricted to described the erosion and/or beginning of transportation. After Ristenpart (1995) and Zanke (2004) sufficiently results can be achieved with them when the specific characteristics of the channel sediments are treated with care. Nalluri and Alvarez (1992) developed two transport equations, which can compute the wall shear stress for cohesive and non-cohesive sediments.

2.4.4 Transportation capacity

The transport of solids generally depends on the transportation capacity of the sewage runoff [Kuehn & Gebhard, 1998]. Deposits develop, if the sediment entry into the sewer system is larger than the transportation capacity of the flow [Wang & Han, 1996]. The distribution of the solid concentration $c(y)$ over the cross section of a channel is represented in figure 2.10.

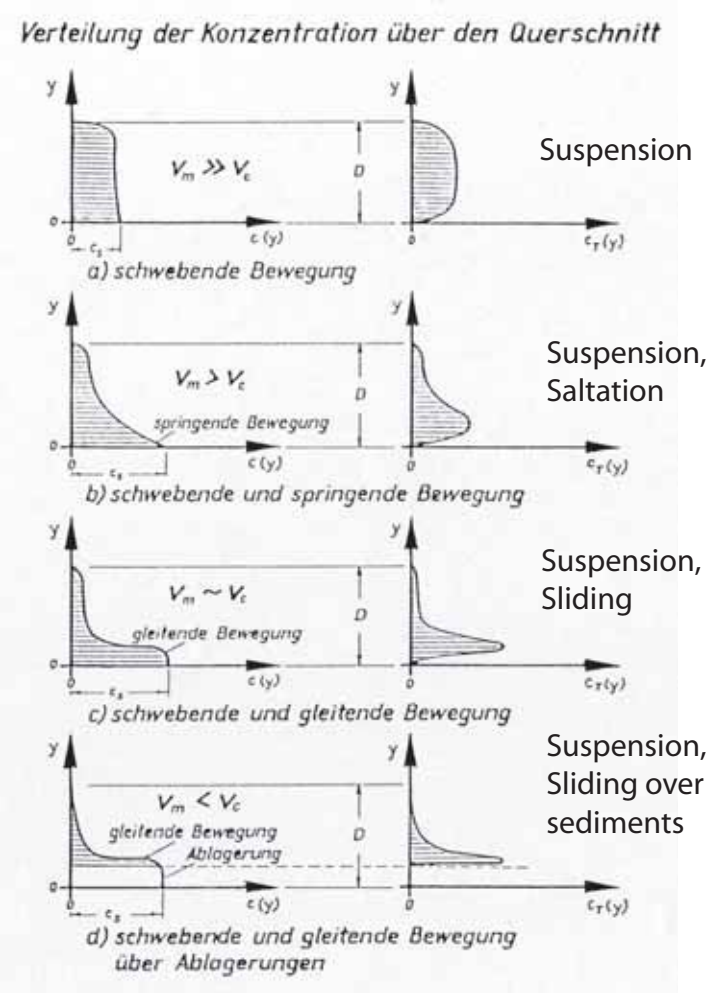

Figure 2.10: Concentration profiles as a function of the mean flow velocity [Sander, 1989]

The volume-referred transportation capacity used here is calculated as follows:

$$c_T = \frac{Q_s}{Q_s + Q_w}. \tag{2.2}$$

Regarding the transportation capacity of solids in combined sewage systems the work of Dette et al. (1996) will be presented.
Thereby one of the goals was the development for model components and recommendations for the structure and the use of quantity and quality models. For this verifiable computation approaches for the erosion and sediment procedures in sewers had to be developed. Therefore it was tried to evaluate critical values, which allow statements about

erosion and sedimentation depending on the solid transport parameters. For this, in the hydrologic year 1989/90 numerous measurements were made in the combined sewage net of the city of Braunschweig. A closer inspection of the deposit dynamics in the sewer of the William Bode road an apparent contradiction turned out, since it came here to the formation of deposit during a rain event. This led to the conclusion that in a network the sediment build up is distributed. Dette et al. (1996) deduced the theoretical background where the following transport equations are used.

$$Q_s = Q \cdot c_T \tag{2.3}$$

The transport rate of solids corresponds to the following approach. The exponent n corresponds to a value within the range between two and three after Karakassonis (1936).

$$Q_s \cdot A = \tau^n \tag{2.4}$$

Due to the increase in concentration during storm events, the transport capacity of the sewer is not sufficient in order to transport all solids. The formation of deposits are the result. A confirmation of this statement is still pending, since so far still no results of measurement in sand traps at sewage plants were made. [Dette et al., 1996] In the case of use of the transport equation for deposit-free sewer pipes after Macke (1982) and consideration of the determined transportation concentrations, increased solid transport rates are the result. Dette et al. (1996) points out that with small wall shear stresses of τ=0.6 N/m^2 a stable transportation condition is to be registered for the channel section concerned. But it is stressed that even for a small decrease of the shear stresses substantial deposits will be encountered. The transportation capacity of a sewer channel is determined by controlling values, according to Ristenpart (1995):

- Consistence of the solids (Grain size and shape)
- Reciprocal effects among themselves (Aggregation and decay, obstructed sedimentation)
- Consistence of the deposits (Cohesive properties)
- Prehistory of the system condition (Duration previous dry-weather period)
- Location and geometry of the sewer channel

Regarding different investigations concerning the hydraulic solid transport of in sewer pipes, the following grain sizes (heterogeneous mixtures) can be assigned to different movement conditions [Sauermann, 1983]:

- Suspension: 50 μm - 0.2 μm
- Transition zone: 0.2 - 2 mm (coarse sand)
- Moveable deposits: 2 mm

In table 2.7 a selection of literature resources concerning the computation approaches for solid transport in sewer systems are indicated. An overview of different approaches to the transport of sewer deposits with consideration of the calculation in main sewers is

presented in Hager (1998). Concerning the different computation approaches it must be stated that a transmission of the empirical approaches is not so easily applicable to each catchment and/or each type of deposit. Arthur (1996) for example, showed on basic experiments that, compared with other approaches, for the description of the transport of so called near bed solids a modified approach after Perrusquia & Nalluri (1995) is best suited for rough material as well as an empirical equation after Arthur & Ashley (1997) for the organic freight. [Chebbo et al., 2003]. Despite a multiplicity of computation approaches for the transport of solids in sewerage systems the remarks of Nalluri (1991) and Perrusquia (1991) show that there is a large need for further research.

Source	Reference / Material
Ab-Ghani (1993)	starting from t/D 10 - 15 % optimum conditions for permanente deposits
Ackers & White (1973)	Major parameters: Shear stress, total load transport
Ackers (1991)	Permanente (moveable) deposits
Arthur (1996)	
Coghlan et al. (1996)	Major parameters: Velocity, total load transport
El-Zaemey (1991)	Transport in sewer systems over a stationary deposit layer
Macke (1982, 1983)	Assumption of non-cohesive solids
Mark (1991)	
May (1982)	
May et al. (1989)	Deposit thickness up to 1 % of sewer diameter
Mayerle (1988)	Permanente (moveable) deposits
Mayerle et al. (1991)	
Nalluri & El-Zaemey (1993)	Major parameters: Shear stress, bed load transport
Nalluri et al. (1994)	Transport in sewer systems over a stationary deposit layer
Novak & Nalluri (1975)	Assumption of non-cohesive solids
Perrusquia (1991)	
Perrusquia & Nalluri (1995)	Bed load transport
Robinson & Graf (1972)	
Sander (1989)	Assumption of non-cohesive solids
Schmitt (1985)	Major parameters: Velocity, total load transport
Wotherspoon (1994)	Major parameters: Shear stress, remobilisation

Table 2.7: Literature sources concerning sewer deposit transport equations [Kirchheim, 2005]

2.5 Roughness

2.5.1 Definition of roughness

Schroeder (1990) gives a general definition of the term roughness:
"*In the scientific sense roughness is called a surface finish of a wall or a sole. This characterizes more exactly the manifestation of the wall or sole roughness, which either naturally or technically occurs. It is artificially created, fixed or variable.* "

Generally there are three different types of roughness:

- Absolute roughness k
- Equivalent roughness k_s
- Relative roughness k/d

The absolute roughness k designates a transverse measure for the deviation of the surface outline from its even, straight-line zero level, perpendicularly to this measured. An example can be here the deviation of a surveyed profile of the wall and/or bottom roughness. The equivalent roughness (sand roughness) goes back to investigations of Nikuradse (1932) in the 30's. He defined sand roughness as a surface formed from sand particle of same grain size in closest packing, whose only characteristic is the diameter of the grain. He did not regard the shape of the individual grains. The grain diameters of this sand roughness then describes the equivalent sand roughness k_s. Thus a comparable roughness is defined, who characterizes the real conditions of a wall or the bottom of a channel.
The relative roughness k/D is a dimensionless characteristic number, which results from the reference of the absolute roughness k on a typical transverse dimension of the flow process (normally measured to the direction of flow). As base factor for the formation of this relative value the pipe diameter d or the depth of water h is applicable. [Schroeder, 1990]
The channel roughness is one of the boundary conditions, which affects the form and speed of the flush wave considerably. The main problem is the estimation or determination of the roughness at the channel bottom, which is dependent on the existing sediments. Contents and the consistency of the channel deposits depend on the respective catchment, which is attached to the regarded channel. Normally the deposits consist of a mixture of paper, hair, fabric materials, textile fiber and small fragments of channel walls. Blumberg and Bauer (1994) characterized channel deposits as a paste with mineral inclusions.

2.5.2 Size of sewer deposits

A literature study for the investigation of roughness with different deposit heights and/or the particle size distribution curves of sediments in sewers was accomplished by Kirchheim (2003). Thereby it became clear that a large range of particle sizes for sewer sediments is possible. In the regarded literature sources the size of the deposit particles

varied between 0.6 mm to 15 mm. In addition, the differences were also depending on the catchment and the seasonal fluctuations.
In order to consider the particle sizes of the sewer deposits in a numerical model, it is necessary to formulate a relationship between the diameter d of the deposit particle and the sand roughness k_s, which enters the logarithmic wall law.
Bollrich (2000) defined the roughness k as the 90% value of the mesh grading curve. Ashley et al. (1994) indicated a particle size between 0.25 to 20 mm for the 90% value, while Sakakibara (1996) measured in his investigations 0.4 to 6 mm. Investigations in inlet and main sewers of Arthur et al. (1996) resulted in an average particle size of 10 mm in the case of 90 % mesh passage.
The study of further literature sources resulted in numerous statements for a functional relationship between the particle diameter and equivalent sand roughness. In Schroeder (1990) the following authors were quoted (Table 2.8):

Source	$k_s = \mathrm{f}(d_i)$
Bollrich, Garbrecht (2000)	$k_s = 1.0\, d_{90}$
Einstein (1942)	$k_s = 1.0\, d_{65}$
Engelund / Hansen (1966)	$k_s = 2.0\, d_{65}$
Hey (1979)	$k_s = 3.5\, d_{84}$
Kamphuis (1990)	$k_s = 2.0\, d_{90}$
Taylor / Brooks (1962)	$k_s = 1.0\, d_{50}$
Van Rijn (1948)	$k_s = 3.0\, d_{90}$

Table 2.8: Relationship sand roughness - particle diameter [Schroeder, 1990]

A further source of literature is the publication of Kabir and Torfs (1992). Beside functional relations they also made the absolute value of the sand roughness in several investigations available. (Table 2.9)

Source	$k_s = \mathrm{f}(d_i)$	Sand roughness k_s[cm]
Ackers-White (1973)	$k_s = 1.25\, d_{35}$	0.42
Engelund-Hansen (1967)	$k_s = 2.0\, d_{65}$	0.96
Hey (1979)	$k_s = 3.50\, d_{85}$	2.08
Kamphuis (1990)	$k_s = 2.5\, d_{30}$	1.50
Mahmood (2000)	$k_s = 5.1\, d_{84}$	2.98
van Rijn (1948)	$k_s = 3.0\, d_{90}$	1.80

Table 2.9: Relationship sand roughness - particle diameter, roughness values [Kabir & Torfs, 1992]

For the numerical modelling of the reservoir sewer August Bebel Ring in Offenbach, which is described later in detail, first a mean roughness of 5 mm was selected, which was varied in the course of the computations.

3 Basics of numerical modelling

3.1 Introduction

Flush waves created by sewer cleaning devices are similar to dam-break waves. Especially in the initial phase they posses a three-dimensional character and it is obvious that the turbulence in the front wave plays a significant role for the cleaning effect of a flush wave. Numerical models are a very good way to calculate and describe highly turbulent flows as encountered in flush waves. The flow velocity and the bottom shear stress are the major values to evaluate the effectiveness of a flush wave. Therefore it is necessary to calculate them both in a high spatial and temporal resolution as offered by three-dimensional models. The use of turbulence models like the $k - \epsilon$ model of Launder and Spalding (1972) helps to close the set of flow equations in the three-dimensional models and to approach the chaotic movement inside the flush wave. In the following chapter the basics of the numerical modelling will be explained to understand the background of the later investigations using the commercial three-dimensional model StarCD, which is described in detail in chapter 5.5.

Using three-dimensional models the discretisation of local areas in a sewer system like narrows, steps or curves can be modelled with a high decomposition. Existing CAD drawings of a sewer system can then be read in and used for a plain mesh generation. The main drawback of a high-resolution three-dimensional calculation is the large amount of grid cells because of the length of a sewer channel. Reservoir sewers can easily exceed 200 m, which leads to very long calculation times. The usage of small iteration time steps in connection with very small grid cells for a detailed discretisation of the flow around the flushing device also increases the calculation times. Therefore it is necessary to reduce the numerical grid to the essential cells to keep the computational times in realistic dimensions.

The description of the theoretical basics of the numerical modelling is divided into the following parts:

- Mass- and momentum conservation
- Turbulence modelling
- Numerical basics - Finite Volume Method
- Calculation of the free surface - Volume of Fluid Method
- Boundary conditions

3.2 Reynolds averaged Navier-Stokes equations

3.2.1 Conservation of mass

The continuity equation specifies the conservation of mass for a volume element in a fluid. Therefore the mass balance to the volume element with all in- and outflows is formed. Equation 3.1 applies for a compressible fluid

$$\frac{\partial \rho}{\partial t} + \frac{\partial (\rho u_i)}{\partial x_i} = 0. \tag{3.1}$$

For incompressible fluids the density ρ = constant. The continuity equation is then reduced to

$$\frac{\partial u_i}{\partial x_i} = 0. \tag{3.2}$$

3.2.2 Conservation of momentum

The momentum equations of the Navier-Stokes equations characterize the conservation of momentum within a control volume. For the available case the momentum equations are limited to isothermal flows of incompressible Newtonian fluids.

$$\rho \left(\frac{\partial u_i}{\partial t} + u_k \frac{\partial u_i}{\partial x_k} \right) = -\frac{\partial p}{\partial x_i} + \mu \frac{\partial^2 u_i}{\partial x_k^2} + \rho g_i \tag{3.3}$$

The kinematic viscosity

$$\nu = \frac{\mu}{\rho} \tag{3.4}$$

leads to equation 3.5

$$\frac{\partial u_i}{\partial t} + u_k \frac{\partial u_i}{\partial x_k} = -\frac{1}{\rho} \frac{\partial p}{\partial x_i} + \nu \frac{\partial^2 u_i}{\partial x_k^2} + g_i. \tag{3.5}$$

The Navier-Stokes equations, consisting of the continuity and the momentum equations, describe laminar and turbulent flows. Theoretically they can calculate all details of turbulent structures with direct numerical modelling (DNS). [Rodi, 1993] At present this approach is limited to simple geometries and low Reynolds numbers (<4000). The calculation of high Reynolds numbers to resolve all vortex structures needs super-computational resources. The most applications of numerical modelling for engineering purposes in urban drainage do not need a resolution of turbulent fluctuations. Averaged values a adequate and the Navier-Stokes equations can be reduced to the Reynolds-averaged Navier-Stokes equations (RANS).

3.2.3 Reynolds averaging - Reynolds equations

In turbulent flows the energy is transformed with vortex cascades into heat. The mean kinematic energy of the flow and the temperature is raised on a molecular basis by large, small and microscopic eddies. The superposition of different scales of motion leads to local and temporal fluctuating flow field. The mean flow field is overlaid by fluctuations with a chaotic character. The hydrodynamic values in a turbulent flow are also chaotic distributed, but the mean flow shows a steady behaviour, which can be defined and solved in differential equations. Therefore the mean values of a flow are determined and the Navier-Stokes equation is averaged to describe the mean turbulent flow in a legality. This approach is based on the publication of Osborne Reynolds in 1895 [Reynolds, 1895]. The physical values in a time slice are separated into a mean and a fluctuation value. Equation 3.6 shows this principle with the flow velocity u.

$$\underbrace{u(x_i,t)}_{\text{Momentary value}} = \underbrace{\bar{u}(x_i,t)}_{\text{Mean value}} + \underbrace{u'(x_i,t)}_{\text{Fluctuation value}} \tag{3.6}$$

The Reynolds averaging will now be applied on the Navier-Stokes equations, which leads to the Reynolds averaged Navier-Stokes equations for the conservation of mass and momentum.

Conservation of mass

$$\frac{\partial \bar{u}_i}{\partial x_i} = 0 \tag{3.7}$$

Conservation of momentum

$$\frac{\partial \bar{u}_i}{\partial t} + \frac{\partial \bar{u}_k \bar{u}_i}{\partial x_k} = -\frac{1}{\rho}\frac{\partial \bar{p}}{\partial x_i} + \frac{\partial}{\partial x_k}\left[\nu \frac{\partial \bar{u}_i}{\partial x_k} - \overline{u'_k u'_i}\right] \tag{3.8}$$

3.2.4 Reynolds stresses

In contrast to the Navier-Stokes equations the Reynolds equations possess terms of correlated fluctuating values $\overline{u'_k u'_i}$, which are termed Reynolds stresses. These stresses represent the exchange of momentum between the fluid elements due to the turbulent motion. They are defined in the Reynolds stress tensor $(\tau_{ki})_{turb.}$.

$$(\tau_{ki})_{turb.} = -\rho\overline{u'_k u'_i} = -\rho \begin{pmatrix} \overline{u'_1 u'_1} & \overline{u'_1 u'_2} & \overline{u'_1 u'_3} \\ \overline{u'_2 u'_1} & \overline{u'_2 u'_2} & \overline{u'_2 u'_3} \\ \overline{u'_3 u'_1} & \overline{u'_3 u'_2} & \overline{u'_3 u'_3} \end{pmatrix} \tag{3.9}$$

3.2.5 Closure problem

The Reynolds equations, in opposition to the original Navier-Stokes equations, imply more unknown values than equations. Beside the velocities and the pressure the Reynolds stresses are newly added. They are unknown by quantity and lead to the problem that the equation system is unclosed which means there is no closed solution possible.
One further equation is necessary to solve the Reynolds equations. The formation of this equation and the quantification of the Reynolds stress are the assignments of the turbulence modelling. Turbulence models should be universally valid and able to describe many different flows with preferably few additional equations. [Malcherek, 2001a,b]

3.3 Turbulence modelling

3.3.1 Fundamentals

The approaches in turbulence modelling can generally be separated into eddy viscosity models and models which calculate the Reynolds stress tensor directly. The eddy viscosity models are based on the assumption of Boussinesq (Equation 3.10) and imply isotropic turbulent structures.
Reynolds stress models (RSM) use further differential equations to solve the Reynolds stress tensor. They employ transport models to describe the individual stresses $\overline{u_i u_j}$ and transport equations for the heat and mass fluxes $\overline{u_i \varphi}$ with exact equations which have to be modelled to obtain a closed system. Algebraic Stress Models (ASM) calculate the Reynolds stress tensor with algebraic equations. They reduce the equations for the Reynolds stresses $\overline{u_i u_j}$ and the scalar fluxes $\overline{u_i \varphi}$ to algebraic expressions by using model approximations to convert differential equations to algebraic equations. [Rodi, 1993]

The assumption of Boussinesq is an extension of the Boussinesq analogy (1877) between the molecular diffusion and the turbulent exchange of momentum.

$$\tau_{tur,ik} = -\rho\overline{u_i' u_j'} = -\nu_t \left(\frac{\partial \bar{u}_i}{\partial \bar{x}_j} + \frac{\partial \bar{u}_j}{\partial \bar{x}_i} \right) + 2\delta_{ij} k \tag{3.10}$$

Momentum, concentration or temperature inside a fluid are redistributed for both procedures to reduce the gradients. The eddy viscosity approach, formulated by Boussinesq, calculates the turbulent stresses with an enlarged viscosity, called eddy viscosity, in the diffusion term in equations 3.10. This expansion was implemented to ensure that the sum of the normal components of the stresses equal the double kinetic turbulent energy (2k). The kinetic turbulent energy is defined in equation 3.11. The newly introduced eddy viscosity varies local and temporal as a function of the flow which makes it necessary to calculate it with a turbulence model. [Rodi, 1993]

$$k = \frac{1}{2}\overline{u_i' u_i'} = \frac{1}{2}\overline{(u_1'^2 + u_2'^2 + u_3'^2)} \tag{3.11}$$

Eddy viscosity models are differentiated by the number of additional transport equations in zero-equation, one-equation and two-equation models. Zero-equation models do not involve transport equations for turbulent quantities. They are based on the eddy viscosity concept. The specification of the eddy viscosity is done directly from experiments with empirical formulae or by relating it to the mean-velocity distribution. Examples are constant-eddy-viscosity model, the mixing-length model or the Prandtl free-shear-layer model.
One-equation models determine the mean velocity gradient by an additional transport equation. The velocity fluctuations are characterised by the kinetic energy k. The Bradshaw et al. model is an example for an one-equation turbulence model.
The two-equation models close the Reynolds equation with the introduction of two new differential transport equations. The first equation is the k-equation, which describes the turbulent kinetic energy k. The second equation can include the length scale L which characterizes the size of the large energy-containing eddies. But the length scale L does not have to be necessarily the depended variable of the second equations. It could also be the turbulent kinetic dissipation rate ϵ. [Rodi, 1993]
In the following the two-equation models and here especially the $k-\epsilon$ model, which was used for the later investigations, will be looked at. Detailed references for turbulence modelling are Durbin and Pettersson (2001), Ferziger and Peric (1996), Oberlack (1994), Oertel and Laurien (2003), Rodi (2004), Rotta (1972) and Wilcox (1998).

3.3.2 The $k-\epsilon$ turbulence model

The first $k-\epsilon$ model was published by Jones and Launder (1972). The standard $k-\epsilon$ model as it is known today was developed by Launder and Spalding also in 1972 [Launder & Spalding, 1972].
The $k-\epsilon$ model is still the most used and best-tested turbulence model which provides the best results for small computational costs. It was the first one to be developed, widely accepted and used for example in industrial applications like aircraft construction. There are various turbulence models, who provide more precise results, but the $k-\epsilon$ model is most widespread turbulence model. The calculation of complex flows like anisotropies in turbulence or rotation in the flow shows the weakness of the $k-\epsilon$ model. These effects cannot be calculated using the eddy viscosity approach.

The purpose of the $k-\epsilon$ model is the prediction of the eddy viscosity ν_t. Therefore a coherency between the turbulent kinetic energy k, the dissipation rate ϵ and the eddy viscosity is formulated due to the fact that for large Reynolds numbers the dissipation rate and the production rate have an similar magnitude.

$$\nu_t \sim \frac{k^2}{\epsilon} \tag{3.12}$$

The introduction of the constant $C_\mu = 0.09$ leads to

$$\nu_t = C_\mu \frac{k^2}{\epsilon} \tag{3.13}$$

Energy is extracted from the main flow by large elements of turbulence and is transferred to smaller elements until the energy is dissipated by the smallest eddies. The dissipation rate ϵ equals the turbulent kinetic energy, which is transformed into internal heat.

To solve the Reynolds system with a sufficient number of equations compared to the unknown variables, respectively one equation for the turbulent kinetic energy k and one for the kinetic dissipation rate ϵ is imposed. The turbulent kinetic energy describes the velocity scale $\hat{V}$ and the kinetic dissipation characterizes the length scale L.

$$\hat{V} = k^{\frac{1}{2}} \tag{3.14}$$

$$L = \frac{k^{\frac{3}{2}}}{\epsilon} \tag{3.15}$$

3.3.2.1 Reynolds stress equation

The Reynolds stress equation (I_i') is derived by the subtraction of the Reynolds averaged Navier-Stokes equation ($\bar{I}_i$) from the momentum equation with Reynolds averaging (I_i).

$$I_i' = I_i - \bar{I}_i \tag{3.16}$$

Momentum equation with Reynolds averaging (I_i)

$$\frac{\partial(\bar{u}_i + u_i')}{\partial t} + \frac{\partial(\bar{u}_k + u_k')(\bar{u}_i + u_i')}{\partial x_k} = -\frac{1}{\rho}\frac{\partial(\bar{p} + p')}{\partial x_i} + \nu\frac{\partial^2(\bar{u}_i + u_i')}{\partial x_k^2} \tag{3.17}$$

Reynolds averaged Navier-Stokes equation ($\bar{I}_i$)

$$\frac{\partial \bar{u}_i}{\partial t} + \frac{\partial \bar{u}_k \bar{u}_i}{\partial x_k} = -\frac{1}{\rho}\frac{\partial \bar{p}}{\partial x_i} + \frac{\partial}{\partial x_k}\left[\nu\frac{\partial \bar{u}_i}{\partial x_k} - \overline{u_k' u_i'}\right] \tag{3.18}$$

Reynolds stress equation (I_i')

$$\frac{\partial u_i'}{\partial t} + u_k'\frac{\partial \bar{u}_i}{\partial x_k} + \bar{u}_k\frac{\partial u_i'}{\partial x_k} + u_k'\frac{\partial u_i'}{\partial x_k} = -\frac{1}{\rho}\frac{\partial p'}{\partial x_i} + \frac{\partial}{\partial x_k}\left(\nu\frac{\partial u_i'}{\partial x_k} + \overline{u_k' u_i'}\right) \tag{3.19}$$

3.3.2.2 General k-equation

To formulate the general k-equation, the Reynolds stress equation is multiplied with the turbulent fluctuation value of the flow velocity u_i' and subsequently the term is averaged.

$$\overline{u_i' I_i'} = 0 \tag{3.20}$$

The general k-equation is then defined by:

$$\underbrace{\frac{\partial k}{\partial t}}_{\text{I}} + \underbrace{\bar{u}_k\frac{\partial k}{\partial x_k}}_{\text{K}} = \underbrace{-\overline{u_i' u_k'}\frac{\partial \bar{u}_i}{\partial x_k}}_{\text{P}} - \underbrace{\frac{\partial\overline{(u_i' u_i' u_k'/2)}}{\partial x_k}}_{\text{Diff1}} - \underbrace{\frac{1}{\rho}\frac{\partial\overline{p' u_i'}}{\partial x_i}}_{\text{Diff2}} + \underbrace{\nu\frac{\partial^2 k}{\partial x_k^2}}_{\text{mol. Diff}} - \underbrace{\nu\frac{\overline{\partial u_i'}\partial u_i'}{\partial x_k \partial x_k}}_{\text{Diss}} \tag{3.21}$$

3.3.2.3 Model equations for the $k-\epsilon$ model

The terms of the turbulent diffusion, $Diff1$ $Diff2$, are summarised and replaced by a gradient-transport model to close the k-equation. [Durbin & Pettersson, 2001]

$$-\frac{\overline{(u_i'u_i'u_k'/2+p'u_k')}}{\partial x_k} = \frac{\partial}{\partial x_k}\left(\frac{\nu_t}{Pr_k}\frac{\partial k}{\partial x_k}\right) \tag{3.22}$$

The k-equation is then defined by:

$$\frac{\partial k}{\partial t} + \bar{u}_k\frac{\partial k}{\partial x_k} = P - \epsilon + \frac{\partial}{\partial x_k}\left(\frac{\nu_t}{Pr_k}\cdot\frac{\partial k}{\partial x_k}\right) + \nu\frac{\partial^2 k}{\partial x_k^2} \tag{3.23}$$

with

$$P = \left[\nu_t\left(\frac{\partial \bar{u}_i}{\partial x_j} + \frac{\partial \bar{u}_j}{\partial x_i}\right)\right]\frac{\partial \bar{u}_i}{\partial x_i} \tag{3.24}$$

and

$$\epsilon = \nu\frac{\overline{\partial u_i'\partial u_i'}}{\partial x_k \partial x_k} \tag{3.25}$$

The transport equation for ϵ cannot be derived directly. It is rather a dimensional consistent analogy to the k-equation. [Durbin & Pettersson, 2001]

$$\frac{\partial \epsilon}{\partial t} + \bar{u}_k\frac{\partial \epsilon}{\partial x_k} = \frac{\epsilon}{k}(C_{\epsilon 1}P - C_{\epsilon 2}\epsilon) + \frac{\partial}{\partial x_k}\left(\frac{\nu_t}{Pr_\epsilon}\cdot\frac{\partial \epsilon}{\partial x_k}\right) + \nu\frac{\partial^2 \epsilon}{\partial x_k^2} \tag{3.26}$$

For large Reynolds numbers the molecular diffusion term of the k-equation and the ϵ-equation will be set to zero. Compared to the turbulent diffusion term the molecular diffusion is very small, which makes it negligible.

The constants of the $k-\epsilon$ model were acquired experimentally by Launder and Spalding (1972). (Table 3.1)

C_μ	Pr_k	Pr_ϵ	$C_{\epsilon 1}$	$C_{\epsilon 2}$
0,09	1,0	1,3	1,44	1,92

Table 3.1: Constants of the $k-\epsilon$ model [Launder & Spalding, 1972]

The introduction of the k-equation and the ϵ-equation produce, together with the continuity and momentum equations, a set of six differential equations. With six unknown variables $(\bar{u}_1, \bar{u}_1, \bar{u}_1, \bar{P}, k, \epsilon)$ the system of equations can be solved.

3.4 Finite Volume Method

3.4.1 General notes

The general approach of numerical modelling is based on the definition of an artificial system, which presents a section of a natural system with all its important processes and

physical magnitudes for the chosen application.
After the definition of the modelling system, the necessary data will be determined and the equations will be set up to characterize the physical problem. Then follows the decision about the appropriate solution algorithm, which is implemented in a software.
The numerical model interacts with is surroundings by boundary conditions as well as input and output values. Initial values describe the state of the system at the beginning of the computation, while the simulation itself calculates the processes and results during a defined period of time.
Generally hydrodynamic models are conceptional models, which means that they are, in contrast to empirical models, defined physically correct. Because of the included turbulence models and their simplifications or empirical assumptions the physical correctness is understated. Numerical models possess a deterministic character by calculating a future condition out of processes that happened in the past. The non-linearity of numerical models is justified by the fact that different impacts on the system cannot be regarded separately from each other.
The equations to describe a certain system must be discretised. Therefore the system is divided in several points, where the relevant equations are solved in time and space. According to the requirements of the calculation this can happen in one, two or three dimensions. The discretisation of the equations can be done by different methods. The most well known are:

- Finite Difference Method
- Finite Volume Method
- Finite Element Method

The Finite Volume Method is used for following investigations. This method is based on the balancing of fluxes through a defined control volume. The equations are discretised indirectly, which means that the conservation of mass and momentum is assured.

3.4.2 Discretisation in space

3.4.2.1 Numerical grids

To solve the basic flow equations the flow domain is divided in single control volumes Ω_i. A knot in its core defines each control volume. The choice of the numerical grid, which describes the flow domain, is of particular importance for the precision of the calculations. Basically it can be distinguished between structured and unstructured grids. (Figure 3.1)
Structured grids are orthogonal grids which means that the meshes are nearly vertical to each other's. For equidistant grids the distances between the single meshes are equal. The nodes in unstructured grids are distributed arbitrarily. Each point is connected to several neighbour points. Thereby faces are generated who feature the shape of triangles or alike. This shape allows a better adaptation of the numerical grid to complicated geometries. The high resolution of the unstructured grids leads to a higher computing time because the flow equations have to be solved more often for the same flow domain.

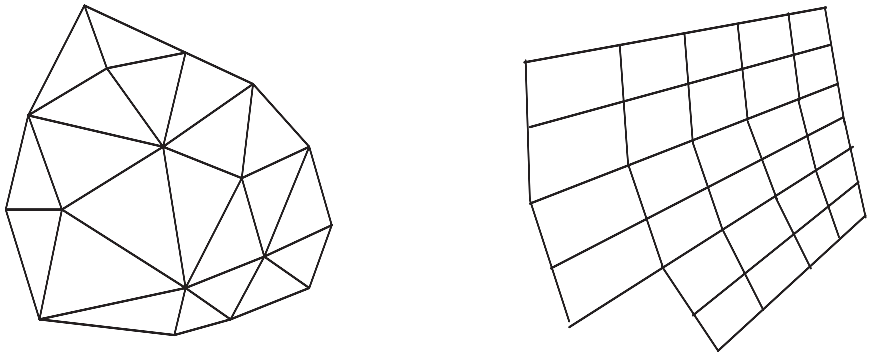

Figure 3.1: Unstructured - structured numerical grids [Valentin & Rinaldi, 2001]

Local refinements are necessary at important places of the flow domain to get more detailed results. The transition between the original grids the refined one should not be abrupt. To ensure a stable calculation the difference in size between two neighbouring cells should not exceed the factor two.
Beside the static grids, which keep their shape during the calculation, there are adaptive grids to illustrate the flow domain. These grids can change their shape and adjust themselves to the water level. They do not move along the river for example like the third kind of grids the moveable grids. They can describe the forward movement of a wave along a dry bottom. More information's on numerical grids can be found for example in Buergisser (1998) and Oertel and Laurien (2003).

3.4.2.2 Divergence form

The discretisation in space is carried out by the definition of the basic hydro-dynamic equations in divergence form.

$$\frac{\partial f}{\partial t} + div\ \Phi_f = q_f \tag{3.27}$$

The terms of the three-dimensional incompressible Navier-Stokes equation are shown in table 3.2.

Equation	f	Φ_f	q_f
x-momentum	u_1	$u_1 u_i - \nu\ grad\ u_1$	$-\frac{1}{\rho}\frac{\partial p}{\partial x_1} - g_1$
y-momentum	u_2	$u_2 u_i - \nu\ grad\ u_2$	$-\frac{1}{\rho}\frac{\partial p}{\partial x_2} - g_2$
z-momentum	u_3	$u_3 u_i - \nu\ grad\ u_3$	$-\frac{1}{\rho}\frac{\partial p}{\partial x_3} - g_3$
Continuity	ρ	$\rho\ u_i$	0

Table 3.2: Terms of the divergence form [Malcherek, 2001a]

3.4.2.3 Integral form of the basic flow equations

The divergence form of the basic flow equations are integrated across the control volumes Ω_i. Then they are transformed by the Gau integral theorem. (Equation 3.28) The usage

of the Gauss integral theorem reduces the volume integral to a boundary integral by leaving out the divergence.

$$\underbrace{\int_{\Omega_i} \frac{\partial f}{\partial t}\, d\Omega}_{\text{I}} + \underbrace{\int_{S} \Phi_f\, dS}_{\text{II}} = \underbrace{\int_{\Omega_i} q_f\, d\Omega}_{\text{III}} \tag{3.28}$$

I: Integration of time
II: Flux term: Summation of all fluxes across the boundaries
III: Source term: Energising forces of the flow, for example the pressure gradient

This equation states that each temporal change of the value f in the volume Ω_i is defined by the balance of the fluxes Φ_i across the boundaries and through the sources and sinks. Derivation terms of the basic flow equations drop out because of the integration of the divergence term. The second order derivations of the diffusion terms are reduced to first order derivations. This makes the differential equations easier to solve.

3.4.2.4 Treatment of the single terms

Integration of time

$$\int_{\Omega_i} \frac{\partial f}{\partial t}\, d\Omega = \frac{\partial}{\partial t} \int_{\Omega_i} f\, d\Omega \simeq \frac{\partial}{\partial t}(V_i\, f_i) \simeq V_i \frac{f_i^{n+1} - f_i^n}{\Delta t} \tag{3.29}$$

The integration of the derivation of time is calculated approximately by the volume V_i of the control volume Ω_i.

Source term

The integration across the finite volumes Ω_i are substituted by a product with V_i.

$$\int_{\Omega_i} q_f\, d\Omega \simeq V_i\, q_{f_i} \tag{3.30}$$

Flux term

The in- and out-flows are summed up across the according boundaries with the length of their edges. (Figure 3.2)

$$\int_{S} \Phi_f\, dS \simeq -\Phi_{i-1/2} \cdot \Delta y + \Phi_{i+1/2} \cdot \Delta y - \Phi_{j-1/2} \cdot \Delta x + \Phi_{j+1/2} \cdot \Delta x \tag{3.31}$$

A negative algebraic sign in equation 3.31 means a flow into the grid cell. A positive algebraic sign stands for an outflow of the grid cell. The interpolation of the fluxes across

the respective borders has to be done with the known values from nodes of the grid cells. [Valentin & Rinaldi, 2001]

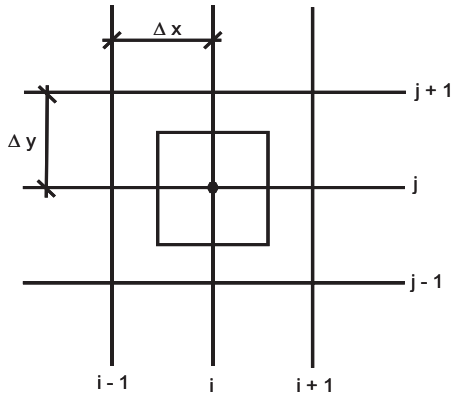

Figure 3.2: Definition of nodes for the flux term [Valentin & Rinaldi, 2001]

3.4.2.5 Interpolation methods

The calculation of the fluxes across the cell boundaries is done using interpolations with the known values of the cell nodes. Therefore numerous methods are available. Generally it can be divided between first, second or higher order methods.
First order methods generate discrete equations, which are easy to solve but mostly the results are not very precise. Steep gradients are not reproduced sharp, they smear because of numerical diffusion. One solution to overcome this problem is to refine the numerical grid but this leads to much longer calculation times. Example for first order methods are Centrale methods, Upstream methods or Upwind difference methods.
Due to their higher accuracy second or higher order methods can reproduce steep gradients better, but they also more fragile to numerical instabilities. In this case a refinement of the numerical grid can lead to stable calculation but also to longer computational times. Examples for high order methods are the Quick method, the Centrale difference method and the Linear upwind differencing method. Further methods of interpolation are documented in the StarCD Methology (2002).
One alternative to avoid the interpolation is the usage of so called staggered grids. They define nodes for each physical value at favourable locations and control volumes for each basic equation. [Valentin & Rinaldi, 2001]
The calculations in the following chapters were carried out using the First Order Upwind Differencing Scheme in the numerical model StarCD. The reason for choosing a first order method was the size of the flow domain which had to be reproduced with a numerical grid. The investigated reservoir sewer has a length of 336 m and a width of 3.2 m which leads, even for a first order scheme, to a large number of grid cells and long calculation times. To use a high order interpolation method it would have been necessary to increase the number of grid cell to get stable results. But the main focus of the investigations was based on the calculation of the bottom shear stress and the cleaning effect of the flush wave for long distances. It was not the target to reproduce the breaking wave in its initial phase precisely. Therefore the time saving first order

scheme was chosen. In an additional investigation the initial phase was modelled with a lengthwise short but refined grid to reproduce the breaking wave.

The First Order Upwind Differencing Scheme in the model StarCD is based on different assumptions to the before mentioned ones. The flux term of equation 3.28 is split into a convective (C_j) and a diffusive term (D_j). The conservation of mass is assured in this method but a too large iteration time step δt can lead to numerical diffusion.
The diffusive ratio is described with equation 3.32.

$$D_j \approx \Gamma_{\Phi,j}[f_j^{\ell}(\Phi_N - \Phi_P) + \{grad\ \Phi \cdot S - f_j^{\ell}\ grad\ \Phi \cdot d_{NP}\}] \tag{3.32}$$

The first summand in equation 3.32 describes the common diffusion between the points P and N. The second summand in the cambered brackets involves the cross-diffusion. [Star-CD Version 3.15, 2002]

The convective ration is characterized as the product of the mass flux F_j across the cell boundaries and the mean value Φ_j at the border faces of the cells. (Equation 3.33)

$$C_j \equiv F_j \cdot \Phi_j \tag{3.33}$$

The mass flux is defined as follows

$$F_j \equiv (\rho \cdot\ u_r \cdot S). \tag{3.34}$$

Equation 3.35 applies for the First Order Upwind Differencing Scheme.

$$C_j = F_j \cdot \begin{cases} \Phi_P & \text{for} \quad F_j \geq 0 \\ \Phi_{N+} & \text{for} \quad F_j < 0 \end{cases} \tag{3.35}$$

The definition of the adjoining cells and their nodes is displayed in figure 3.3.

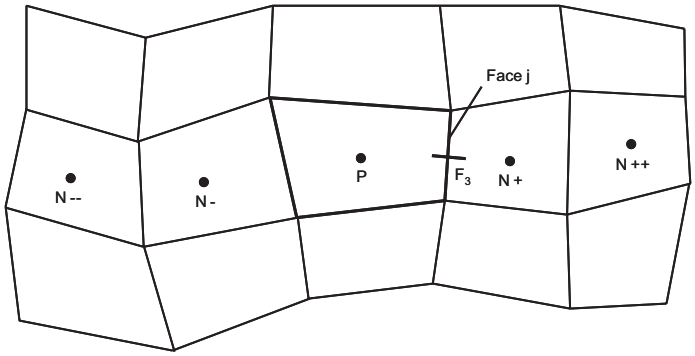

Figure 3.3: Definition of cells and nodes First Order Upwind Differencing Scheme [Star-CD Version 3.15, 2002]

3.4.3 Discretisation in time

The temporally dependency of transient flows is fixed in the temporal derivations of the basic hydrodynamic equations. To describe a flow in its progression it is necessary to discretisize the modelled time step as well as the investigated domain. Therefore single time steps are defined, at which the equations have to be solved. (Equation 3.36)

$$t^n = t^0 + n \cdot \Delta t \tag{3.36}$$

It is assumed that all relevant values are known as initial conditions for the time t^0.
The calculation methods to inquire t^n can be divided into single- or multi-step methods. Starting from an initial condition each system of equations is solved for one time step.

$$\frac{\partial u}{\partial t} = DGL(u) \tag{3.37}$$

The right side of equation 3.37 incorporates all non time dependent ratios of the differential equation. To calculate the unknown time step $n + 1$ the known solutions at already calculated time steps are accessed. [Malcherek 2001b]
Single-step methods use the immediate previous time step to solve the differential equation. The temporal derivation is then approximated with a difference. (Equation 3.38)

$$\frac{\partial u}{\partial t} = \frac{u^{n+1} - u^n}{\Delta t} \tag{3.38}$$

The non time dependent ratios can be calculated with different methods. Some of them are

- Euler method (Consistency 1st order),
- Implicit method (Consistency 1st order),
- Crank-Nicholson method (Consistency 2nd order),
- Taylor method (Consistency 2nd order), also called Lax-Wendroff method,
- Runge-Kutta method (Consistency 4th order).

The order of consistency characterizes the quality of each method. Malcherek (2001 b) gives a detailed description of numerous single step methods.

Multi-step methods not only use the past time step t^n to calculate t^{n+1}, they also include further time steps into the calculation. This procedure creates a higher degree of accuracy. The Leap-Frog method is one example for a multi-step method of a 2nd order consistency. (Equation 3.39)

$$\frac{\partial u}{\partial t} = \frac{u^{n+1} - u^{n-1}}{2\ \Delta t} \tag{3.39}$$

The numerical model StarCD uses optionally the Fully-Implicit method or the Crank-Nicholson method. [Star-CD Version 3.15, 2002] For the following investigations the Fully-Implicit method was chosen.

3.4.3.1 Fully-Implicit Method

The fluxes of the new time step are calculated by using the known physical values of the new time step. The size of the time step δt must be kept small for transient calculations to minimize the temporal estimation error. The differential expression of the unknown numerical function u^{n+1} remains and the partial differential equation still has to be solved, which makes this method very time consuming but more stable than explicit methods. See equation 3.40.[Star-CD Version 3.15, 2002] [Malcherek, 2001 b]

$$\frac{u^{n+1} - u^n}{\Delta t} = DGL(u^{n+1}) \tag{3.40}$$

3.4.4 Treatment of the pressure term

The calculation of the pressure term is carried out with pressure correction scheme. The pressure p will be decomposed into the following terms in equation 3.41 at the unknown time step t^{n+1}.

$$p^{n+1} = p' + p^* \tag{3.41}$$

The momentum equation of the Navier-Stokes equations is uncoupled by the usage of an operator separation and split in two parts. (Equation 3.42 and 3.43)

$$\frac{u_i^{n+1/2} - u_i^n}{\Delta t} + u_i \cdot grad\ u_i = -\frac{1}{\rho}\ grad\ p' + \nu\ \Delta u_i \tag{3.42}$$

$$\frac{u_i^{n+1} - u^{n+1/2}}{\Delta t} = -\frac{1}{\rho}\ grad\ p^* \tag{3.43}$$

The addition of both equations results in the original momentum equation where the pressure term is calculated at the unknown time step. A known value of the pressure is then inserted for p'. This can be either the hydrodynamic pressure at the time step n or the hydrostatic pressure.
The divergence is generated in equation 3.43 with the equation 3.44 as a constraint.

$$div\ u_i^{n+1} = 0 \tag{3.44}$$

This leads to equation 3.45.

$$\Delta p^* = \frac{\rho}{\Delta t}\ div\ u_i^{n+1/2} \tag{3.45}$$

The right side of equation 3.45 is known after the solution of equation 3.42. Now it is possible to calculate the pressure p. [Malcherek, 2001 a]

3.4.5 Solution of the finite volume equations

The high temporal and spatial discretisation of the basic hydrodynamic equations creates large systems of equation, which have to be solved. These are often symmetrical matrices with a band structure. They can be solved with two categories of solution algorithms.
Direct solution algorithms transfer the stiffness matrix into a triangular matrix. The solution vector is obtained by a back substitution. The exact solution, apart from rounding errors, is found after a finite number of calculations. Examples for direct solution algorithms are the Gauss-Elimination Scheme and the Kramer rule.
Iterative solution algorithms are based on a starting vector, which is constantly iterative improved until a solution in preassigned limits is found. An exact solution is theoretically found after an infinite number of iterations. Example for iterative methods are the

- Conjugated-Gradient Method,
- Jakob Iteration,
- Gauss-Seidel Iteration,
- Relaxation Method,
- Block-Iteration Method and
- L-U Iterations Method.

[Oertel & Laurien, 2003]

In practice the number of operations and the computational time for direct algebraic solutions are high and therefore iterative methods are the most economical. Depending on the chosen fault tolerance they offer fast and efficient solutions, especially for non-linear problems.
The numerical model StarCD solves the algebraic finite volume equations with implicit methods. Three different methods can be chosen.

- SIMPLE (Semi-Implicit Method for Pressure-Linked Equations) Method
- PISO (Pressure-Implicit with Splitting of Operators) Method
- SIMPISO Method (Combination of SIMPLE and PISO method)

The SIMPLE and SIMPISO Method are used for steady flow calculations. The PISO Method can be either used for the solution of steady or transient flows. A detailed description of these methods is given in the StarCD methology. [Star-CD Version 3.15, 2002]
The equations are uncoupled for every dependent variable. The non-linear advective terms, the diffusion and the convection, are linearised explicitly or with the Newton-Raphson method. In succession large linear algebraic equation systems are emerging. To solve these systems the Conjugated-Gradient Method and the Multiple-Grid Method

are available. The detailed description of the mentioned methods can be found in the StarCD methology. [Star-CD Version 3.15, 2002]

3.5 Determination of the free surface - Volume of Fluid Method

The location of the free surface, which is the boundary face between the water and the air is temporal and spatial variable. It is strongly dependent on boundary conditions like exterior pressure, wind or surface tension. The flow domain is subject to continuous changes.
There are several methods available for the determination of the free surface but only a few are commonly accepted. The direct modelling of the free surface is possible with the Height-Function Method and the Line-Segment Method. The Marker-in-Cell Method (MAC) is used to characterize the free surface with the aid of mass less marker particles. This method is frequently chosen for simulations with moving grid meshes. [Jankowski, 1999] A well known method is the Volume of Fluid Method, which implemented in the chosen numerical model StarCD.
The Volume of Fluid Method (VOF) is used for fixed tree-dimensional numerical grids including a water and a air phase. The calculation of boundary faces for multi-phase flows is also possible. The shape of the free surface is determined by the grid cells partly filled with water and air. Therefore the concentration C describes the fraction of water in a grid cell. A completely water filled grid cell has the concentration $C = 1$ and for $C = 0$ the cell is void of water.
The calculation of C needs the introduction of a new transport equation additional to the already known mass and momentum equations. The concentration C is subject to advection in the flow field of U and not to diffusion. (Equation 3.46)

$$\frac{\partial C}{\partial t} + div(C \cdot U) = 0 \tag{3.46}$$

The main problem is now the discretisation of the convective term of equation 3.46. Using first order upwind schemes lead to a smearing of the free surface and an artificial mixing of the fluids, which does not match the reality. Hence upwind schemes with a higher order are better suited to model the free surface. The choice of the discretisation scheme is depending on their ability not to over- or underfill the grid cells with water. The constraint of $\leq C \leq 1$ is maintained by the Additional Flux-Limiting algorithm. [Jankowski, 1999]
The interpolation of the free surface with the Volume of Fluid Method is subject to numerous investigations. Sulzer (2001) for example used an implicit scheme to describe steady flows while Jankowski (1999) applied an explicit scheme. The Volume of Fluid Method was originally developed by Hirt and Nichols (1981) and was also referred as the Donor-Acceptor System. The Geometric Reconstruction Scheme of Youngs (1982) and the High Resolution Interface Capturing Scheme of Muzaferija et al. (1998) are well known. They are published in Rhee et al. (2004). Further calculation methods can be found in Rudman (1997) and Barkhudarov (2003).

As an example the Geometric Reconstruction Scheme will be described in the following. It is based on the assumption that the boundary face between two fluids in each grid cell possesses a linear slope. This assumption is used for the calculation of the advection flow of the fluids through the cell surfaces.
The first step is to locate the position of the linear boundary relative to the centre of the partly filled grid cell. This is based on the information of the filling degree and their derivation in a grid cell. The second step will be the calculation of the in- and outflow of fluids as a result of advection through each cell face. Therefore the position of the fluid face inside the cell as well as the information concerning the velocity distribution in normal and tangential direction are inserted. The last step calculates the in- and outflows and the volumetric content of water and air for each considered cell.[Jankowski, 1999]

The versions of the VOF method are different in their approach to involve the fluids and their physical properties into the calculation of the free surface. The approach of Hirt and Nichols (1981) solves the transport equation for the whole flow field but the mass and momentum equations are solved for the liquid phase only. The VOF method in StarCD threats both fluids, water and air, equal and their physical properties are considered for the solution of the conservative equations. Both fluids are used for the modelling according to the volumetric content in each grid cell. Equation 3.47 displays the calculation of the averaged density ρ_m.

$$\rho_m = C\rho_1 + (1 - C)\rho_2 \tag{3.47}$$

All other properties like the viscosity are calculated in the same way. The free surface is then regarded as a discontinuity in the fluid properties.
The VOF approach can be used for complicated overturning surfaces like breaking waves. Lift forces will not be considered if gaseous parts are mixed with the fluid. The results will be unrealistic in this case.
The free surface is not sharp or exactly defined; usually it is smeared over two or three grid cells. To reproduce a free surface in a high resolution it is necessary to provide a high refinement of the numerical grid. Therefore all cells who satisfy the condition $0 \leq C \leq 1$ should be refined. But this leads to long computational time and raises the calculation costs of an investigation. [Sulzer, 2001]

3.6 Boundary conditions

3.6.1 General remarks

The numerical simulation of fluids with the Navier-Stokes equations and a turbulence model demands the definition of boundary conditions. They describe the behaviour of the flow at the borders of the flow domain.
The free surface and the bottom of the sewer channel limit the investigated flow domain vertically. These faces are called the upper and lower boundary conditions. Fixed impermeable walls embed the flow domain sideways but in- and outflows are also possible.

The up- and downstream end of the flow domain is defined by inflow, outflow or pressure boundaries depending on the geometry of the channel. With these definitions it is possible to describe the boundaries of the flow domain as exact as physically possible and close to reality. The size of the single boundaries can change temporally and is dependent of the unsteady free surface. An impervious wall can be the lateral boundary for small runoffs but for large runoffs it can change to an outflow region, like an overflown side weir.

3.6.2 Impervious walls - Logarithmic law of the wall

The usage of turbulence models to solve the flow equations, as described earlier, has its limitation in the region close to impervious walls, where the $k-\epsilon$ model for example is not valid anymore.
The isotropy of turbulence, the basic of the $k-\epsilon$ model, is not given close to fixed walls due to the dampening of the turbulent fluctuations. Also the $k-\epsilon$ model is only valid for large Reynolds numbers and not for small Reynolds numbers due to the low flow velocity at fixed walls. The Reynolds stresses grown when approaching the wall but directly at the wall surface they disappear. The viscose effects come to the fore close to the wall but at the derivation of the $k-\epsilon$ model they were neglected.
Turbulent flows at impervious walls form a fine boundary layer, which consists of three regions. The flow velocity directly at the wall is very low due to the adhesion of the fluid. The flow in this boundary layer is laminar and dominated by the viscosity. The Reynolds numbers are approaching zero. This region is called viscous sublayer.
The next region above the viscous sublayer is the transition zone where the flow will be locally instable and the logarithmic velocity profile starts. The molecular viscosity and the Reynolds stresses are equal. With a growing distance off the wall the influence of the Reynolds stresses increases. In the following turbulent region the flow is dominated by the Reynolds stresses and the $k-\epsilon$ model is valid again. [Griebel et al., 1995] [Oberlack, 1994]
Figure 3.4 shows the different regions inside the boundary layer.

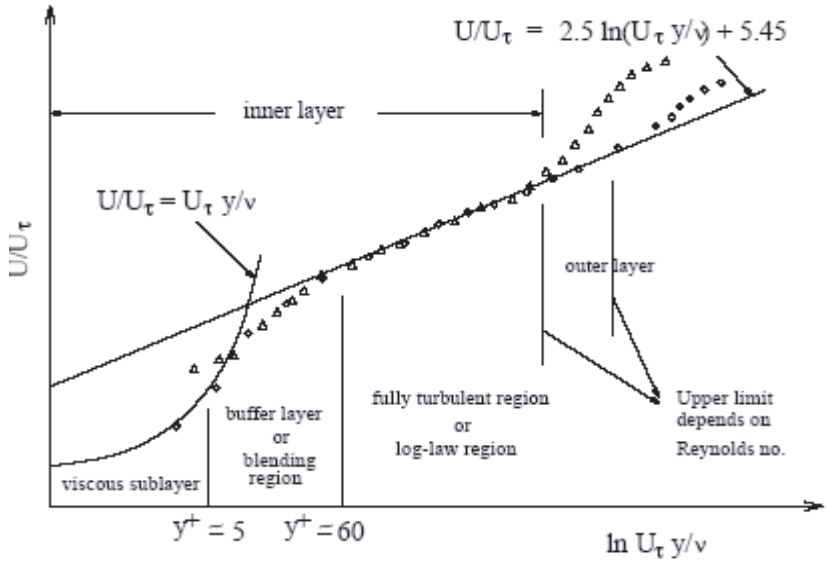

Figure 3.4: Boundary layer regions, [Kivekaes et al., 2006]

The characteristically thickness of a turbulent boundary layer is small compared to the out flow field. Because of the steep gradients numerous grid cells are necessary to model the boundary layer in a numerical simulation. Using the Finite Volume Method the centre of the boundary cell is chosen within distance so that the viscous shear stresses are reduced and the transport of momentum is controlled by the Reynolds stresses.
To describe the flow behaviour close to a fixed boundary a wall function, the Logarithmic Law of the Wall is introduced. The viscous sublayer and the log-region are eliminated of the flow domain. To model the flow at the impervious wall the boundary condition is modelled by using the wall function. The flow is discretizesed and calculated only for the turbulent region.

The derivation of the Logarithmic Law of the Wall is based on the following assumptions:

- Steady flow conditions $\frac{\partial \bar{u}_i}{\partial t} = 0$
- No pressure gradients $-\frac{1}{\rho}\frac{\partial \bar{p}_i}{\partial x_i} = 0$
- Incompressible flow
- Homogeneous flow for a constant distance to the wall x_2

Due to the last assumption all statistical functions are exclusively depended of x_2. It is essential that

- $\bar{u}_1(x_2) \neq 0$,
- $\bar{u}_2 = 0$,
- $\bar{u}_3 = 0$.

The Reynolds averaged momentum equation is reduced to equation 3.48.

$$0 = \nu \frac{\partial^2 \bar{u}_1}{\partial x_2^2} - \frac{\partial \overline{u_1' u_2'}}{\partial x_2} \tag{3.48}$$

A singular integration and the consideration of the boundary condition, here the introduction of the wall shear stresses leads to equation 3.49.

$$\tau_w = +\mu \frac{d\bar{u}_1}{dx_2} - \rho \overline{u_1' u_2'} \tag{3.49}$$

The Reynolds averaged momentum equation is now defined in equation 3.50.

$$\nu \frac{\partial \bar{u_1}}{\partial x_2} - \overline{u_1' u_2'} = \frac{\tau_w}{\rho} = u_\tau^2 \tag{3.50}$$

The friction velocity u_τ stands for the characteristic velocity. The dimensionless mixing length l^+ is introduced in equation 3.51.

$$l^+ = \frac{\nu}{u_\tau} \tag{3.51}$$

The dimensionless wall distance x_2^+ is defined in equation 3.52.

$$x_2^+ = \frac{x_2}{l^+} \tag{3.52}$$

The boundary layer is divided in three different parts as already mentioned. The Reynolds stresses are nearly zero in the viscous sublayer close to the wall. Equation 3.53 is valid.

$$\nu \frac{\partial \bar{u_1}}{\partial x_2} = \frac{\tau_w}{\rho} = u_\tau^2 \tag{3.53}$$

The introduction of the dimensionless velocity $\bar{u}_1^+$ leads to equation 3.54.

$$\bar{u}_1^+ = \frac{\bar{u}_1}{u_\tau} \tag{3.54}$$

Integration of 3.52 and using 3.52 and 3.54 defines the viscous sublayer in the region of $x_2^+ \leq 10$.

$$\bar{u}_1^+ = x_2^+ \tag{3.55}$$

The parts of molecular viscosity and Reynolds stresses are of the same order of magnitude in the buffer layer.
With an increasing distance off the wall the Reynolds stresses start to grow while the molecular forces decrease. The flow can be regarded independent of the molecular viscosity in a distance of $x_2^+ \geq 60$. The transport of momentum is due to the Reynolds stresses.

$$\overline{u_1' u_2'} = \frac{\tau_w}{\rho} = u_\tau^2 \tag{3.56}$$

The buffer layer ends at x_2^+=100. Afterwards starts the region where the $k-\epsilon$ turbulence model is valid again.

Von Kármán (1930) proposed for the logarithmic region of $100 \leq x_2^+$ the following similarity theorem.

$$\frac{\partial \bar{u}_1}{\partial x_2} = \frac{u_\tau}{\kappa x_2} \tag{3.57}$$

After the integration of equation 3.57 and the introduction of dimensionless variable the universal or logarithmic law of the wall is given.

$$\bar{u}^+ = \frac{1}{\kappa} ln(x_2^+) + C^+ \tag{3.58}$$

The calculation of the turbulent kinetic energy k and the kinetic dissipation rate ϵ is given by Wilcox (1998) in equation 3.59 and 3.60.

$$k = \frac{u_\tau^2}{\sqrt{C_\mu}}, \tag{3.59}$$

$$\epsilon = \frac{u_\tau^3}{\kappa y}. \tag{3.60}$$

The logarithmic law of the wall was proven in numerous experiments and numerical investigations. [Nikuradse, 1932] [Moin & Kim, 1982] The logarithmic law of the wall is valid for flows with a small curvature of the streamlines without displacement and approximately for flows with small pressure gradients. The Kármán constant was determined in experiments to the value of $\kappa = 0.41$. The additive constant C^+ is a function of the sand roughness k_s. [Schlichting & Gersten, 1997] For hydraulic smooth walls applies $C^+ = 5.5$. [Oberlack, 1994] [Sulzer, 2001] [Rodi, 2004]

3.6.3 Upper boundary condition

The upper boundary condition is defined by the free surface between water and air. It is determined with the Volume of Fluid Method and is restricted as follows:

- No in- or outflows through the free surface what means no convective or diffusive fluxes vertical to the surface.
- Velocities normal to the surface equal zero.
- Gradients of variables normal to the surface equal zero.

3.6.4 Lower boundary condition

The lower boundary condition is represented by the bottom of the channel and the same rules apply here as for the fixed impervious walls in chapter 3.6.2. The bottom of the channel is assumed to be impervious. Main sewer channels or older channels can be affected by sewer infiltration water or groundwater leakage. In this case a local inflow boundary would be defined.

3.6.5 Inflow boundary condition

The flow conditions in the inflow region are usually known or can be assigned by measurements. Therefore a Dirichlet boundary condition can be defined for the border face where velocity, density, free surface, pressure or temperature are known. Often only the influx Q is constituted and the gradients normal to the water depth are set to zero.
All values of the variables except the pressure must be given in the centre of the boundary cell faces to apply the model StarCD for incompressible flows. Then the fluxes are calculated directly and the pressure will be determined with an extrapolation out of the flow field. The variables of the turbulence model are defined separately. The turbulent kinetic energy k is sometimes known by measurements. If this is not the case it can be calculated by the turbulent intensity I.

$$I = \frac{u'}{U_m} \approx 0,16 \cdot Re^{-1/8} \tag{3.61}$$

The turbulent kinetic energy k is calculated by equation 3.62.

$$k = \frac{3}{2}(U_m \cdot I)^2 \tag{3.62}$$

The dissipation ϵ is measured seldom and is usually calculated directly.

$$\epsilon = C_\mu^{3/4} \cdot \frac{k^{2/3}}{\ell} \tag{3.63}$$

The mixing length ℓ is determined as a function of the hydraulic radius L.

$$\ell = 0,07 \cdot L. \tag{3.64}$$

The water and the air phase are calculated separately during the three-dimensional simulations. The mentioned variables for water are defined or calculated as described. The inflow velocity of the air will be chosen similar to the surface velocity of the water to prevent shear stresses. The turbulent kinetic energy k and the dissipation ϵ are set to zero for the air phase. [StarCD, 2002]

3.6.6 Outflow boundary condition

3.6.6.1 General description

The distribution of flow magnitudes at the outflow boundaries is usually unknown and gradient conditions are allocated there. They can be explicit or implicit and frequently zero-gradient conditions are specified.

$$\frac{\partial U_i}{\partial x_n} = \frac{\partial k}{\partial x_n} = \frac{\partial \epsilon}{\partial x_n} = 0 \tag{3.65}$$

The estimation of the outflows is carried out in two steps by the model StarCD. At first the distribution of unknown variables at the boundary faces is extrapolated with existing upstream flow conditions. A zero-gradient is assumed along the streamlines that cross the boundary face. The preciseness of the extrapolation is dependent on the proximity to the physical reality. Therefore the direction of the extrapolation should be placed exactly in flow direction. A steady flow leads to better results at this point than a strongly unsteady runoff. The estimation does not constitute the final value of the runoff. A further requirement for the runoff is based on the conservation of mass, which leads to the next step.
The velocities are adjusted to preserve the conservation of mass in the flow domain. Subsequently the runoff is determined for the boundary face. The normal-vectors of the velocity are set to zero for the cell faces into the flow domain and no inflow can occur through the boundary faces. This artificial interference can lead to errors or wrong results if there is the possibility of inflows due the model geometry or the to expected flows. Changing tidal flows for example make it necessary to define a pressure boundary instead of an outflow boundary. [Sulzer 2001] [Schoenung, 1990] [StarCD, 2002]

3.6.6.2 Pressure boundary condition

The pressure boundary condition is used for example when there is no inflow to the flow domain and outflow at the downstream border. The usage of an outflow boundary condition is not possible in this case. The conservation of mass would be violated due to the missing inflow.
The later used model StarCD offers the possibility to integrate a pressure boundary condition in the numerical model. Therefore the distribution of the pressure is necessary at the boundary face and must be provided. It can be choosen between static, piezometric and atmospheric pressure. To calculate the flow velocities at the boundary face two different methods are available.
The first method connects the velocity of the boundary grid cells with the local pressure gradients by a separate momentum equation. Their coefficients for the centre of the grid cells are equated with the already existing coefficients. This equation allows, together with the continuity condition, the calculation of the modulus and the direction of the in- and outflows across the boundary faces of the flow domain.
The second method presets the two components of the flow velocity in an adequate local coordinate system. The velocity normal to the boundary face is calculated with an

extrapolation of the inner flow domain. The turbulence parameters I and ℓ are applied for the calculation of the pressure in the case of an inflow. [StarCD, 2002]

3.7 Definition of the wall shear stress

3.7.1 General approaches

The mathematical derivation of the wall shear stress for channel flows τ_0 compares the slope drift component of the current F_G as well as the friction force F_R, which is directed contrary to the main flow direction. (Figure 3.5) The regarded flow is accepted to be stationary and homogeneously, which means that two neighbouring cross section profiles exhibit the same distribution of velocity. The friction slope I_0, the water level slope I_W and the energy slope I_E have an equal value.

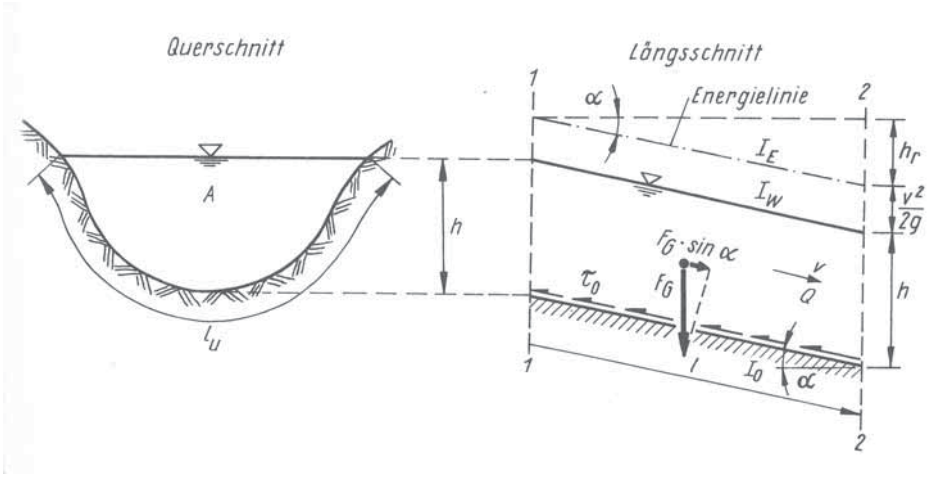

Figure 3.5: Cross- and longitudinal view of the channel [Bollrich, 2000]

The flow is generated by the slope drift component of the gravity force.

$$F_G \cdot sin\alpha = A \cdot l \cdot \rho \cdot g \cdot sin\ \alpha \tag{3.66}$$

The energy slope is defined by

$$I_E = \frac{h_V}{l} = sin\ \alpha. \tag{3.67}$$

This leads to

$$F_G \cdot sin\ \alpha = A \cdot l \cdot \rho \cdot g \cdot I_E. \tag{3.68}$$

The friction force is defined by

$$F_R = \tau_0 \cdot l_U \cdot l. \tag{3.69}$$

The slope drift component is balanced to the friction force, which is created by the wall shear stress τ_0 along the wetted perimeter l_u over the length l.

$$F_R = F_G \cdot sin\alpha \tag{3.70}$$

The wall shear stress τ_0 will then be

$$\tau_0 = \frac{A \cdot \rho \cdot g \cdot I_E}{l_U}. \tag{3.71}$$

With

$$r_{hy} = \frac{A}{l_U} \tag{3.72}$$

and

$$I_E = I \tag{3.73}$$

the general calculation approach for the wall shear stress results in

$$\tau_0 = \rho \cdot g \cdot r_{hy} \cdot I_E. \tag{3.74}$$

Due to the different velocity distribution along the wetted perimeter the wall shear stress is not distributed homogeneous. (Figure 3.6)

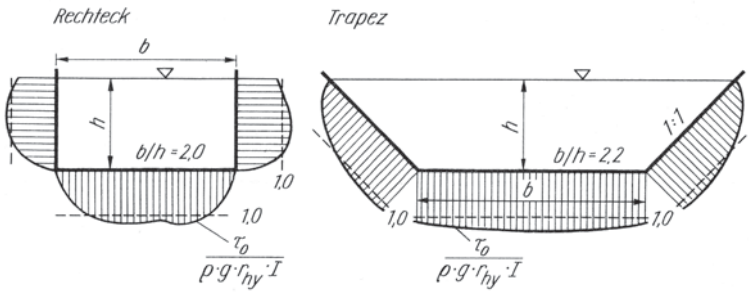

Figure 3.6: Distribution of the wall shear stress [Bollrich, 2000]

A further possibility to determine the wall shear stress origins from the derivation of the flow equation of Brahms and Chezy. [Bollrich, 2000] It is postulated that the wall shear stress is proportional to the squared mean value of the flow velocity for a fully developed turbulent flow and hydraulic rough conditions.

$$\tau_0 \sim v \tag{3.75}$$

On the right side of the equation, for dimensional reasons and regarding the later solution, the density ρ and the friction coefficient λ is introduced. Thus the wall shear stress results to

$$\tau_0 = \frac{\lambda}{8} \cdot \rho \cdot v. \tag{3.76}$$

In the actual sense this equation applies only to pipe flows, but with the introduction of the Strickler value k_{st} it can be used too for channel flows with a free surface. Therefore the Manning Strickler equation and the Darcy Weisbach equation is solved for I_E and then both equations at set equal. [Bollrich, 2000]

Then the friction coefficient λ =f(k_{st}) will be

$$\lambda = \frac{2 \cdot g \cdot d}{k_{st}^2 \cdot (r_{hy})^{4/3}} = \frac{124.58}{k_{st}^2 \cdot \sqrt[3]{d}} \tag{3.77}$$

with

$$d = 4 \cdot r_{hy} \tag{3.78}$$

and

$$k_{st} = \frac{26}{k^{1/6}}. \tag{3.79}$$

Prandtl formulated with the law of the mixing length a differentiated view of the wall shear stress distribution τ = f(x_2) for turbulent flows outside the viscous sub layer which should not be regarded here. [Bollrich, 2000] Kirchheim (2003) presented the approach of Wittmann and Vollmers [Volmers & Pernecke, 1976] to calculate the wall shear stress for non-uniform flows.

3.7.2 Determination of the wall shear stress using the turbulent kinetic energy

The previous two computational approaches, which were defined in chapter 3.7.1, are based on the steady and uniform flow. The flush wave to be investigated is highly unsteady and non-uniform. For this reason it is not possible to determine the wall shear stress of a flush wave with these equations.
For near wall flows the law of the mixing length of Prandtl [Schlichting & Gersten, 1997] is only valid above the viscous sub layer. This means that a calculation of the wall shear stress directly at the wall is not possible. The approach of Wittmann and Vollmers [Volmers & Pernecke, 1976] is valid for non-uniform flows with a mean velocity v_m but it is not useable for unsteady flows like flush waves for example.
In the available investigation the results of the numeric modelling were used in order to determine the wall shear stresses. Therefore the turbulent kinetic energy k in the

grid cells at the bottom and the wall of the channel were calculated by using the $k-\epsilon$ turbulence model and/or the logarithmic wall law. The following equation forms the connection between turbulent kinetic energy and wall shear stress.

$$k = \frac{v_\tau^2}{\sqrt{C_\mu}} = \frac{\tau_w/\rho}{\sqrt{C_\mu}} \tag{3.80}$$

The wall shear stress can then be calculated for each wall or bottom cell of the numerical grid by using [Rodi, 1993]

$$\tau_w = \rho \cdot \sqrt{C_\mu} \cdot k. \tag{3.81}$$

Due to the turbulent mixing in the head of the flush wave with air, the cells near the bottom and the walls are filled with a mixture of air and water.

By using the Volume of Fluid method (VOF) the water content C of the concerned cells confirmed this assumption and made it necessary to determine the mean density ρ_m in these locations. A weighting of the water and/or air content of the grid cells lead to

$$\rho_m = C \cdot \rho_W + (1 - C) \cdot \rho_L. \tag{3.82}$$

Figure 3.7 shows an example of the possible air and water distribution in a cross section of the channel.

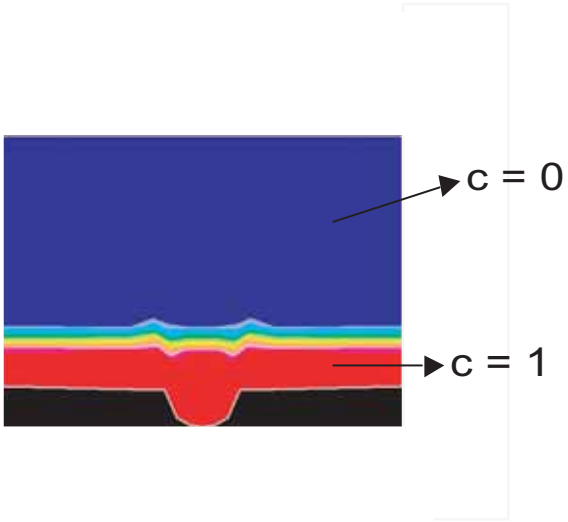

Figure 3.7: Distribution of the water content C

The wall shear stress is defined as a function of the mean density.

$$\tau_w = \rho_m \cdot \sqrt{C_\mu} \cdot k \tag{3.83}$$

4 Analytical determination of dam-break waves

4.1 Overview

Dam-break waves are created by the break down of a free standing water body due to gravitation and pressure forces. Depending on the boundary conditions they run on a dry or a wetted channel bottom. Flush waves in sewer channels created by flush gates or shields are similar in their hydraulic behaviour. A water volume is stored and released by the sudden opening of the flush gate. Then the created wave runs along the sewer channel to clean it by removing the deposits. The boundary conditions can also be compared with the ones of a river which is affected by a dam-break wave.
The boundary condition of a dry bottom will usually take place when cleaning stormwater tanks or large reservoir sewer like the investigated one in chapter 12. (Figure 4.1) The wetted bottom boundary condition can be compared with the conditions in a main-sewer. Depending on the duration to store the desired flushing volume and the slope of the flushing length main-sewers will not fell completely dry. Usually they possess a remaining water body at the end of its length which affects the flushing wave and its cleaning efficiency.

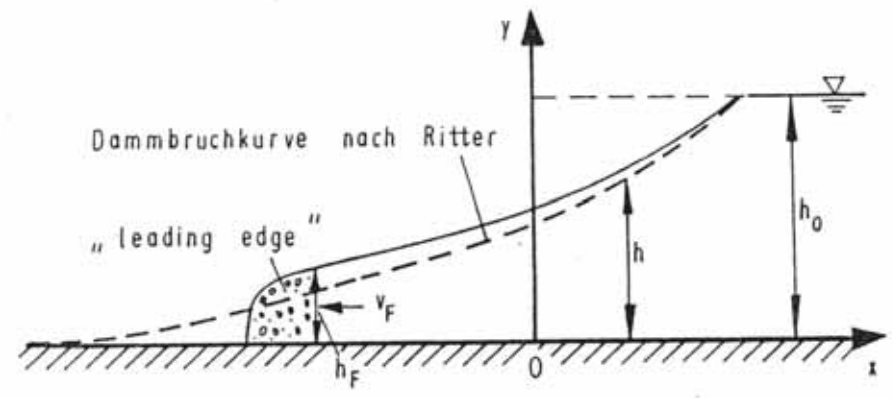

Figure 4.1: Dambreak wave on a dry bed [Martin & Bollrich, 1983]

Dam-break waves can be described using numerical modells (one-dimensional - three-dimensional) and with limitations by analytical solutions. The derivation for the three-dimensional modelling with the averaged Navier-Stokes equation is given in chapter 3. The derivation of the two-dimensional shallow water equations (chapter 4.2) and the one-dimensional approach with the Saint-Venant equation (chapter 4.3) presents the way from the three-dimensional modelling to the analytical solutions.

The oldest analytical approach to describe a dam-break wave is the Ritter formula developed in 1892. [Ritter, 1892] [Bollrich, 2000][Vischer & Hager, 1997] Whitham (1955) created a further solution, which is based on the boundary layer theory using the Polhausen Method. Other solutions were established by Pohle (1952) or Martin and Bollrich (1983). Both approaches are only valid for rectangular channels to describe the initial phase of a dam break wave close to the dam wall. A very detailed description of the Pohle solution can also be found in the dissertation of Liem (2003).
A recent investigation of the dam break problem was carried out by Stansby et al. (1998), where he compared analytical solutions with laboratory experiments. One of the results was the graphical display of acceleration vector field and the pressure distribution in from of the dam wall. (Figure 4.2) It is obvious that the free surface is moving downward due to the influence of gravity that shows that the vertical acceleration in the initial phase cannot be disregarded. [Martin, 1989][Schaffner, 2003a]

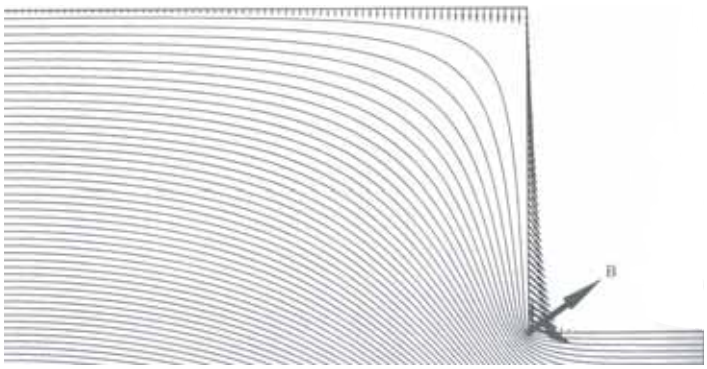

Figure 4.2: Acceleration vectors and pressure distribution [Stansby et al., 1998]

Yu and Tan (2006) were using the Lauber and Hager (1998a,b) solution for the calculation of the wave height, wave velocity and shear stresses to analyze the cleaning effects of a flush gate system analytically and in a physical experiment.
Incontrast to the solutions assuming a dry channel bed Stoker (1957) derived an analytical solution for a dam-break wave on a wetted channel bottom. The chapters 4.4 and 4.5 will present the equations of the Ritter dam-break wave and the solution of Dressler (1952).

4.2 Derivation of the two-dimensional shallow water equations

The numerical modeling of flows with the three-dimensional Navier-Stokes-Equations (NSE) is accurate but very time consuming. The free water surface is initially unknown and must be adjusted iteratively to the calculated pressure and velocity conditions. The depth-averaging of the 3-d NSE leads to the 2-d Classical Shallow Water Equations (CSWE), where the free surface can be calculated explicitly.
For the CSWE constant horizontal velocity profiles over flow depth, no vertical velocities

and a hydrostatic pressure distribution are assumed. [Krueger, 2001] To gain more detailed information over the water depth an extended approach was developed. These Extended Shallow Water Equations (ESWE) contain a linear horizontal velocity and quadratic vertical velocity and pressure distribution over depth. [Steffler & Jin, 1993]

4.2.1 Navier-Stokes Equations

Continuity Equation

$$\frac{\partial \rho}{\partial t} + \frac{\partial \rho u_k}{\partial x_k} = 0, \tag{4.1}$$

Momentum Equations

$$\rho \left(\frac{\partial u_i}{\partial t} + u_k \frac{\partial u_i}{\partial x_k} \right) = -\frac{\partial p}{\partial x_i} + \mu \frac{\partial^2 u_i}{\partial x_k^2} + \rho g_i \tag{4.2}$$

which means in detail:

Equation for the x1-momentum

$$\rho \left(\frac{\partial u_1}{\partial t} + u_1 \frac{\partial u_1}{\partial x_1} + u_2 \frac{\partial u_1}{\partial x_2} + u_3 \frac{\partial u_1}{\partial x_3} \right) = -\frac{\partial p}{\partial x_1} + \mu \left(\frac{\partial^2 u_1}{\partial x_1^2} + \frac{\partial^2 u_1}{\partial x_2^2} + \frac{\partial^2 u_1}{\partial x_3^2} \right) + \rho g_1, \tag{4.3}$$

Equation for the x2-momentum

$$\rho \left(\frac{\partial u_2}{\partial t} + u_1 \frac{\partial u_2}{\partial x_1} + u_2 \frac{\partial u_2}{\partial x_2} + u_3 \frac{\partial u_2}{\partial x_3} \right) = -\frac{\partial p}{\partial x_2} + \mu \left(\frac{\partial^2 u_2}{\partial x_1^2} + \frac{\partial^2 u_2}{\partial x_2^2} + \frac{\partial^2 u_2}{\partial x_3^2} \right) + \rho g_2, \tag{4.4}$$

Equation for the x3-momentum

$$\rho \left(\frac{\partial u_3}{\partial t} + u_1 \frac{\partial u_3}{\partial x_1} + u_2 \frac{\partial u_3}{\partial x_2} + u_3 \frac{\partial u_3}{\partial x_3} \right) = -\frac{\partial p}{\partial x_3} + \mu \left(\frac{\partial^2 u_3}{\partial x_1^2} + \frac{\partial^2 u_3}{\partial x_2^2} + \frac{\partial^2 u_3}{\partial x_3^2} \right) + \rho g_3. \tag{4.5}$$

One can also write for (4.1)

$$\frac{\partial \rho}{\partial t} + \frac{\partial \rho u}{\partial x} + \frac{\partial \rho v}{\partial y} + \frac{\partial \rho w}{\partial z} = 0, \tag{4.6}$$

with

$$\begin{aligned} u_1 &= u, \\ u_2 &= v, \\ u_3 &= w, \end{aligned} \tag{4.7}$$

for the velocities and

$$\begin{aligned} x_1 &= x, \\ x_2 &= y, \\ x_3 &= z, \end{aligned} \tag{4.8}$$

for the coordinates. Then, with the same substitutions, the momentum equations (4.3) - (4.5) of the Navier-Stokes equation will turn to:

Equation for the x-momentum

$$\frac{\partial \rho u}{\partial t} + \frac{\partial \rho u^2}{\partial x} + \frac{\partial \rho uv}{\partial y} + \frac{\partial \rho uw}{\partial z} + \frac{\partial p}{\partial x} - \left(\frac{\partial \tau_{xx}}{\partial x} + \frac{\partial \tau_{xy}}{\partial y} + \frac{\partial \tau_{xz}}{\partial z} \right) = 0 \tag{4.9}$$

Equation for the y-momentum

$$\frac{\partial \rho v}{\partial t} + \frac{\partial \rho uv}{\partial x} + \frac{\partial \rho v^2}{\partial y} + \frac{\partial \rho vw}{\partial z} + \frac{\partial p}{\partial y} - \left(\frac{\partial \tau_{yx}}{\partial x} + \frac{\partial \tau_{yy}}{\partial y} + \frac{\partial \tau_{yz}}{\partial z} \right) = 0 \tag{4.10}$$

Equation for the z-momentum

$$\frac{\partial \rho w}{\partial t} + \frac{\partial \rho uw}{\partial x} + \frac{\partial \rho vw}{\partial y} + \frac{\partial \rho w^2}{\partial z} + \frac{\partial p}{\partial z} - \left(\frac{\partial \tau_{zx}}{\partial x} + \frac{\partial \tau_{zy}}{\partial y} + \frac{\partial \tau_{zz}}{\partial z} \right) + \rho g = 0 \tag{4.11}$$

Figure 4.3 shows the definition of the coordinate systems and the heights.

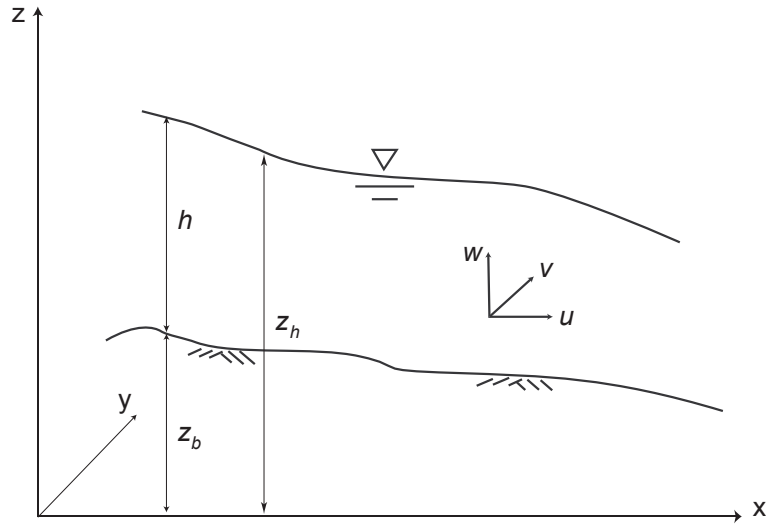

Figure 4.3: Definition coordinate systems

4.2.2 Boundary conditions

Boundary condition are necessary to fix the solution of the differential equations. They must be established for all boundaries of the flow domain. For the derivation of the shallow water equations kinematic and dynamic boundary conditions are required for the free water surface and the solid bottom.
The dynamic boundary condition at the bottom (index b) is the "no-slip" condition where the tangential velocity component disappears

$$u_b = v_b = w_b = 0 \tag{4.12}$$

The free surface pressure p_h equals the atmospheric pressure p_A and is set to zero.

$$p_h = p_A = 0 \tag{4.13}$$

The tangent of the shear stress to the water surface is

$$\tau_{hx} = -\tau_{hxx}\frac{\partial z_h}{\partial x} - \tau_{hxy}\frac{\partial z_h}{\partial y} + \tau_{hxz}, \tag{4.14}$$

and the tangent to bed of the flow domain is

$$\tau_{bx} = -\tau_{bxx}\frac{\partial z_b}{\partial x} - \tau_{bxy}\frac{\partial z_b}{\partial y} + \tau_{bxz} \tag{4.15}$$

for the y- and z-direction respectively.
The kinematic boundary condition allow no flux through the bed or the free surface. The solid bottom stands for a no-flux condition so the normal velocity component vanishes

$$u_b\frac{\partial z_b}{\partial x} + v_b\frac{\partial z_b}{\partial y} - w_b = 0. \tag{4.16}$$

Therefore the water surface can be moving and the relative normal velocity component must vanish at the surface

$$\frac{\partial z_h}{\partial t} + u_h\frac{\partial z_h}{\partial x} + v_h\frac{\partial z_h}{\partial y} - w_h = 0, \tag{4.17}$$

where

$$z_h = z_b + h. \tag{4.18}$$

4.2.3 Depth-Averaged Equations

The first part in the derivation of the classical shallow water equation constitutes in the integration of the 3-d NSE (4.6, 4.24-4.11) from the bottom boundary z_b to the free surface z_h. The depth-averaging is accomplished with the Leibnitz theorem. [Ploechinger, 1995]

$$\frac{\partial}{\partial t}\int_{a(y,t)}^{b(y,t)} f(x,y,t)dx = \int_{a(y,t)}^{b(y,t)} \frac{\partial f}{\partial t}dx - f(a,y,t)\frac{\partial a}{\partial t} + f(b,y,t)\frac{\partial b}{\partial t} \tag{4.19}$$

The Leibnitztheorem is now applied for the depth-averaging of the continuity equation (4.6).

$$\int_{z_b}^{z_h} \left(\frac{\partial \rho}{\partial t} + \frac{\partial \rho u}{\partial x} + \frac{\partial \rho v}{\partial y} + \frac{\partial \rho w}{\partial z} \right) dz = 0 \tag{4.20}$$

$$\begin{aligned} &\frac{\partial}{\partial t} \int_{z_b}^{z_h} \rho dz + \rho_b \frac{\partial z_b}{\partial t} - \rho_h \frac{\partial z_h}{\partial t} \\ &+ \frac{\partial}{\partial x} \int_{z_b}^{z_h} \rho u dz + \rho_b u_b \frac{\partial z_b}{\partial x} - \rho_h u_h \frac{\partial z_h}{\partial x} \\ &+ \frac{\partial}{\partial y} \int_{z_b}^{z_h} \rho v dz + \rho_b v_b \frac{\partial z_b}{\partial y} - \rho_h v_h \frac{\partial z_h}{\partial y} \\ &+ \frac{\partial}{\partial z} \int_{z_b}^{z_h} \rho w dz + \rho_b w_b \frac{\partial z_b}{\partial z} - \rho_h w_h \frac{\partial z_h}{\partial z} = 0 \end{aligned} \tag{4.21}$$

Solving the integrals leads to:

$$\begin{aligned} &\frac{\partial}{\partial t} \bar{\rho} h - \rho_h \frac{\partial z_h}{\partial t} + \frac{\partial}{\partial x} \overline{\rho u} h + \rho_b u_b \frac{\partial z_b}{\partial x} - \rho_h u_h \frac{\partial z_h}{\partial x} \\ &+ \frac{\partial}{\partial y} \overline{\rho v} h + \rho_b v_b \frac{\partial z_b}{\partial y} - \rho_h v_h \frac{\partial z_h}{\partial y} - \rho_b w_b + \rho_h w_h = 0. \end{aligned} \tag{4.22}$$

Inserting the kinematic boundary conditions (4.16) and (4.17) the surface and the bottom terms cancel. The compressible depth-averaged continuity equation can now be written as

$$\frac{\partial}{\partial t} \bar{\rho} h + \frac{\partial}{\partial x} \overline{\rho u} h + \frac{\partial}{\partial y} \overline{\rho v} h = 0. \tag{4.23}$$

The same procedure will be applied for the momentum equations (4.24) - (4.11) and will be shown for the x-momentum (4.24). After the use of the Leibnitz theorem the surface and the bottom terms of the equation disappear due to the kinematic boundary conditions.

$$\underbrace{\frac{\partial \rho u}{\partial t}}_{I} + \underbrace{\frac{\partial \rho u^2}{\partial x} + \frac{\partial \rho u v}{\partial y} + \frac{\partial \rho u w}{\partial z}}_{II} + \underbrace{\frac{\partial p}{\partial x}}_{III} - \underbrace{\left(\frac{\partial \tau_{xx}}{\partial x} + \frac{\partial \tau_{xy}}{\partial y} + \frac{\partial \tau_{xz}}{\partial z} \right)}_{IV} = 0 \tag{4.24}$$

$$I \qquad \frac{\partial}{\partial t}\int_{z_b}^{z_h} \rho u dz + \rho_b u_b \frac{\partial z_b}{\partial t} - \rho_h u_h \frac{z_h}{t} = \frac{\partial}{\partial t}\overline{\rho u} h - \rho_h u_h \frac{\partial z_h}{\partial t} \tag{4.25}$$

$$\begin{aligned} II \qquad \int_{z_b}^{z_h} \frac{\partial \rho u^2}{\partial x} dz &= \frac{\partial}{\partial x}\int_{z_b}^{z_h} \rho u^2 dz + \rho_b u_b^2 \frac{\partial z_b}{\partial x} - \rho_h u_h^2 \frac{\partial z_h}{\partial x} = \frac{\partial}{\partial x}\overline{\rho u^2} h \\ &\quad + \rho_b u_b^2 \frac{\partial z_b}{\partial x} - \rho_h u_h^2 \frac{\partial z_h}{\partial x} \\ \int_{z_b}^{z_h} \frac{\partial \rho uv}{\partial y} dz &= \frac{\partial}{\partial y}\int_{z_b}^{z_h} \rho uv dz + \rho_b u_b v_b \frac{\partial z_b}{\partial y} - \rho_h u_h v_h \frac{\partial z_h}{\partial y} = \frac{\partial}{\partial y}\overline{\rho uv} h \\ &\quad + \rho_b u_b v_b \frac{\partial z_b}{\partial y} - \rho_h u_h v_h \frac{\partial z_h}{\partial y} \\ \int_{z_b}^{z_h} \frac{\partial \rho uw}{\partial z} dz &= \rho_b u_b w_b \frac{\partial z_b}{\partial z} - \rho_h u_h w_h \frac{\partial z_h}{\partial z} = -\rho_b u_b w_b + \rho_h u_h w_h \end{aligned} \tag{4.26}$$

$$III \qquad \int_{z_b}^{z_h} \frac{\partial p}{\partial x} dz = \frac{\partial}{\partial x}\int_{z_b}^{z_h} p dz + p_b \frac{\partial z_b}{\partial x} - p_h \frac{\partial z_h}{\partial x} = \frac{\partial}{\partial x}\overline{p} h + p_b \frac{\partial z_b}{\partial x} \tag{4.27}$$

$$\begin{aligned} IV \qquad \int_{z_b}^{z_h} \left(\frac{\partial \tau_{xx}}{\partial x} + \frac{\partial \tau_{xy}}{\partial y} + \frac{\partial \tau_{xz}}{\partial z} \right) dz &= \frac{\partial}{\partial x}\int_{z_b}^{z_h} \tau_{xx} dz + \tau_{bxx} \frac{\partial z_b}{\partial x} - \tau_{hxx} \frac{\partial z_h}{\partial x} \\ &\quad + \frac{\partial}{\partial y}\int_{z_b}^{z_h} \tau_{xy} dz + \tau_{bxy} \frac{\partial z_b}{\partial y} - \tau_{hxy} \frac{\partial z_h}{\partial y} \\ &\quad + \frac{\partial}{\partial z}\int_{z_b}^{z_h} \tau_{xz} dz + \tau_{bxz} \frac{\partial z_b}{\partial z} - \tau_{hxz} \frac{\partial z_h}{\partial z} \\ &= \frac{\partial}{\partial x}\overline{\tau_{xx}} h + \tau_{bxx} \frac{\partial z_b}{\partial x} - \tau_{hxx} \frac{\partial z_h}{\partial x} + \frac{\partial}{\partial y}\overline{\tau_{xy}} h \\ &\quad + \tau_{bxy} \frac{\partial z_b}{\partial y} - \tau_{hxy} \frac{\partial z_h}{\partial y} + \tau_{hxz} - \tau_{bxz} \end{aligned} \tag{4.28}$$

Inserting the kinematic boundary conditions (4.14) and (4.15) and considering the tangential stress $\tau_{hx} = 0$ follow the momentum equations in x,y and z direction:

$$\frac{\partial \overline{\rho u} h}{\partial t} + \frac{\partial \overline{\rho u^2} h}{\partial x} + \frac{\partial \overline{\rho u v} h}{\partial y} + \frac{\partial \overline{p} h}{\partial x} + p_b \frac{\partial z_b}{\partial x} - \frac{\partial \overline{\tau_{xx}} h}{\partial x} - \frac{\partial \overline{\tau_{xy}} h}{\partial y} - \tau_{bx} = 0 \tag{4.29}$$

$$\frac{\partial \overline{\rho v} h}{\partial t} + \frac{\partial \overline{\rho u v} h}{\partial x} + \frac{\partial \overline{\rho v^2} h}{\partial y} + \frac{\partial \overline{p} h}{\partial y} + p_b \frac{\partial z_b}{\partial y} - \frac{\partial \overline{\tau_{xy}} h}{\partial x} - \frac{\partial \overline{\tau_{yy}} h}{\partial y} - \tau_{by} = 0 \tag{4.30}$$

$$\frac{\partial \overline{\rho w} h}{\partial t} + \frac{\partial \overline{\rho u w} h}{\partial x} + \frac{\partial \overline{\rho v w} h}{\partial y} - p_b + \bar{\rho} g h - \frac{\partial \overline{\tau_{zx}} h}{\partial x} - \frac{\partial \overline{\tau_{zy}} h}{\partial y} - \tau_{bz} = 0. \tag{4.31}$$

The lateral stresses (4.32) include viscous friction and turbulent friction. They are obtained by depth-averaging equation 4.33.

$$\overline{\tau_{i,j}} = \frac{1}{h} \int_{z_b}^{z_h} \tau_{ij} dz \qquad with \quad i,j = x,y,z \tag{4.32}$$

$$\tau_{i,j} = \mu \left(\frac{\partial u_i}{\partial x_j} + \frac{\partial u_j}{\partial x_i} \right) - \rho \overline{u_i' u_j'} \qquad with \quad i,j = x,y,z \tag{4.33}$$

4.2.4 Classical Shallow Water Equations

The shallow water theory defines the water depth as the major vertical length scale. The main assumption is that the water depth is much smaller than the horizontal dimension. This assumption signifies that the vertical velocity component is smaller than the horizontal velocity component by the same factor as the length scales. This reduces the vertical momentum equation 4.11 to

$$\frac{\partial p}{\partial z} - \left(\frac{\partial \tau_{zx}}{\partial x} + \frac{\partial \tau_{zy}}{\partial y} + \frac{\partial \tau_{zz}}{\partial z} \right) + \rho g = 0. \tag{4.34}$$

The second assumption regards the viscosity formulation 4.35

$$\tau_{i,j} = \mu \left(\frac{\partial u_i}{\partial x_j} + \frac{\partial u_j}{\partial x_i} \right), \tag{4.35}$$

which is applied for the vertical momentum equation 4.11.

$$\frac{\partial \tau_{zy}}{\partial x} = \frac{\partial}{\partial x} \left(\mu \frac{\partial u_z}{\partial y} + \frac{\partial u_y}{\partial x_z} \right) = \mu \left(\frac{\partial u_z^2}{\partial x \partial y} + \frac{\partial u_y^2}{\partial x \partial x_z} \right) \tag{4.36}$$

The second derivatives, which arises now are small compared to the first derivatives and can be neglected. The vertical momentum equation is now reduced to the hydrostatic pressure equation.

$$\frac{\partial p}{\partial z} = -\rho g \tag{4.37}$$

Assuming a constant density over depth and integration of equation 4.37 leads to depth-averaged pressure.

$$\bar{p} = \frac{g}{2}\frac{\partial}{\partial x}\left(\rho h\right) \tag{4.38}$$

The process of depth-averaging in the previous section lead to nonlinear terms in the equations 4.23, 4.29, 4.30 and 4.31. The variables can be split up in a depth-averaged mean and a random variation.

$$\begin{aligned}\overline{\rho u_i u_j} h &= \int_{z_b}^{z_h} \left(\bar{\rho} + \rho'\right)\left(\bar{u}_i + u_i'\right)\left(\bar{u}_j + u_j'\right) dz \\ &= \bar{\rho}\bar{u}_i\bar{u}_j + \int_{z_b}^{z_h} \left(\bar{\rho}u_i'u_j' + \bar{u}_i\rho' u_j' + \bar{u}_j\rho' u_i' + \rho' u_i' u_j'\right) dz \qquad with \quad i,j = 1,2,3\end{aligned} \tag{4.39}$$

The integral describes the lateral momentum exchange due to differences in velocity and is called differential advection. In the Classical Shallow Water Equations, the differential advection terms are zero due to the uniform horizontal velocity over the depth. The density is assumed to be constant over depth so the last three terms in the equation disappear.

$$\frac{\partial}{\partial t}\bar{\rho}h + \frac{\partial}{\partial x}\left(\bar{\rho}\bar{u}h\right) + \frac{\partial}{\partial y}\left(\bar{\rho}\bar{v}h\right) = 0 \tag{4.40}$$

$$\frac{\partial}{\partial t}\left(\bar{\rho}\bar{u}h\right) + \frac{\partial}{\partial x}\left(\bar{\rho}\bar{u}^2 h\right) + \frac{\partial}{\partial y}\left(\bar{\rho}\bar{u}\bar{v}h\right) + \bar{\rho}gh\frac{\partial z_h}{\partial x} + \frac{1}{2}gh^2\frac{\partial \bar{\rho}}{\partial x} - \frac{\partial \overline{\tau_{xx}}h}{\partial x} - \frac{\partial \overline{\tau_{xy}}h}{\partial y} - \tau_{bx} = 0 \tag{4.41}$$

$$\frac{\partial}{\partial t}\left(\bar{\rho}\bar{v}h\right) + \frac{\partial}{\partial x}\left(\bar{\rho}\bar{u}\bar{v}h\right) + \frac{\partial}{\partial y}\left(\bar{\rho}\bar{v}^2 h\right) + \bar{\rho}gh\frac{\partial z_h}{\partial y} + \frac{1}{2}gh^2\frac{\partial \bar{\rho}}{\partial y} - \frac{\partial \overline{\tau_{xy}}h}{\partial x} - \frac{\partial \overline{\tau_{yy}}h}{\partial y} - \tau_{by} = 0 \tag{4.42}$$

Calculating flows with a large water-level gradient can cause discontinuities of water depth and velocity using the non-conservative CSW. The derivatives in the CSW get theoretically infinite. The infinite velocity gradients lead to an error in the reproduction

of the wave velocity. The conservative formulation of the CSW will help to overcome these problems. The velocities are expressed in discharges.

$$\begin{aligned} \bar{q} &= \bar{u}h \\ \bar{r} &= \bar{v}h \end{aligned} \tag{4.43}$$

Discontinuities of discharge cannot occur with this formulation. The derivatives are finite and the wave velocity can be reproduced. The conservative CSW reads as follows

$$\frac{\partial}{\partial t}\bar{\rho}h + \frac{\partial}{\partial x}\left(\bar{\rho}\bar{q}\right) + \frac{\partial}{\partial y}\left(\bar{\rho}\bar{r}\right) = 0, \tag{4.44}$$

$$\frac{\partial}{\partial t}\left(\bar{\rho}\bar{q}\right) + \frac{\partial}{\partial x}\left(\frac{\bar{\rho}\bar{q}^2}{h}\right) + \frac{\partial}{\partial y}\left(\frac{\bar{\rho}\bar{q}\bar{r}}{h}\right) + \bar{\rho}gh\frac{\partial z_h}{\partial x} + \frac{1}{2}gh^2\frac{\partial\bar{\rho}}{\partial x} - \frac{\overline{\partial\tau_{xx}}h}{\partial x} - \frac{\overline{\partial\tau_{xy}}h}{\partial y} - \tau_{bx} = 0, \tag{4.45}$$

$$\frac{\partial}{\partial t}\left(\bar{\rho}\bar{r}\right) + \frac{\partial}{\partial x}\left(\frac{\bar{\rho}\bar{q}\bar{r}}{h}\right) + \frac{\partial}{\partial y}\left(\frac{\bar{\rho}\bar{r}^2}{h}\right) + \bar{\rho}gh\frac{\partial z_h}{\partial y} + \frac{1}{2}gh^2\frac{\partial\bar{\rho}}{\partial y} - \frac{\overline{\partial\tau_{xy}}h}{\partial x} - \frac{\overline{\partial\tau_{yy}}h}{\partial y} - \tau_{by} = 0. \tag{4.46}$$

The two-dimensional shallow water equations are solved using numerical models as described in chapter 5.3.

4.2.5 Extended Shallow Water Equations

The extended shallow water equations (ESW) regard, in contrast to the CSW, additional information over water depth including approximated distributions for horizontal and vertical velocities and for pressure. The exact derivation can be found in Krueger (2001), who used the ESW for the two-dimensional numerical model FEMTOOL.

4.2.6 Bottom Stress

The bottom shear stress is unknown in the shallow water equations. It must be expressed with already existing variables to close the equation system. The bottom stress is described with the aid of the friction terms τ_{bx} and τ_{by}. The channel depth is assumed to be much smaller than the channel width and therefore the effect of the side friction is smaller than the one of the bottom friction. The friction terms treats only the bottom friction, the friction at the channel walls is neglected.
The friction terms τ_{bx} and τ_{by} are assumed to depend quadratically on the depth-averaged velocities which is in accordance with turbulent boundary layer theory (Schlichting &

Gersten, 1997). Therefore the assumption may be correct for the shallow water flow. The friction terms can be expressed with:

$$\tau_{bx} = c_f \bar{\rho} \frac{\bar{q}}{h^2} \sqrt{\bar{q}^2 + \bar{r}^2} \tag{4.47}$$

$$\tau_{by} = c_f \bar{\rho} \frac{\bar{r}}{h^2} \sqrt{\bar{q}^2 + \bar{r}^2} \tag{4.48}$$

The friction coefficient c_f is depending on the channel roughness, channel shape, fluid viscosity and flow velocity. It is possible to calculate c_f with several approaches. Here the friction coefficient is defined by the Manning's coefficient n or alternatively with the Chezy C coefficient:

$$c_f = \frac{g n^2}{h^{\frac{1}{3}}} \tag{4.49}$$

$$c_f = \frac{g}{C^2} \tag{4.50}$$

4.3 Derivation of the one-dimensional Saint-Venant equations

4.3.1 General assumptions

The modelling of long river or channel sections for the flood forecast can be done by two-dimensional numerical modells but these calculations are still time consuming. Therefore it is common today for engineering companies and water authorities to use one-dimensional modells to save computational resources and calculation time. In urban water applications like the hydrodynamic modelling of large sewer systems, the one-dimensional modells based on the Saint-Venant equations are favoured.
The Sain-Venant equations describe the unsteady flow with depth- and width-averaged variables. The effect of the turbulence, the vertical and lateral dispersion, the bottom shear stress and the influence of secondary flows are all summarized in the energy slope I_E, which makes it impossible to model these single processes in detail. The Sain-Venant equations can be derived from the two-dimensional shallow water equations or direct from the three-dimensional Navier-Stokes equations. They are a system of partial differential equations of the first order, which is called a hyperbolic system, for the unknown functions $h(x,t)$ and $u(x,t)$. [Malcherek, 2001b]

The assumptions for the Saint-Venant equations are:

- incompressible flow medium
- the vertical pressure distribution is hydrostatic
- the transversal velocities are constant over a cross-section
- vertical accelerations are negligible

- the horizontal velocites are constant over the water depth
- the viscous stresses are constant over the water depth
- the density of the flow medium is constant over the water depth

4.3.2 Basic equations

The calculation of the water level in channels are based on the Navier-Stokes equations including the continuity equation 4.51 and the momentum equation 4.52.

$$\frac{\partial u_i}{\partial x_i} = 0 \tag{4.51}$$

$$\frac{\partial u_i}{\partial t} + u_k \frac{\partial u_i}{\partial x_k} = -\frac{1}{\rho}\frac{\partial p}{\partial x_i} + \nu \frac{\partial^2 u_i}{\partial x_k^2} + g_i. \tag{4.52}$$

4.3.2.1 Continuity equation

The x-axis is placed parallel to the channel axis, which leads to $u_1 = u$. The velocities in tranversal direction to the channel axis will be negligible ($u_2 = 0, u_3 = 0$). The integration of the continuity equation 4.51 over the cross section surface (depth and width) results in

$$\frac{\partial A}{\partial t} + \frac{\partial Q}{\partial x} = 0 \tag{4.53}$$

,

with the cross section surface $A = B\bar{h}$ and volume flow $Q = \overline{uh}B$. [Malcherek, 2001b]

4.3.2.2 Momentum equation

The integration of the three-dimensional momentum equation 4.52 follows the same assumptions as for the continuity equation and is described in detail in Malcherek (2001b). It results in equation 4.54

$$\frac{\partial Q}{\partial t} + \frac{\partial uQ}{\partial x} = -gA\frac{\partial z_s}{\partial x} - gAI_E. \tag{4.54}$$

The formulation of the equations 4.53 and 4.54 in dependency of the water level h and the flow velocity u was carried out by Malcherek (2001b) by using the cain and product rule under the assumption that the cross section surface as a function of h will be known. The continuity equation 4.53 can then be written as

$$\frac{\partial h}{\partial t} + u\frac{\partial h}{\partial x} + h\frac{\partial u}{\partial x} = 0. \tag{4.55}$$

The momentum equation 4.54 changes to

$$\frac{\partial u}{\partial t} + u\frac{\partial u}{\partial x} + g\frac{\partial h}{\partial x} = g\frac{\partial z_s}{\partial x} - gI_E. \tag{4.56}$$

With $I_E = \frac{\partial z_s}{\partial x}$ equation 4.57 is formulated

$$\frac{\partial u}{\partial t} + u\frac{\partial u}{\partial x} = g(I_S - I_E) - g\frac{\partial h}{\partial x}. \tag{4.57}$$

[Malcherek, 2001b][Kinzelbach, 2006]

4.3.3 Calculation of the energy slope

The energy slope I_E can be calculated with the equation of Manning Strickler and Darcy-Weisbach. The Manning Strickler equation uses the Strickler value k_{st} to calculate the energy slope.

$$I_E = \frac{Q^2}{(k_{Str} A R_{Hy}^{2/3})^2} \tag{4.58}$$

The Dary-Weisbach equation uses the friction coefficient λ for the calculation of I_E.

$$I_E = \lambda \frac{Q^2}{8gA^2 R_{Hy}} \tag{4.59}$$

The dimensionless coefficient λ is defined by the equation of Colebrook-White

$$\frac{1}{\sqrt{\lambda}} = -2log\left(\frac{2.51}{Re\sqrt{\lambda}} + \frac{k_s}{3.71 d_{Hy}}\right) \tag{4.60}$$

with the effective bottom friction k_s and the Reynolds number

$$Re = \frac{u d_{Hy}}{\nu}. \tag{4.61}$$

The equation of Colebrook-White 4.60 consists of two parts. The first part includes the Reynolds number and describes the effects of the turbulence on the energy slope. The second parts includes the effective bottom friction and represents the influence of the boundary layer near the bottom on the turbulent production. [Malcherek, 2001b]

4.3.4 Solutions of the Saint-Venant equations

4.3.4.1 Steady flows

The Saint-Venant equations (4.55) and (4.57) can be solved for steady flows with an approximation and an exact analytical solution.

Approximation

The approximate solution assumes that

$$v\frac{\partial u}{\partial x}, \quad g\frac{\partial h}{\partial x} \ll I_S \tag{4.62}$$

and that for steady flows

$$\frac{\partial u}{\partial t} = \frac{\partial h}{\partial t} = 0 \tag{4.63}$$

will be valid.

This lead to the uniform flow condition that the bottom slope equals the energy slope ($I_S = I_E$). The energy slope is defined as:

$$I_E = \frac{\lambda}{8}\frac{1}{R_{Hy}}\frac{v^2}{g} = I_S. \tag{4.64}$$

The flow velocity u is then given with:

$$u = \sqrt{\frac{8gI_S R_{Hy}}{\lambda}}. \tag{4.65}$$

The water level h_N for uniform flows must be calculated iteratively by using the Colebrook-White equation 4.60.

Exact solution

The exact solution combines the continuity equation 4.66 for steady flows

$$\frac{du}{dx} = -\frac{u}{h}\frac{du}{dx}. \tag{4.66}$$

and the momentum equation 4.67 for steady flows

$$u\frac{du}{dx} = g(I_S - I_E) - g\frac{dh}{dx}. \tag{4.67}$$

Inserting the continuity equation 4.66 into the momentum equation 4.67 leads to

$$-u\frac{u}{h}\frac{du}{dx} = g(I_S - I_E) - g\frac{dh}{dx} \tag{4.68}$$

and

$$\frac{dh}{x}\left(1 - \frac{u^2}{gh}\right) = I_S - I_E. \tag{4.69}$$

With the Froude-Number

$$Fr^2 = \frac{v^2}{gh} \tag{4.70}$$

the exact solution for the level of the water surface is

$$\frac{dh}{dx} = \frac{I_S - I_E}{1 - Fr^2}. \tag{4.71}$$

[Kinzelbach, 2006]

4.3.4.2 Unsteady flows

Flush or dam-break waves are highly transient flows which need therefore unsteady solutions. The Saint-Venant equations can be solved for unsteady flows in different stages of approximation, which are shown for the momentum equation 4.57

$$\underbrace{\frac{\partial u}{\partial t} = -u\frac{\partial u}{\partial x} - g\frac{\partial h}{\partial x} + \underbrace{\underbrace{g(I_S - I_E)}_{1.Approximation,\ KinematicWave}}_{2.Approximation,\ DiffusiveWave}}_{Exact,\ DynamicWave} \tag{4.72}$$

1. Approximation: Kinematic wave
The basic assumptions for the approximation of the kinematic wave are

$$u\frac{\partial u}{\partial x} \ll gI_S \tag{4.73}$$

$$\frac{\partial u}{\partial t}, \frac{\partial h}{\partial x} \ll I_S, \tag{4.74}$$

which leads to the uniform flow condition $I_S = I_E$. The further derivation, given in Kinzelbach (2006), defines the kinematic wave velocity c:

$$c = k_{str} \cdot I_S^{1/2} \cdot R_{Hy}^{2/3} + \frac{2}{3}k_{str} \cdot I_S^{1/2} \cdot h \cdot R_{Hy}^{-1/3} \cdot \frac{\partial R_{Hy}}{\partial h} \tag{4.75}$$

For wide channels the hydraulic radius R_{Hy} will equal the water depth h

$$R_{Hy} \approx h. \tag{4.76}$$

The kinematic wave velocity c will then be

$$c \approx \frac{5}{3} k_{str} \cdot I_S^{1/2} \cdot h^{2/3} = \frac{5}{3} u \tag{4.77}$$

2. Approximation: Diffusive wave
The diffusive wave is a further approximation of the Saint-Venant equation. The basic assumptions are again

$$\frac{\partial u}{\partial t}, u\frac{\partial u}{\partial x} \ll g I_S. \tag{4.78}$$

The derivation of Kinzelbach (2006) ends in an advection-dffusion equation

$$\frac{\partial h}{\partial t} + c \cdot \frac{\partial h}{\partial x} - D \cdot \frac{\partial^2 h}{\partial x^2} = 0 \tag{4.79}$$

with

$$c = \frac{5}{3} u \tag{4.80}$$

for the wave velocity and

$$D = \frac{3}{10} \frac{ch}{I_S - \frac{\partial h}{\partial x}}. \tag{4.81}$$

for the diffusion coefficient. D is always positive because of the energy slope $I_E = I_S - \frac{\partial h}{\partial x}$, which is positive in flow direction. The wave has a diffusive movement downstream. [Kinzelbach, 2006]

3. Approximation: Dynamic wave
The complete Saint-Venant equations can be solved numerically using the following methods:

- Method of characteristics
- Finite-Element Method
- Finite-Differences Method
- Finite-Volume Method

To solve the Saint-Venant equations boundary and initial condition must be given for $h(x,t)$ and $u(x,t)$. At the start of the calculations the water level and the flow velocity must be known for the complete flow domain, therefore the initial condition are local functions. Usually uniform flow is assumed.
The boundary conditions are temporal functions. The water level and the flow velocity have to be know at the upper and downstream boundary of the flow domain at any time step. The description of the numerical methods can be found in numerous sources like Oertel & Laurien (2003).

4.4 Analytical solutions

4.4.1 Ritter solution

Ritter(1892) investigated the dam-break problem by analyzing the wave formation induced by the movement of a dam-wall. The basic assumptions were a horizontal bottom with no slope, no influence of friction, a prismatic rectangular channel and an unlimited water supply for the dam-break wave.
Ritter observed a dam-wall which was moving with an uniform velocity $\hat{U}$ into a stored water body. The nearest part of the water body was moved forward and the water level was raised. The distant part of the water body still rested undisturbed. The developing boundary between the resting and the moving water has the relative velocity $\tilde{u}$. (Figure 4.4)

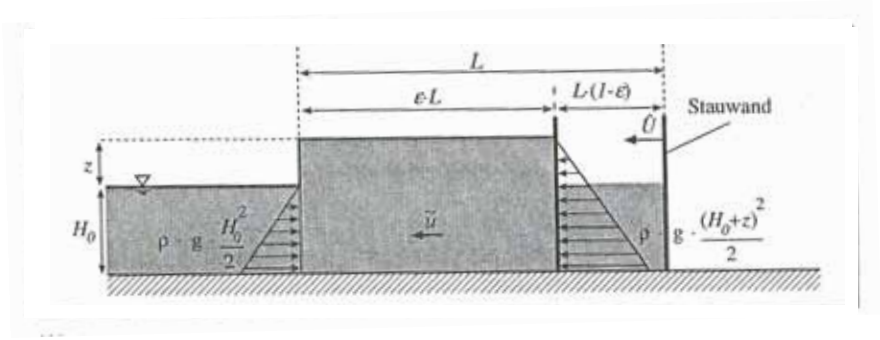

Figure 4.4: Balance of forces, Liem (2003)

With the help of continuity conditions and with respect to the conservation of energy Ritter derived the height and the velocity of the moving wave. The relative velocity $\tilde{u}$ was defined with

$$\tilde{u} \approx \sqrt{gz} \tag{4.82}$$

The velocity $\hat{U}$ was defined by Ritter with

$$\hat{U} \approx \sqrt{gH_0} \tag{4.83}$$

The movement of the boundary layer was then reversed by Ritter for the following observation. The dam-wall was now moved away (downstream) from the initial water body with a constant velocity. The water followed the moving wall and a surge wave was developed moving upstream into the reservoir. The border case selected when the movement of the dam-wall was just lower than possible velocity of the water following the wall. This case describes the dam-wave with the velocity of a positive front wave. The velocity of the boundary layer $\hat{U}$ was defined by Ritter for this new case by the equation

$$\hat{U} \approx \sqrt{g(H_0 - z)} \tag{4.84}$$

with $c_0 = \sqrt{gH_0}$ as the wave propagation velocity.

The relative velocity $\tilde{u}$ is shown in equation 4.85

$$\tilde{u}(z) = 2 \cdot c_0 - 2 \cdot \hat{U} \tag{4.85}$$

and the absolute velocity at the front wave consists of

$$u_F(z) = \tilde{u}(z) - \hat{U} = 2c_0 - 3\hat{U} = 2\sqrt{gH_0} - 3\sqrt{g(H_0 - z)}. \tag{4.86}$$

A temporal integration of the velocity allows the determination of the location x_F in dependence of the dam-break height z and the time t.

$$x_F(z,t) = \tilde{u}(z)t = (2 \cdot c_0 - 3\hat{U}) \cdot t \tag{4.87}$$

The water level of the dam-break wave is defined by

$$h(x,t) = \frac{1}{9g}(2\sqrt{gH_0} - \frac{x}{t})^2 \tag{4.88}$$

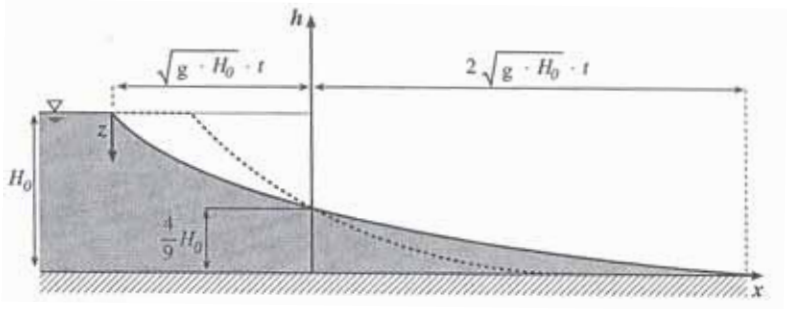

Figure 4.5: Ritter wave by Liem (2003)

Figure 4.5 shows the Ritter wave. The curve is parabolic with a vertical axis. The vertex of the wave front is equal to the channel bottom. The water level at the breach is constant for $\frac{4}{9}H_0$ and describes the turning point for the water level.

Regarding the case of $z = H_0$ the velocity at the front wave is then

$$u_F(z = H_0) = 2\sqrt{gH_0} = 2c_0 \tag{4.89}$$

The front wave is located at

$$x_F(h = 0, t) = 2\sqrt{gH_0} \cdot t \tag{4.90}$$

The velocity and the location of the surge wave moving upstream are described by the equations 4.91 and 4.92.

$$u_S(z = 0) = -\sqrt{gH_0} = -c_0. \tag{4.91}$$

$$x_S(h = z, t) = -\sqrt{gH_0} \cdot t. \tag{4.92}$$

During his investigation of dam-break waves Stoker (1957) found also the equations of the Ritter wave by solving the one-dimensional shallow water equations with the method of characteristics under the assumption of a dry channel bottom.
De Saint-Venant (1871) detected the equations for the Ritter wave twenty years earlier, when he was analyzing unsteady flood waves from rivers entering the open sea. The solution is based on the one-dimensional shallow water equations named after Saint-Venant. [Liem, 2003] Hager and Lauber (1996) and Hager and Chervet (1996) give a good overview on the historical development of the dam-break waves.
The physical assumptions of Ritter for the dam-break waves are [Stoker, 1957]:

- The front wave moves independent of time with a constant velocity c and is only dependent on the water depth h.
- The flow velocity u_F at the front wave is equal to the propagation velocity.

[Bornschein, 2005][Briechle, 2006]

4.4.2 Dressler solution

In contrast to the Ritter equations the solution of Dressler (1952) considers the influence of friction on the shape, propagation and the velocity of dam-break waves. The shape of the Ritter wave shows a front with a horizontal tangent. The front of a real wave under the influence of friction appears with a nearly vertical tangent and a convex curve on its top. (Figure 4.6) Several historical experiments given in Bornschein (2005) confirm this observation.

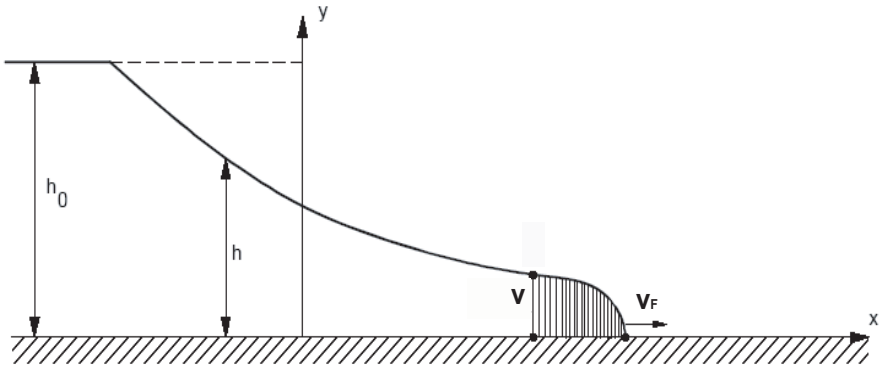

Figure 4.6: Dam-break wave by Dressler, Bornschein (2005)

The front wave is characterized by a high turbulence and an non-uniform velocity distribution. Dressler assumed that the water volume at the wave front is moved with the velocity v_F by the following flow. He introduced the friction approach of Chezy (Bollrich, 2000) into the one-dimensional shallow water equations to create a new description of dam-break waves for a wide, rectangular and horizontal channel. The initial velocity was assumed to be zero. [Bollrich, 1989] The mathematical discussion of the equation terms and the solution of the initial and boundary condition lead to a analytical solution. The higher-order terms were neglected and dimension-less values were introduced

$$X = \frac{x}{h_0}, \quad T = t\frac{g}{h_0}, \quad V = \frac{v}{w_0}, \quad W = \frac{w}{w_0} \quad and \quad R_z = \frac{g}{C_z^2} \tag{4.93}$$

with the Chezy factor

$$C_z = M \cdot R_{hy}^{1/6} \approx M \cdot h^{1/6}. \tag{4.94}$$

M the Manning-Strickler value represents the friction, w_0 the relative wave velocity in the region of the undisturbed flow and w the relative wave velocity.
Due to validation restriction it was not possible to apply the approach of Dressler to the front of the dam-break wave. His approximation was to regard the front wave as an independent part of the wave moving ahead and being followed by a surge wave. Therefore velocity v at the boundary between the front and the surge wave stands for an approximation of the front velocity v_F. The water level h and the velocity v can be calculated using the following equations.

$$n^{(*)} = n = \frac{X}{T} \tag{4.95}$$

$$v^{(*)}(n) = -\frac{108}{7(2-n)^2} + \frac{12}{2-n} - \frac{8}{3} + \frac{8\sqrt{3}}{189} \cdot (2-n)^{2/3} \tag{4.96}$$

$$w^{(*)}(n) = \frac{6}{5(2-n)} - \frac{2}{3} + \frac{4\sqrt{3}}{135} \cdot (2-n)^{3/2} \tag{4.97}$$

$$V(X,T,R_z) = \frac{2}{3}(n+1) + v^{(*)}(n) \cdot R_z \cdot T \tag{4.98}$$

$$W(X,T,R_z) = \frac{1}{3}(2-n) + w^{(*)}(n) \cdot R_z \cdot T \tag{4.99}$$

$$h = \frac{W^2 \cdot w_0^2}{g} = W^2 \cdot h_0 \tag{4.100}$$

$$v = V\sqrt{gh_0} \tag{4.101}$$

The velocity v_F, the location x_F and the height of the front wave h_F are calculated with the equations 4.102, 4.103 and 4.104.

$$v_F = \sqrt{gh_0} \cdot \left[\frac{2}{3}(n^{(*)}+1) + v^{(*)}(n^{(*)})R_z \cdot T\right] \tag{4.102}$$

$$x_F = n^{(*)} \cdot h_0 \cdot T \tag{4.103}$$

$$h_F = h_0 \cdot \left[\frac{1}{3}(2-n^{(*)}) + w^{(*)}(n^{(*)})R_z \cdot T\right]^2 \tag{4.104}$$

Dressler recognized that the water particles stay in the front wave during the propagation of the dam-break wave. Therefore the front wave will be regarded as a single wave with a constant shape and a negligible vertical acceleration. The validity of his equations are restricted to less than one third of the distance between the breaking point ($x = 0$) and the point where v equals zero.
Dressler gave also a dimension-less equation for the front wave velocity.

$$V_F = \frac{2}{3}(n^{(*)}+1) + v^{(*)}(n^{(*)})R_z \cdot T \tag{4.105}$$

The approximation of equation 4.106 is

$$V_F = 2 - a(R_z T)^{1/3} \quad with \quad a = 3,59. \tag{4.106}$$

Whitham (1955) investigated the front wave on an initially dry channel with the Pohlhausen Method and came to a value of $a = 4,58$ for equation 4.105.
Whitham and Dressler assumed an one-dimensional flow with negligible vertical acceleration. Therefore their approaches can not be valid for the initial phase of the breaking wave where the vertical acceleration have a large influence of the propagation of the wave. Both approaches can only be significant after the initial phase described by Ritter and Pohle described in Liem (2003).
The velocity v_F is reduced with the progression of time (4.102) due to the effect of

the friction. The time when there is no further wave propagation can be derived from equation 4.105. [Bornschein, 2005]

$$T_E = \frac{8}{R_z \cdot a^3} \tag{4.107}$$

The width-averaged runoff q in the breaking point ($x = 0$) is given by Dressler with

$$q = \frac{8}{27} \cdot (1 - 0.239 \cdot R_z \cdot T) \tag{4.108}$$

The derivation of the Dressler solution can also be found in Bollrich (1989).

5 Literature review - Hydrodynamic simulation models

5.1 Introduction

The oldest approach to describe the motion of fluids is the mathematical or analytical approach, which use equations based on physical fundamentals to investigate the behaviour of fluid particles. Physical models in laboratories where the next step to prove the reliability of the analytical equations in practical experiments. The influence of boundary conditions, which were sometimes neglected in analytical solutions, was now the subject of detailed investigations. The results led to better analytical equations and more precise characterisations of fluid motion.
With the availability of computational resources it was possible to use numerical methods based on the same differential equations as for analytical solutions to investigate and simulate fluid dynamics. One-dimensional models were the first ones to be developed but due to the fast growing computational power it is possible today to use three-dimensional models for all kind of applications in fluid dynamics.
The choice for a certain numerical model is based on a number of requirements, which have to be satisfied by the model. The available computational resources, the size of the flow domain and the accuracy of the results are some of the criteria that have to be considered when choosing a numerical model. Beside from the ability to calculate certain processes every model has advantages and disadvantages that have to be taken into account. The number of dimensions indicates the degree of simplification of the calculated differential equations. Therefore the choice of dimensions of the numerical model is the most important one before starting an investigation. In the following one-, two- and three-dimensional models are described by their numerical basics, their application ranges and their advantages and disadvantages. Many examples of suitable numerical models for the calculation of flush- or dam break waves are given. For a detailed description of the following models please see Oberlack et al. (2005).

Beside their number of dimensions they can be divided into three different groups:

Commercial models
These models are distributed by software companies like Danish Hydraulic Institute, Boss, HR Wallingford, CD adapco Group or Fluent for example. Some of their codes origin from universities or from national research institutes and some of them are developed by themselves.

Academic models
Many numerical models are developed and grown within universities during the work on research projects. Some of these models are free and some are kept to the departments for future research.

National research institutes
Organizations like the US National Weather Service or US Army Corps of Engineers developed numerical models for their own demands and made some of the them available to the open public.

5.2 One-dimensional models

5.2.1 Numerical basics

One-dimensional models can be differentiate into hydrological and hydraulical models. Hydrological models use approaches like the Muskingum or the Kalinin-Miljukov to analyse approximately the propagation of gradually unsteady flows like flood waves for example. Hydraulic approaches are based on the Saint- Venant equation. Depending on the number of terms of the Saint- Venant equation a diffusive, kinematical or dynamic approach is used. Only if all terms of the Saint-Venant equation are taken into account it is possible to model accelerated processes like a dam-break (flush) wave with its back-water effects and the calculation of in- and outflows also needs a dynamic approach. [Schramm, 2003]
Usually the complete Saint- Venant equation is described as a system of non-linear, partial differential equations to calculate the conservation of mass and momentum. This set of equation is solved using mathematical numerical methods to create a system of algebraic equations. These will be solved with the aid of boundary and initial conditions. The results are depth- and width averaged values. Therefore it is not possible to calculate for example the shear stress at the bottom of a sewer precisely. It is also not possible to model the turbulence which dominates unsteady flows.
The discretisation of the investigated flow domain is usually carried out using the Finite Volume or the Finite Differences Method. Methods like the one from Preissmann are used to solve the Saint- Venant equations for sub- and supercritical flows. [Schramm, 2003] Some models also include a transport approach to calculate the movement of sediments within the flow.

5.2.2 Application

Some of the first one-dimensional models had been created especially to calculate wide river systems with large temporal and spatial scales. With these models it was possible to simulate the long-term runoff of flood waves and give predictions for flooded areas. These models were not able to give detailed results in a high temporal and spatial resolution. Other one-dimensional models were developed to calculate the flow over dams, weirs or certain special structures. The modelling of possible dam-break wave is one very important issue for the operators of big reservoir lakes. The requirements to the numerical code were very high in this case because of the unsteady flows and the originally dry parts of the flow domain. Another field of application for one-dimensional models is the simulation of sewer channels or systems of sewers within bigger cities. Here it is also necessary to model structures like combined sewer overflows, culverts or retention tanks for example.

5.2.3 Assets and drawbacks

The major advantage of one-dimensional models is the fast calculation time. Large systems of channels or creeks can be simulated in a very short time. Usually one-dimensional models are easy to learn and this fact together with the fast computational time makes these models very interesting for engineering companies with less time to spend. The accuracy of the results is not very high due to the fact that all flow values will be averaged in width and height. But for many engineering purposes it is absolutely sufficient.
A big drawback is the mostly rough spatial resolution of the flow domain, which makes it difficult to include complicated geometries. The need for large time steps in the temporal resolution is another drawback which makes it sometimes impossible to model temporal small transient processes.

5.2.4 Selection of one-dimensional models

Floodwave:
DWOPER (Dynamic Wave Operation Model)
DAMBRK (Dam Break)
FLDWAV (Flood Wave Routing Model)
US National Weather Service
(www.weather.gov/oh/hrl/rvrmech/documentation/fldwav_doc.pdf)

FLUVIUS-1Di
Institut fuer Wasserbau und Wasserwirtschaft, RWTH Aachen
(www.rwth-aachen.de/iww/)

HEC-RAS
Hydrologic Engineering Centers River Analysis System
US Army Corps of Engineers
(www.hec.usace.army.mil)
Commercial versions like HEC-6 available from Boss International
(www.bossintl.com)

InfoWorks CS
HR Wallingford Software
(www.hrwallingford.co.uk/software/software.html)

Mike11
Danish Hydraulic Institute (DHI)
(www.dhisoftware.com)

Mouse
Danish Hydraulic Institute (DHI)
(www.dhisoftware.com)

Sobek
WL — Delft Hydraulics
(www.sobek.nl)

Flooris2000
Flood Routing in River Systems
(www.tkconsult.ch, www.scietec.com)

5.3 Two-dimensional models

5.3.1 Numerical basics

Two-dimensional models are based on the shallow-water theory, which includes the following assumptions:

- the vertical velocity is very small compared to the two horizontal velocities and can be neglected
- Hydrostatical pressure distribution over the water depth
- Horizontal velocity and acceleration is constant over depth
- Water level fluctuations are very small compared to the water depth
- Incompressible fluid with constant density
- the impact of friction forces is summarized in a bottom roughness term
- Wind, coriolis forces and turbulence are neglected

[Liem, 2003] [Vreugdenhil, 1994]

The turbulence, which is originally neglected for the two-dimensional models, is subject to discussions. Jankowski (1999) states that the effect of friction, induced by turbulence and viscosity, is negligible small. Rodi (1993, 2004), in contrast, developed a $k-\epsilon$ model for depth-averaged calculations. His approach was rather empirical but his results were promising. [Rastogi & Rodi, 1975]
The spatial discretisation of the flow domain is done using the Finite Differences, the Finite Volume or the Finite Element Method. The application of these different methods on the same problem can lead to different results regarding the wave velocity. Details of the advantages or disadvantages of the mentioned numerical methods can be found in Forkel (1995). Implicit, semi-implicit or explicit methods are used for the temporal discretisation, which can be solved with numerous mathematical approaches. Oertel and Laurien (2003) give an in-depth view into these techniques.
The investigation of flows with discontinuities like hydraulic jumps or dam-breaks, using common numerical approaches, lead to the problem of inaccurate results. These discontinuity flows need special numerical algorithms, which are implemented into the models so that they can solve the flow equations precisely. Numerical instabilities in the results can also occur when the bottom friction or the bottom slope of a channel is regarded in the solution. Methods like shock fitting, implementation of numerical viscosity or high-resolution techniques were developed to overcome these problems. They are explained in detail in Oertel and Laurien (2003) and Naef (1997).

5.3.2 Application

Two-dimensional models are used, like the one-dimensional ones, to investigate stationary and transient flow in rivers, channels or lakes. They model the flooding of originally dry areas caused by discharge of flood waves along rivers or river systems. The influence of weirs, bridges or other buildings on the flow is the subject of many two-dimensional models. Some of the advanced models are able to simulate dam-breaks or hydraulic jumps as well as transport sediments or pollution loads. They can also regard turbulent flows using turbulence models like the $k - \epsilon$ model. Especially the river models can be linked to geographical information systems to reproduce the river catchments or possible flood plains.

5.3.3 Assets and drawbacks

Two-dimensional models possess the advantage to be more accurate than one-dimensional models due to the fact that the results averaged in just horizontal dimension. The computational time is depending on the fineness of the numerical grid but generally they are slower than the one-dimensional models. Compared to three-dimensional models the depth-averaged approach is still fast and combined with a turbulence model they can offer a good accuracy in comparison with realistic calculation times. This fact makes them very appealing for investigations where no super-computational resources are available.
The calibration of the numerical model on the bottom roughness against a measured water level, run-off or flow velocity is absolutely necessary to achieve reliable results. Liem (2003) presented an investigation where the calibration of a two-dimensional model with the Strickler roughness k_{st} showed differences in the flow velocity of a dam-break wave up to 40 %.
One disadvantage of most of the models is disability to calculate the influence of air and sediment intrusion to the propagation of the dam-break wave. Usually only the water phase is regarded when applying two-dimensional flow models for dam-break waves. Liem (2003) states that due to the differential results depending on the chosen numerical approach and if there is no possibility to calibrate a model it is acceptable to choose an analytical method to calculate the propagation of a dam-break wave. Analytical approaches like the Ritter solution, presented in chapter 4.4, offer very basic results with a small expenditure of time. But it must be kept in mind that these plain solutions are based on many estimations, which strongly restrict the calculated results.
Two-dimensional models offer a good compromise between the fast but basic one-dimensional approaches and the very detailed three-dimensional models, which require large computational resources.

5.3.4 Selection of two-dimensional models

AquaDyn
Hydro-Qubec and Synexus Global
(www.technum.com)

BCE-2D
Bjoernsen Beratende Ingenieure
(www.bjoernsen.de)

DELFT FLS (Delft Flooding System)
Delft Hydraulics
(http://www.wldelft.nl)

DGflow Institut fuer Wasserbau und Wasserwirtschaft, RWTH Aachen
(www.rwth-aachen.de/iww/)

FESWMS-2DH (Finite Element Surface Water Modeling System)
U.S. Gelogical Survey, Boss International
(www.usgs.gov),(www.bossintl.com)

FLUMEN v.1.3 (FLUvial Modelling ENgine)
Fluvial.ch
(www.fluvial.ch)

Hivel 2D
U.S. Waterways Experiment Station, Coastal and Hydraulics Laboratory
(http://chl.erdc.usace.army.mil)

Hydro_AS-2D
Hydrotech
(www2.hydrotec.de)

HYDRO-2D
E-Planung GmbH
(www.EplanungGmbH.de)

Hydro2de
Fluvial.ch
(www.fluvial.ch)

Kalypso-2d
Arbeitsbereich Wasserbau, TU Hamburg Harburg
(http://elbe.wb.tu-harburg.de)

Mike Flood
Danish Hydraulic Institute
(www.dhisoftware.com)

RISMO 2D (River Simulation Model)
Institut fuer Wasserbau und Wasserwirtschaft, RWTH Aachen
(www.rwth-aachen.de/iww/)

RMA2
Coastal and Hydraulics Laboratory US Army Corp of Engineers
(http://chl.wes.army.mil/software/tabs/rma2.htp)

5.4 Three-dimensional models

5.4.1 Numerical basics

The numerical basics of three-dimensional models are described in detail in chapter 3. They are divided into the general flow equations, the turbulence modelling, the discretisation with Finite Volume Method and the calculation of the free surface using for example the Volume of Fluid Method (VOF). The treatment of the boundary is explained as well as the implementation of initial conditions. More literature for computational fluid dynamics with three-dimensional models can be found in Durbin and Pettersson Reif (2001), Ferziger and Peric (1996), Hirt and Nichols (1981), Launder and Spalding (1972), Malcherek (2001 a), Oertel and Laurien (2003), Rodi (1993), Versteeg and Malalasekra (1995) and Wilcox (1998).

5.4.2 Application

Three-dimensional models are usually general commercial codes for the investigation of numerous flow applications. Most of them were developed to be used in scientific research projects as well as for industrial studies and a few were designed for military projects. The program modules for the calculation of free surfaces flows are just a small part of the possibilities offered by three-dimensional models. A literature survey by Oberlack et. al (2005) showed the following applications:

- Flow in porous media
- Thermodynamic flows
- Multiphase flows
- Particle or chemical transport (dispersion - advection)
- Combustion or chemical reactions
- Dam-break waves
- Acoustic waves
- Cavitation
- Rotating bodies
- Transfer between gas- fluid and solid phases
- Water Quality
- Free surface flows in rivers, lakes and oceans
- Sediment transport with erosion
- Drop formation

The commercial codes are supplied with pre- and postprocessors and they feature interfaces to further post processing software for example to create animations of flows.

5.4.3 Assets and drawbacks

Turbulence in the front wave plays an important role concerning the cleaning effect of a flush wave and can be described best in a three-dimensional model using a turbulence model such as the $k-\epsilon$ model of Launder and Splading (1972). With a three-dimensional model it is possible to calculate the velocity and shear stress for the bottom cells in a locally and temporally high resolution to describe the movement and the cleaning effect of the flush wave without depth-averaged values.
The accurate calculation of the hydraulic losses induced by the flush gate at the end of its rotation movement is of high importance when modelling flush waves. Therefore it is necessary for the chosen model to be able to create an unstructured numerical gird or to read existing CAD files and convert them in unstructured grids. Three-dimensional models also offer the possibility to reproduce local differences in boundary conditions like the bottom roughness to suit the conditions found in long sewer channels.
Many one- or two-dimensional codes show difficulties in their numerical stability when including originally dry zones into the flow domain when they only can simulate the water phase. This common initial condition for the calculation of flushing devices can lead then to an abort of the simulation. The most three-dimensional models can imply several phases in the flow domain like air and water for example. So these models can handle the situation of an initially dry-bed without problems due to their ability to solve the differential equations for all phases.
The computational time for the simulation of flow domains with a large number of grid cells is usually very high so it is convenient to stop a simulation run and to control the results. After this most of the three-dimensional models are able to restart the calculation at a chosen time step to save time in the duration of the computation. Some models offer the possibility to create a moving numerical grid to simulate rotating bodies like flushing device or turbines. This option which can be important in calculation of the initial phase of a flush wave is provided by commercial three-dimensional models.
The initial stages of a flush wave can be compared with a dam-break wave, which has a three-dimensional character. Therefore it is necessary to provide a high temporal and spatial resolution of the flow domain and a three-dimensional algorithm to describe the movement of a flush wave in detail. But a fine resolution of the numerical grid leads to a long simulation times and requires high computational resources. Three-dimensional models are usually run on workstations or super-computers to handle the large number of cells of a fine grid. Personal computers can be soon overstrained with the calculation of hundred thousands of cells. So it is the accuracy of the needed results against the computational costs, which has to be considered for the user of a three-dimensional model.
The next chapter shows a list of three-dimensional models, which are suitable for the simulation of flush waves in sewer channels. Detailed descriptions of their abilities can be found in Oberlack et. al (2005).

5.4.4 Selection of three-dimensional models

CFX 4, CFX 5
ANSYS, Inc.

(www.ansys.com)

CH3D
Costal Hydraulics Laboratory US Army
(http://hlnet.wes.army.mil/software/ch3d/)

FEMTOOL Versuchsanstalt fuer Wasserbau (VAW), ET Zuerich
(http://water2.uibk.ac.at/de/index.html)

FIDAP
Fluent Inc.
(www.fluent.com)

Flow-3D
Flow Science
(www.flow3d.com)

FLUENT
Fluent Inc.
(www.fluent.com)

HYDRO-3D
E-Planung GmbH
(www.EplanungGmbH.de)

Mike 3
Danish Hydraulic Institute
(www.dhisoftware.com)

PASTIS-3D (Projection Algorithm Solver for Transient Incompressible flow Simulations in 3D)
Institut fuer Wasserbau und Wasserwirtschaft, RWTH Aachen
(www.rwth-aachen.de/iww/)

Phoenics
Cham Corporation
(www.cham.co.uk)

RMA10
Coastal and Hydraulics Laboratory US Army Corp of Engineers
(http://chl.erdc.usace.army.mil/)

SSIIM (Sediment Simulation In Intakes with Multiblock Option)
Universitaet NTNU Trondheim
(www.bygg.ntnu.no/∼nilsol/ssiimwin/)

StarCD
CD adapco Group
(www.cd-adapco.com)

TABS-MD (Multi-Dimensional) Numerical Modeling System
Costal Hydraulics Laboratory US Army
(http://chl.erdc.usace.army.mil/)

TELEMAC
Laboratorie National de Hydraulique
(www.hrwallingford.co.uk/software/telemac.html)

5.5 Description of the applied 3-D Model StarCD

The model StarCD of the CD adapco Group is a three-dimensional CFD (Computational Fluid Dynamics) code for the calculation of different flow processes. Steady and transient flows can be modelled as well as sub- and supercritical free surface flows. The transition from free surface to pressured flows and hydraulic jumps are modelled in detail. StarCD can use Newtonian or non-Newtonian fluids for the simulations. The Volume of Fluid Method (VOF) defines the location of the free-surface between water and air. The size of the iteration time steps can be chosen freely but very large time steps can lead to numerical instabilities in the calculation.
StarCD solves the Reynolds-averaged Navier-Stokes equation to calculate three-dimensional flow processes. Therefore the Finite Volume Method is used which reproduces the flow geometry by unstructured grid meshes with hex, tetra, and triangle elements. The calculations can be executed alternatively with implicit or explicit solvers. Moving grids to model rotating bodies like turbines are also possible.
The calculation of the turbulence is carried out with the aid of different turbulence models. StarCD uses the standard models like the $k-\epsilon$ model as well as the Large Eddy Models (LES), the $k-\omega$ model and the Detached Eddy Simulation Model (DES). The latest version of StarCD offers additionally two-layer models and hybrid wall functions, which calculate the flow conditions at fixed walls in a high resolution. A large choice of boundary conditions makes it possible to define borders of the flow domain in detail. The calculation of initially dry parts of the flow geometry is without problems for the stability of the simulations of StarCD.

Additional calculation modules of StarCD are:

- Multi-phase flows
- Heat- and mass transfer
- Chemical reactions and combustion
- Euler Two-phase flows with detailed boundary faces
- Radiation processes
- Acoustics
- Fluid - Structure Interactions
- Flow in porous media
- Cavitations
- Flows in rotating bodies
- Multi-phase Lagrange flows with combined changes Gas/Solid/Fluid

The ProStar Software can be used for the pre- and post processing. It is also possible to utilize the interfaces of StarCD for well-known commercial software like AutoCad or Tecplot. The user of StarCD is also able to work with user-defined functions to interfere the calculation process actively and connect own subprograms with the source code to solve individual flow problems. (www.cd-adapco.com)

6 Literature review - Flushing devices

6.1 Historical background

The usage of flush waves is one of the oldest methods to clean sewer channels from deposits. The first reported flushing of a sewer system, the Cloaca Maxima in Rome, was 500 - 550 BC. [Bertrand-Krajewski, 2003] Ehnert (1980) reports of large water supply tanks in 32 BC, which were opened abruptly to create a flush wave that cleaned the water pipes. During the middle age, the Roman heritage and knowledge was not kept. One flushing system from this age in Germany in the city of Bunzlau is reported where the sewer system was cleaned periodically by flushing with drinking water.
The first cleansing service for sewers in France was established in Paris in 1663. In England, the first ideas about a regular sewer cleaning were found in 1678. The main problems of the old sewer systems were the flat inverts combined with low flow velocities and insufficient volumes. There were no or only a few gully pots so most of the debris and solids from the streets entered the sewer system.

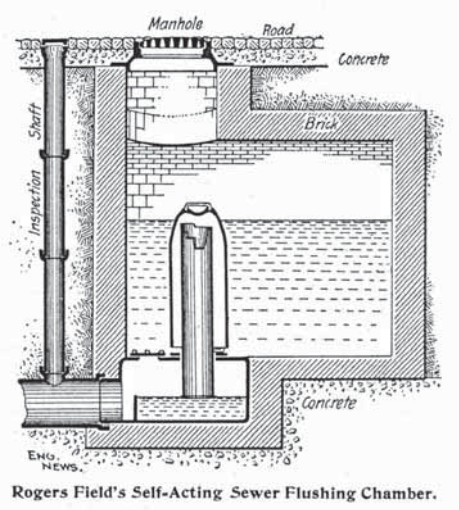

Figure 6.1: Roger Field's self-acting sewer flushing chamber, 1896 [N.N., 1896]

At the end of the 19th century flushing tanks were introduced in many European cities. (Figure 6.1) In 1899 Paris had 3500 flushing tanks and Berlin possessed 1220 flushing tanks in 1906. Parallel to the development in Europe the need of continuous sewer cleaning using flushing techniques was also discovered in the United States. Memphis for example used 180 flushing tanks in 1879. [Bertrand-Krajewski, 2003]

Flushing tanks could be differentiated into manual devices, where the gate or the valve was opened by hand and automatic flushing tanks, which used counterweights, floating

valves or tipping devices. The effective flushing distance of the tanks was estimated between 150 and 300 m.
The first flushing doors were installed in sewer systems in the middle of the 19th century to activate storage volume in the sewer channels and to flush them. A sanitary report by Edwin Chadwick (1942) cited the English engineer John Roe, who implemented the first flushing doors in the sewer systems of Holborn and Finsbury, England. The gates invented by Roe are described in his 1842 paper. [Roe, 1842) Further and similar flushing doors were implemented for example in Hamburg, Germany by William Lindley (1845) or in Paris. [Leo, 1969][Bertrand-Krajewski, 2008] For the flushing itself sewage, water from nearby rivers or fresh water was used. [Fruehling, 1910] [Guerschner & Benzel, 1921] An early dissertation by Schween (1936) described the movement of flush waves in sewer pipes. An example of a flushing door is shown in figure 6.2.

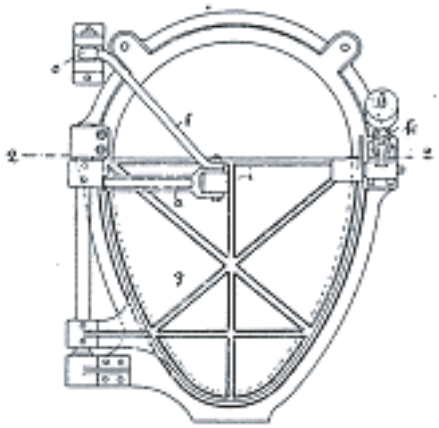

Figure 6.2: Automatic flushing door 1924 [Genzmer, 1924]

The improvement in sewer design since the late 1950 led to higher self-cleansing velocities, less street sediments and higher volumes of water in the channels. Combined with the development of powerful hydraulic and mechanical cleansing tools like high-pressured water jets and economical concerns like costs of maintenance the flush cleaning was displaced. In the end of the 20th century the flush cleaning was reinvented and new technologies where developed. The disadvantages of the jetting with freshwater became obvious and ecological practices had to be found. Especially in Germany many companies started to investigate the principles of sewer flushing and invented numerous new flushing devices.
The following chapters show the principles of flush cleaning and the problems connected with this approach. The different groups of flushing devices will be presented as well as their functionality.

6.2 The principle of flush cleaning

Flush cleaning follows the same mode of action as the first flush in sewer network as a cause of a storm event in an urbanised area. The sudden runoff of a large volume

of water leads to a flush wave with a highly turbulent wave head. (Figure 6.3) The necessary precondition for the function of a flush wave is a dry runoff region downstream of the flushing device. Even a low water level downstream slows the flush wave down and influences the cleaning effectiveness negatively. The flow has to act with high shear stresses on the deposits at the sewer bottom to be able to lift and transport them with the current.

Figure 6.3: Head of dam break induced wave [Stansby et al., 1998]

Flush waves are translation waves, which move a volume flow in the direction of their propagation. They are generated by a discontinuous change of the runoff cause by the opening of a sluice or the break of a reservoir dam that lets out large amounts of water. They are also called shock waves. When these shock waves lead to rise of the water level they are called flush waves. [Bollrich, 1989] This means that a the principle of a flush wave is based on a sudden changing transient flow.
A low filling level downstream of the flushing device is of advantage regarding the effectiveness of the flush wave because a resting water volume does not stop the runoff of the wave. [Haussmann, 1999] [Lorenzen et al, 1997] Flush waves like a dam break wave running on an initially dry bottom are called breaking wave because of the formation of their head. The wave head can be regarded as a moving hydraulic jump with a surface roller. [Martin, 1989]

6.3 Effects of flush cleaning

The flush cleaning, aside from its positive cleaning results, underlies the criticism of the abrasion of the sewer pipes caused by the transport of water and solids mixture. Sand, gravel or metal parts could harm the surface of the sewer pipes but in the literature there are no reports about demonstrable damages caused by flush waves. The same applies for the forming of deposits directly upstream of a flushing device. [Jaervenkylae & Haavisto, 1993]

Investigation by Lorenzen et al. (1996) showed that a complete cleaning of a sewer from its deposits by flushing is not possible. Ristenpart (1998) observed during his investigations that it is possible to keep a sewer channel free of deposits for long space of time with the aid of flushing once it was cleaned with a high pressured water jet before the flushing campaign started. Afterwards the amount of work was restricted to the maintenance of the flushing device. The effects of flush cleaning in sewer channels can be outlined as follows by the results of Lorenzen et al. (1997):

- Deposits are detached and transported
- The cleaning can be effective for long distances
- A backwater effect in connected sewers can be possible
- The high flow velocity of the flush waves, which have to be released periodically, reduces the formation of new deposits
- The first flush during a storm event will contain only a low pollution load caused by decrease of deposits when the sewer is flushed and therefore cleaned continuously

6.4 Applications of flush cleaning

Flushing devices can be found in many different shapes and applications. Usually they are fixed installations which can be controlled from the outside or work automatically. Some flushing devices are fixed in a certain location for a limited time to clean a sewer stretch. Some old flushing devices like the trolley that draws the silt in were real mobile devices. But they were connected with a large amount of work and not effective in heavily polluted sewers. Some big flushing devices like the Drehbogen or the HydroGuard can be used for the management of a part of the sewer system. [Barth et al., 1993] [Barth, 1996]
The main determination is the hydraulic principles on which the different flushing devices are based on. These are:

- Dambreak induced flush waves
- Flush waves created by weirs or siphons
- Flushing devices with storage installations

In the following the above-mentioned flushing devices will be examined regarding their hydraulic principles, their design and their functionality.

6.4.1 Dam-break induced flush waves

Flush waves created by the lifting of a locking device can be compared with dam-break waves who are the result of a sudden opening of a barrier. Martin (1989) regarded this abrupt release a downstream movement of the barrier with the velocity $v_w \leq -2w_0$.
After the break of the barrier a wave front with a vertical front head is formed. Figure 6.4 shows such a wave. The influence of the roughness in dry river or channel bed leads

to deformations and cushions on the dam break wave once it is running downstream. The front wave, "'leading edge"', is characterised by a high degree of turbulence and inhomogeneous velocity. [Martin, 1989]

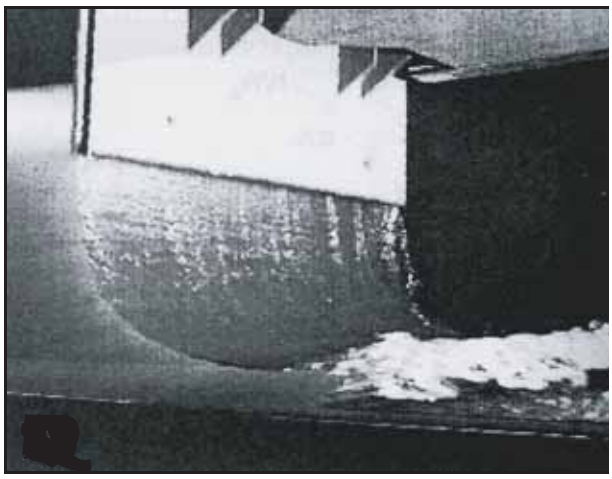

Figure 6.4: Dam-break induced waves [Lauber, 1997]

In chapter 4 two approaches are described to calculate dam-break waves analytically. The devices, which created dambreak induced flush waves can be split in different types. They are specified in table 6.1 with the developer or the distribution company.

Type of flushing device	Product name	Developer / Distributer	Reference
Flush gate	Stauspuelklappe Rotaria	ROTARIA Energie- und Umwelttechnik	www.rotaria.com
Flush gate	Berliner Klappe (Hydrass valve)	Physiker Buero Berlin	www.dr-lorenzen.de [Lorenzen& Laplace, 1998]
Flush shield	HydroFlush© GS	Steinhardt Wassertechnik	www.steinhardt.de
Flush gate valve	Spuelschieber	AWK Passa-vant GmbH	www.awk-passavant.de
Flush valve	SD - Schieber	ASATechnik GmbH	www.asatechnik.de
Flush sluice	HydroGuard	Steinhardt Wassertechnik	www.steinhardt.de
Flush sack	AWS - Spuelsack	Hydro-System-technik-GmbH	www.systemtechnik.net [IKT, 2004]
Pulsator	Pulsator	LIWATECH	www.liwatech.de
Tube weir	Schlauchwehr	Floecksmuehle Energietechnik	www.floecksmuehle-et.com

Table 6.1: Flushing devices and producers

Detailed descriptions of the different flushing devices can be found in Dettmar (2003), Dettmar et al. (2001), Dohmann and Dettmar (2003), Gebhard (2000), Kirchheim (2003), Kirchheim (2005), Schueler (2002) and Oberlack et al. (2005).

6.4.2 Flush waves created by weirs or siphons

Special types of flushing devices are concealed weirs and the rotary arch (Drehbogen). The original idea behind these devices was the controlling of parts of the sewer system. Therefore the moveable weirs and siphons are used in large sewers above DN 1000 and in reservoir sewers to store the storm water sewage and give it throttled back to system. But it is also possible to release the large water volume abruptly to create a flush wave that lifts the deposits from the bottom of the sewer. In some cases it was possible to clean a sewer stretch of 2000 m.
Their hydraulic principle is based on the free overfall described by the equation of Poleni. [Bollrich, 2000]

$$Q = \frac{2}{3} \cdot \mu \cdot b \cdot \sqrt{2 \cdot g} \cdot h^{\frac{3}{2}} \tag{6.1}$$

A typical example for a concealable weir is the vertical weir of the company ASA Technik as shown in figure 6.5.

Figure 6.5: Vertical weir for the dynamic control of a reservoir sewer, ASA-Technik (2003)

A recent development of the engineering consultants Hesse und Partner [N.N., 2001] is the usage of several vertical moveable weirs in one long reservoir sewer. The arrangement of the weirs as a cascade along the reservoir sewer makes it possible the control the runoff dynamically and cleans it with flush waves over a length of eight kilometres permanently.

The rotary arch was developed research program sponsored by the Deutsche Bundesstiftung Umwelt (DBU) while the scientific research was carried out by the TU Dresden. Originally it was designed as a control element for sewer systems but it was also used to create flush waves, which can clean large sewers for a long distance. The functional principle is based on three contrarious pipe bends, which can be moved about the pipe axis and in 0 - 90 degrees against the horizontal. Figure 6.6 shows the functional principle.

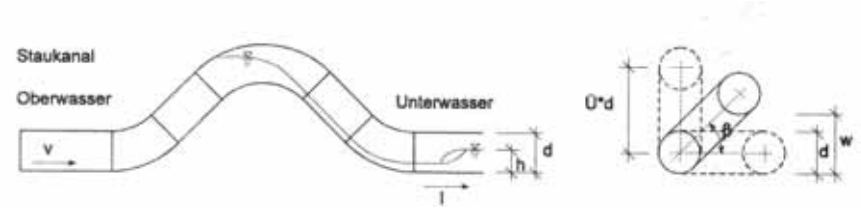

Figure 6.6: Functional principle of the rotary arch [Barth et al., 1993]

The main drawback of the rotary arch are the high expenses in the investment and maintenance. The rotary arch is only useable for sewer with a circular profile otherwise it needs a special building which connects the arch to the following sewer. More information about the rotary arch can be found in Barth et al.(1993).

6.4.3 Flushing devices with storage installations

Flushing devices with storage installations are based on the same hydraulic principle as flushing devices mentioned in chapter 6.4.1. They also create dambreak induced flush waves to clean the sewer but they store the sewage in special structures. Flush valves or flush sluices for example use the main sewers to store the necessary water volume, which generates the flush wave. Flushing devices like gates with flushing chambers or tipping buckets are placed in storm water holding tanks or reservoir sewers in sub-main sewers. Flushing manholes are used for smaller sewers below 400 mm diameter.
Some installations need fresh water, which is pumped into their reservoir; others use the available rainstorm sewage to fill up the needed flushing volume. Flush tanks work on the siphon principle and store the dry-weather runoff for the flush waves in a manhole.

6.4.3.1 Flush gates with storage chambers

These flushing devices own a special building, the storage chamber, where they stock the water volume for the flush waves to clean large reservoir sewers or storm water holding tanks. The systems can be divided into gate-flushing devices and vacuum-flushing devices.

Gate-flushing devices

Gate-flushing devices possess a storage chamber which is filled with storm water sewage. Therefore the gate in front of the storage chamber needs to be locked. When the reservoir sewer or the storm water holding is emptied, the gate is opened and the flush wave released. The potential energy of the stored water is transformed into kinetic energy and creates a high velocity flush wave, which runs along the sewer. The gate-flushing system of the Steinhardt company for example is able to clean sewer stretches up to 200 m from deposits. [Steinhardt, 2005] Figure 6.7 shows the principle of the gate-flushing system.

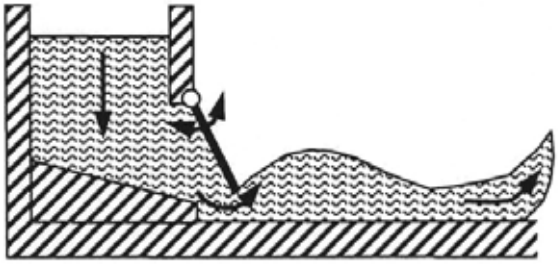

Figure 6.7: Gate-flushing system [Dettmar, 2001]

Vacuum-flushing devices

A modified version of the gate-flushing devices is the vacuum-flushing system of the Biogest company. [Biogest, 2005] The flushing volume held in an airtight storage chamber under vacuum conditions. This vacuum above the water column is created by pumps, which are placed on top of the storage chamber. The flushing volume can consist of storm sewage or it can be filled up with fresh water. The maximum flushing distance of this system is around 250 m. Drawbacks of this system are the high noise level created by the air valves when the pressurisation takes place and cost intensive air-tight concrete for the storage chamber. Figure 6.8 shows the principle of the vacuum-flushing device.

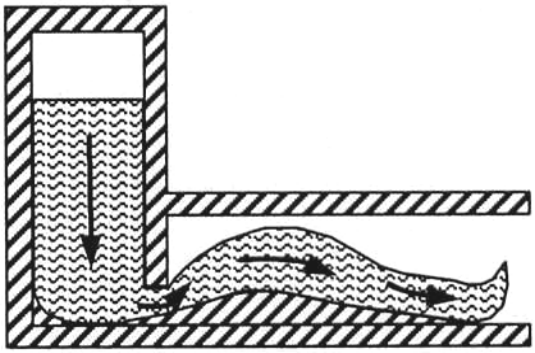

Figure 6.8: Vacuum-flushing device [Dettmar, 2001]

Both systems need a flushing sump at the end of the flushing lane to prevent the flushing wave from being reflected. Therefore deposits in end sections of the flushing lanes can be avoided. Because of the detached deposits the volume of the flushing sump needs to be 1.3 times bigger then the water volume that is used for flush waves. Table 6.2 gives an overview on the available flushing systems.

Product name	Producer	Type of flushing device
HYDROSELF	Steinhardt GmbH	Gate-flushing
Klappenlose Schwallspuelung	Vollmar GmbH	Vacuum-flushing
Typ KS	BIOGEST AG	Gate-flushing
Typ KS-OF	BIOGEST AG	Gate-flushing
Typ MF	BIOGEST AG	Vacuum-flushing
Typ OF	BIOGEST AG	Vacuum-flushing
Schwallspuelung	Niehues GmbH	Vacuum-flushing

Table 6.2: Flushing devices and producers

6.4.3.2 Tipping bucket

Tipping buckets are usually used to clean storm water retention tanks with flushing lanes up to 50 m and smaller reservoir sewers. Figure 6.9 shows the operating principle.
The bucket is placed at least 2.5 m above the bottom of the tank to obtain the necessary potential energy for a powerful flush wave. When bucket rotates around its axis the water volume is accelerated along the curved back wall to the bottom of the tank. The potential energy of the stored water is transformed into kinetic energy, which forms a flush wave with a high velocity.

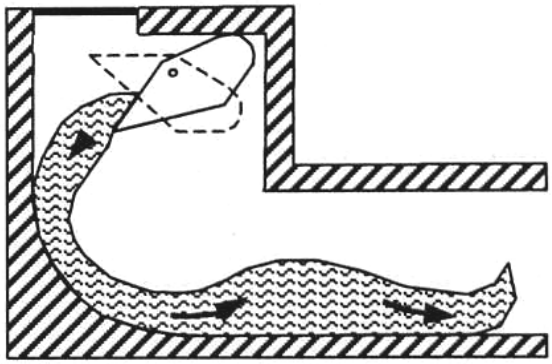

Figure 6.9: Tipping bucket [Dettmar, 2001]

At the end of the flushing lane a sump should be installed as mentioned before for the gate-flushing devices. Usually the tipping bucket is filled with fresh water from a well, which makes a pump necessary, but it is also possible to use storm water sewage. Table 6.3 shows different tipping bucket systems and their producers.

Product name	Producer
HydroSelf Tipping Bucket	Steinhardt GmbH
FluidFlush	UFT GmbH
HST-AWS	HST GmbH
Schwallspueltrommel	bgu GmbH
Spuelkippe	Vollmar GmbH
Spuelkippe	Niehues GmbH
Tipping bucket	Copa Limited

Table 6.3: Tipping buckets and producers

6.4.3.3 Flush tanks

Flush tanks are some of the oldest flushing devices and usually designed for smaller channels at the beginning of the sewer system. They are placed in manholes where they stock the dry-weather runoff. When the desired volume is reached the device is opened and the flush wave released. Flush tanks like the FABEKUN Spuelschacht or the HydroFlush from the Steinhardt company work on the siphon principle. Other flush tanks like the Spueltopf are arranged in cascades and placed aside the main sewer. They are filled with storm water sewage, which is used for the flushing when the storm event has ended. [Moine & Madiec, 1994]

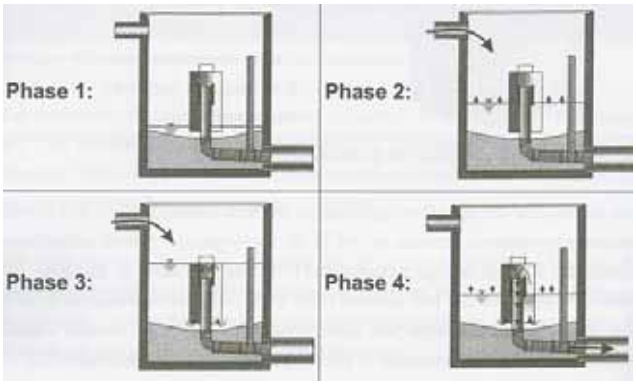

Figure 6.10: Working principle HydroFlush-Kanalspueler [Steinhardt Wassertechnik, 2005]

Figure 6.10 shows the siphon principle with the HydroFlush device. The dry-weather runoff fills the manhole until the water level reaches the height of the runoff pipe. Then the siphon starts to drain the manhole and a flush wave runs along the connected sewer channel. [Oberlack et al., 2005]

7 Literature review - Investigations on flush cleaning

The aim of investigations on flush waves are usually the hydrodynamic description and the optimization of the cleaning effectiveness. Furthermore it is also the target to investigate the boundary conditions for the application of certain flushing devices. Scientific investigations are carried out in laboratories or chosen sewer stretches by universities or research institutes. Scientific publications by developers of flushing devices are the exception.
The early investigations were restricted to measurements of the flush waves, the newer investigation combine these measurements with numerical calculations in one or more dimensional models. In single cases the sediments or the deposits in sewer channels are investigated.
The approximated solutions and results concerning the cleaning effectiveness of a certain flushing device are always connected with the problem to describe the characteristics of the local deposits. These are depending on the development of the sewer system and further local circumstances like connected catchments. [Kirchheim, 2005] Therefore it is difficult to transfer the results of single investigations to general statements. Numerical models, calibrated by field measurements, can lead to general statements concerning the cleaning effectiveness and the flush wave behaviour.
The following chapter presents the major investigations in the field of flushing and the list does not claim to be complete. The results are summarized shortly, for further information one should search the given references.

7.1 General investigations

The first serious field investigations, known to the author, were carried out by Ogden (1899) in 1897 in Ithaca, NewYork, USA. He measured the propagation of flush waves in sewers and the efficiency of the flushing regarding the scouring of stones and sand. Some of his results are given in Bertrand-Krajewski (2008).
Brombach (1982) investigated the longitudinal transport of pollutants inside a flush wave in combined sewer systems. Therefore he set up a hypothesis for the behaviour of sediments with different densities inside a flush wave by using the Helen-Shaw model. This model indicated the development of a wave after a long running time. To prove his hypothesis he investigated the movement of a real flush wave in a field test. He chooses a main sewer of nearly 2 km length, which could be flushed by opening a gate valve of a storm water tank. Potatoes, apples, tennis balls and a coloured saline solution substituted the real sediments or deposits of the sewer. The distribution of the sediments was controlled on four measuring points.

The results of the field tests confirmed his hypothesis. The heavy sediments (potatoes) move to the back of flush wave and stay in the tail. The sediments with a light buoyancy (apples) float in the front vortex of the wave and the highly buoyant sediments (tennis balls) ride in the front of the wave. The colour and the measured saline concentration of the wave core confirmed that the dissolved sediments move inside the main wave body where a secondary current is existing. (Figure 7.1)

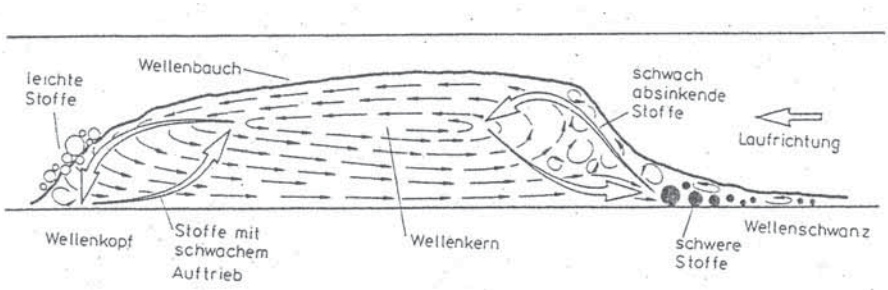

Figure 7.1: Secondary flow in a flush wave [Brombach, 1982]

The turbulence was found to be stronger in the tail of the wave than in the front. But the front turbulence was strong enough to lift deposits at the bottom of the sewer like the bio-film. The concentration of deposits was the highest in the front and in the tail of the wave. Waves with a shorter running had the highest concentration of pollutants in the front head due to the fact that the pollutants had no enough time to move inside the flush wave.

Investigations on the rotary arch are given by Barth (1996) where a real size model was installed in Dresden, Germany. The results of the flushing tests can be found in his publication. The rotary arch was described previously in chapter 6.4.2.

Campisano and Modica (2002) presented in their paper a numerical investigation on flushing sewer collectors in order to derive indications on sewer cleansing effects. The analysis was performed using the dimensionless fully dynamic De Saint Venant equations solved by the TVD McCormack numerical scheme. A large number of simulations had been run considering circular and straight sewers and adequate ranges of values of three dimensionless parameters characterising the hydraulic of the phenomena. The simulations have shown a rapid decreasing of the flow velocities and shear stresses values in the upstream part of the collector. A high influence of the flushing duration and of the flushing volume was discovered. Finally, on the basis of all simulation results, useful regressive equations have been proposed for evaluating the section length where shear stresses exceed minimum threshold values for determining the minimum shear stress maintained in a prefixed collector section. [Campisano & Modica, 2002]
Uphoff and Toews (2004) investigated the effectiveness and performance of a flush tank to compare the results with the publication of Pisano et al. (1979). The main statement of Uphoff and Towes was that several small flush waves are more effective than single large ones. To prove this they choose four different substitutes for the real sewer deposits for investigations. The first one was a single object with the density of sand, which is not described in detail. In addition sand, cellulose and flower soil were chosen. The test plant consisted of a plastic pipe with a length of 100 m and a diameter of 200 mm. The flush tank had a capacity of 450 - 500 litre. The pipe was able to be tilted with a slope

of 0 - 0.4 %.
The results showed that the shortest flushing length was achieved with sand, where the pipe slope had no influence. The flushing length of the single object was strongly dependent on the slope and it was easier affect by the flush wave due to its larger surface. The flushing length of cellulose and flower soil was also strongly dependent on the slope of the pipe. The cellulose was mostly transported in suspension in contrast to the sand, which was split up into two fractions. The lighter fraction of the sand was also in suspension with the flow but the heavier parts were moved at the bottom as a bed load.
Generally the effective flushing length was strongly dependent on the volume of the substitutes but there is no common rule given by Uphoff and Towes. The flushing length for cellulose and flower soil with a thickness of 1 cm was formulated as a function of the bottom slope. This curve was then compared with the findings of Pisano et al. (1979) with the result that the effective flushing length could never be zero.

Flushing gates and vacuum flushing are the most common cleaning devices for removing sediments in stormwater tanks and combined sewers. Guo et al. (2004) compared both in laboratory tests using a 4.57 m long flume and a connected flush tank. The tank was closed with a vertical gate on its downstream end to simulate the gate flushing device. For the vacuum flushing the tank was closed on the top and the vacuum was created using a PVC air valve. Sand was chosen for a non-cohesive sediment in grain sizes between 0.075 and 0.25 mm with an initial thickness of 2.5 cm. After each flushing run the sediment flushed into the trap at the end of the flume was collected, dried and weighted. The sediment layer thickness before and after the flushing was measured to record the sediment distribution.
The movement of the water and the sediment was videotaped and digitised to obtain data on the flow velocity, the shape of the flush wave and the draining velocity in the flushing tank. Initial conditions in the flume varied from a dry sand bed to a filling with water of 5.1 cm. In total 34 flushing runs were carried out with different sediment weights (17 kg and 34 kg) and initial water depths in the flushing tank of 86.4 cm and 44.5 cm height.
For equal initial conditions the gate and the vacuum flushing showed similar weights of moved sediments. Generally the weight of the flushed sediment increased with the initial water depth in the flushing tank. The double depth of water lead to a triple weight of sediments. The weight of the flushed sediment decreased with an initial water depth in the flume. The rise of the water level from zero to 2.5 cm reduced the weight of the collected sediment by 51 %. A change in the opening height of the flushing gate resulted in an only slightly changing weight of flushed sediment. The larger gate opening height increased the flushing velocity but decreased the flushing duration. The effect of the flushing velocity was smaller then for the flow duration.
The digitised video recordings showed the flush wave in form of a moving hydraulic jump with deeper water level in the middle of the wave, smaller water level in the front and in the end of the wave. Existing chosen fluvial sediment transport equations were calculated and found to be inadequate to predict the sewer sediment transport.

The aim of an investigation of Dettmar and Stauffer (2005b) was to determine the behaviour of the activated storage volume of flush waves on the cleaning performance. To optimise the flushing with so-called Storage-Volume-Activated-Devices numerical studies were carried out. The cleaning performance was described by the value of the bottom

shear stress, which had to exceed the value of 5 N/m^2 to assume a cleaning effect. Therefore a one-dimensional numerical model based on the Saint-Venant equations solved by the Finite Volume Method was used to investigate the propagation of the generated flush waves. The model was designed to analyse transient flows in complex geometric environments and steep slopes. [Dettmar & Stauffer, 2004]
To describe the effects of the responsible variables(slope, dam-height and storage length) on the cleaning performance, several runs simulating flush waves were carried out changing a single parameter for each run whilst the sewer diameter and the roughness were kept constant. When the shear stress went below the critical limit the effective flushing distance ended.
By varying the slope of the storage section, the achieved flushing distance increased with a rising volume. It seemed that the maximum flushing distance stays within a limit. Thus a maximum value for the volume is to be expected. If this value is exceeded for a given dam-height additional volume will not contribute further to the cleaning performance. The results for the influence of an additional storage length showed that enlarging the volume by increasing the storage length will generally advance the flushing distance. As seen before, the calculated values proceeded towards a limit. Regarding the effect of enlarging the flushing volume by raising the dam-height, a higher dam-height caused a longer flushing distance. If the same volume was created with a shorter storage length but with a higher dam-height, the cleaning performance was more favourable. This indicated a major influence of the dam-height on the cleaning performance. It is reasonable that the strong impact of the dam-height is due to the stored potential energy, which is higher and closer to the flushing line if the dam-height is raised instead of extending the body of water towards the storage section.
As a result of the dominant effect of the dam-height and its upper restrictions within sewers, longer flushing distances were achieved in big sized sewers. For a sewer with a diameter of 2000 mm and a dam-height of 1.6 m, a flushing distance of above 1500 m was calculated. This underlines the primary use of such devices in main sewers. [Dettmar & Stauffer, 2005b]
Further detailed practical and numerical investigations on flush cleaning of Dettmar can be found in his dissertation. [Dettmar, 2006]

The paper of Kirchheim et al. (2005) presents a scientific research carried out on the flushing of a 350 m long stormwater holding tank in the sewer system of Wetzlar, Germany using a flushing gate system. The analysis is based on three-dimensional numerical modeling solving the averaged Navier-Stokes equations using the $k-\epsilon$ turbulence model. The free surface water-air interaction is handled by the Volume of Fluid (VOF) method. Several scenarios for different boundary conditions concerning the flushing device have been tested. To evaluate the cleaning efficiency it was very important to investigate the shear stress created by the flush wave. It could be shown that the influence of the initial condition is less important for long-term purifications. The length of the channel, which could be cleaned by a flush wave depends predominantly on the flushing volume.
It was possible to calculate different scenarios in the sewer channel and to approximate the cleaning capacity of a flushing system. The results showed that the flushing volume and the roughness at the bottom and walls are the key parameters, which should be subject to further investigations. With an increasing flushing volume higher shear stress rates were achieved and longer channels could be cleaned. The geometry of the flushing gate had only an effect on the flow conditions close to the gate and was less important

for the design of flushing systems for long sewers. The efficiency of this flushing system and the effectiveness to clean a very long sewer section was shown.

Another investigation describing a flushing gate system, here the HydroSelf system of the Steinhardt Company, is presented by Yu and Tan (2006). Their paper presents an investigation of the performance of the hydraulic and sediment removal of a flushing system in a detention basin in Singapore. A hydraulic criterion for the design of the flushing system is proposed and an equation for the maximum height of the flushing wave front as a function of the distance from the gate, the initial water depth in the chamber and the chamber length is proposed. The Lauber and Hager equation [Lauber & Hager, 1998] for the maximum velocity of a flushing wave is also verified by the authors. They state that effective removal of sediment particles on the bed is a direct function of the bed shear stress generated by the flushing flow. The study also reveals that the bed shear stress on the channel bed induced by the flushing flow can be attributed to the hydrostatic pressure, the flow acceleration, and the convection-induced momentum. The shear stress associated with fluid distortion and the turbulent viscosity may be neglected. An significant error would occur if the hydrostatic pressure component were used as an estimate of the bed shear stress on a mild slope channel. The energy slope method may provide an overestimation of the bed shear stress. Finally, an appropriate equation to evaluate the maximum bed shear stress is proposed. [Yu & Tan, 2006]

One of the most recent investigations on the effect of sewer flushing was carried out by Steinhard and Schaffner (2006). Sewer deposits up the 15 cm height affected the investigated main collector running towards the treatment plant of the city of Frankenberg. During dry-weather periods they were solidified at the bottom of the sewer and parts of them were removed after storm events. The cleaning of the main collector was necessary to save the connected river and the operation of the treatment plant.
The main collector to the treatment plant had as diameter of 1100 mm and a dry-weather runoff in the main sewer differs between 40-80 l/s. The storm-weather runoff can be up to 2000 l/s. The investigated sewer had a length of 713 m from an overflow to the treatment plant and two lateral inflows (DN 300 and DN 400) were discharged. The average slope in this stretch was 0.9 ‰ with some parts having no slope. The HydroFlush GS DN 1100 flushing shield was installed in an overflow structure, which was place within the main sewer. The storage level behind the gate can was varied between 0.6 - 0.8 m.
Measurements of the available sewer deposits were taken. The sediments downstream of the flushing shield were measured before the release of the first flush wave. The HydroFlush GS was deactivated for 6 month before the flushing tests started. During this time sediments were accumulated to a height of 8 cm at the bottom of the sewer channel. Close to the flushing shield deposits of 10 - 15 cm height were measured. The flush waves created by the HydroFlush GS were measured to obtain the necessary data for the calibration of the numerical model. Therefore the temporal heights of numerous flush waves were recorded in manholes using five ultra sonic probes. The flush waves were displayed along the sewer for different time steps so it was possible to calibrate the numerical model.
The numerical investigations were carried out using the three-dimensional simulation model SSIIM (Sediment Simulation In Intakes With Multiblock Option) developed by Prof. Olsen (Norwegian University of Science and Technology, Trondheim, Norwegen) for hydraulic calculations of free-surface runoffs and sediment transport. [Olsen, 2002]

[Schaffner et. al., 2004] The bottom shear stresses were calculated with the turbulent kinetic energy k of the $k-\epsilon$ turbulence model as described in chapter 3.3.2. The structured numerical grid of the main collector in Frankenberg consisted of 52250 grid cells. The width was divided into 11 grid cells (δy = 0.22m) and the total length of 1423.5 m was split up into 950 cells (δy = 1.5 m). The actual water level was discretized with 5 cells of 20 % depth each. The size of the iteration time step was 0.05 s. The roughness of the channel was chosen to a Manning Strickler value of 100, which is equal to 0.3 mm, and the storage level at the HydroFlush GS was chosen to 70 cm. The calibration of the numerical model was carried out comparing a measured wave with an initial storage level of 70 cm with a modelled wave at the location of relevant ultrasonic probe.

Beside the calculation of the water level the determination of the bottom shear stresses for the evaluation of the cleaning effectiveness was the main aim of this investigation. The mode of flush cleaning had also to be considered when the shear stresses are regarded. The HydroFlush GS sends regular flush waves into the sewer channel. Depending on the dry-weather runoff this happens several times a day. Therefore it is in contrast to flushing devices in storm tanks, which flushes only once after a storm event with long dry-weather periods in between. The regular flushing of the HydroFlush GS prevents the permanent consolidation of the deposits and makes it easier to remove them. The maximum downstream values for the shear stress during the initial phase of the flush wave were between 5 - 10 N/m^2. Along the main sewer the maximum shear stress generated by the flush wave was calculated to 4 N/m^2. This value was not reached with the front wave, it was achieved by the main part of flush wave and was kept persistently. The measurements in Frankenberg revealed that the sewer was not completely drained because of its length and low slope before the flushing started. To overcome this problem the flushing volume for the HydroFlush in Frankenberg was increased to create a flush wave with more backwater.

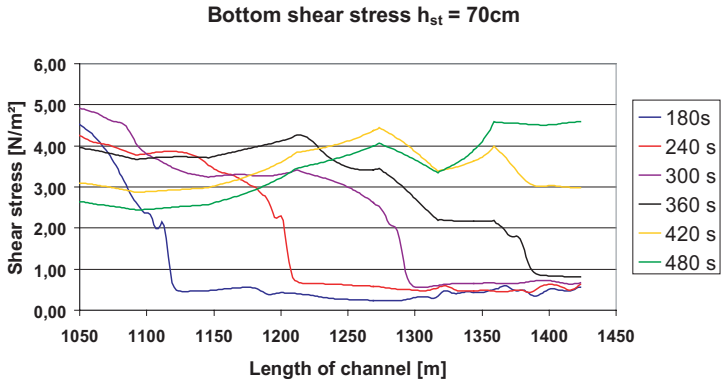

Figure 7.2: Distribution of shear stress at the end of the sewer channel [Steinhardt & Schaffner, 2006]

Figure 7.2 shows the progression of the shear stress at the end of the sewer at different times steps. It shows the distribution of the shear stresses between 3 - 4 N/m^2 which were created by the main part of the flush wave. Especially at the end of the sewer is necessary to maintain the cleaning effectiveness of the flush wave. In the present case it was possible to achieve this result under difficult boundary conditions.

The investigation of the shear stresses of the sunk wave upstream of the flushing shield showed an interesting development. An inverted siphon with a diameter of 700 mm placed 100 m upstream of the HydroFlush GS. Siphons can, depending on their shape, create high hydraulic losses for flush waves. The wave can lose much of its cleaning power when it is passing a siphon. Therefore it was the idea in Frankenberg to use the sunk wave, which moves upstream to clean the sewer channel and the siphon. The siphon in Frankenberg had no significant jump at the bottom of the sewer, so it is relatively easy for the flush wave to flow through it. The reduction of the diameter from 1000 to 700 mm leads to higher flow velocities and therefore higher shear stresses. Within the siphon shear stresses up to 16.8 N/m^2 were calculated. (Figure 7.3)

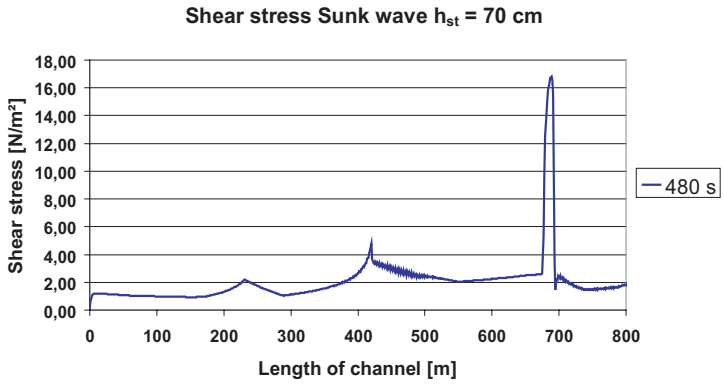

Figure 7.3: Distribution of shear stress upstream of the flushing shield [Steinhardt & Schaffner, 2006]

These values indicate a good cleaning effectiveness of the sunk wave in the siphon. The maximum shear stresses of the sunk wave upstream of the siphon were calculated to 4 N/m^2, which is still a good result for the design of the flushing system. The observations of the sediment transport during the measurements support the result of the calculations. The results of the numerical calculation also showed that 50 % of the storage length upstream of the flushing shield can be cleaned effectively by the sunk wave.
The numerical investigations of the shear stresses at the bottom of the main collector in Frankenberg created by the flush wave proved the excellent cleaning results of the HydroFlush GS observed by the representatives of the city of Frankenberg. They showed that it is possible to clean sewer channels with difficult boundary conditions like a very low channel slope or a remaining water level effectively for long distances. [Steinhardt & Schaffner, 2006]

Butler et al. [2005a, 2005b] analysed the movement and behaviour of large solids in small sewers in several experiments. They investigated the forces on sanitary solids and develop the model SOLID, which describes the movement of solids in small sewers based on the Method of Characteristics solution of the Saint Venant equations.

Further, very early, investigations on sewer flushing were published by Pisano et al. in the year 1979 in the EPA report *Dry-Weather Deposition and Flushing for Combined Sewer Overflow Pollution Control*. [Pisano et al., 1979] Pisano also published in 1998 a detailed overview on sewer flushing systems, case studies in Germany and a cost analysis of sewer and tank flushing systems. [Pisano et al., 1998] Another EPA report concerning

corrosion and pollution control was published by Fan et al. (2001). A case study of the sewer and drainage flushing system in Cambridge, Massachusetts shows the successful application the HydroSelf flushing system. [Pisano et al., 2003] Later results of a case study in Cambridge, Massachusetts and a cost analysis are presented by Fan (2004).

7.2 Flushing with gate valves

Macke and Froehlich (1981) investigated the cleaning efficiency of a closing gate valve to use the stored water volume for the removal of downstream deposits. Therefore they constructed a physical sewer model with two channels of 290 mm and 192 mm diameter using the Froud similarity. The real channel had a diameter of 2600 mm. With the aid of a model sediment (Sand $n' = 0{,}52$) the cleaning length, the temporal distribution and the height of the sediment layers was determined.

The following observations were made:

- The main part of the sand vacation (93,2 %) took place in middle of the flush wave.
- The initial concentration of solids was reduced slowly.
- After 50 s the flow regime changed from supercritical to subcritical.
- The subcritical flow showed a low transport volume.

The final cleaning situation of two consecutive flush waves showed a relocation of the deposits by the first wave and a comparatively low cleaning success by the second wave. (Figure 7.4)

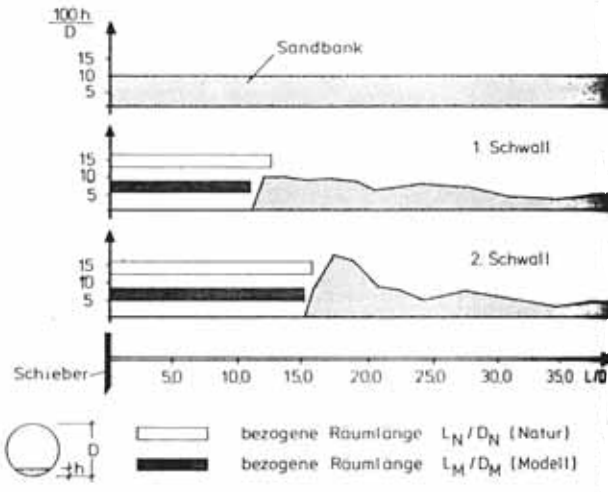

Figure 7.4: Final cleaning situation for two flush wave with an initial sediment height of $h/D = 0{,}06$ [Macke & Froehlich, 1981]

Measurements of Drews (1979) in the sewer system of the city of St. Pauli / Hamburg proved the low cleaning effectiveness of the flushing with gate valves as shown by Macke and Froehlich (1981).

To optimise the flush cleaning with a gate valve the following list of recommendations are formulated by Drews:

- To create an optimal front wave the width of the gate opening a in ratio to the pipe diameter D should be chosen according to the following values:

$$0,23 \leq \frac{a}{D} \leq 0,26 \tag{7.1}$$

- The cleaning effect is favoured by a fast opening of the gate valve.
- The cleaning effectiveness could not be improved when the storage length exceeded 300-fold the diameter of the sewer pipe. (for $I_s = 1 : 1500$ to 3.000)
- The cleaning effectiveness is constant and independent of the storage length for subcritical flows.
- A complete opening of the gate valve increases the cleaning effectiveness for subcritical flows.
- The cleaning effectiveness of gate valves is comparative small for a low sewer slope and deposits with a high mineral content. Therefore the usage of gate valves is recommended only for carefully chosen locations in the sewer system with ideal boundary conditions.

Lorenzen investigated the effects of two gate valves in main sewer channels in the city of Hannover, Germany to prove their cleaning abilities in chosen sewer reaches. [Lorenzen et al., 1997] The sewer channel for mixed sewage had a length of 2400 m with a diameter of 1800 - 2400 mm. After 1340 m length it had a lateral inflow. One part of the sewer with a length of 50 m had a width of 4 m, a height of 2 m and was called Wide Chamber. The bottom slope of the channel was between 1.2 ‰ and zero, which led, together with four bends, to sediment accumulation after 1200 m length. The flushing device consisted of two, not described, gate valves. One was placed after 611 m and the second was installed in the inflowing channel. The storage height was 1.9 m with a storage time of 12 hours. There was no information given concerning the storage volume. The opening time for the gate valves was given with 5 min. Due to the slow opening time the created flush wave can not be considered as a dam-break wave, which makes the results difficult to compare to standard flushing devices. The measured sediments showed a height of up to 20 cm in the wide chamber. The texture of the deposits consisted of sand at the bottom and muddy organic material in the top layers. The mean particle size was measured with $d_{50} = 0.6$ mm. Additionally the water level and vertical velocity distribution were measured with an induction device. After the measurement of the initial conditions five flush waves were created before the sediment heights were taken for the second time. The results showed, that for 600 - 700 m the flushing was effective. The deposits at the bottom of the channel were removed and transported with the wave. In the wide chamber only the organic material was moved by the flush wave. The heavier parts, sand and gravel, remained at the bottom. Even after further 24 flushes the situation did not change. The second part of the investigation was regarding the effect of the flush waves on the long-term cleaning of an initially high-pressured cleaned sewer. It became obvious that the flush waves created by the gate valves were not strong enough to keep the sewer free of sediments. Even the combination of both gate valves were not powerful

enough to create the necessary bottom shear stress to avoid sedimentation.
Lorenzen made several conclusions on the results of the flushing test. He stated that the cleaning success of a flush wave is depending on the storage height, the flow velocity and the duration of the flushing. He did not regard the storage volume but he gave the general statement that a long flush wave is equally effective as a short flush wave. The turbulence and the shear stresses in the front wave are responsible for the lifting of the deposits. In contrast to his investigations Lorenzen stated that is more effective to create several consecutive flushes than single large flush waves. He also concluded that a remaining water body would degrade the energy of a flush wave and therefore the cleaning success. Flush waves will remove most of the biogenetic material of the deposits and this leads to less pollution of receiving waters during rain events. These investigations and the results were also published in Lorenzen et al. (1996).

Ristenpart (1998) carried out flushing test with gate valves in two parallel sewer channels (diameter 1500 mm) in Hildesheim, Germany. By measuring the water level, the flow velocity, the deposit level and the deposit volume before and after the flushing, he found that frequent but less intensive flushing is more effective than a single flush wave of high intensity.
Ristenpart was not able to clean the sewer on the whole investigated stretch using the flushing device. Only 6.30 m were totally cleaned. (Figure 7.5) He determined that for a certain deposit volume no further cleaning was possible, which would be due to a balanced condition of the deposits. The complete cleaning of a sewer with deposit bed would not be possible under the circumstances in Hildesheim, but keeping a sewer clean for a long duration by regular daily flushing after an initial cleansing could be achieved.

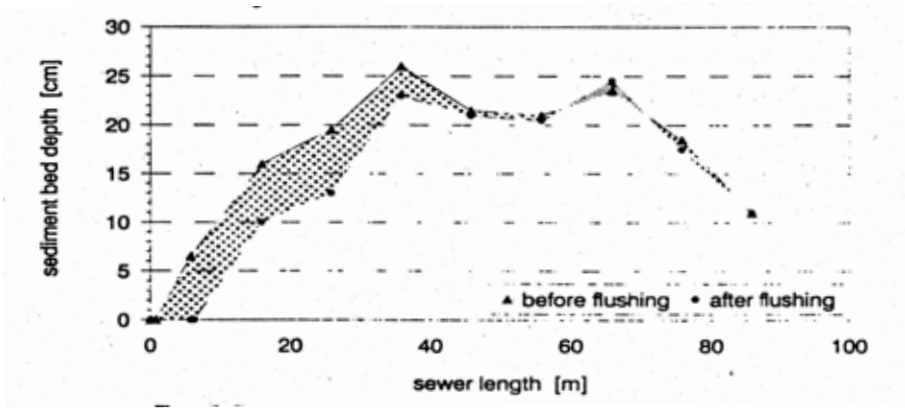

Figure 7.5: Change of the deposit level caused by flush waves [Ristenpart, 1998]

These results were confirmed by Gendreau et al. (1993), who investigated the effect of flush waves on sand in laboratory tests. Therefore Gendreau use a servo-controlled weir to create flush waves from a tank into a 24 m long flume to observe the motion of the sand. He determined that the sand is transported for a longer time when the weir was opened fast with a high storage level. The complete drainage of the storage tank ($V = 4.8\ m^3$) led to the best transport results for the sand particles.

Experimental and numerical investigations on the scouring effects of flushing waves on sewer sediment deposits were presented by Campisano et al. (2004). An experimental series was carried out in a laboratory channel using a simple flushing device and consid-

ering different boundary conditions. The main idea was to develop a simple model to describe the scouring effects of flush waves on a non-cohesive sediment deposited on the bottom of a sewer channel. The results of the numerical model were then compared with the results of the laboratory experiments to derive indications on the scouring processes due to the flushing operations.
The flush tests were carried out in a 3.9 m long and 0.15 m wide rectangular channel with a slope of 0.145 %. The flushing device consisted of a stainless steel plate, which could be opened very fast to create a dam-break flush wave. Volcanic sand was used as a substitute for sewer deposits. The one-dimensional numerical model was based on the Saint-Venant equations for unsteady flow and Exner equation for the sediment continuity. The bed-load transport of the sediments due to the unsteady flow conditions caused by the flush waves was calculated by the equations of Meyer-Peter and Kalinske. The Saint-Venant equations were solved numerically using the second order MacCormack scheme. This scheme is shock-capturing, which means it is able to describe discontinuities such as hydraulic jumps and shock waves over an initially dry bed. It is well suited to analyse the movement of flush waves. To reduce the numerical oscillations caused by high gradients in water level and flow rates the total variation diminishing (TVD) scheme was also applied.
The results of the numerical model for the progression of the flush wave were compared with the experimental data and showed a very good agreement up- and downstream of the flushing gate. The movement of the sediment was well reproduced for the first flushes but with an increasing number of flush waves the differences between measured and simulated results became obvious. Tests with changing boundary conditions and different variable for the Meyer-Peter and Mueller formulae led to better results. A good agreement was also found for the comparison of the washed out sediment weights and the scoured section lengths after a number of n successive flushes. To summarize the results it can be stated that the numerical model offered a good reproduction of the experimental data from the laboratory channel.

Campisano et al. (2005) also presented the results of a dimensionless numerical investigation on the scouring performances of flushing waves. The investigation has been performed using the numerical model mentioned before. It was validated on the basis of laboratory data. The evaluation of the dimensionless sediment transport rate Q_s has been derived from the Meyer-Peter and Muller's formula. The flush waves were created by a vertical lift gate in a laboratory channel.
The experimental evaluation of the performances of the flushing waves was carried out by measuring the scoured flume lengths L_s, the distance between the initial position of the upstream deposit front and its position after n flushes. The bed profile evolution was also monitored by measuring the sediment heights h_s along the flume at the end of each flush. The numerical simulations have allowed evaluating the scoured channel lengths downstream of the flushing device, as a function of the number of performed flushes and for different values of the identified dimensionless parameters. The results have pointed out the increase of the scouring effects as the channel slope increases and the sediment grain size decreases. The results have also provided information on the design and set-up of the flushing devices, with a specific reference to the evaluation of the most effective hydraulic conditions of the flush. In particular, the results have shown a slight convenience in operating a small number of flushes with high water heads instead of frequent flushes with lower water heads. [Campisano et al., 2005]

The most recent investigation of Campisano et al. (2006) was carried out on flushing experiments with cohesive sediments. The aim was to evaluate the effects of fine cohesive sediments include into a granular sediment bed. Therefore a bed of sandy material was formed in a 17 m long laboratory flume as a reference condition for the first experiments. Then a clay-silt mixture was added to the sand in measured values of 10 and 20 % weight content. The addition of the fine particles allowed keeping the initial experimental conditions equal to the one performed with purely sand deposits. The fine material was able to fill a part of the sand porosity without changing the initial height of the sediment bed. The critical shear stress τ_{crit} for the erosion of the sediment mixture was evaluated between 1.4 - 3.3 N/m^2 depending on the percental content of fine material. A vertical lifting gate at the upstream end of the flume generated the flush wave. The deposit bed evolution was measured as well as the sediment masses flushed out by the waves.
The observation of the erosion processes during the experiments showed the prevalence of bed-load transport for sand particles while the silt-clay material was observed to move mainly as suspended-load. It also became obvious that for the first flushes the addition of fine material slowed down the advancement of the sediment bed. The more the content of fine material increased the more the movement of the sediment bed was slowed down. Differently from what was expected, with an increasing number of flushes, higher erosive effects occurred in beds with fine material. The removed sand masses were larger for deposits with fine material.
The experimental data derived from this investigation will be taken by Campisano for the validation of numerical models developed for the effects of flush waves on sewer deposits with cohesive properties. [Campisano et al., 2006]

7.3 Investigations on the Hydrass or Berlin flushing gate

Several investigations are concentrated on the optimisation of the Hydrass or Berlin flushing gate, which is described in chapter 6.4.1. (Figure 7.6)

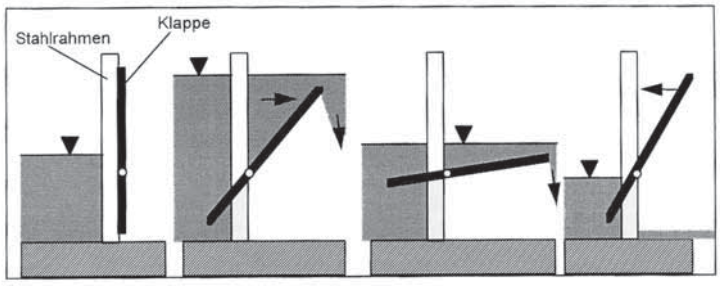

Figure 7.6: Function principle of the Hydrass gate [Haumann, 1999]

The Hydrass valve is widespread in usage in large French cities like Paris or Marseille. [Sikora, 1989] The velocity of a flush is depending on the dry-weather runoff, the geometry of the sewer channel, the height of the flushing gate and the storage length. [Bachoc, 1992] The characterisation of the flush wave by its height, velocity and duration can give an extent of the potential cleaning success. The time and the frequency of the flushing are also vital for the cleaning result. [Lorenzen et al., 1997]

Lorenzen et al. (1998) presented in their publication the results of an investigation in an egg-shaped sewer in Marseille, France. A Hydrass gate was installed in this main sewer to observe the effects of the flush waves on the downstream sediments. The storage height was 0.72 m and the time between two flushes was 18 minutes. The measured sediment with a mean size of $d_{[50]}= 3$ mm were coarse compared to the sediments Lorenzen found in Hannover. The main goal of the installation of the Hydrass gate was to lift the deposits and transport them to a downstream sewer, which had a higher self-cleaning ability. After 700 flushes during one month all the sediments were removed from the investigated sewer. In the following no further sediments could be measured at the bottom of the sewer. The numerous flush waves created by the Hydrass gate were able to remove all sediments and keep the sewer clean on a long-term basis. (Figure 7.7)

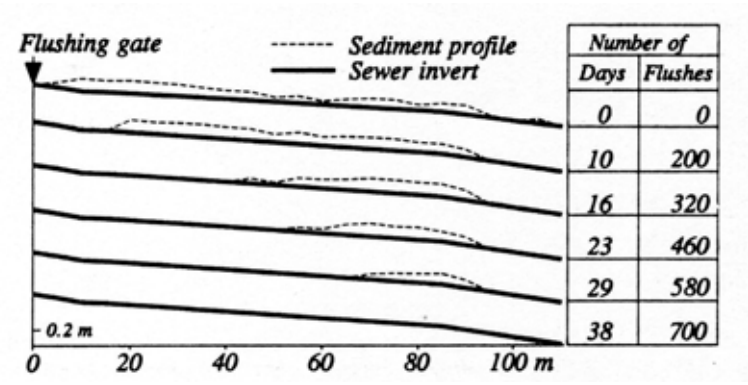

Figure 7.7: Movement and reduction of the deposit level after the installation of a Hydrass flushing gate in Marseille [Chebbo et al., 1996]

In his publication in the year 2000, Dettmar gave an overview of the most used flushing devices and their operational areas. He also showed water level measurements of a flush wave created by a Berlin flushing gate in a sewer channel in the city of Goettingen.
The investigations of Dettmar on flush waves created by the Berlin gate were carried out in Aachen and Goettingen to observe the application of the gate in large and small sewers. The design of the Berlin gate is based on the before mentioned Hydrass gate. It uses the dry-weather sewage of main sewer channels to create flush waves for the cleaning of deposits. The functional principle of the Berlin gate depends on the rotatable gate parts. The lower parts with the smaller area are heavier than the upper part. The flushing volume is stored in the vertical position of the gate. When the torsional moment of the lower gate part is exceeded by the torsional moment of the upper part the gate swings into a horizontal position. Then the flush wave is released. (Figure 7.8)

Figure 7.8: Berlin gate [Dettmar et al., 2003]

A further investigation carried out by Dettmar (2001) was concentrated on a small sewer, which is not accessible by man. Therefore the installation of the gate had to be done in a manhole. The regarded sewer had a diameter of 400 mm and a length of nearly 500 m. The water level and the velocity of the flush waves were measured to document the propagation of the wave. (Figure 7.9)

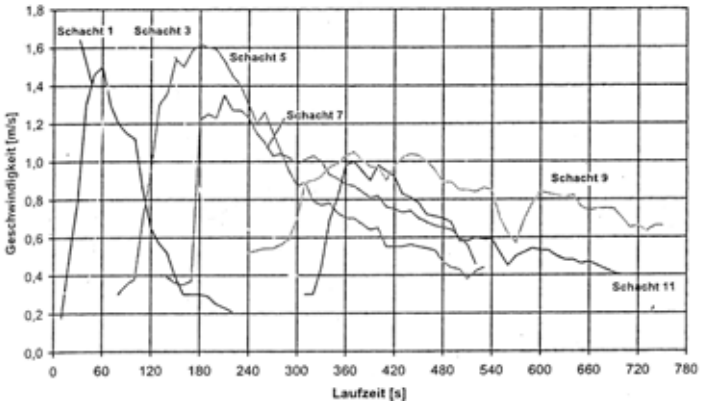

Figure 7.9: Distribution of flow velocity at different locations of the investigated sewer [Dettmar et al., 2001]

The nature of the flush wave is clearly visible. At the beginning close to the flush gate the wave is steep and short formed. After a longer distance the shape of the wave is longer and more flat due to the influence of the bottom friction. During the test 50 flush waves were created daily and all of the deposits in the observed sewer were removed.

Another analysis was carried out in a larger sewer of 1200 mm diameter and 500 m length. A flush volume of 180 m^3 was stored by the Berlin gate which was now installed inside the sewer. Dettmar measured the height of the deposits on the bottom of the sewer before and after the flushing tests. He found moveable and consolidate mineral deposits of up to 20 cm height. After the investigation the lighter deposits were removed

by the continuous flushing but the consolidate sediments remained in their locations. Dettmar suggested a longer usage of the flush gate to remove them too.
The bottom shear stress created by the flush waves was also calculated in several locations along the sewer by measuring the water depth and the flow velocity at the same time. Directly at the flush gate a maximum shear stress of $\tau_{max} = 15.3$ N/m^2 was recorded. In a distance of 200 m to the gate $\tau_{max} = 3.8$ N/m^2 was measured and close to the end of the sewer, 480 m away from the gate, $\tau_{max} = 1{,}7$ N/m^2 could be surveyed. Beside the advantage of the flexibility of the Berlin gate Dettmar also mentioned the drawbacks. The leakage rate of the gate can cause problem if the dry-weather runoff is lower the leakage of the gate. Then no water will be stored and sediments will contaminate the gate and the upstream sewer, which influences the efficiency negatively. [q.v. Lorenzen & Laplace, 1998] The application of the Berlin gate is also restricted for sewer with a very large dry-weather runoff. Here the flush gates tips to often and releases many waves in a short period of time. The flush waves overlay each other and this will cut down their cleaning efficiency. Dettmar suggests that the flushing should take place between 8 and 72 times a day and the height of Berlin gate should not exceed 2/3 of sewer diameter. The overflow of the gate during storm events in case of a gate failure must be possible. [Dettmar et al., 2001]

The dissertation of Linehan (2001) outlines a study into the effects of using various flushing devices on sewer sediment beds. Experiments were carried out in a laboratory channel and two styles of gate were tested, lifting and tipping. Two lifting and two tipping gates were studied for different boundary conditions. The hydraulics of each gate were investigated and each gate was tested using a sediment bed made up of silica sand on a length of 6 m with 10 mm depth. The gates flushed over this sediment bed and the sand was picked up from the channel end, dried and weighed. The results from this were then compared with a control value to assess the transport occurring in each situation. The results showed that the most effective style of gate for the transportation of sediments is the lifting gate. (Figure 7.10)

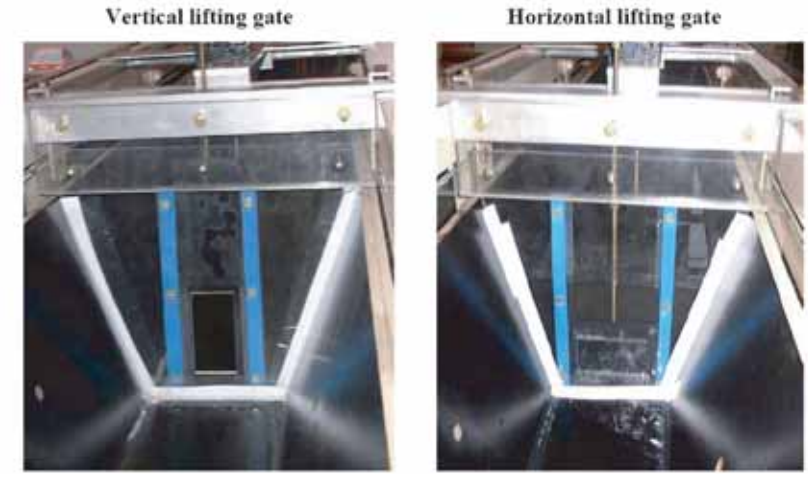

Figure 7.10: Horizontal and vertical lifting gate [Linehan, 2001]

This type of gate out performed the tipping gates in all the sediment transport experiments. (Figure 7.11) It is also supposed to be better due to the initial velocity of

discharge from the gate is in a lateral direction, whereas the tipping gates drop a large volume into the channel, which then accelerates downstream. This lateral discharge continues downstream with a good velocity, thus transporting a higher amount of sediment.

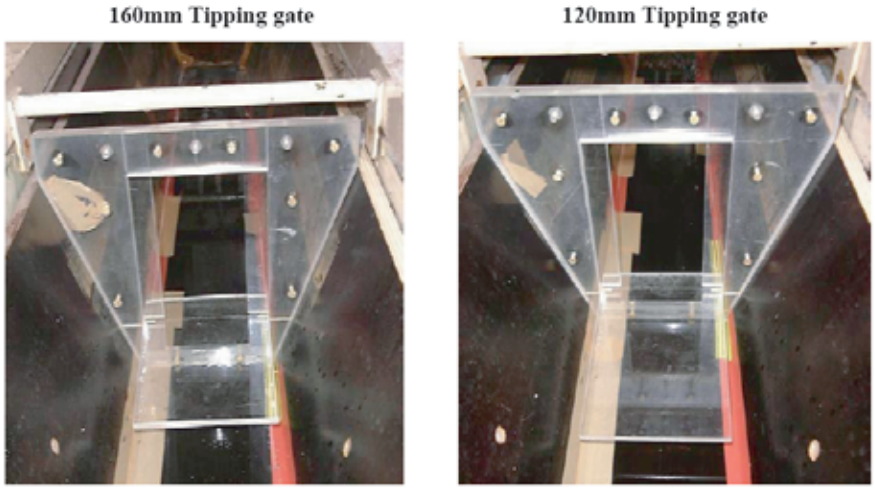

Figure 7.11: Horizontal and vertical tipping gate [Linehan, 2001]

The most effective lifting gate was the horizontal lifting gate. This is proven by the results of the sediment transport experiments, where the horizontal lifting gate moved the most sediment from the first meter downstream of the gate. The horizontal gate was better than the vertical lifting gate due to the higher average pressure acting over the area of the orifice. This higher pressure causes a higher velocity of discharge from the gate, and thus moves more sediment. The reason the horizontal orifice has a higher average pressure acting over it is because this gate is at a lower average level than the vertical orifice. The results of the further sediment transport experiments showed that a higher upstream starting head is more effective than a lower one, even with the a similar volume of fluid being flushed. The experiments also showed that the first flush of a set is the most effective at transporting sediment and subsequent flushes do transport sediment to a lesser degree. The discharge experiments revealed how the discharge through the horizontal lifting gate decreases as the head decreases. Finally, the bed form experiments demonstrated how velocity and depth of flow decrease slightly, as the upstream head falls. This is a direct consequence of the decreasing pressure over the orifice, and therefore decreasing discharge. [Linehan, 2001]

In Lyon, France investigations on the hydraulics and the efficiency of the Hydrass flushing gate were carried out by Bertrand-Krajewski et al. (2002). Therefore a Hydrass gate was installed into an egg-shaped sewer of 1.8 m height under the Pompidou Avenue. The main objects were to define an empirical relationship giving the flow discharged by the gate as a function of the upstream water level, to observe how the flush propagates in sewers and evaluate the distance along which the gate may potentially remove sediments. The downstream reach had a length of 300 m and the upstream sewer was 275 m long where the flushing volume of 57.70 m^3 was built up. The initial storage level at the flushing gate was 0.86 m.
The flush waves were measured up- and downstream using ultrasonic probes for the

water level and Doppler velocimeter for the calculation of the flow off rate and observe its evaluation in time. The downstream sensors were moved to several positions to gain measurements at different locations along the sewer reach. The flushing gate tipped every 45 minutes and the drainage time was measured to 2.5 minutes in dry-weather conditions.
According to the author it was difficult to formulate an equation for the relation between the runoff Q_v and the upstream water level h_{am} due to the complex hydraulic situation with an over- and underflow of the flushing gate. Field observations showed that most of the flow is under the tipping gate. With the measurements of 10 different flushes the following polynomial relationship was derived which has to be calibrated for each new location. Equation 7.2 is valid between storage levels of 0.86 m (Opening of the gate) and 0.49 m (Closure of the gate). The model was tested successfully in further investigations.

$$Q_v = -276.86h_{am}^4 + 767.32h_{am}^3 - 776.85h_{am}^2 + 341.76h_{am} - 55.086 \qquad (7.2)$$

The evaluation of the cleaning efficiency was carried out by calculating the bed shear stress τ_0 using formulae 3.85. The maximum values of the shear stresses were 7 - 9 N/m^2 with mean values of 5.4 - 6 N/m^2. According to the Shields criterion for sand particles this would be large enough to move sediments of 7 - 9 mm diameter during the peaks and 5 -6 mm considering the mean bed shear stresses.

The problem of the hydraulic description of the outflow through the horizontal tipping gate lead to further investigations by Bertrand-Krajewski et al. (2004, 2005a). Here an experimental study of a scale model under steady conditions was carried out to determine the behaviour of the device during the flushing phase and outflow relations for different boundary conditions. For unsteady conditions a numerical model was set up to validate the data of the previous investigations in the Lyon sewer system.
The experimental site was located at the University of Catania in Italy using a 4 m long flume with a 0.15 x 0.30 m cross section. To approximate the egg-shaped sewer of Lyon custom shaped steel profiles were inserted. The model of the Hydrass gate was built in a relation of 1:7.
To derive outflow relations for different hydraulic conditions measurements of the water level upstream and the flow rate in the flume were carried out for different inclinations of the gate. The authors considered the outflow over upper part as flow over an inclined weir. Depending on the upstream water level, the outflow through the lower part of he Hydrass gate can be considered as the flow through a pressurized orifice or as the flow over a weir, made up by the lower frame of the gate. The discharge coefficients μ_i were evaluated with three series of experiments where the boundary conditions like the flow rate were changed.
To confirm the equations and to describe the outflow through the tipping gate the outflow relations were tested under unsteady conditions using data from the experiments on the Hydrass flushing gate in Lyon. [Bertrand-Krajewski et al., 2002] The relations were implemented into the numerical model as used by Campisano et al. (2004). In addition a further procedure based on the theory of Total Variation Diminishing (TVD) was coupled to the McCormack scheme for reducing the numerical oscillations generated in case of high gradient in hydraulic variables.

The before mentioned sewer reach of the Pompidou Avenue in Lyon was simulated using this model. The results showed a good agreement for the up- and downstream propagation of the flush wave created by the Hydrass gate.

Analyses on long term monitoring of sewer sediment accumulation and flushing experiments were carried out by Bertrand-Krawjewski et al. (2005b) for 4 years starting in 2000, to contribute the knowledge and the modelling by investigating a 1.8 m high and 400 long egg shaped combined sewer in Lyon/France.
This sewer shows a very flat profile ($I_s = 0.02$ %) with some negative slopes. The dry-weather flow is 40 l/s. Measurements of the water level and the flow velocity were taken continuously with a 2 min time step. The sediment build-up was measured manually every week with a space step of 5 m over a period of 36 month. During this time no cleaning of the sewer took place. Samples of the sediments were taken periodically to determine the grain size distribution, density, water content, total organic carbon (TOC) and the organic fraction. Structure investigations were carried out with frozen samples of sewer sediments. The sediments were mainly mineral and all mentioned characteristics appeared stable in both time and space. The accumulation of the sediment is shown in figure 7.12.

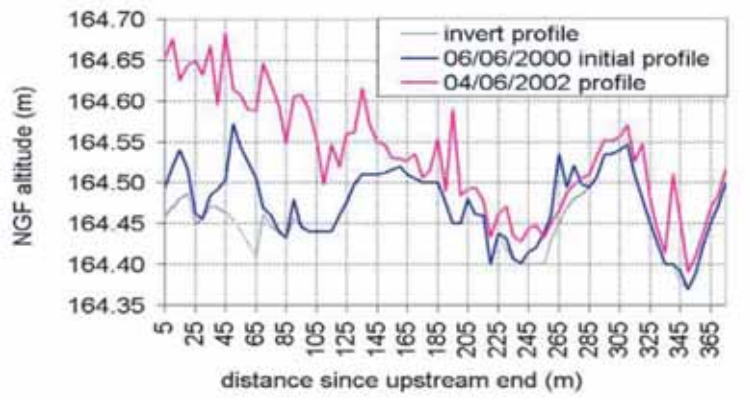

Figure 7.12: Sediment accumulation after 24 month [Bertrand-Krawjewski et al., 2005b]

The mean bottom slope increases progressively and tends towards an asymptotic value. This tendency can either mean that the energy of the flow is sufficient for a further transport of the particles or that a balance exists between erosion and settling process.

To investigate the sediment movement under the influence of flush waves a Hydrass gate was installed in sewer after 36 month of sediment accumulation. Due to dry-weather runoff it tipped every 2 minutes and showed a drainage time of 30 seconds. A progressive movement of the sewer sediments towards the downstream end of the sewer reach could be observed. (Figure 7.13) Despite the large number of flushes created by the Hydrass gate the sediments stayed in the sewer reach.

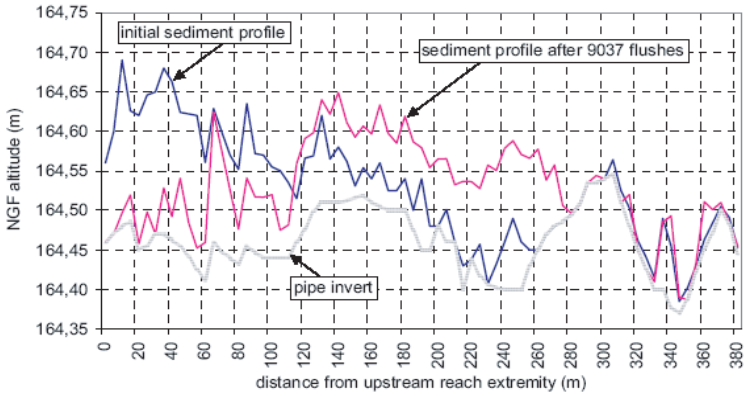

Figure 7.13: Effect of flushes on the sediment profile [Bertrand-Krawjewski et al., 2005b]

Another task during these investigations was to simulate the sediment accumulation with an empirical conceptual model and with the Velikanov model. The calibration of both models was carried out using the before mentioned measurements. The conceptual model was based on a three parameter approach and rather simple. Once calibrated it showned useful results for operators who want to establish a sewer cleaning strategy. The uncertainty of the simulated results against the measured values was plus/minus 20 %.
The Velikanov model was initially developed to calculate suspended solids transport rates in rivers. In the available case it simulated the global trend well and showed a good reproduction of sediment profiles. It seems to be suitable for operational purposes but it is very sensitive to input data and parameter values. To create transferability to other sewer sites both models will need further investigations to discover relationships between the models parameters and the sewer characteristics. [Bertrand-Krawjewski et al., 2005b]

A further investigation using the Hydrass gate was carried out by Laplace et al. (2002). It was based on the idea to remove the organic surface layer of deposits, which is situated at the water-sediment interface. This layer contributes to a large extent to the pollution of CSO's, with 40 - 70 % of suspended solids and the organic fraction. The erosion of this layer during dry-weather times would lead to a protection of receiving waters and a reduction of shock loads to the treatment plant. Therefore the available investigation used a Hydrass gate in a trunk sewer in combined sewer system of the city of Marseille. The sewer has an ovoid form with a height of 1.7 m. The studied section was 120 meters long and had a slope of 0.02 - 0.03 %. Deposits occurred over the whole length of the sewer reach. The Hydrass gate was installed to wash the coarser deposits towards a sediment trap 150 m downstream, where a mechanical extraction of the deposits would take place. To describe the effects of the flush waves the water level and the flow velocity were measured at two locations downstream of the Hydrass gate. The flushing volume stored by the gate was 6 m^3. The shear stresses of the flush waves were calculated with the measured water depth and the flow velocity to 14 N/m^2 as maximum values. The flow velocity during dry-weather runoff was measured with 0.35 - 0.40 m/s with a shear stress of 1 N/m^2.
The sediments height was measured with a measuring rod every 5 meters. The particles size of the deposits showed a sandlike material. The surface of the deposits was measured

with an endoscope to detect the presence of an organic layer. [Oms et al., 2002] The eroded pollutant mass was calculated taking the difference in concentrations of samples during the dry-weather flow and the flushes into account. The available mass of the organic layer was calculated with the measured surface size of the endoscope observations. The analysis of the flushing experiments showed that the concentration increased for the first and the second flush where 65 % of the eroded mass was removed. After the third flush the concentrations decreased to a stable value. Further long-term investigations showed that even with one year difference between two flushing investigations the eroded masses are of the same magnitude. It can therefore concluded that erodeable sediments reform to the same level and measurements showed that this process needs less then 8 days. Inspections after a flushing series revealed that the organic layer was removed to a large extend and larger particles were eroded by the flush waves. [Laplace et al., 2002]

The numerical model mentioned in Campisano et al. (2004) has been used for further investigations substituting the stainless steel plate with a Hydrass gate model. [Campisano et al., 2005] Again numerical results were compared with experimental results from a laboratory channel. The Hydrass gate as used by Bertrand-Krajewski et al. (2002) in Lyon was reduced to a 1:7 scale model to investigate the unsteady flow conditions caused by the gate. The Hydrass gate outflow relations (Bertrand-Krajewski et al., 2004) were implemented into the numerical model as internal conditions. The results showed a good agreement of the model, which is suitable to reproduce the unsteady flow of flushing operations and the steady outflow through the Hydrass gate.

The dissertation of Creaco (2005) gives a very good and detailed summary of all the investigations carried out at the University of Catania in Italy. [Campisano et al., 2002, 2004, 2005, 2006] [Bertrand-Krajewski et al., 2004, 2005a]

7.4 Investigations on reservoir sewers

Gathke and Borchering (1996) carried out an early investigation of the cleaning effectiveness of flush waves by using the numerical simulation. They built a physical model of a reservoir in a scale of 1:24 with respect to the model law of Froude. The measured results of the physical model allowed the calibration of the one-dimensional numerical model, which was based on the Saint-Venant equations. The investigated reservoir sewer had a length of 2 km and a width of 4.5 m. The flushing volume of 360 m^3 was stored in a height of 15.5 m. The results of the calculation showed a good agreement concerning the propagation of the flush wave. The simulated water levels diverged from the measured water levels up to 20 %. Especially at the end of reservoir the measured wave differed from the calculated one. (Figure 7.14)

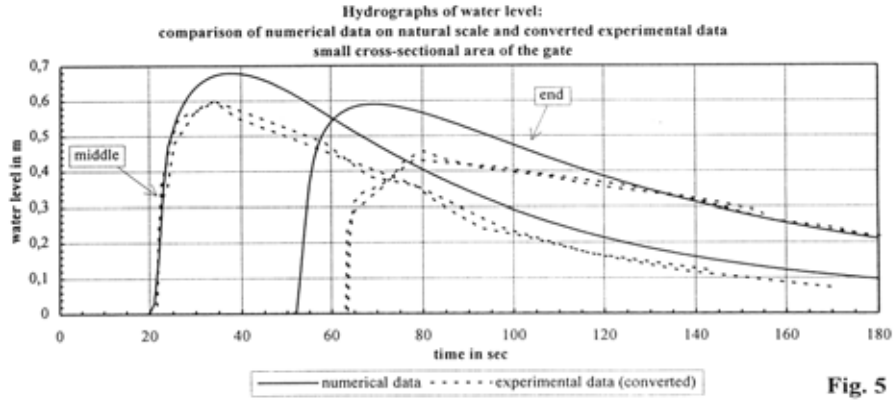

Figure 7.14: Hydrograph of the water level and the velocity [Gathke und Borchering, 1996]

The velocity of the opening of the flush gate was also of importance for the propagation of the flush wave. The slow opening of the flush gate resulted in a lower (77 %) and slower (10 s) flush wave compared to the flush wave created by a fast opening. But in a distance of 450 m to the flush gate the difference of both flush waves is not visible any more. The opening time is important for the sewer range close to the gate but not for longer flushing distances.
The controlling parameters for the remobilisation of the deposits are based on a minimum flow velocity of 1 m/s and a bottom shear stress of 4 N/m^2. [Mittelstaedt, 1981] [Sander, 1989] These values are still exceed in a flushing distance of 1800m. (Figure 7.15)

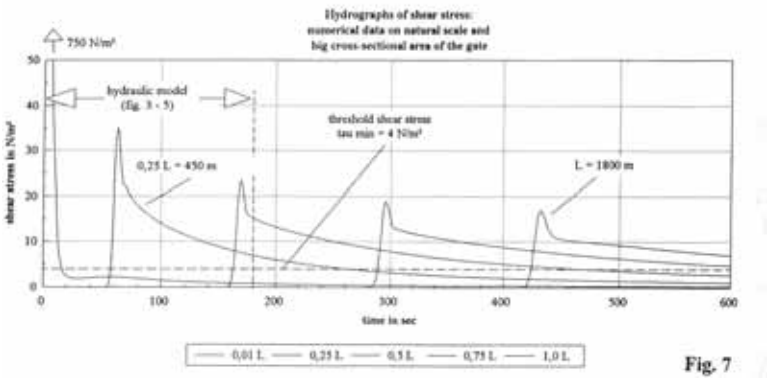

Figure 7.15: Hydrograph of bottom shear stress [Gathke und Borchering, 1996]

A further statement was the massive reduction of the water level during the wave progression. At the end of reservoir sewer the flush wave had a height of 30 cm ($\sim$ 1/15 DN). The loss of energy of the flush wave was given with 80 % for the first quarter of the sewer length. The loss of energy caused by erosion and transport was not considered.

Numerical and practical investigations in Bochum on the flushing of combined sewers with storage capacity and overflow are given by Dettmar and Stauffer (2004). The field investigations were carried out in a large sewer with storage capacity and bottom-end overflow. The size of the channel ranged between pipe diameters of 2500 mm to 3400

mm and a length of about 400 m. The bed slopes of the sewer varied between 3.6 and 4.6 ‰.

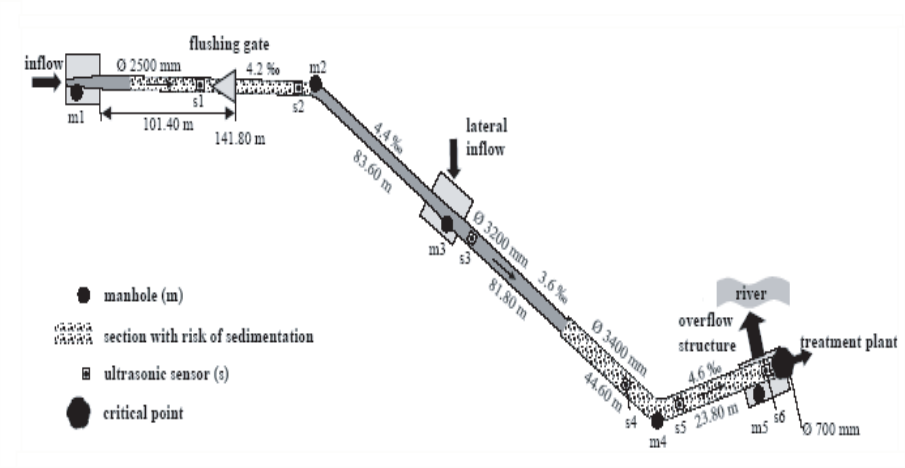

Figure 7.16: Overview of the investigated sewer [Dettmar & Stauffer, 2004]

An automatic flushing gate was installed in the upper part of the sewer to remove settled particles and bed-load material. The gate divided the sewer in a 300 m flushing section downstream and in a 100 m storage section upstream. In both parts of the sewer deposit are found. The throttle at the outlet of the sewer channel was a pipe with a diameter of 700 mm and a maximum discharge of 0.71 m^3/s. Figure 7.16 shows an overview of the investigated sewer.

At the end of the sewer channel the concentration of flow at the throttle reduced the bottom shear stresses and limited the sediment transport rates. Therefore the flow rate of the flushing waves needed to be optimised at the outlet to minimise the risk of sedimentation of remobilised solids and of transportating the solids back into the sewer by reflection of the flushing waves. For an optimised flushing concept the authors chose a bottom shear stress of 5 N/m^2 to exceed the erosion shear stresses.
The flushing gate used for the investigations was based on a new concept with an automatic operation using a pneumatic drive. The parts were of stainless steel and synthetic materials. The field investigations included recordings of the water level during the progression of the flush wave and measurements of the sediment height and location. The composition of the sediments was also analysed. The measurements of the flush wave at four locations along the sewer showed a mean velocity of the flush wave of 3.6 m/s.
For the numerical investigations the program Fluvius-1D was used which is a one-dimensional hydrodynamic model. The model was developed for calculating non-steady and discontinuous discharges in near-natural channels and is bases on the Saint-Venant equations, which were discretised conservatively by the method of Gudonov. The method of Gudonov characterises the transition between two areas of continuous flow by the Riemann's problem for non-linear equations of conservation. In this case the Riemann's problem is solved with the method of Roe. Parameters for the calibration of the numerical model using the measurements of the real sewer were the discharges and the roughness for several sections along the channel. The flush waves behaved highly unsteady and discontinuously and were described as dam-break waves. The calibration of the modelled flush waves at two locations of the sewer channel are shown in figure 7.17.

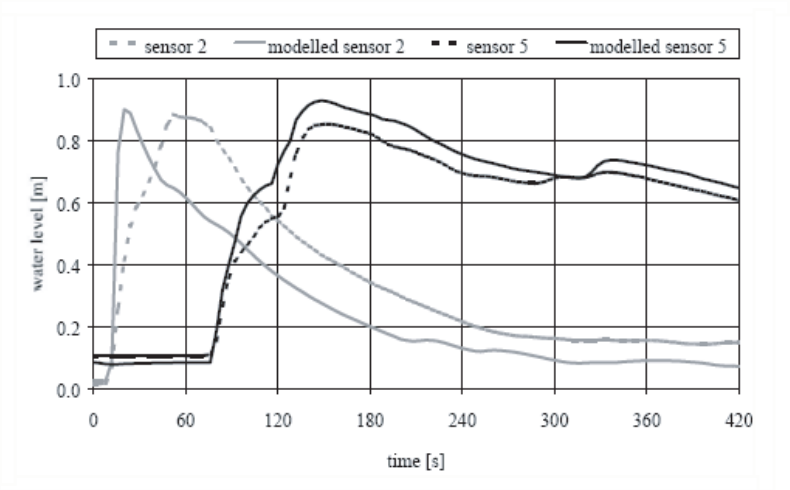

Figure 7.17: Measured and calculated water levels over time [Dettmar & Stauffer, 2004]

The results of the numerical calculations lead to the fact that the critical shear stress of 5 N/m^2 was exceeded by the calculated mean shear stresses at the bottom for at least 240 s for the lowest dam height of H = 0.80 m. Taller dam heights caused even higher shear stresses up to 140 N/m^2 for H = 1.40 m at the gate. Therefore the process of erosion was started and the deposits were transported downstream. As expected the cleaning success at that point was greater with a bigger wave than those created with a smaller dam height.
When choosing the dam height at the flushing gate the backwater effect at the end of the sewer channel, at the throttle, had to be taken into account. Only dam heights below H = 0.9 m showed a free discharge at the throttle without any backwater effects and low shear stresses. For larger heights the shear stresses droped as soon as the flow rate exceeded the given limit by the throttle. That might cause re-sedimentation at lower parts of the sewer. The degree of re-sedimentation probably depends on the time the impact of the throttle is activated.

On basis of the simulation results the authors were applying for a two phase cleaning strategy composed of basic and preventive cleaning. The basic cleaning should remove all existing deposits and two different strategies are possible. First numerous small waves (dam height: H < 0.9 m) could remobilise settled solids without a blockage. Therefore up to 20 waves a day would be necessary. Assisting the small waves single big waves can be flushed to loosen consolidated deposit or to transport gross solids towards the outlet. The second choice could be an operation where the dam height at the gate is adjusted smoothly as the height of deposit decreases and the capacity of the outlet rises.
After the basic cleaning the operation for the preventive cleaning would be started. Flushing waves for preventive cleaning are dimensioned with only 1 or 2 waves per day and a dam height at the gate between 1.2 and 1.3 m. According to the authors, with this two-part strategy the sewer the sewer channel could be cleaned permanently without causing overflow events by exceeding the maximum runoff at the throttle. [Dettmar & Stauffer, 2004, 2005a] A detailed report on this investigation can be found in Dettmar and Stauffer (2006).
A comparison of the one-dimensional numerical model Fluvius and the tree-dimensional

model SSIIM was carried out by Stauffer et al. (2006). Here he compared the 3-D results of Schaffner (2003b) with result he achieved by re-modelling the sewer channel originally investigated by Schaffner.
As a result of all the investigations presented in this chapter it can be stated that the flushing volume and the frequency of flushing are the key parameters for a potential successful cleaning of a sewer channel. The initial storage height should not be not less than 50 cm to create a typical dam-break wave. But compared to the flushing volume a large initial storage height does not necessarily lead to long flushing distances. It is more the flushing volume which needs to be large enough for the chosen or demanded sewer stretch to be cleaned. The chosen frequency of flushing should be related to the existing deposits in a sewer channel. Their characteristics can vary to a large extend and should be taken into account. High levels of sediments in old sewers will need a high frequency of powerful flush waves to be cleaned in the long run. New sewers or already cleaned sewers will need a smaller frequency of flush waves to be cleaned of new and mobile sediments.

8 Description of the test-side

8.1 Reservoir sewer August-Bebel Ring / Offenbach

The investigated reservoir sewer August-Bebel Ring in the city of Offenbach is used as a sub-main sewer and is connected to the main collector Frankfurter Strasse by a side weir. It is built and operated as a stormwater holding tank. The length was measured by the author with 336.5 m, the offical plan of the Eigenbetrieb Stadt Offenbach (ESO) showed 341.75 m. Figure 8.1 displays a simplified longitudinal view of the reservoir sewer in Offenbach.

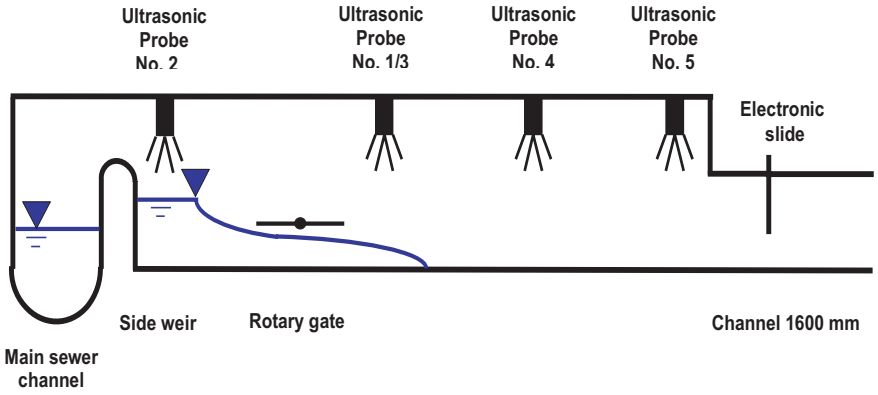

Figure 8.1: Longitudinal view of the reservoir sewer in Offenbach August-Bebel-Ring

The width of the sewer dithers between 3.1 - 3.2 m and the average height of the sewer channel amounts to 2.5 m. The cross slope varied between 1.5 - 3 %. The longitudial slope changes from section to section among 0.8 und 5.81 ‰ with a weighted mean value of 1.96 ‰. A detailed list can be found in the appendix A.
In its center the sewer channel has a half tube of 600 mm made out of stoneware with clinker for the dry-weather runoff. The reservoir sewer itself consist of concrete. Figure 8.2 shows a cross view of the channel in flow direction.

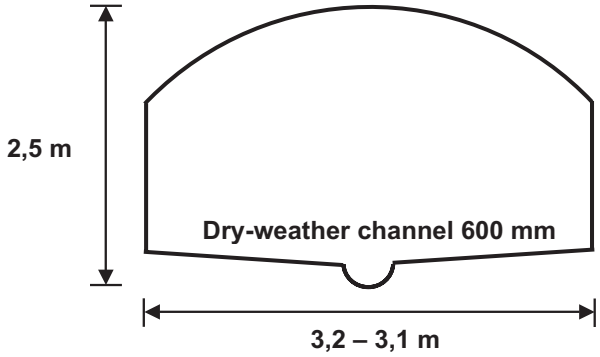

Figure 8.2: Cross view reservoir sewer Offenbach August-Bebel-Ring

At the downstream end the reservoir sewer is connected to a pipe sewer with 1600 mm diameter which consists first of fiberglass (GFK) and later of concrete. This pipe has a total length of 257.38 m with a averaged longitudial slope of 0.32 ‰. It links the reservoir sewer to the main collector Bernhardstrasse. A velocity and ultrasonic probe is installed 19 m after the beginning of the pipe and after a further 17 m follows a manhole with a electronic slide which was deactivated and remained in a fixed position of 0.41 m about the bottom of the sewer. For a maximum filling of the reservoir sewer it allows a runoff of 2.106 m^3/s. The figures 8.3 und 8.4 show the inlet and the outlet of the reservoir sewer. These pictures were taken in November 2004.

Figure 8.3: Inlet of the reservoir sewer Offenbach August-Bebel-Ring

Figure 8.4: Outlet of the reservoir sewer Offenbach August-Bebel-Ring

8.2 Description and functionality of the rotary gate

The rotary gate is installed at the beginning of the reservoir sewer in a distance of 35.5 m downstream of the side weir. It is 1.80 m high and it axis is located 1.06 m above the ground.
The gate itself is frameless and made of stainless steel. It can be customised according to the geometry of the sewer channel. The sealing of the rotary gate at the sewer walls is achieved with the aid of a compressed-air tube. To prevent this tube from damage is is pressed with up to 11000 kp against a stainless plate which it tightly screwed to the sewer wall. (8.5)

Figure 8.5: Rotary gate in reservoir sewer Offenbach August-Bebel-Ring

The opening mechanism is also pneumatic operated and is, like the sealing tube, connected to a hydraulic power pack that generates the compressed air. The pneumatic gear of the rotary gate can be found in its vertical bar. The gate swing freely and can be opened in 0.8 s then it is locked in the horizontal position.

The operation of the rotary gate is done with a SPS control type Mitsubishi KS 1468. It refers to the water levels up- and downstream of the rotary gate recorded by two ultrasonic probes (Type Nivus P 6). In the present case the probes no.1 and no.2 were used for the control of the rotary gate.
After a storm event and a filling of the reservoir sewer the probe downstream of the gate measures the falling water level. When the minimum level is reached the control closes the rotary gate. At this time usually no water flows across the side weir so it is necessary to fill the flushing volume over the gate to the desired level. Therefore a underwater pump is installed on the downstream side of the rotary gate. It pumps the remaining stormwater into the flushing volume behind the gate. The pumping starts when the gate is closed and the water level downstream is recorded with 70 cm above the bottom of the sewer channel. The pump is able to deliver 30 m^3/h.
The probe upstream the gate measures the filling level of the flush volume. At a water level of 1.82 m at the gate the pumping is stopped. To ensure a completely draining of the reservoir sewer the gate remains in the locked position for two hours after the sinking water level passed the 0.35 m mark above the sewer bottom. Then the rotary gate is opened and the flush wave runs along the channel of the reservoir sewer.
It is necessary to empty the reservoir sewer so that the flush wave runs along a dry bottom. If it would run into a remaining water body or a backwater a lot of the energy of the flush wave would be lost and no satisfying cleaning result should be expected.

The flush volume can be described as a function of the dam height at the rotary gate.

$$V_{Store} = 113.6 \cdot h_{Store} - 41.7552 \tag{8.1}$$

For the maximum dam height of 1.82 m at the rotary gate a flush volume of 163 m^3 is available.

8.3 Location of the measuring probes

The investigation of the flush wave was done with the aid of three further ultrasonic probes (Type Nivus P6). They were installed along the reservoir sewer to document the development of the flush wave during its course. In theory the probes were able to take a measurement of the water level every second, practically they measured in intervals from three to ten seconds which was sufficient for the investigations. Table 8.1 displays the location of these three probes and the two probes controlling the gate.

Notation of the measuring probe	Distance to the rotary gate [m]	Distance to the side weir [m]
Probe no.2	-35.5	0
Probe no.1	17.72	53,22
Probe no.3	19.01	54,51
Probe no.4	143.5	179
Probe no.5	300.5	336

Table 8.1: Location of the measuring probes

Figure 8.6 shows measuring probe no. 1 which is located at the ceiling of the reservoir sewer.

Figure 8.6: Measuring probe no.1

8.4 Measuring technique

The data of the flush waves measured by the ultrasonic probes no. 3 - 5 had to be stored and transmitted to the LIWATECH company in Bad Koenig. Therefore it would have been possible to use the already available Mitsubishi SPS control. But this SPS control did not posses sufficient data memory to record the measured data of a flush wave. Because of this the company LIWATECH decided to remove the Mitsubishi control and installed an already tested computer process control by the company Schraml.
Due to the fact that there was no access to the conventional telephone network at the reservoir sewer, the data transmission had to be done via GSM mobile phone network. The measuring and transmission procedure was as follows:

1. Collection of data through ultrasonic probes
2. Computer process control relates each a time to each measurement
3. Temporal storage of the data in the process control

4. Transmission of data packets from Offenbach to LIWATECH central office via GSM mobile phone network
5. Storage of the data on a personal computer

A detailed description of the measuring technique used in the Offenbach reservoir sewer can be found at Oberlack et al. (2005).

9 Measurement of flush waves in the reservoir sewer

One major aspect for the success of the numerical modeling in the following investigations is the measurement of data taken from real flush waves in the reservoir sewer August-Bebel Ring / Offenbach. The calibration of the numerical model with measured data and known boundary conditions makes it possible to achieve reliable modeling results. It is not possible to create and simulate different scenarios with changing boundary condition without the use of a calibrated numerical model. Therefore it is necessary to take reliable measurements of several different flush waves to calibrate the model and validate it for further investigations.

The original strategy to use storm sewage from intense rainfalls to create flush waves with different storage levels could no be realized because of the following reasons.
After the installation of the measurement technique by the company LIWATECH in November/December 2002 a disfunction in the rotary gate prevented the first flush tests. The official reason for this was the incorrect maintenance of the rotary gate by the operating company of the Offenbach sewer system ESO. In May 2003 the rotary gate was repaired. In the following months transmission problems between the measurement technique and the head office of LIWATECH in Bad Koenig made it impossible to carry out flush tests. This unsatisfying situation remained until April 2004. During this time it was not possible to record any data resulting from storm events to recognize how many times and to which water level the reservoir sewer was flooded.
After the apparent solution of this problem the company LIWATECH was still not able to carry out the necessary flush tests. The official statement was that the intense storm events occured during the night hours or at weekends when head office of LIWATECH was not occupied.
At the beginning of October 2004 the operating company of the Offenbach sewer system (ESO) supposed to remove the side weir to the main sewer Frankfurter Strasse temporarily so that the dry-weather runoff would discharge through the reservoir sewer. The main sewer itself was closed with an artificial sewer bubble. Now it was possible to fill the flush volume selectively for different storage levels and carry out the flush tests.

The first two flush tests took place at the 13th of October 2004. The dry-weather runoff was damed to a height of $h_1 = 0.897$ m und $h_2 = 0.567$ m at probe no.2 which is located between the side weir and the rotary gate. The water level at probe no.2 is situated 0.2 m below the water level at the rotary gate. Therefore the storage levels for the first two flush tests at the rotary gate were $h_1 = 1.097$ m und $h_2 = 0.767$ m. Using equation 8.1 the tests were carried out with flush volumes of $V_1 = 82{,}864$ m^3 and $V_2 = 45{,}376$ m^3. Unfortunately the analysis of the recorded water levels of the ultrasonic probes no. 4 and 5 could not used for the model calibration because of failures at the probes.
Further flush tests were carried out between the 11th and the 14th of November 2004 by

the company LIWATECH. The storage levels and the flush volumes of these tests are displayed in table 9.1.

Storage level at probe no.2 [m]	Storage level at rotary gate [m]	Flush volume [m^3]
0.529	0.729	41.0592
0.8035	1.035	75.8208
1.053	1.253	100.5856
1.259	1.459	123.9872
1.437	1.637	144.208
1.619	1.819	164.8832

Table 9.1: Storage levels and flush volumes of the flush tests, 11.-14.11.2005.

The comparison of the water levels of the flush waves measured at the ultrasonic probes are shown in the figures 9.1 - 9.3. The legend of these figures refers to the storage level at the rotary gate. A more detailed presentation of the flush waves and their water levels can be found in appendix B.

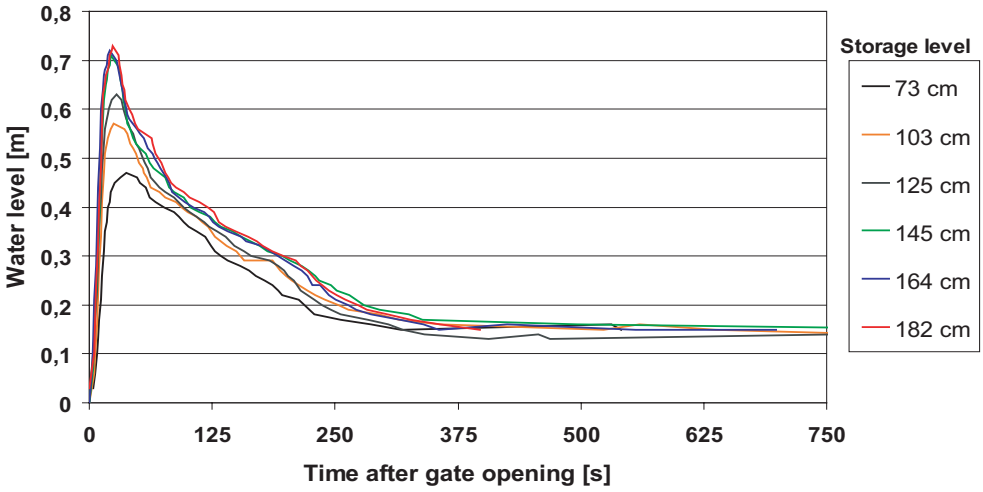

Figure 9.1: Measured data probe no.1

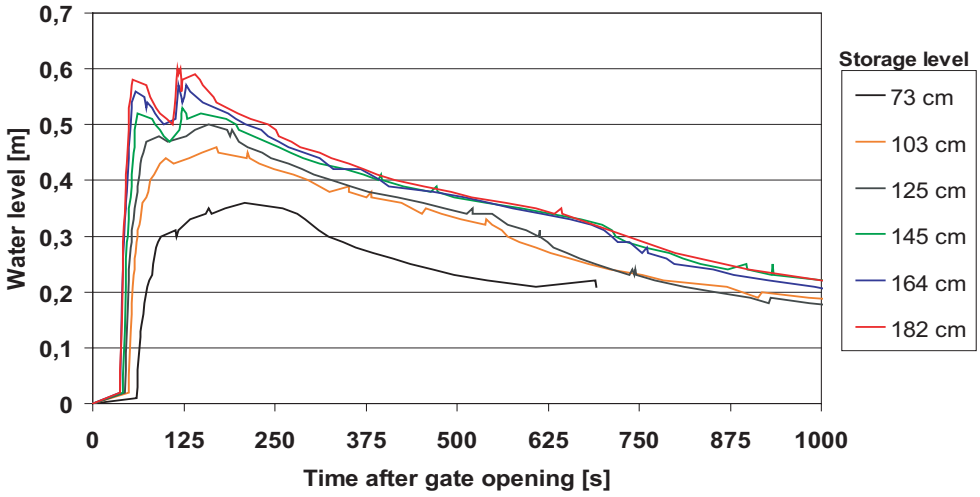

Figure 9.2: Measured data probe no.4

The jagged lines at probe no. 5 seem to be caused by the backwater of the flush wave unable to leave the reservoir sewer undisturbed.

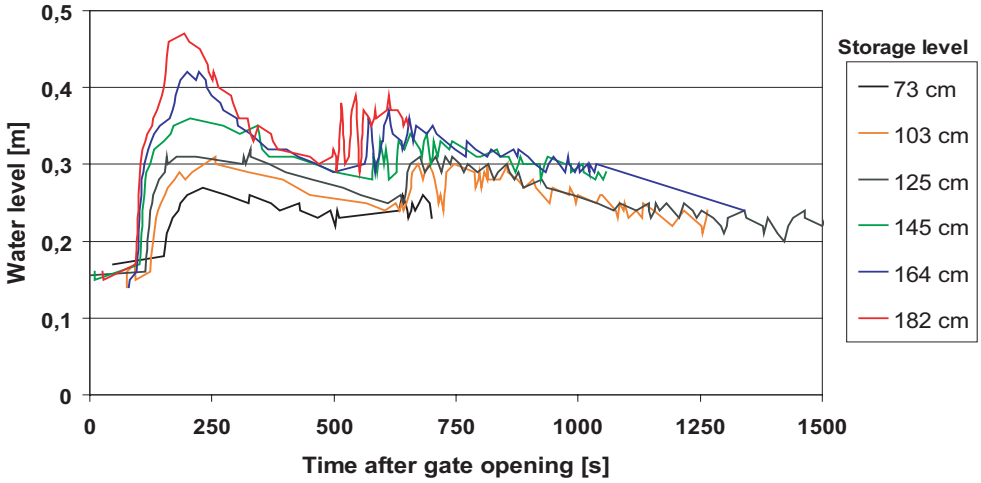

Figure 9.3: Measured data probe no.5

10 Setup of the data record

The data record contains all relevant information necessary for the definition of the flow domain and settings to run the numerical model. The spatial definition of the flow domain is carried out by the set up of the numerical grid. The temporal distribution of the flow is defined by the time step size and the chosen numerical algorithm. In the present case the fully implicit scheme was chosen. The data record also contains the definition of the boundary conditions like the bottom roughness for example and the initial conditions like the storage level or the flushing volume.
The numerical simulation of the flush waves in the reservoir sewer August-Bebel Ring was carried out with the three-dimensional finite volume model StarCD. The general description of the model can be found in chapter 5 and the numerical basics are defined in chapter 3. Further in-depth information can be found in the methology of StarCD. [Star-CD Version 3.1, 2002]
The representation of the reservoir sewer and the included flushing gate was carried out in two steps. First a shortened model was generated which covers the first 200 m of the sewer. In the next step the complete reservoir sewer with a length of 336.5 m was constructed. For both versions of the model the flushing volume was regarded as a freestanding water body.

10.1 Shortened reservoir sewer

The first numerical calculation was made with a model version, which represented the first 200 m of the reservoir sewer. The ultrasonic probes no. 1 and 4 are placed within this distance and it was possible to use their measurements of the flush waves for the calibration of the numerical model.
The shortened model had the advantage of less grid cells and therewith shorter calculation times compared to the complete model of the sewer. The calibration of the numerical model was based on the adjustment of variables like the bottom roughness of the sewer and required numerous computational runs to obtain good results. The application of the shortened sewer model for the calibration process lead to a major saving of time.

10.1.1 Generation of the numerical grid

In this variant the reservoir sewer was divided in two sections. The first section of 35.5 m length represented water storage area with the flushing volume. The second section displayed the flushing distance of 164.5 m. Eight cross-sections with 11 coordinates each were defined to describe the geometry of the reservoir sewer and to generate the numerical grid. (Appendix C)

The cross-sections were joined together to one block and the number of grid cells in each coordinate direction were determined. They are displayed in table 10.1.

Coordinate direction	Width/Heigth/ Length [m]	Number of grid cells	Width/Height/Length of the grid cells [m]
x	3.2 / 3.1	16	0.2 / 0.194
y	2	20	0.1
z	200	400	0.5

Table 10.1: Definition of the numerical grid, 200 m model

The number of grid cells resulted in 128000. Figure 10.1 shows a cross-section of the generated numerical grid for the 200 m model.

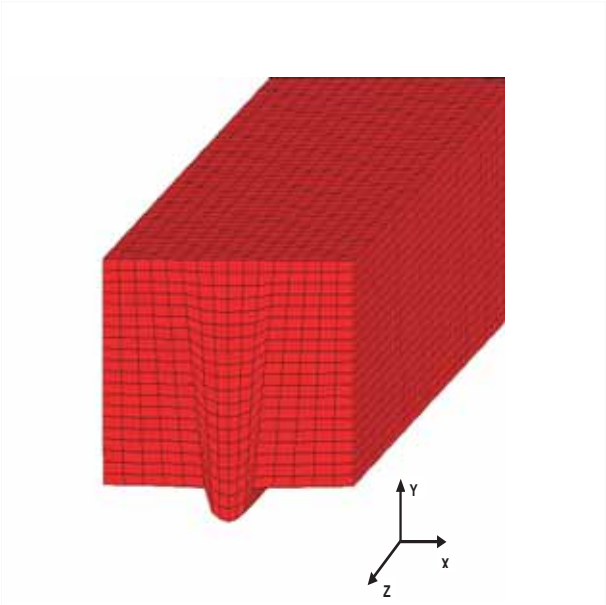

Figure 10.1: Cross-section of the numerical grid

The model StarCD can calculate several phases inside the flow domain. In the present case the movement of the water as well as the air above it is modelled. To evaluate the cleaning efficiency of the flush wave it is necessary to investigate the motion of the water, the air can be partly neglected. Therefore the number of the grid cells and the computing time can be reduced significantly by cutting out numerous cells just filled with air until a certain limit.
The height of the numerical grid can be reduced step by step due to fact that the flush wave is getting shallow in it progression along the sewer. A minimum cover of 5 grid cells filled with air above the water is needed to avoid numerical divergence of the solution. Figure 10.2 and figure 10.3 show the reduced numerical grid with a number of 55518 grid cells for the investigated part of the reservoir sewer.

Figure 10.2: Reduced numerical grid

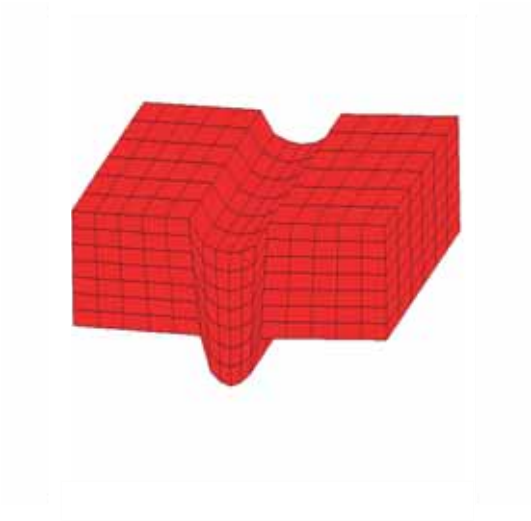

Figure 10.3: Cross-section of the numerical grid

10.1.2 Boundary and initial conditions

For the case of the shortened model the accumulated water volume was considered to be a freestanding water body, which breaks down due to gravity force and hydrostatical pressure. During the practical flush tests in the reservoir sewer it became obvious that up to an initial storage level of 1.45 m the flush wave slides under the flush gate when its rotary movement had ended. For initial water level higher than 1.45 m the gate was over flown for a short period of time. Therefore it was not necessary for this first model to regard the roughness and the flow resistance of the flush gate. The chosen storage level for the first numerical model was $h_{Store} = 1.03$ m. (Figure 10.4)

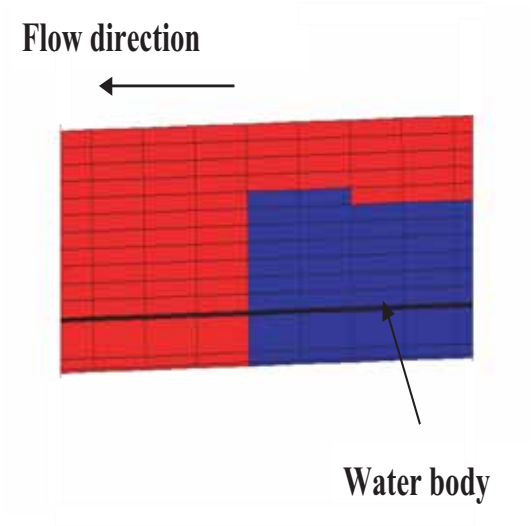

Figure 10.4: Storage area of the flushing volume (cut-out)

The upper boundary condition declares that the numerical flow domain like real the reservoir sewer has no upstream inflow during the calculation time. A suitable pressure boundary was chosen at the shortened end of the sewer to ensure a free outflow of the flush wave. The time step size for the single iteration steps were chosen to $\Delta t = 0.025$ s. In summation 50000 iteration steps were considered which resulted in a flow duration of 1250 s. The investigated results were restricted to the water level, the propagation of the flush wave and the bottom shear stress. The water level and the location of the flush wave was calculated by the water content c of the grid cells as a result of the Volume of Fluid method. The bottom shear stress was computed by turbulent kinetic energy k.
All boundary cells of the modelled reservoir sewer, except the ones at the end of channel, were defined to be impermeable for fluxes. The roughness of the boundary cells was defined by the value of k. The dry-weather channel in the real sewer channel showed a significant biofilm caused by the continuous dry-weather runoff, which was very slippery. The roughness was set according to Kraus (2002) to a value of $k = 0.6$ mm. The slopes and the walls of the reservoir sewer are made of concrete with a formerly wooden boarding. The roughness of the concrete was determined with $k = 2$ mm according to Bollrich, (2000).

10.2 Complete reservoir sewer

10.2.1 Generation of the numerical grid

The numerical modelling of the complete reservoir sewer with a length of 336 m was analogue to the shortened model of 200 m. The geometry of the reservoir sewer was defined by 14 cross profiles which were connected to one block. Table 10.2 shows the number of the grid cells and their size for the complete reservoir sewer.

Coordinate direction	Width/Height/ Length [m]	Number of grid cells	Width/Height/Length of the grid cells [m]
x	3.2 bzw. 3.1	16	0.2 bzw. 0.194
y	2	20	0.1
z	336.5	673	0.5

Table 10.2: Definition of the numerical grid, 336.5 m model

The number of grid cells for the complete reservoir sewer resulted in 215360. To save computational time during the calculations most of the grids cells containing air were cut out and the total number of cells was reduced to 148128. (Figure 10.5)

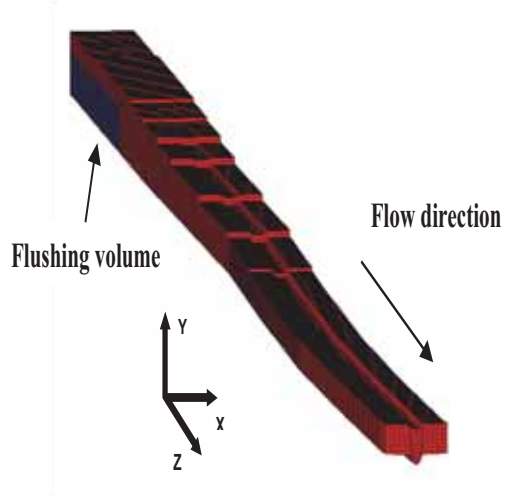

Figure 10.5: Reduced numerical grid for the complete reservoir sewer

In contrast to the reality the following sewer channel with a diameter of 1600 mm was modelled only on a length of 20 m using 2560 grid cells. Table 10.3 shows the measurements of the circular profile and the distribution of the grid cells.

Coordinate direction	Width/Height/ Length [m]	Number of grid cells	Width/Height/Length of the grid cells [m]
Radius	0.8	4	
Perimeter	5.02 (360)	14	
z	20	40	0.5

Table 10.3: Numerical grid of the circular sewer channel

The circular cross-section is connected evenly to the dry-weather channel according to the real conncection in the reservoir sewer August-Bebel Ring. (Figure 10.6)

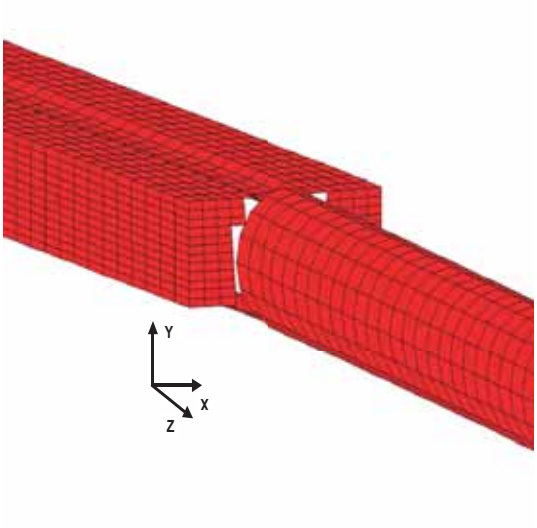

Figure 10.6: Transition main channel - circular channel

To drain the flushing volume unresisted and without backwater effects, a collection tank was defined as the last element of the complete model. This collection tank received and stored the flushing volume as the downstream boundary condition. Figure 10.7 shows the collection tank and its connection to the circular sewer channel.

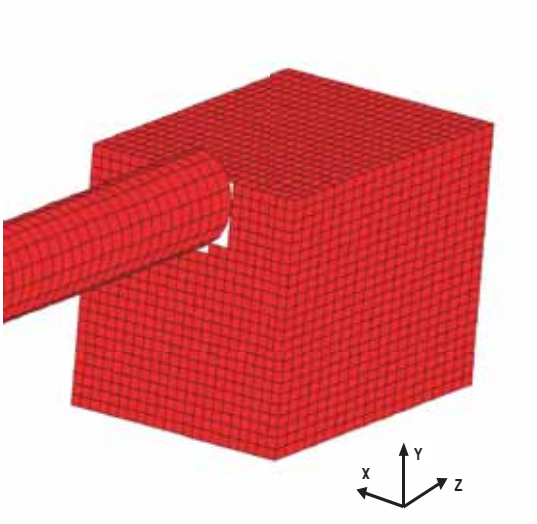

Figure 10.7: Transition circular sewer - collection tank

The collection tank consist of 10560 grid cells. Their distribution is shown in table 10.4. The numerical grid of the complete reservoir sewer consisting of main channel, circular channel and collection tank contains in summation 161248 grid cells.

Coordinate direction	Width/Height/ Length [m]	Number of grid cells	Width/Height/Length of the grid cells [m]
x	5	22	0.227
y	4,8	24	0.2
z	10	20	0.5

Table 10.4: Numerical grid collection tank

10.2.2 Boundary and initial conditions

The boundary conditions for the numerical model of the complete reservoir sewer were not changed compared to the shortened model except for the pressure boundary at the end of the shortened model. Instead of the free outflow the circular channel and the collection tank were included to guarantee a free outflow of the flushing volume of the main reservoir sewer and to ensure the comparability of the measurements and the simulation results. The number of iteration steps was reduced to 28000, which resulted in a running time of 700 s for the flush wave.

11 Calibration and validation of the numerical model

11.1 Calibration - Variation of the roughness

First the numerical modelling of the flush waves was concentrated on the preferably detailed reproduction of the measured waves in the reservoir sewer August-Bebel Ring in Offenbach. Therefore the shortened model of 200 m length was chosen which offers shorter calculation times in contrast to the complete model of the reservoir sewer. The temporal progression of the modelled waves at the probes no. 1 and no. 4 were evaluated and compared to the measured real waves. Manual calibration of the roughness for the slopes and the dry-weather channel adjusted the calculation results according to the measurements at the ultrasonic probes no. 1 and no. 4.
The variation of the channel roughness was carried out separately for the dry-weather channel and the slopes. Inspections in the reservoir sewer showed that the dry-weather channel is affected by the grow of bio-films despite of the regular cleaning. The roughness of the bio-film is lower than for the slopes according to Kraus (2002). The initial storage level at the flush gate was chosen to h_{Store}=1.03 m and kept for all other variants.

11.1.1 Roughness variant 1

The roughness for the first calculations was chosen to $k = 0.6$ mm for the dry-weather channel and $k = 2$ mm for the slopes. The progression of the measured and the modelled flush wave is shown in figure 11.1.
The maximum value of the water level at probe no. 1 is 0.57 m for the modelled wave and is similar to the real wave. The modelled wave reaches probe no. 1 after 5 s while the measured wave passes the probe after 9 s. Regarding the temporal progression the modelled maximum is reached 5 s earlier then the measured maximum. After the maximum level the calculated flush wave declines significantly slower than the measured one.

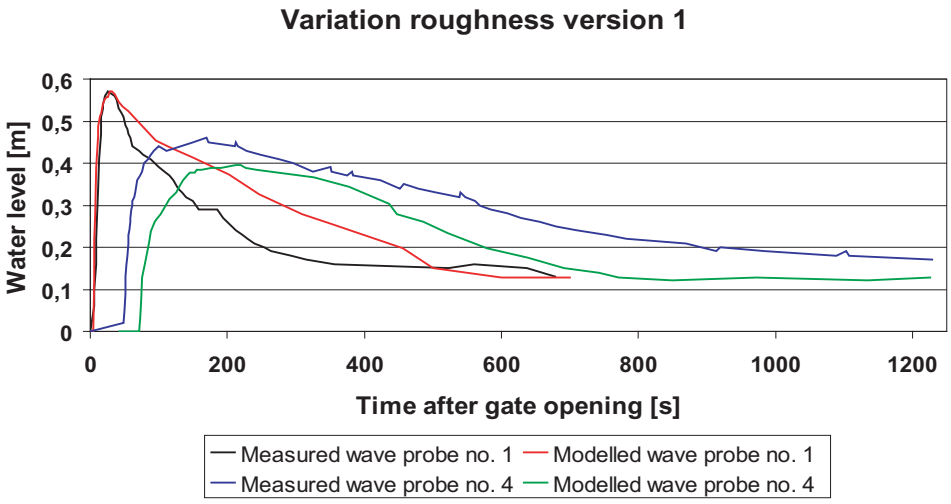

Figure 11.1: Comparison of the measured and the modelled flush wave

Regarding the modelled flush at the two different locations shows an incomprehensible behaviour of the flush wave. At probe no. 1 the flush wave shows a high velocity and is declining slowly, at probe no. 4 the wave is slower and declining faster than the measured wave. The progression of the flush wave at probe no. 1 is strongly influenced by the estimation of the boundary conditions at the flushing gate. A flush wave developing out of the chosen free standing water body will move faster in its initial phase than the real wave, which is slowed down by the flow resistance of the flushing gate.
At the probe no. 4, after a running distance of 179 m, the flush wave is now fully developed and should not be influenced by the flow resistance of the flushing gate. At this point it is obvious that the flush wave is too slow compared to the measured wave. The roughness for the slopes and the dry-weather channel had to be reduced in the same degree to increase the velocity of the flush wave constantly. A one-sided reduction of the roughness for the dry-weather channel would lead to a small and shallow runoff, which would flow ahead of the main water body. The shape of the flush wave would be flattened caused by the loss of water volume. The difference in the maximum water level of the modelled wave compared to the measured wave would be even higher.

The fast declination of the calculated wave compared to the measured one can be justified with the difference of the peak values. If the calculated wave would be shifted 7 cm higher the characteristics of both waves would be nearly equal. This means the tendency of the modelled wave is acceptable with the peak water level being too small.

11.1.2 Roughness variant 2

In the variant 2 the roughness of the dry-weather channel was kept with $k = 0.6$ mm and the roughness of the slopes was set to $k = 1$ mm.
The analysis of the calculated flush wave at probe no. 1 showed that it has a similar velocity compared to the measured wave and the peak-level is about 2 cm lower. The declination of the measured flush wave is again faster than for the modelled wave. (Figure 11.2)

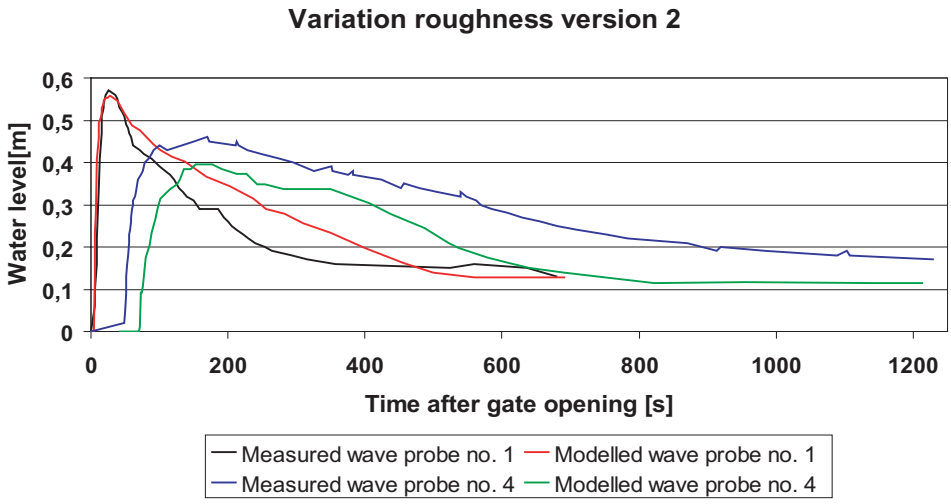

Figure 11.2: Comparison of the measured and the modelled flush wave

The investigation of the modelled flush wave at probe no. 4 showed that the reduction of the roughness lead to an insignificant increase of velocity. The measured wave is still 20 s faster than the modelled one. The peak level remains at 0.39 cm for the modelled wave. The declination can be compared with roughness variant no. 1. For the next variant a larger reduction of the roughness was necessary to adapt the modelled wave better to the measured wave.

11.1.3 Roughness variant 3

In variant 3 the roughness was reduced for the dry-weather channel to $k = 0.15$ mm and $k = 0.25$ mm for the slopes.
This reduction had no influence on the velocity of the wave at probe no. 1. The maximum water level of the modelled flush wave is at 0.54 m and it passes the probe after 25 s. The difference to the measured wave is 3 cm. The declination of both waves is similar to each other. The modelled wave showed a good adaptation to the measured wave.
The effects of the roughness reduction are more visible at probe no. 4. The calculated flush wave reaches the probe after 58 s, which is only 8 s before the measured wave. (Figure 11.3)
The maximum water level is now at 0.41 m, which 4 cm below the measured wave. The temporal phase of the peak levels is placed between 136 s and 166 s equal to the measured wave. The declination of the modelled wave is faster than for the variant 1 or 2.

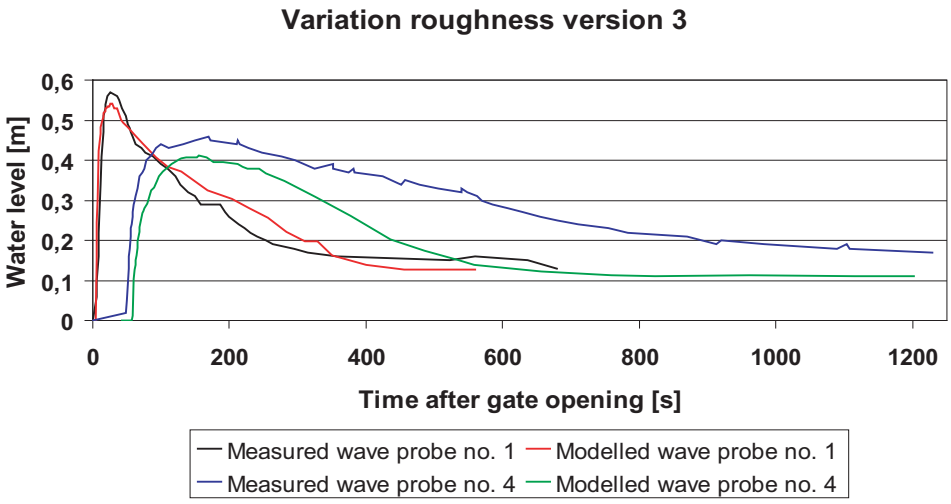

Figure 11.3: Comparison of the measured and the modelled flush wave

The calibration of the numerical model of the reservoir sewer showed the best results for variant 3. The adaptation of the modelled wave is good for the location of the probes no. 1 and 4. It would have been possible to increase the velocity of the flush by decreasing the channel roughness but this would have lead to a further reduction of the peak water levels and a faster declination of the wave at probe no. 4. The further reduction of the roughness would result in unrealistic values for the roughness, which would not meet the reality in the reservoir sewer.

11.2 Variation of the iteration time step

In the following section the influence of the iteration time step on the progression of the flush wave is investigated. The basis of the calculations will be the roughness variant 3 of the numerical model as used in the prior section. For the variants 4 and 5 the boundary conditions remained the same only the size of the iteration time step $\Delta\ t$ was varied. Table 11.1 shows the investigated time steps.

Variant	Iteration time step Δt [s]
3	0.025
4	0.05
5	0.01

Table 11.1: Variation of the iteration time step

Figure 11.4 shows the comparison of the temporal progression of variant 3, 4 and 5 at probe no. 1.

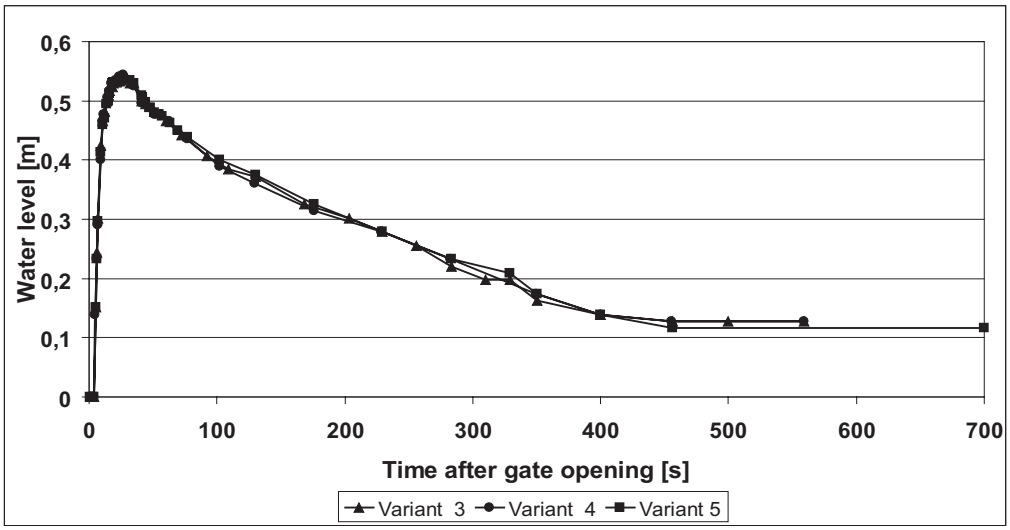

Figure 11.4: Comparison of iteration time step, probe no. 1, storage level 1,03 m

There is no difference in the initial velocity of the different waves. The maximum values are nearly identical and in the declination the waves crosses each other several times but with no significant differences.
Figure 11.5 shows the progression of the waves for the different iteration time steps at probe no. 4. The differences in the water levels of the investigated wave are around 2 cm which makes no difference. The velocities of the waves are also nearly equal.

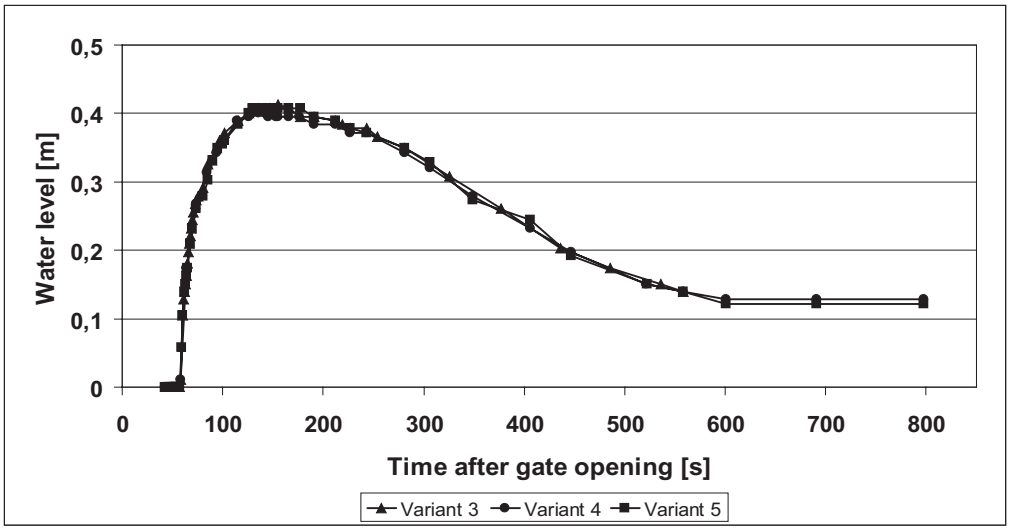

Figure 11.5: Comparison of iteration time step, probe no. 4, storage level 1,03 m

The variation of the iteration time step Δt in the shown range leads to not significant differences in the progression of the flush wave. Further investigations with smaller time steps were not made due to large amount of needed calculation time.

11.3 Validation of the numerical model

The calibration of the numerical model in the prior section was carried out using the shortened numerical grid with a storage level of $h_{Store} = 1.03$ m. In this section the calibrated model will be used to calculate all other chosen storage levels and compare the results with the measured waves regarding the dry-weather channel and the slopes. Therefore the complete numerical grid with a total length of 336.5 m was chosen to include the results of probe no. 5.
The first calculation was carried out with a storage level of $h_{Store} = 0.73$ m.

11.3.1 Probe no. 1

The comparison of the measured and the modelled wave at probe no. 1 at $z = 53.22$ m shows a good agreement. (Figure 11.6) The modelled wave is only a few seconds slower compared to the measured wave but around 6 cm lower in the maximum height. During the declination both waves progress very similar.

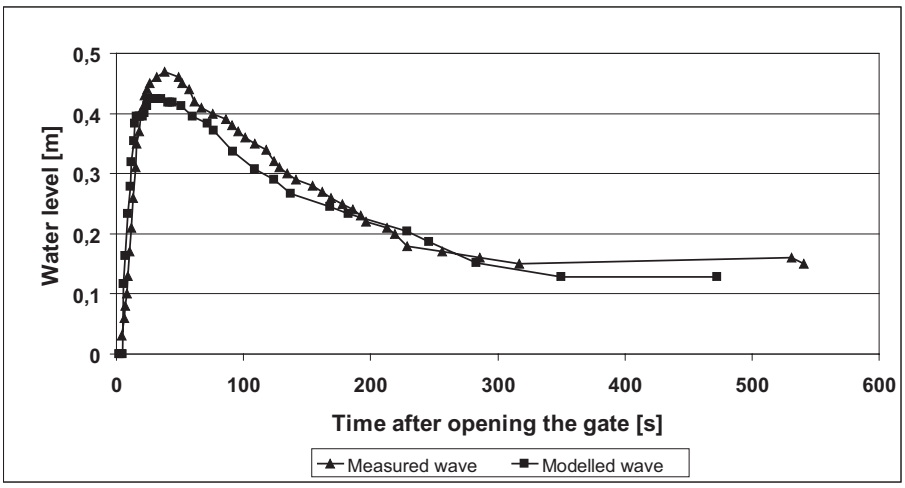

Figure 11.6: Comparison of flush waves, probe no. 1, storage level 0.73 m

11.3.2 Probe no. 4

The modelled wave reaches probe no. 4 at $z = 179$ m 5 seconds after the measured wave. The maximum water level of the modelled wave is around 5 cm lower than for the measured wave. During the declination the modelled wave shows a steeper gradient. (Figure 11.7)

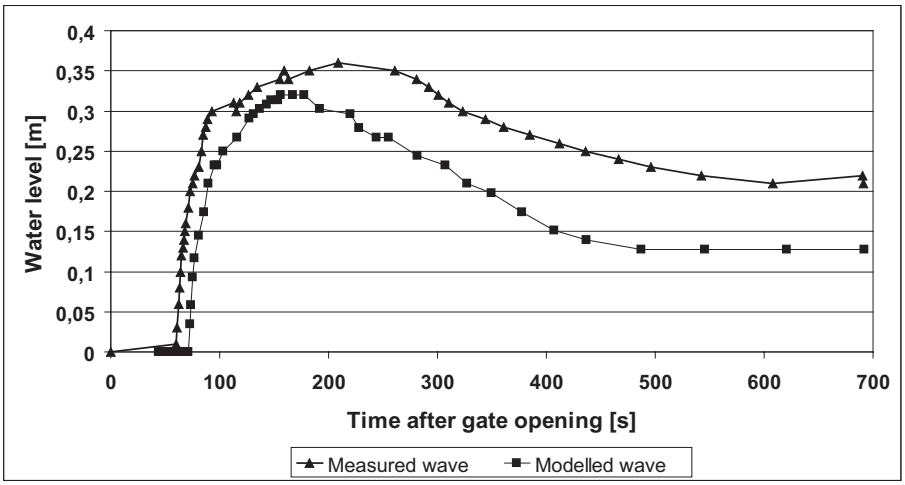

Figure 11.7: Comparison of flush waves, probe no. 4, storage level 0.73 m

11.3.3 Probe no. 5

Probe no. 5 is located at the end of the reservoir sewer after 336 m length. The measured wave reaches probe no. 5 after 152 seconds whilst the modelled wave needs 205 seconds for the same distance. The difference in the maximum water level is 7 cm. The modelled wave declines faster then the measured wave which shows a fluctuant progression in the water level. (Figure 11.8)

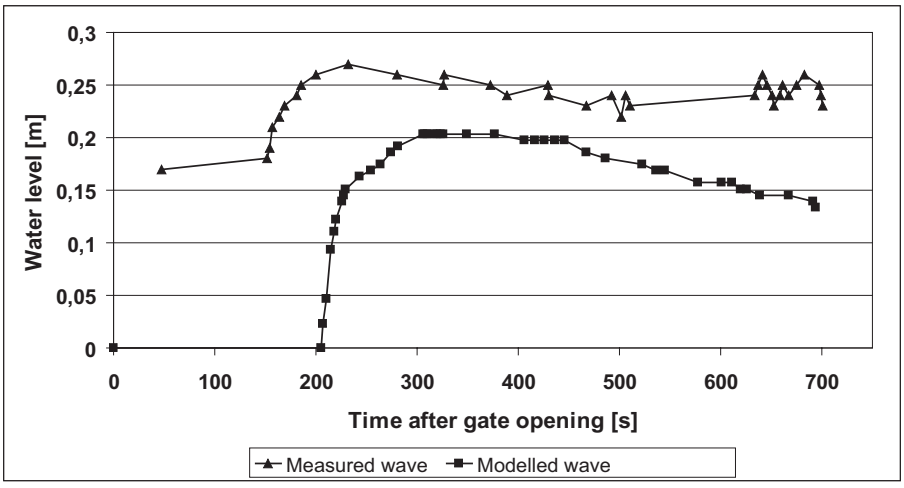

Figure 11.8: Comparison of flush waves, probe no. 5, storage level 0.73 m

11.3.4 Conclusion

The numerical calculations show a very good agreement at probe no. 1 after a relative short running length of 17.5 m. At the probes no. 4 and 5 both flush waves show a tendency to a similar behaviour. Both times the modelled wave is slower than the

measured wave. The differences in the maximum water level of both waves can be justified with inaccuracies of the measurements and the Volume of Fluid Method used by the numerical model StarCD. In the VOF Method the free surface is not exactly defined. It is a band where the boundary between the water and the air is located. Therefore the critical value for the concentration at the VOF was chosen to $C = 0.5$ to define the free water surface. This approach is more or less a good approximation of the location of the free surface. A lower value of C would lead to a faster wave which arrives earlier at the probes but the maximum water level would rise significantly.
The acceleration of the numerical flush wave by a reduction of the bottom roughness would lead to an adjustment of the main flow velocity but it would also lead to a faster declination of the flush wave. It is then very likely that the maximum water level of the modelled wave would decrease due the stretch forming of the flush wave.
The chosen roughness for the dry-weather channel and the slopes offer a good compromise for the agreement of the modelled and the measured wave. This is also shown in appendix D, where the flush waves are compared for the remaining storage levels.

12 Results of the numerical simulations

12.1 Description of the initial phase

Chapter 4 describes two analytical approaches to calculate dam-break waves. They are both subject to certain assumptions and limitations that restrict their validity. To analyse the behaviour or the effects of a flush wave fast and simple calculations are sometimes necessary for practical applications without the usage of supercomputers. In the following chapter the well know analytical solutions of Ritter and Dressler are shown for an initial water level of 1.82 m at the flush gate and they are compared to a detailed numerical solution of the initial phase of the flush wave. The three calculations investigate the first 20 seconds of the moving flush wave. The mean longitudinal slope of the reservoir sewer in this part is 0.55 % and the friction was appraised to $k = 0.15$ mm for the dry-weather channel and $k = 0.25$ mm for the slopes.

12.1.1 Determination of the initial phase using the Ritter solution

The solution of Ritter (1892) is probably the oldest approach to calculate a dam-break wave analytically. The calculation is limited to a rectangular horizontal channel with no friction. The water supply for the dam-break wave is assumed to be unlimited. In the present case of the reservoirs sewer the cross section is supposed to be rectangular. The Ritter wave was first calculated for a horizontal channel and then it was transformed according to the slope of the reservoir sewer.
Taking a storage level of 1.82 m at the gate means that at $x = 0$ the same water level arises. In the reservoir sewer in Offenbach the water level at $x = 0$ is at 1.58 m due to the inclination of the bottom. To make the results of the Ritter solution comparable to the following Dressler and the numerical results, the horizontal channel was shifted according to the real slope. The water level was then adjusted to be horizontal starting from the gate, which lead to a water level of 1.58 m at the start of the reservoir sewer. This violation of the Ritter solution is supposed to be small to make the results comparable. To give a general impression of the propagation of the Ritter wave figure 12.1 shows the transformed Ritter solution for the first 20 seconds for the whole length of the wave distribution. The flush gate is located at $x = 35.5$ m.

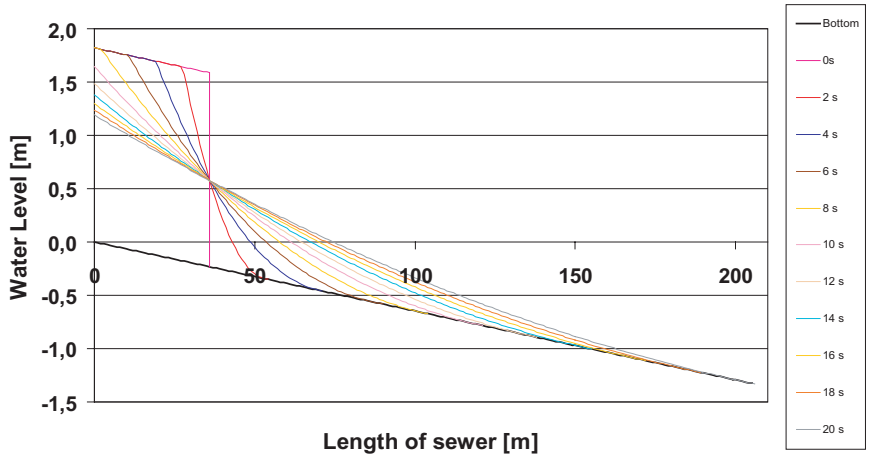

Figure 12.1: Results for the initial phase of the Ritter wave 0 - 210 m

Figure 12.2 displays the behaviour of the dam-break wave according to Ritter for the first 50 m of the reservoir sewer.

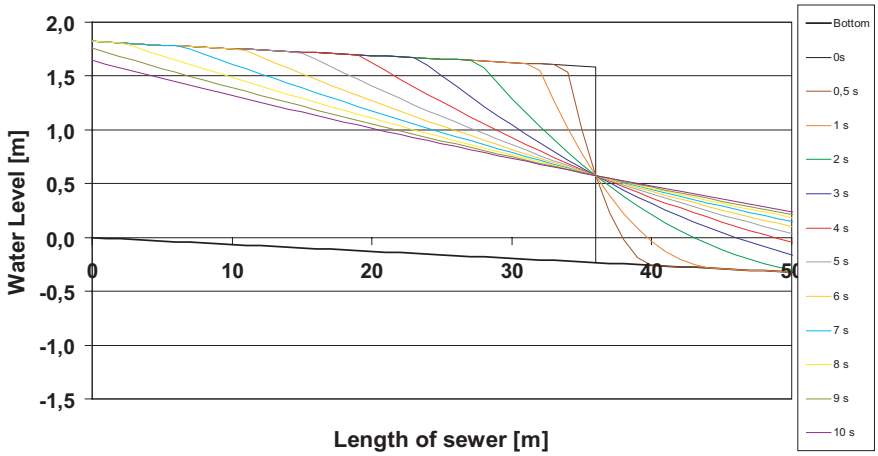

Figure 12.2: Results for the initial phase of the Ritter wave 0 - 50 m

The water level at the flush gate is constant for $\frac{4}{9} \cdot h_0 = 0.81$ m. The front of the dam-break wave converges steadily towards the bottom of the channel and it is obvious that the wave is undisturbed by resistance.

12.1.2 Determination of the initial phase using the Dressler solution

In contrast to the Ritter solution the real dam-break or flush wave is deformed in its front part by the flow resistance of the channel bottom. The leading edge is characterized by a high turbulence and non-uniform distribution of velocity. The front of the wave is formed nearly vertical. Observations of several flush waves showed, that the front head and its development is strongly dependent on the roughness of the sewer. The more deposits are found at the bottom of the sewer the more turbulent and higher the head

of the flush wave will be. This effect is part of the analytical solution of Dressler (1952) as it can be seen in figure 12.3.
The solution of Dressler approximates the progress of a dam-break wave in a horizontal and rectangular channel. The bottom friction is introduced by the Chezy coefficient, which describes the friction with the Manning value. The approach of Dressler only calculates the course of the flush wave downstream of the flush gate. The upstream part of the wave can not regarded. [Bollrich, 1989] In the present case the solution of Dressler was calculated for a horizontal channel and was then transformed according to the slope of the reservoir sewer.

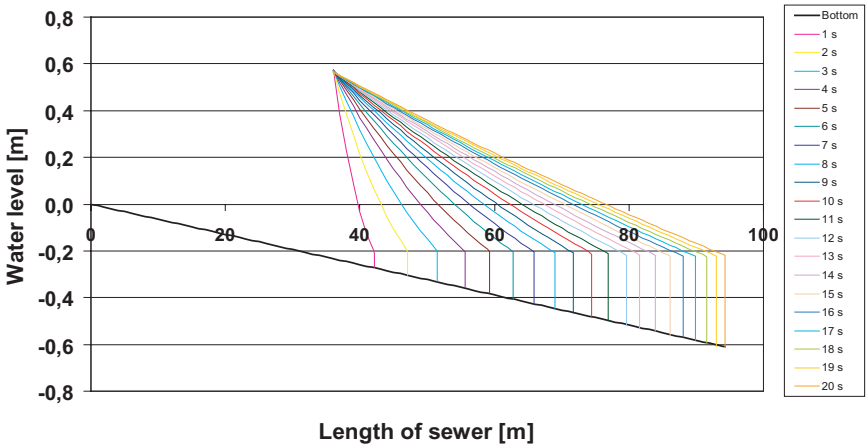

Figure 12.3: Results for the initial phase of the Dressler wave

12.1.3 Numerical simulation of the initial phase

The initial phase of the breaking wave and the behaviour of the sunk wave was modelled in a refined numerical grid.

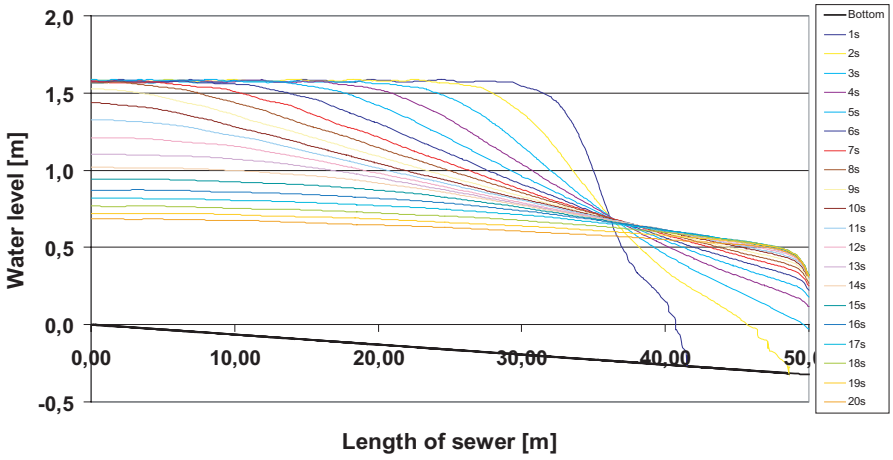

Figure 12.4: Results for the initial phase of the modeled flush wave

The size of the grid cells was 0.125 m in length, 0.025 in height and 0.2 m in width. Only the first 50 m of the reservoir sewer were investigated to cut down the calculation times due the fine grid with 499456 cells. At the end of the flow domain an open pressure boundary was chosen so that the water could leave the grid undisturbed. The modelled storage level was 1.82 m. In figure 12.4 the dropping water level in front of the gate and the sunk wave in its progression in time can be seen.

12.1.4 Comparison of the analytical solutions and the modelled flush wave

At the flush gate the modelled wave shows behaviour similar to the Ritter solution. The flush wave has a nearly constant water level at $x = 0$ at h_{av}= 0.92 m until 15 seconds, then the water level drops significantly. (Figure 12.5)

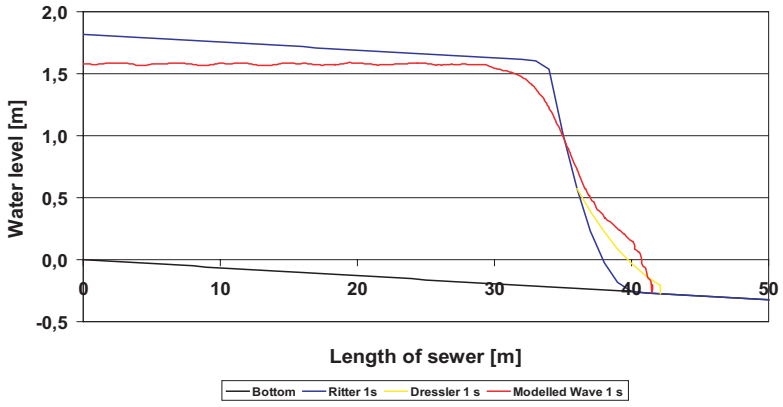

Figure 12.5: Comparison of analytical and numerical solutions, 1s

The constant water level of the Ritter solution is $\frac{4}{9} \cdot h_0 = 0.81$ m which is lower than for the modelled wave. The roughness is considered in the numerical model and leads to a steeper wave compared to the frictionless Ritter wave. (Figure 12.6)

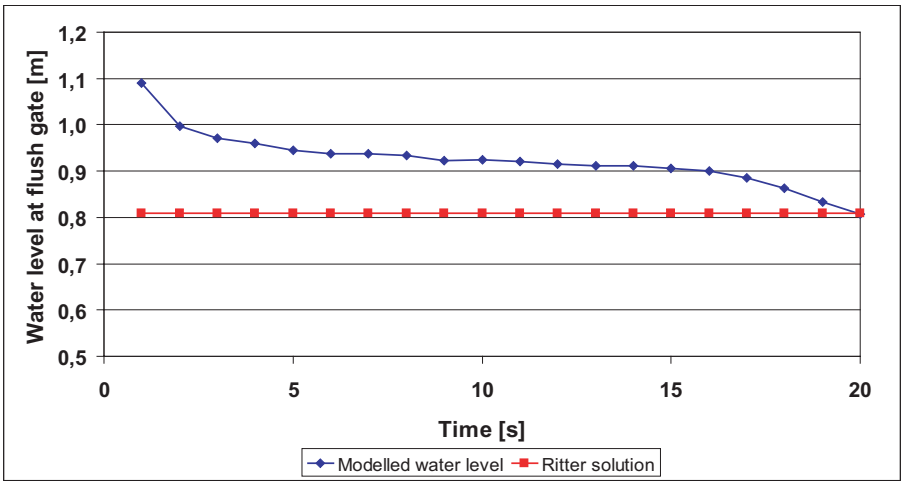

Figure 12.6: Modelled water level at the flush gate

The shape of the front head of the numerical calculated wave is more related to the Dressler solution, which takes the friction into account than to the Ritter solution. A further comparison of the Ritter wave, the Dressler solution and the numerical wave can be found in appendix E.

12.2 Analysis of the bottom shear stresses

The analysis of the bottom shear stresses of the calculated flush waves is used for the evaluation of their cleaning efficiency for different storage levels. The critical value of the bottom shear stress for an efficient cleaning is considered to be $\tau_{crit} = 5$ N/m^2. The determination of the spatial distribution of the bottom shear stresses on the slopes and in the dry-weather channel for a certain storage level was carried out using the results for the turbulent kinetic energy k and the equations as described in chapter 3.7.2.
The investigation of the bottom shear stress maximum values at different times lead then to the formation of trend curves. These curves allow statements about the effective flushing distance for each storage level, which will be shown in the following chapters.

12.2.1 Investigation of the dry-weather channel, storage level 0.73 m

12.2.1.1 Distribution of the bottom shear stresses

Figure 12.7 shows the temporal progression of the modelled bottom shear stress maximum values in the centre of the dry-weather channel (DWC) for an initial storage level of $h_{store} = 0.73$ m. The peak value of the bottom shear stress of 39.74 N/m^2 is reached after 3 s at $z = 42.5$ m. The graph of the bottom shear stresses declines fast after this point and the maximum value falls below the critical value τ_{crit} after 150 s at $z = 230$ m. In the following the shear stresses of the flush wave are below the critical value, which will suggest an unsatisfying cleaning result.

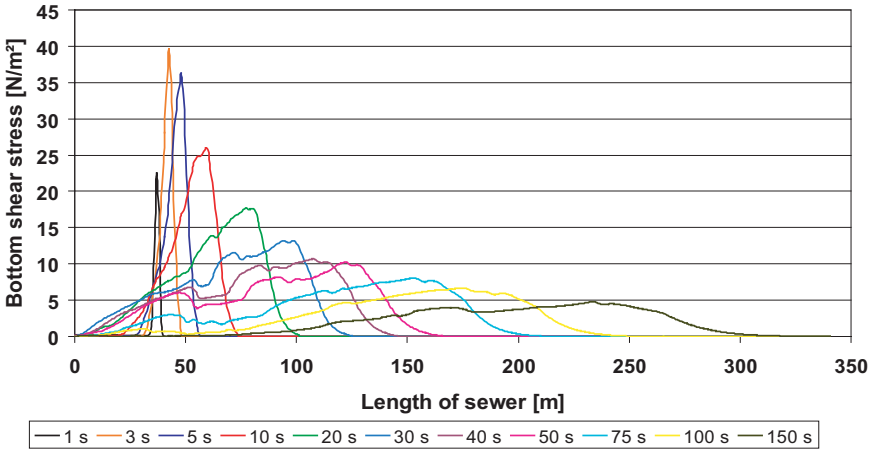

Figure 12.7: Progression of the bottom shear stress, h_{store}=0.73 m, DWC

12.2.1.2 Calculation of the effective flushing distance

The maximum values of the bottom shear stress at different times, shown in figure 12.7, were now used for a regression analysis. Therefore trend curves based on a non-linear regression of exponential functions were generated. These functions describe the possible trend of maximum values for the bottom shear stresses and they vary with the number of chosen time steps out of figure 12.7.
The solution of each trend function with the chosen critical value τ_{crit} = 5 N/m^2 for the bottom shear stress leads to a maximum effective flushing distance depending on the number of implied time steps. Figure 12.8 describes the results for the dry-weather channel for an initial storage level of 0.73 m. Firstly the effective flushing distance increases with a rising number of implied time steps. With only 30 % of the time steps included into the trend function the effective flushing distance decreases.

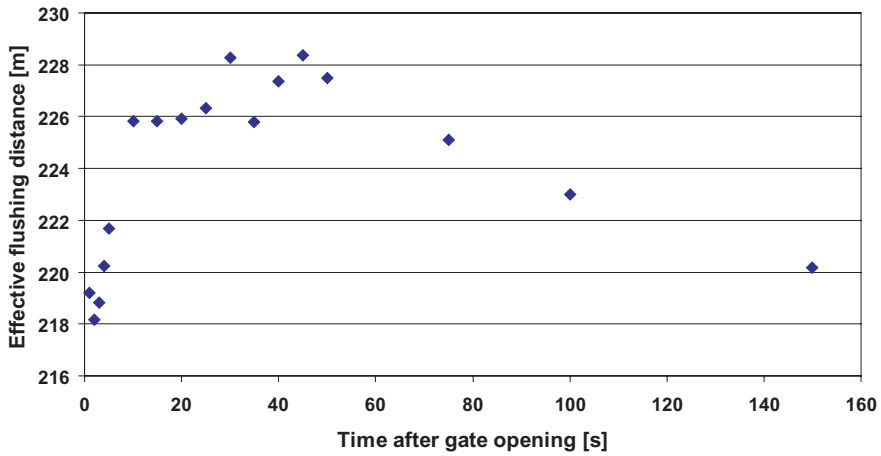

Figure 12.8: Effective flushing distance, h_{store}=0.73 m, DWC

The range for the effective flushing distance of the dry-weather channel will be between z = 218.7 m and z = 228.37 m. The mean value is z = 223.37 m and the standard

deviation $s = 3.54$ m. The confidence interval (95 %) of the effective flushing distance is calculated between $z = 222.16$ m and $z = 225.18$ m. Started from the flushing gate ($z = 35.5$ m) the effective flushing distance will be between 186.66 m to 189.68 m.
The documentation of the progression of the bottom shear stresses and the distribution of the effective flushing distance for all other storage levels can be found in appendix F. Table 12.1 shows the results of the statistical analysis of the regression results regarding the effective flushing distance for all investigated storage levels.

Storage level [m]	Mean value Eff. flushing distance z [m]	Standard-deviation [m]	Confidence-interval 95 % z [m]
0.73	223.97	3.54	$222.16 \leq \mu \leq 225.78$
1.03	331.76	20.78	$319.82 \leq \mu \leq 343.70$
1.25	357.69	15.95	$348.52 \leq \mu \leq 366.86$
1.45	378.55	17.92	$367.81 \leq \mu \leq 389.29$
1.64	400.82	15.70	$391.79 \leq \mu \leq 409.84$
1.82	401.14	4.82	$398.49 \leq \mu \leq 403.79$

Table 12.1: Results of statistical analysis of the effective flushing distance for the bottom shear stresses, DWC

The analysis of the mean values of the effective flushing distance for the dry-weather channel showed their increase with a rising storage level. The maximum flushing distance is reached with 400 m between the storage levels 1.64 m and 1.82 m. (Figure 12.9) After reaching this peak the mean values decrease. This tendency leads to the suggestion that a further increase of storage level above 1.82 m does not increase the effective flushing distance. It seems more effective to increase the flushing volume whilst keeping the storage level to reach a greater flushing distance. In the available case in Offenbach it is not possible due to the boundary condition of the channel. The only possibility would be a relocation of the flushing gate.

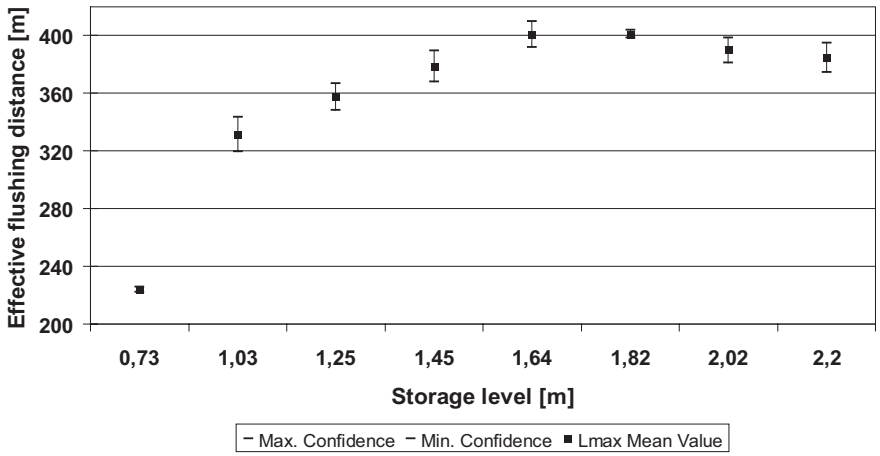

Figure 12.9: Mean values of the effective flushing distance with confidence interval, DWC

Table 12.2 shows the effective flushing distance from the flushing gate ($z = 35.5$ m) for the dry-weather channel.

Storage level [m]	Effective flushing distance [m]
0.73	$186.66 \leq L_{Max} \leq 190.28$
1.03	$284.32 \leq L_{Max} \leq 308.20$
1.25	$313.02 \leq L_{Max} \leq 331.26$
1.45	$332.31 \leq L_{Max} \leq 353.79$
1.64	$356.29 \leq L_{Max} \leq 374.34$
1.82	$362.99 \leq L_{Max} \leq 368.29$

Table 12.2: Effective flushing distance from flushing gate ($z = 35.5$ m), DWC

The distribution of the effective flushing distance depending on the storage level for the confidence interval is displayed in figure 12.10. The trend curves show the same behaviour as the mean values in figure 12.9. The graph approaches a limit value which seems to describe to optimum storage level and the maximum effective flushing distance. This tendency has no real physical background. Further measurements in real sewers and numerical calculations should be made to investigate this tendency about the influence of the storage level.

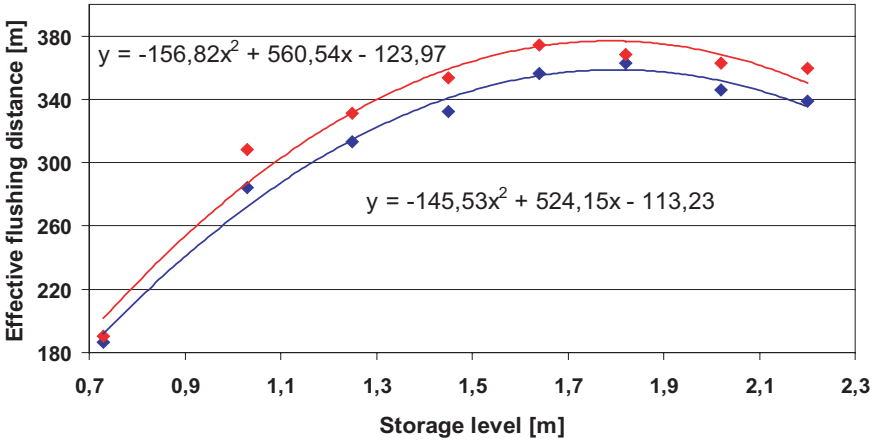

Figure 12.10: Confidence interval effective flushing distance (Minimum and maximum of 95 %), DWC

Figure 12.11 shows the mean value of the effective flushing distance starting from the rotary gate as a function of the storage volume.

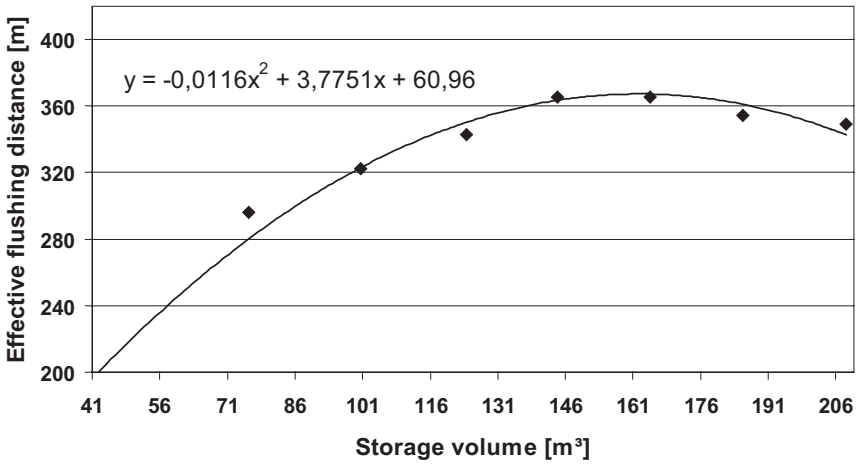

Figure 12.11: Mean value effective flushing distance, DWC

12.2.1.3 Evaluation

Regarding the dry-weather channel the necessary storage level for an effective cleaning of the reservoir sewer on its total length of 336.6 m is $h_{store} = 1.25$ m. The results of the numerical modelling show that with the maximum possible storage level of $h_{store} = 1.82$ m a channel length of 400 m can be cleaned effectively for the dry-weather channel. The cleaning of the sewer slopes along the dry-weather channel is the subject of the next section.

12.2.2 Investigation of the slopes, storage level 0.73 m

12.2.2.1 Distribution of the bottom shear stresses

To evaluate the cleaning efficiency of the flush wave on the slopes the bottom shear stress was calculated at a distance of 0.5 m sideward away from the wall. The analysis is shown in figure 12.12.

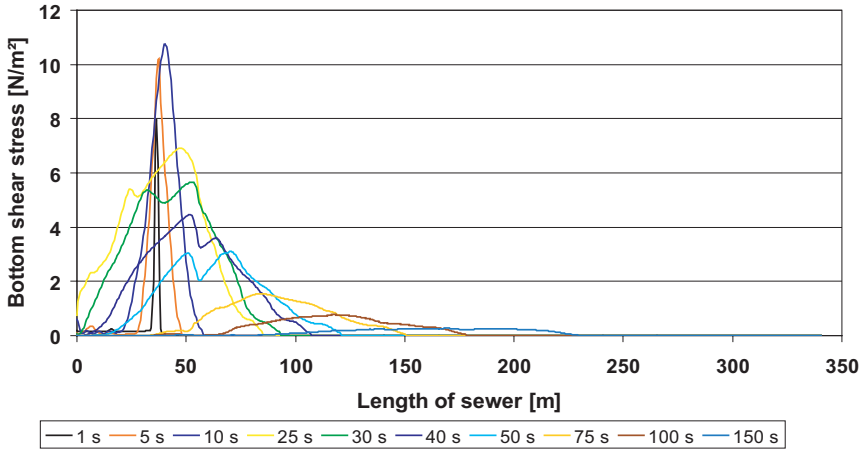

Figure 12.12: Progression of the shear stresses, h_{store}=0.73 m, slopes

The maximum value of the shear stress is 10.75 N/m^2 and was reached after 10 seconds at the location of $z = 40$ m. The critical value of the bottom shear stress was undercut after 35 s at $z = 50$ m. This means that the effective flushing distance for the slopes is significantly shorter than for the dry-weather channel ($z = 230$ m).
Due to the larger hydraulic radius and the cross slope the flow velocity in z-direction is here smaller than in the dry-weather channel. The runoff in the dry-weather channel forms a tongue which flows in front of the main wave body. Figure 12.13 shows a general distribution of flow velocity vector profiles for the bottoms cells after 50 s running time in the dry-weather channel and the slopes.

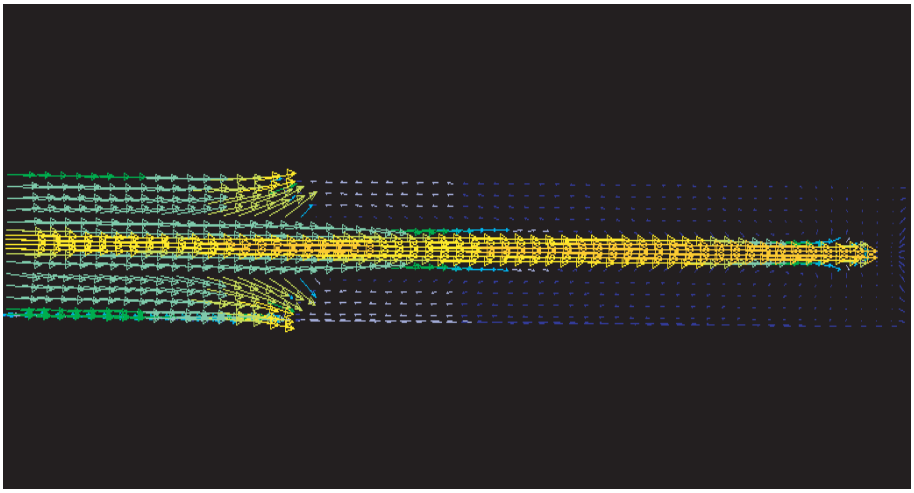

Figure 12.13: Front of the flush wave after 50 s, Vector profiles flow velocity in bottom cells

12.2.2.2 Calculation of the effective flushing distance

The calculation of the effective flushing distance was done analogue to the analysis of the dry-weather channel in the prior section. Figure 12.14 shows the results of the regression analysis for the maximum bottom shear stress values on the slopes at an initial storage level of 0.73 m. The maximum flushing distances, determined by the trend curves, are reduced by an decreasing number of investigated time steps. There is no region visible for the effective flushing distance like in figure 12.8 for the dry-weather channel.

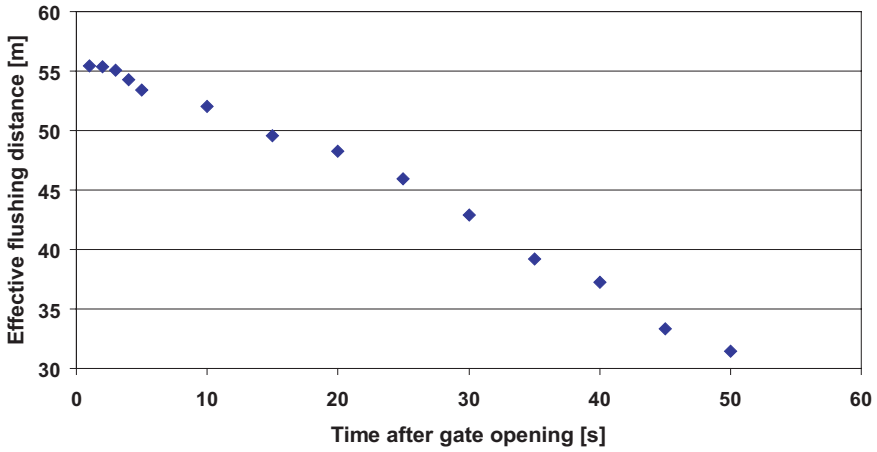

Figure 12.14: Effective flushing distance, h_{store}=0.73 m, slopes

The effective flushing distance for the slopes was placed in a range between $z = 31.42$ m and $z = 55.41$ m. The mean value was calculated to 46.76 m and the standard deviation was 8.49 m. The 95 % confidence interval for the effective flushing distance is located between 41.79 m and 51.55 m. Without the storage length of 35.5 m the effective flushing distance on the slopes for an initial storage level of 0.73 m could be calculated to 6,29 m and 16,05 m.
The progression of the bottom shear stresses and the distribution of the maximum flushing distance for all other storage levels are given in appendix F. Table 12.3 gives the results of the statistical evaluation of the effective flushing distances by the regression analysis.

Storage level [m]	Mean value Eff. flushing distance z [m]	Standard-deviation [m]	Confidence-interval 95 % z [m]
0.73	46.67	8.49	$41.79 \leq \mu \leq 51.55$
1.03	119.15	0.93	$118.59 \leq \mu \leq 119.70$
1.25	153.61	6.84	$149.99 \leq \mu \leq 157.24$
1.45	204.94	1.32	$204.21 \leq \mu \leq 205.67$
1.64	231.53	0.92	$231.02 \leq \mu \leq 232.04$
1.82	266.29	0.58	$265.98 \leq \mu \leq 266.60$

Table 12.3: Results of statistical analysis of the effective flushing distance for the bottom shear stresses on the slopes

In contrast to figure 12.9 the mean values of the effective flushing distances for the slopes show a continuously increasing progression. (Figure 12.15)

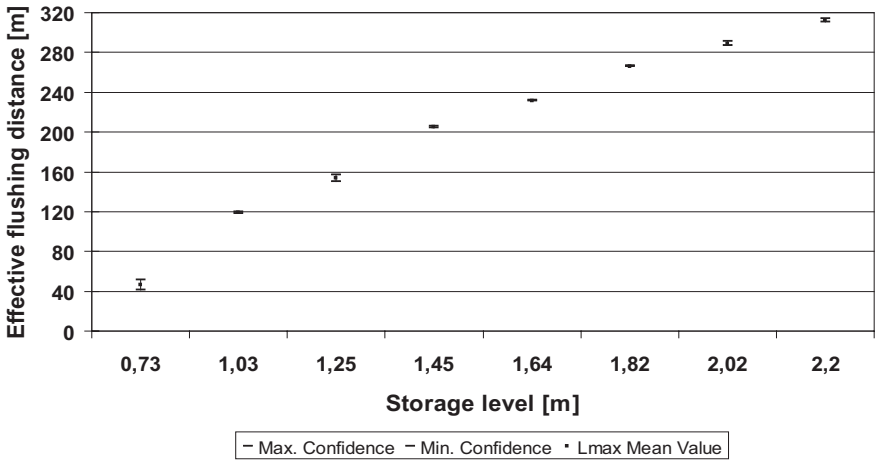

Figure 12.15: Mean values effective flushing distance with confidence interval, slopes

With an increasing storage level it does not seem that the effective flushing distance will approach a limited value. Because of the strong contrast to the behaviour of the mean values for the dry-weather channel the slopes should be the subject of further investigations beyond this thesis.

Table 12.4 displays the range of the effective flushing distance beginning at the flushing gate ($z = 35.5$ m) in dependence of the initial storage level.

Storage level [m]	Effective flushing distance [m]
0.73	$6.29 \leq L_{Max} \leq 16.05$
1.03	$83.09 \leq L_{Max} \leq 84.2$
1.25	$114.49 \leq L_{Max} \leq 121.74$
1.45	$168.71 \leq L_{Max} \leq 170.17$
1.64	$195.52 \leq L_{Max} \leq 196.54$
1.82	$230.48 \leq L_{Max} \leq 231.1$

Table 12.4: Effective flushing distance from flushing gate ($z = 35.5$ m), slopes

The results of the numerical calculations and the regression analysis are summarised in figure 12.16. Similar to the mean values in figure 12.15 the boundaries graphs for the effective flushing distance are increasing continuously. There seems to be no approach to a limit value for higher storage levels. Further investigation should confirm this tendency and will allow more general statements.

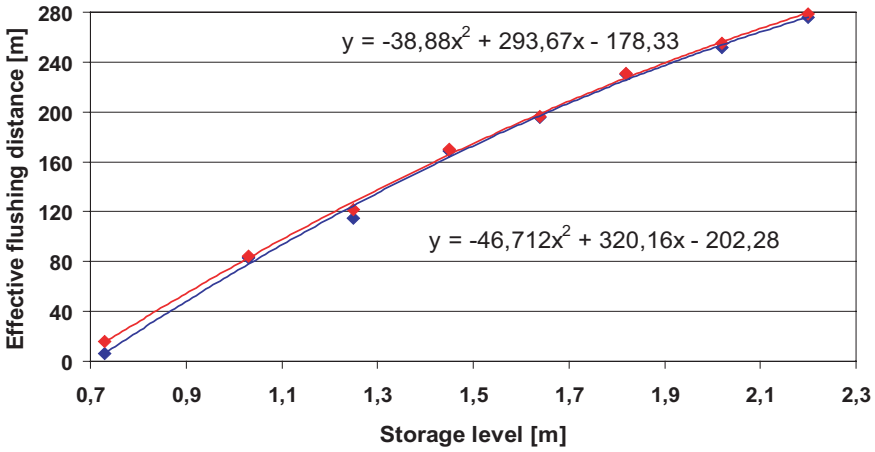

Figure 12.16: Confidence interval effective flushing distance (Minimum and maximum of 95 %), slopes

Figure 12.17 shows the mean value of the effective flushing distance starting from the rotary gate as a function of the storage volume.

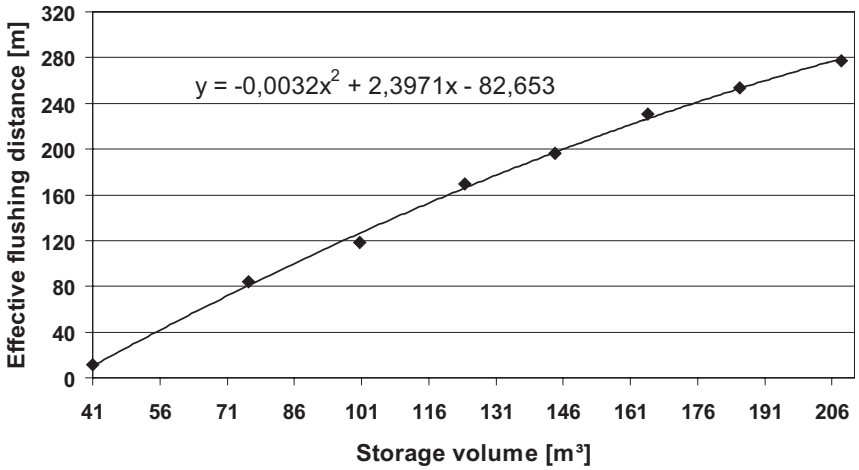

Figure 12.17: Mean value effective flushing distance, slopes

12.2.2.3 Evaluation

The reflection of the results of the numerical calculations reveal that storage levels larger than 1.82 m are necessary to exceed the critical value of the bottom shear stress $\tau_{crit} = 5$ N/m^2 and to clean the slopes of the reservoir sewer efficiently along its total length. The analysis of the trend curve equations in figure 12.16 gives a necessary storage level between 2.56 m and 2.55 m to clean the reservoir on its length of 336.5 m successfully on the slopes.
Inspections of the reservoir sewer in Offenbach showed that due to the thorough cleaning the slopes possessed only small amounts of deposits. Therefore a frequent flushing with

smaller waves and less cleaning efficiency was able to remove these sediments. Long periods of dry-weather without the possibility of creating a flush wave can lead to consolidated and incrusted sediments. Then the flush wave needs to stronger and storage levels above 1.82 m would be necessary to clean the reservoir sewer on its slopes for the complete distance. For this case it would be interesting to investigate the influence of the flushing volume on the cleaning efficiency by keeping a constant storage level.

12.3 Investigation of the gate influence

In this investigation the influence of the gate geometry is analysed and compared with the initial approach of a vertical free standing water body. The flush tests showed that the gate was not overflow in the initial phase for storage levels 1.25 m and below. For larger storage levels the overflow lasted only a few seconds before the flush wave was drained under the gate. Figure 12.18 displays a flush wave running under and above the rotary gate at an initial storage level of 1.82 m.

Figure 12.18: Flush wave running under and above the rotary gate, initial storage level of 1.82 m

To indicate the influence of the flushing gate on the cleaning efficiency a comparison of the bottom shear stresses was carried out. Therefore the flush waves with storage levels of 1.45, 1.64 and 1.82 m were modelled with the flush gate included in the cell grid. The cells for displaying the gate with a thickness of 20 cm were set to impervious. The roughness of the gate was set according to stainless steel with k = 0.08 mm. (Schroeder, 1990) The results were then compared with the bottom shear stresses without the influence of the gate. The figures 12.19 and 12.20 show the bottom shear stress with the gate influence for the dry-weather channel and the slopes at an initial storage level of 1.64 m.

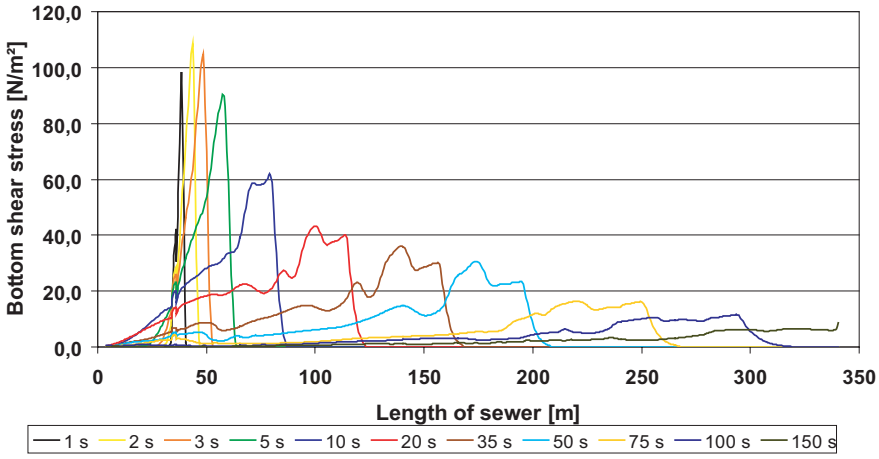

Figure 12.19: Bottom shear stress, Storage level 1.64 m, DWC

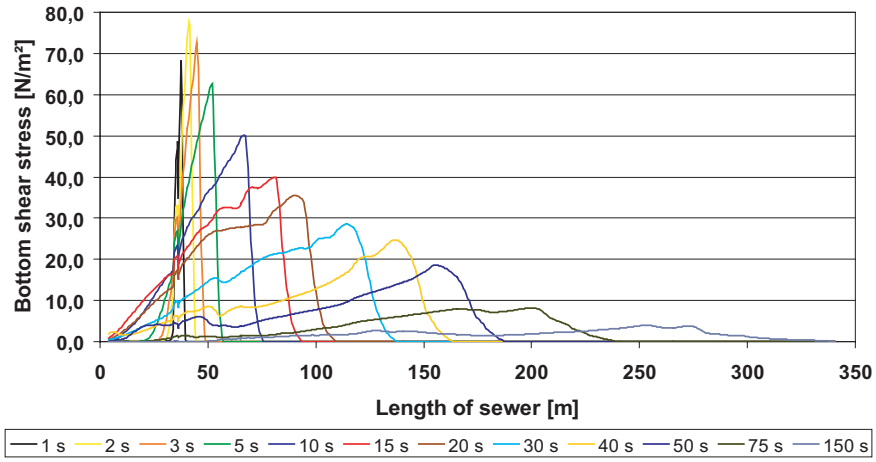

Figure 12.20: Bottom shear stress, Storage level 1.64 m, Slopes

The bottom shear stresses were then compared for the dry-weather channel and for the slopes. In figure 12.21 the comparison between the two approaches shows that for a storage level of 1.64 m the gate does not affect the shear stresses in the dry-weather channel. The curve progression is nearly identical and the differences in the peak values are marginal.

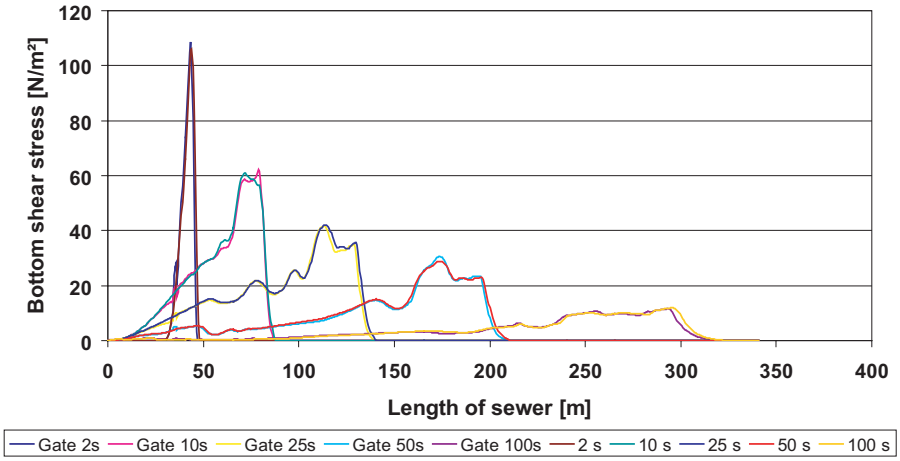

Figure 12.21: Influence of the flushing gate for the dry-weather channel, storage level of 1.64 m.

Figure 12.22 shows the analysis for the shear stresses at the slopes for an initial storage level of 1.64 m. The maximum values of the shear stresses are higher for the flush wave modelled with the gate. This is noticeable for the beginning of the flush wave. The water is constricted at the slopes in its run-off through the gate, so the flow velocity and the shear stresses are higher at the bottom of the sewer. This influence is reduced as the time progresses and the water level drops below the gate. After 100 s the shear stresses for both cases are identical at the slopes.

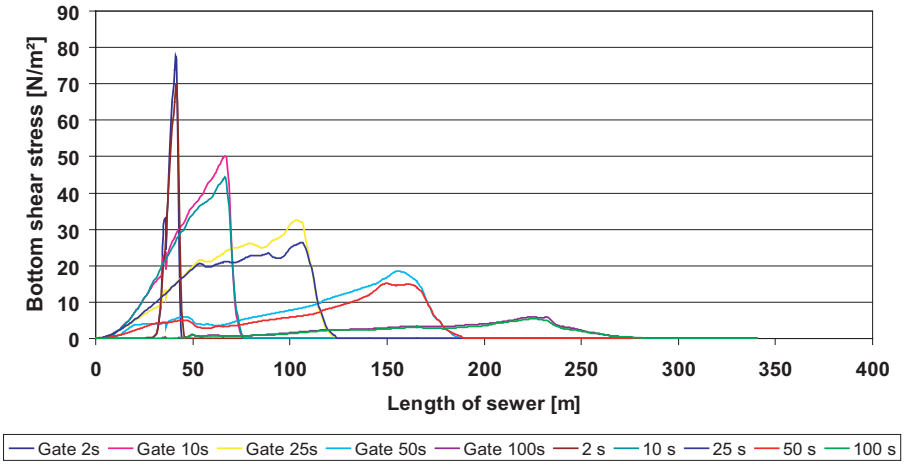

Figure 12.22: Influence of the flushing gate at the slopes, storage level of 1.64 m.

As a result it can be stated that for the flushing of long sewer stretches the hydraulic losses at the flushing gate have a minor influence on the behaviour of the wave and on the cleaning effect. The shear stresses and the comparison for the storage levels 1.45 m and 1.82 m are displayed in appendix G.

12.4 Influence of the flushing volume

The influence of the flushing volume on the effective flushing distance is the subject of the investigations in this chapter. Therefore the flushing volume was varied by reducing the storage length whilst keeping the gate at the location of $z = 35.5$ m and the storage level constant. The numerical grid of the storage upstream of the gate was reduced to 10, 20 and 30 m for two different storage levels of $h_{store} = 1.25$ m and $h_{store} = 1.82$ m. The geometry of the storage length of the reservoir sewer in Offenbach leads to equation 12.1 which describes the flushing volume as function of the storage length L and the storage level h_{store}.

$$V_{store} = 3.2L \cdot h_{store} - 1.1762L \tag{12.1}$$

The influence of the flushing volume will be investigated for the dry-weather channel and the slopes of the reservoir sewer separately.

12.4.1 Storage level h_{store} = 1.25 m

12.4.1.1 Investigation of the bottom shear stresses

The numerical model of the complete reservoir sewer (chapter 10.2) was used for following calculation. The storage level was kept constant at 1.25 m with a variation of the storage length upstream of the flushing gate. Table 12.5 shows the flushing volumes and the storage lengths of each variant with the according percentage of the increase in volume.

Variant no.	Storage length [m]	Storage volume [m^3]	Volume [%]
1	10	28.24	28.16
2	20	56.47	56.32
3	30	84.71	84.50
4	35.5	100.25	100

Table 12.5: Variants of flushing volume, storage level 1.25 m

The bottom shear stresses for each storage volume were calculated by using the before mentioned methods. Then the shear stresses of the different flush waves were compared at different time steps.

Dry-weather channel

Figure 12.23 shows the distribution of the bottom shear stresses in the dry-weather channel 150 seconds after the gate opening for the four different variants.

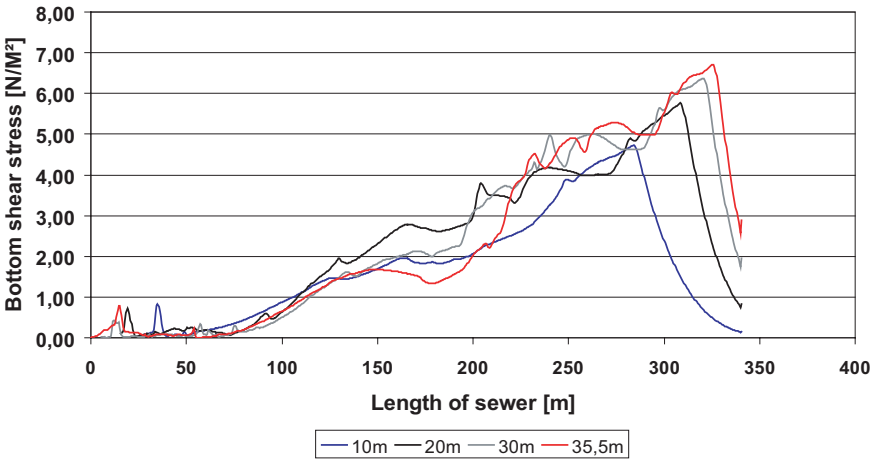

Figure 12.23: Bottom shear stresses 150 s after the gate opening for different storage length, DWC

The illustration of the time steps of 5, 25 and 50 seconds are given in appendix H. It is shown there that after 5 seconds running time the waves are grouped close together. After 25 seconds variant no. 1 with the lowest flushing volume is significant smaller than the other variants. At 50 seconds the variant no. 3 and 4 have two peaks in the bottom shear stress. One small peak in front which is the fast moving water in the dry-weather channel and the main body of the wave who is responsible for the second peak. The variant no. 1 and 2 have one peak, which is slower compared to the other variants. At the end of the channel at 150 seconds all flush wave have a similar distribution of bottom shear stresses. The highest volume (Variant 4) leads to the highest shear stresses. A fact that is not surprising when taking the results of the prior chapter in account. Variant 1 with a flushing volume of 28.24 m^3 just reaches the critical shear stress of 5 N/m^2, which makes it not suitable to clean langer channels distances than shown here.

Slopes

In figure 12.24 the distribution of the bottom shear stresses are shown for 150 seconds after the gate opening. At first after 5 and 25 seconds the progression on the slopes is similar to the one in the dry-weather channel. The shear stresses of variant 1 are low after 25 seconds and this tendency is kept until the waves reach the last part of the sewer after 150 seconds. The progression at this time of all waves is different to the ones in the dry-weather channel. No wave reaches the critical value for the shear stress and shows not the typical peak as for the dry-weather channel. (Appendix H)

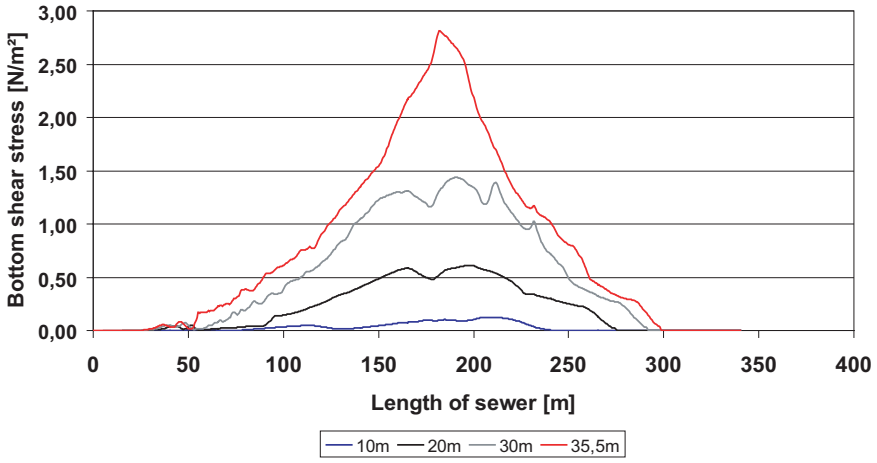

Figure 12.24: Bottom shear stresses 150 s after the gate opening for different storage lengths, slopes

12.4.1.2 Effective flushing distance

Dry-weather channel

The calculation method of the effective flushing distance is equal to the one in section 12.2. For all variants the mean values of the effective flushing distance were determined. (Figure 12.25)

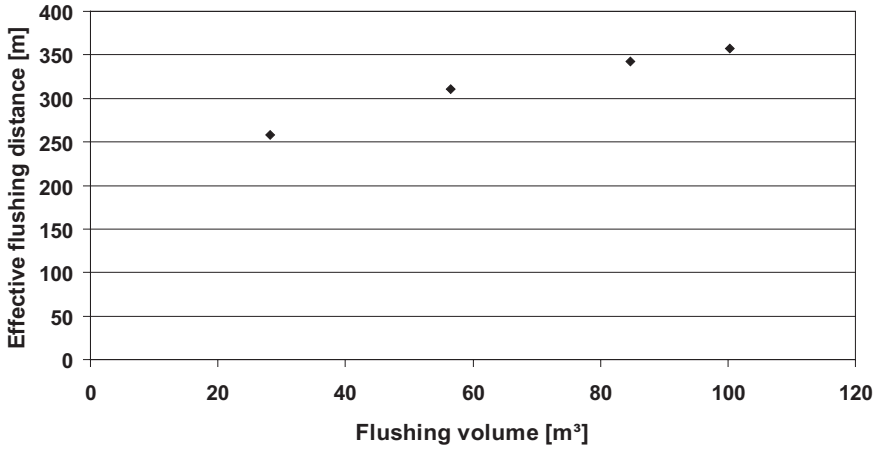

Figure 12.25: Mean values effective flushing distance, DWC

The increase of flushing volume leads only to a small improvement of the effective flushing distance for the dry-weather channel. The double flushing volume rises the effective flushing distance only about 20 %. Figure 12.26 shows the percentages in which 100 % of flushing volume is related to the value of variant no. 1. The effective flushing distance is increasing with a rising flushing volume but the rate of the rise is decreasing.

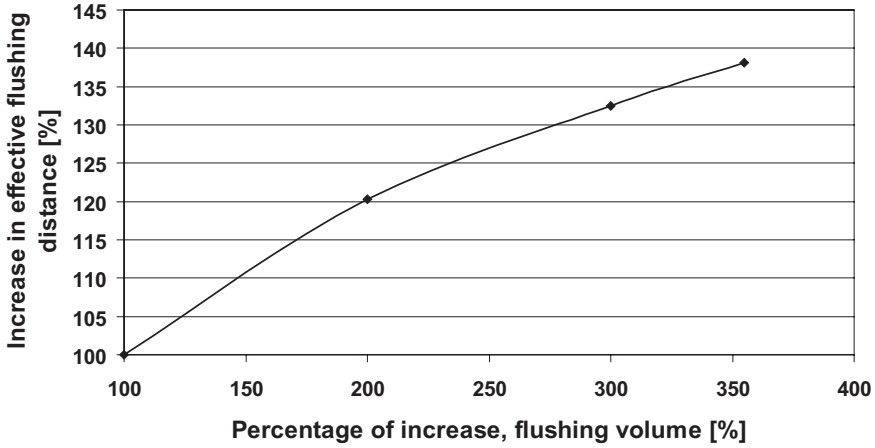

Figure 12.26: Increase of effective flushing distance, DWC

Slopes

The progression of the mean values for the effective flushing distance is much more steeper for the slopes than for the dry-weather channel. So an increase of flushing volume has a greater influence on the cleaning success of the slopes. Figure 12.27 shows the mean values.

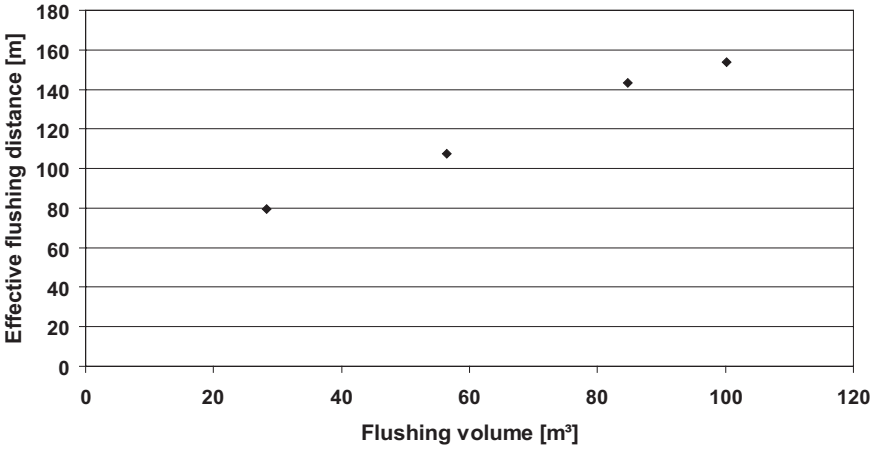

Figure 12.27: Mean values effective flushing distance, slopes

The larger influence of the flushing volume for the slopes is also visible in figure 12.28. An increase of flushing volume of 100 % leads to a rise of the flushing distance of 35 %. The difference between variant no. 1 and no 4 are 93 %.

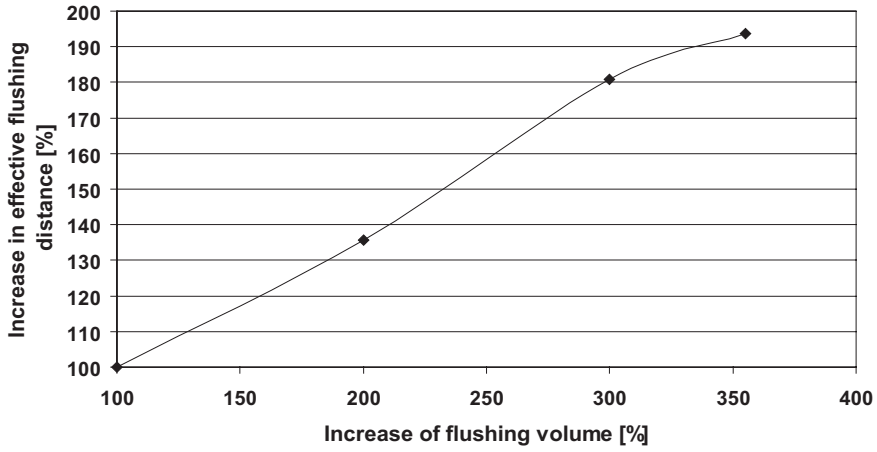

Figure 12.28: Increase of effective flushing distance, slopes

12.4.2 Storage level h_{store} = 1.82 m

12.4.2.1 Investigation of the bottom shear stresses

The flushing volume was varied at a constant storage level of 1.82 as shown in table 12.6. In comparison to the storage level of 1.25 m the storage volumes were significant higher which could lead to a different behaviour regarding the bottom shear stresses or the effective flushing distances.

Variant no.	Storage length [m]	Storage volume [m^3]	Volume [%]
1	10	46.48	28.17
2	20	92.96	56.53
3	30	139.43	84.51
4	35.5	164.99	100

Table 12.6: Variants of flushing volume, storage level 1.82 m

Dry-weather channel

The progression of the bottom shear stresses along the dry-weather channel are similar to the storage level of 1.25 m. Figure 12.29 shows the distribution after 50 seconds. The variants no. 3 and 4 show the significant double peak in the shear stresses and are nearly equal. Variant no. 1 and 2 have lower peaks but they are still well above the critical value for the shear stress. This remains also after 150 seconds running time of the flush wave. (Appendix H)

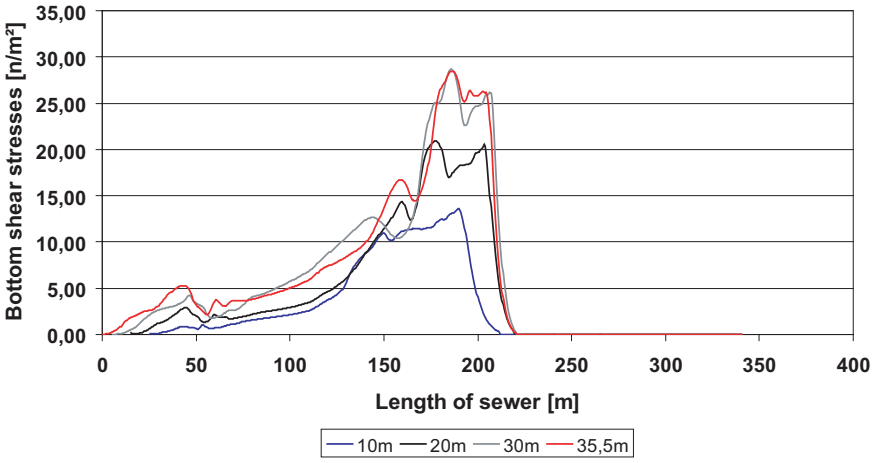

Figure 12.29: Bottom shear stresses 50 s after the gate opening for different storage lengths, DWC

Slopes

The situation of the shear stresses is different for the slopes alongside the dry-weather channel. After 50 seconds variant no. 3 is as fast as variant no. 4 but regarding the shear stresses with no. 4 above no. 3. These two variants show nearly the same distribution after 150 seconds but with a delay of 30 -50 seconds. Variant 4 is having very small values for the bottom shear stresses. None of the variants reaches the critical value for the bottom shear stress after 150 seconds at the end of the sewer. (Figure 12.30)

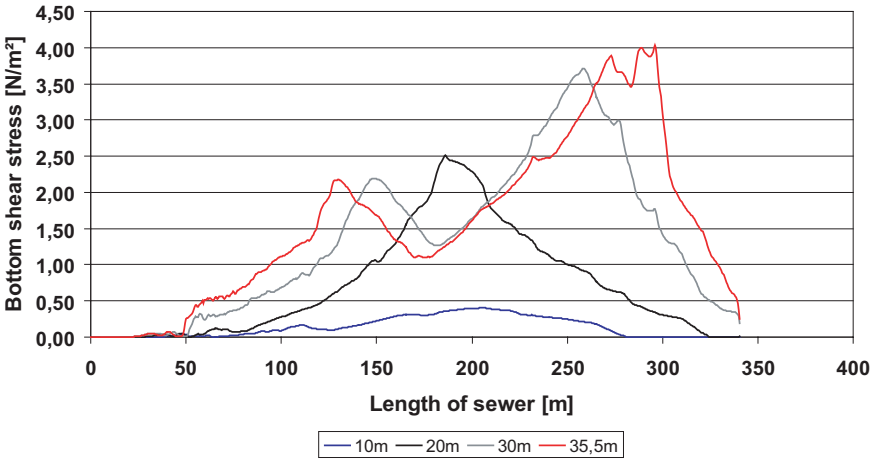

Figure 12.30: Bottom shear stresses 150 s after the gate opening for different storage lengths, Slopes

12.4.2.2 Effective flushing distance

Dry-weather channel

The distribution of the mean values of the effective flushing distance in dependence of the storage volume is shown in figure 12.31. The graph reveals a very shallow curve. It seems that it is approaching a limit value where a further increase of flushing volume will not lead to a significant increase of effective flushing distance.

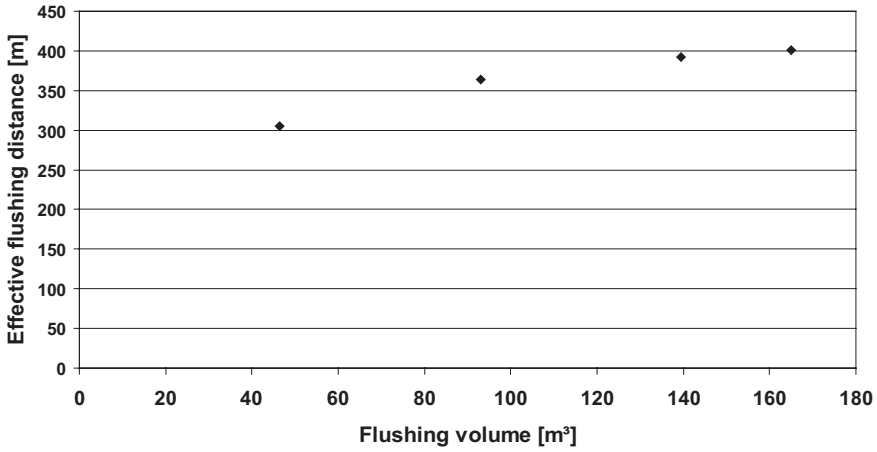

Figure 12.31: Mean values effective flushing distance, DWC

Figure 12.32 displays the increase of the effective flushing distance as a function of the increase of flushing volume. It is apparent an increase of flushing volume of 355 % leads to only to an increase in the flushing distance of 32 %.

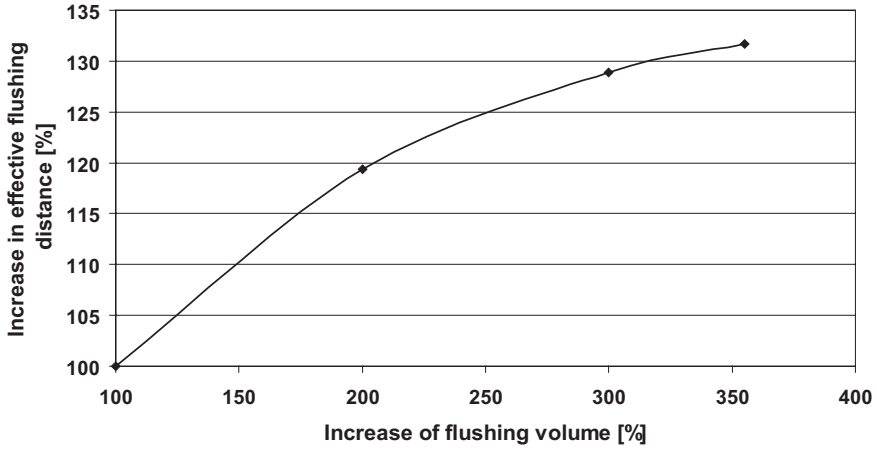

Figure 12.32: Increase of effective flushing distance, DWC

Slopes

A different situation can be found for the slopes. Figure 12.33 gives a steeper curve as for the dry-weather channel. The influence of the storage volume on the effective

flushing distance is significantly greater for the slopes than for the dry-weather channel. For the chosen storage level of 1.82 m an increase of flushing volume of 355 % leads to an increase of the effective flushing length of 159 %. (Figure 12.34)

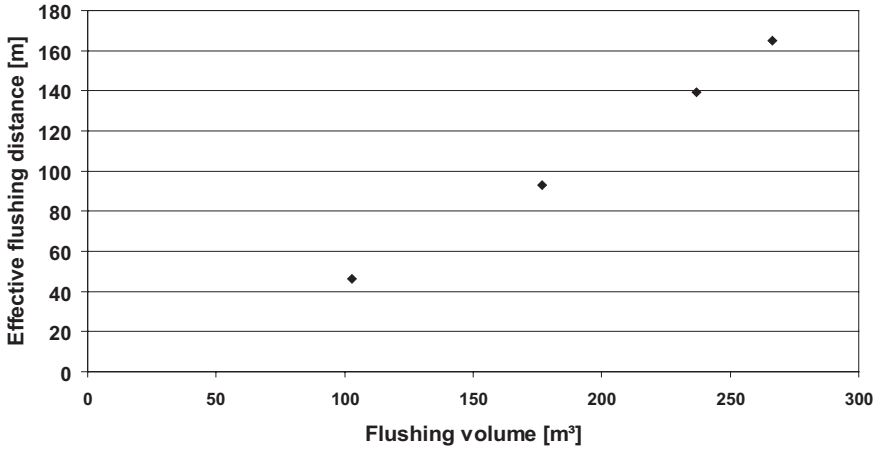

Figure 12.33: Mean values effective flushing distance, slopes

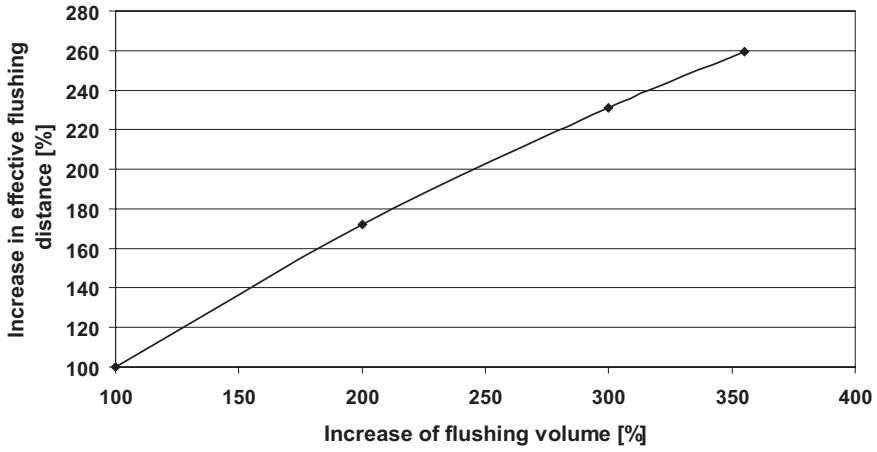

Figure 12.34: Increase of effective flushing distance, slopes

12.4.3 Conclusion

The influence of the storage volume on the effective flushing length is strongly dependent on the location of the flush wave. A flush wave, which cleans successfully the dry-weather channel does not necessarily cleans the slopes too. As shown in this chapter the regional distinctions of the shear stresses can be large and will determine the cleaning result.
The dry-weather channel and the cleaning efficiency there is only weakly influenced by the increase of flushing volume. The slopes must be handled with caution. The influence here is very strong as shown in the prior section. During the operation of a flushing device the conditions on the slopes should be checked regularly especially in the first month

after the installation of the flush gate. When the cleaning of the slopes is not satisfying the storage volume should be increased within the possibilities of the flushing gate until the situation changes.

12.5 Analysis of the time step size

The aim behind the following investigation was, in contrast to section 11.2, to analysis the influence of the time step size on the bottom shear stress. Therefore the reduced numerical model of 200 m length, as used for the calibration, was chosen. The storage level was kept constant for all variants with $h_S = 1.03$ m. The roughness of the dry-weather channel was fixed with $k = 0.6$ mm and $k = 2$ mm for the slopes. The time step size is shown in table 12.7.

Variant	Time step size [s]
1	0.01
2	0.025
3	0.05

Table 12.7: Time step size

The analysis of the bottom shear stresses for the dry-weather channel revealed, that the smaller time step in variant 1 had the highest maximum value and the highest velocity for 1 to 5 seconds running time. Then variant 2 followed before variant 3. (Figure 12.35)

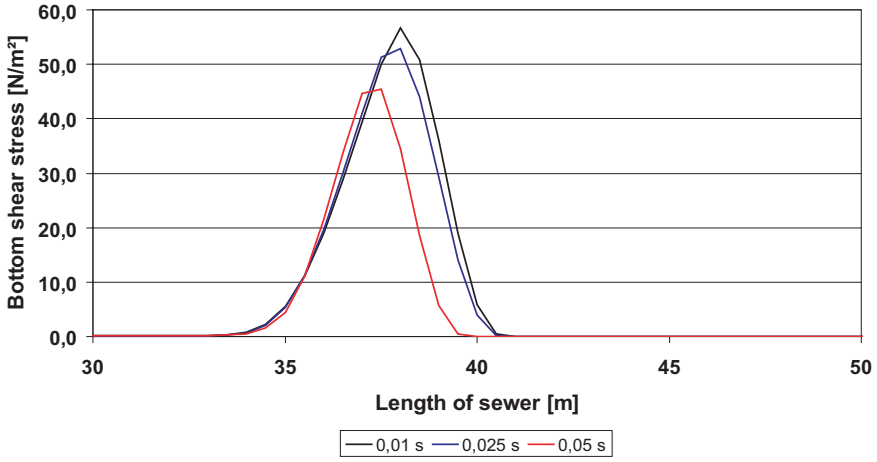

Figure 12.35: Influence of the time step size, 1 second running time, DWC

At 1 seconds running time of the flush wave variant 3 had the highest shear stress followed by variant 2 and 3. After 10 and 50 seconds running time all variants showed equal shear stresses. (Figure 12.36) (Figure 12.37)

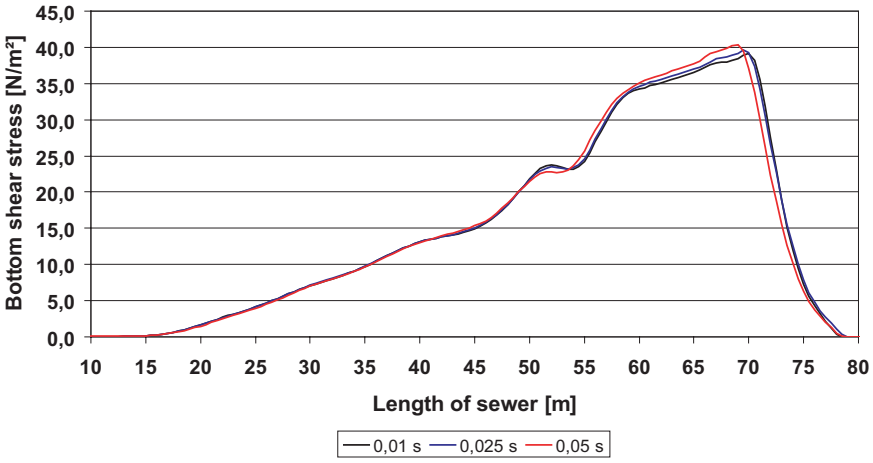

Figure 12.36: Influence of the time step size, 10 second running time, DWC

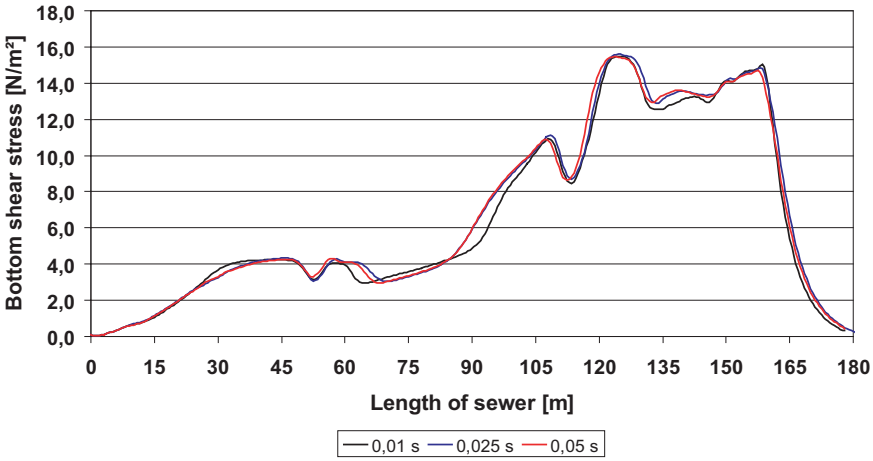

Figure 12.37: Influence of the time step size, 50 second running time, DWC

Regarding the slopes of the sewer channel a similar behaviour of the bottom shear stresses were noticed. For 1 to 5 seconds running time variant 1 and 2 had the same values with variant 3 below the maximum peaks. (Figure 12.38)

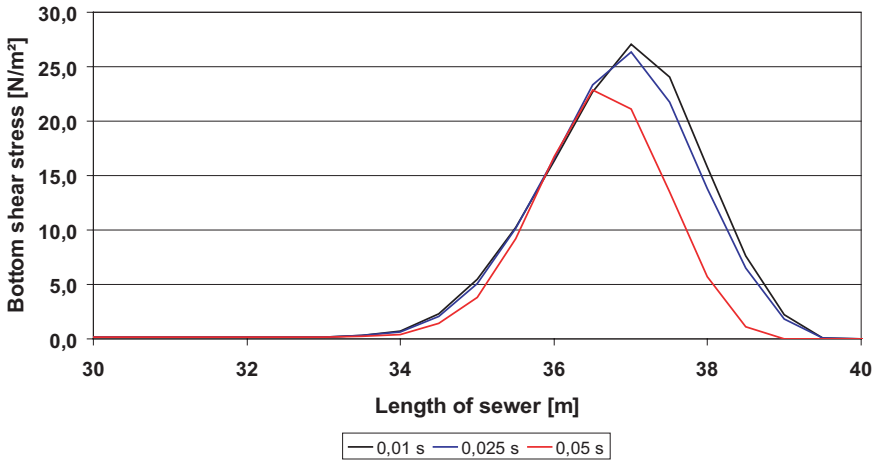

Figure 12.38: Influence of the time step size, 1 second running time, Slopes

Between 10 and 50 seconds running time of the flush wave all variants showed the same progression for the bottom shear stresses and only after 100 seconds variant 1 had an obviously high maximum compared to the other variants. (Figure 12.39) (Figure 12.40)

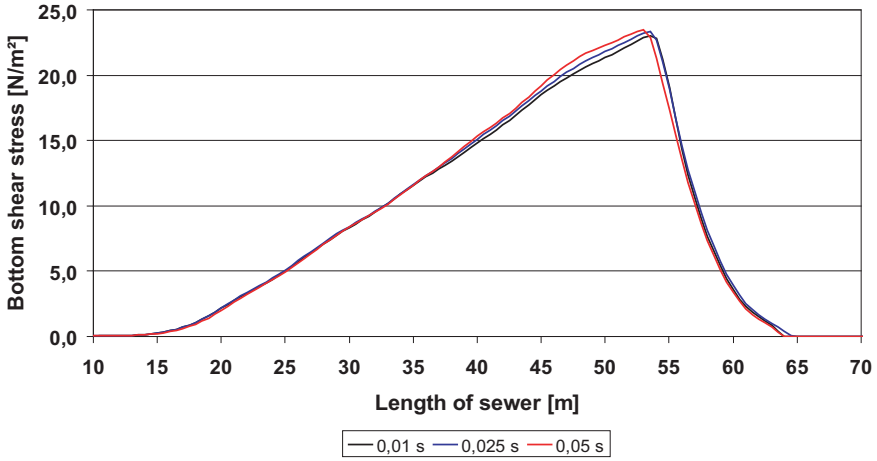

Figure 12.39: Influence of the time step size, 10 second running time, Slopes

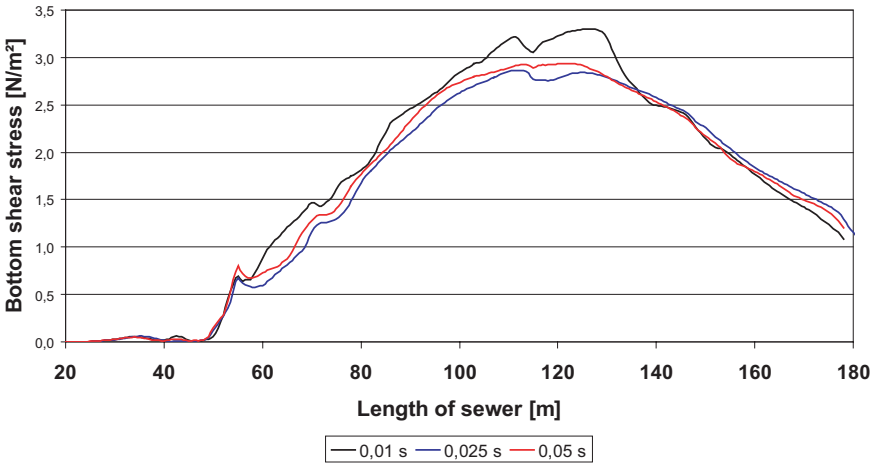

Figure 12.40: Influence of the time step size, 100 second running time

Finally it can be stated that a higher temporal resolutions leads to higher shear stresses for the first 5 seconds of the flush wave running time. Usually the shear stresses in the initial phase are clearly above the critical values for the removement of deposits. Because of this the initial phase is not really important for the cleaning success of a flush wave. Regarding longer running times and therefore longer flushing distances, which are more important, the shear stresses were similar for all variants. In the chosen range the time step size is negligible for the calculation of long distance flush waves. Smaller time steps than the chosen ones may have lead to different results but they would be inappropriate concerning the calculation times of the available computational resources. Therefore it is then more relevant to chose a time step size, which leads to shorter computing times.

12.6 Determination of the log-region

12.6.1 Intention

The calculation of the bottom shear stress with the turbulent kinetic energy k of the $k-\epsilon$ turbulence model was explained in chapter 3.7.2. The value of the shear stress was then a mean value for the thickness of the grid cell at the bottom or the wall of the sewer channel. The validity of the $k-\epsilon$ turbulence model is limited as described in chapter 3.6.2 to a zone where the Reynolds stresses dominate the flow. Beneath this zone, directly at the impervious wall the $k-\epsilon$ turbulence model is not valid. This zone is called the viscous sub-layer where the flow is dominated by the viscosity. Above this zone the buffer layer is placed and here the Reynolds stresses and the molecular viscosity are of equal order.
The modelling approach as already described shows the problem that the grid cells at the walls were larger than the boundary layer. This lead to an averaged value of the shear stresses at the walls. To calculate the shear stress at the walls more detailed it would be necessary to refine the grid in such a way that the lower part of the log-region is resolved. An uncontrolled refinement of the numerical grid leads to a very large number of grid cell and unnecessary long computational times. For a steady flow the boundary

layer can be calculated using the flow velocity but in the available case the flush wave is a highly unsteady flow. Therefore it is necessary to use an iterative to approach to determine the boundary layer depending on the development of the flush wave along the sewer channel.

12.6.2 Approach

The dimensionless wall distance x_2^+ is the major parameter for the determination of the log-layer. The value of $x_2^+ = 100$ limits the log-layer from below. To calculate x_2^+ the shear stress τ_w is calculated for the bottom cells as described in equation 3.85. The shear stress velocity u_τ is then determined with the following equation:

$$u_\tau = \sqrt{\frac{\tau_w}{\rho}} \tag{12.2}$$

The dimensionless wall distance x_2^+ can then be calculated with

$$x_2^+ = \frac{x_2 u_\tau}{\nu} \tag{12.3}$$

If the value of x_2^+ exceeds 100 then the initially chosen grid thickness has to be refined until the dimension less wall distance falls below the limit and indicates the lower limit of the log-layer.

12.6.3 Results

As a first iteration the numerical model with 340 m length of the sewer was refined to a thickness of the bottom cells of 10 cm. The model contained 161.248 grid cells. For a running time of the flush wave of 3 seconds the maximum values of the dimension less wall distance for the dry-weather channel was calculated between $x_2^+ = 579.4$ - 740.1. These values were well above the aimed limit of $x_2^+ = 100$.
For next step a shortened model of 50 m length was created to keep the calculation times in a realistic range. The geometry was chosen to $\delta x = 0.2$ m, $\delta y =$ variable and $\delta z = 0.125$ m. Table 12.8 shows the result for the maximum values in the dry-weather channel and the slopes using an initial storage level of 1.82 m.

Model length [m]	Height bottom cell [cm]	No. grid cells [-]	Wave running time [s]	Max. values x_2^+ [-]
50	2.5	499456	1	237.8
50	2.5	499456	1.5	194.6
50	2.5	499456	2	163.8
50	2.5	499456	2.5	150.4
50	2.5	499456	3	141.6
50	1.25	555291	1	139.5
50	1.25	555291	1.5	141.5
50	1.25	555291	2	131.3
50	1.25	555291	2.5	108.6
50	1.25	555291	3	88.84
50	0.625	591547	1	86.24
50	0.625	591547	1.5	76.76
50	0.625	591547	2	81.46
50	0.625	591547	2.5	82.73
50	0.625	591547	3	71.63

Table 12.8: Determination of dimension less wall distance x_2^+

The results show that a thickness of 0.625 cm is small enough to resolve the log-layer for the initial phase of the flush wave with up to 3 seconds. The steep gradients of the breaking wave make it necessary to refine the grid to such a small grid size. To investigate the thickness of the boundary layer for a flush wave running for a longer time and longer distance a model with a length of 100 m was created. The thickness of the bottom cell was chosen to 2.5 cm, the initial storage level to 1.82 m and the iteration time step to 0.01 seconds. The grid size was δx = 0.2 m, δy = 0.025 m and δz = 0.125 m. The results for a running time of 10 and 15 seconds are given in table 12.9. For 15 seconds running time the front of the flush wave in the dry-weather channel had already left the model limits so it was not possible to locate the front value for x_2^+.

Wave running time [s]	Location z [m]	Max. values x_2^+ DWC	Max. values x_2^+ Slopes
10	35	1.13	9.59
10	40	1.28	10.44
10	50	7.1	81.92 (Front)
10	62	26.73 (Front)	-
15	35	1.09	1.87
15	50	2.19	2.21
15	85	2.70	11.61
15	92	5.19	19.65 (Front)

Table 12.9: Determination of dimension less wall distance x_2^+

The results show that for a running flush wave, disregarding the initial phase, a thickness of 2.5 cm would be sufficient to resolve the boundary layer.

The last step of this investigation was to create a model to cover the complete length of the sewer channel. Therefore a numerical grid with a length of 340 m was modelled. The thickness of the bottom cell was chosen to 2.5 cm and the initial storage level to 1.82 m. The longest possible iteration time step was investigated to 0.002 seconds. The grid size was $\delta x = 0.2$ m, $\delta y = 0.025$ m and $\delta z = 0.125$ m. Due to the number of 725407 grid cells the calculation times were very high. The used personal computer (2.2 GHZ, 512 MB RAM) offered no reasonable solution for calculations of this dimension. A complete run of the flush wave for 200 seconds was not finished after a calculation time of 2 month. The model run was therefore stopped without results. Even for practical purposes it seem not suitable to follow this path of investigations.
To fulfill the original aim of a more detailed calculation of the bottom shear stresses some results are displayed in the following figures. Using the 50 m long numerical model a comparison was made between the calculated bottom shear stresses according to models with a bottom cell thickness of 10 cm and 0.6 cm where the boundary layer is resolved. (Figure 12.41 and 12.42)

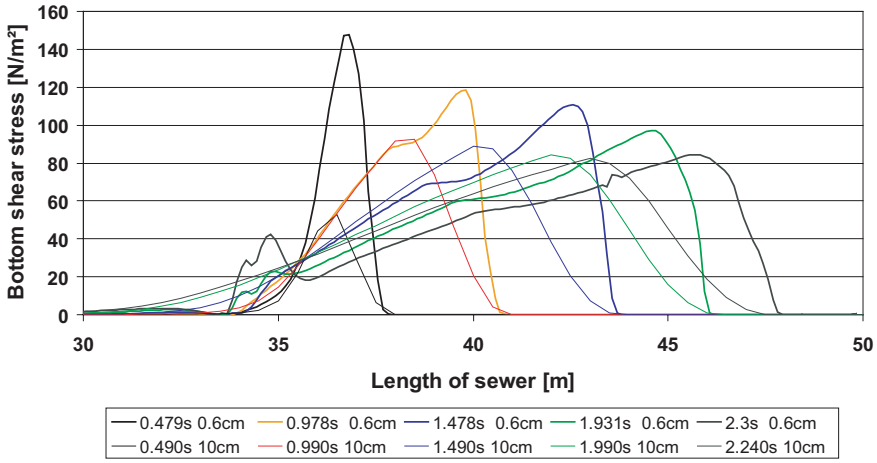

Figure 12.41: Comparsion of bottom shear stresses, DWC

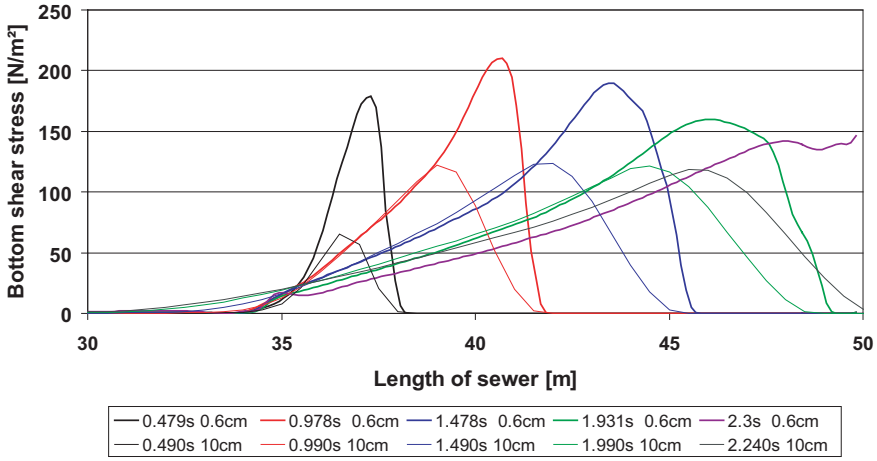

Figure 12.42: Comparsion of bottom shear stresses, Slopes

In the initial phase of the flush wave the differences for the maximum shear stresses are large. The values of the bottom shear stresses with the resolved boundary layer are up 300 % higher than for the 10 cm thickness model. With an increasing running time the difference decreases. The behaviour on the slopes shows a possible trend with nearly equal values for a running time of 2.3 seconds. A further investigation with a longer model and longer running times could reveal the trend of adjustment. It is also obvious that the flush wave modelled with the thinner grid cells is clearly faster than the second wave. The difference in the maximum values seems to be minor especially for longer running times but the differences in flow velocity seem to be increasing. Further investigations could be useful but they should be carried out on larger computational resources than for the present investigations.

12.7 Investigation of the sunk wave

Rapidly varied unsteady flows in open channels can be caused by the sudden opening of valves or by the partly or total break of a dam. These waves are characterized by precipitate changes of variables like the velocity components, pressure distribution and water levels. The upstream moving sunk wave, caused by the opening of the flush gate, leads to a dropping water level against the flow direction. As a first approximation sunk waves can be regarded as decline waves with a nearly vertical front wave but a closer observation reveals that negative surges are not stable in form. The upper portions of the wave travel faster than the lower portions. If the initial profile of the surge is assumed to have a steep front, it will soon flatten out as the surge moves through the channel. (Chow, 1959) The relative wave velocity w is calculated in relation to the undisturbed flow velocity and is a function of the channel cross-section and the height of the shock wave. The absolute wave velocity c describes the velocity in relation to a fixed point at the channel border. The initial undisturbed flow velocity is v_0. For the case of the surge wave moving against the general flow direction equation 12.4

$$c = v_0 - w. \tag{12.4}$$

is valid. Detailed and comprehensive description of the surge wave hydraulics can be found in Bollrich (1989) and Chow (1959).
The initial phase of the breaking wave and the behaviour of the sunk wave was modelled in a refined numerical grid. Only the first 50 m of the reservoir sewer were investigated. The size of the grid cells was 0.125 m in length, 0.025 m in height and 0.2 m in width. At the end of the flow domain an open pressure boundary was chosen so that the water could leave the grid undisturbed. The modelled storage level at the flushing gate was 1.64 m.

12.7.1 Water level

In figure 12.43 the dropping water level in front of the gate and the sunk wave in its progression from 0.1 seconds until 3 seconds is shown. The gradients in the backward

moving wave are steep until 2 seconds running time. Then the water level is dropping slowly.

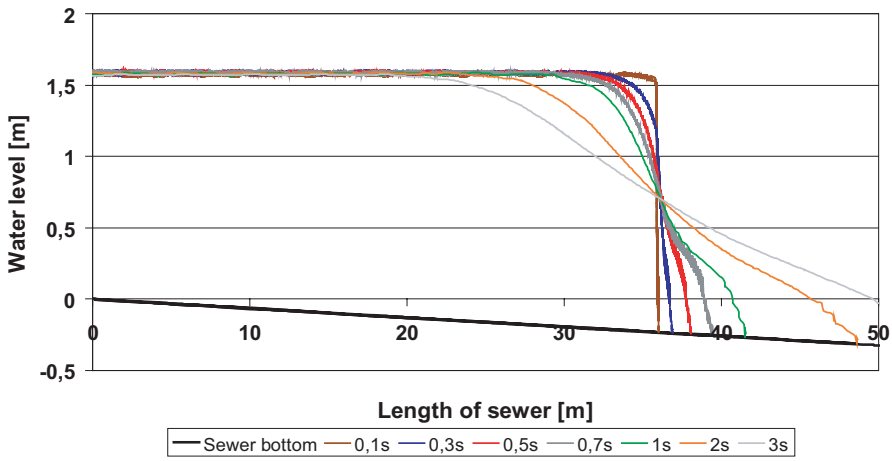

Figure 12.43: Water level propagation of the sunk wave, 0.1 s - 3 s

This tendency is also displayed in figure 12.44. After 9 seconds the sunk wave reaches the upstream boundary, the side weir. The numerical calculations show no reflection of the sunk wave at the side weir. The water level is dropping slowly in the further progression.

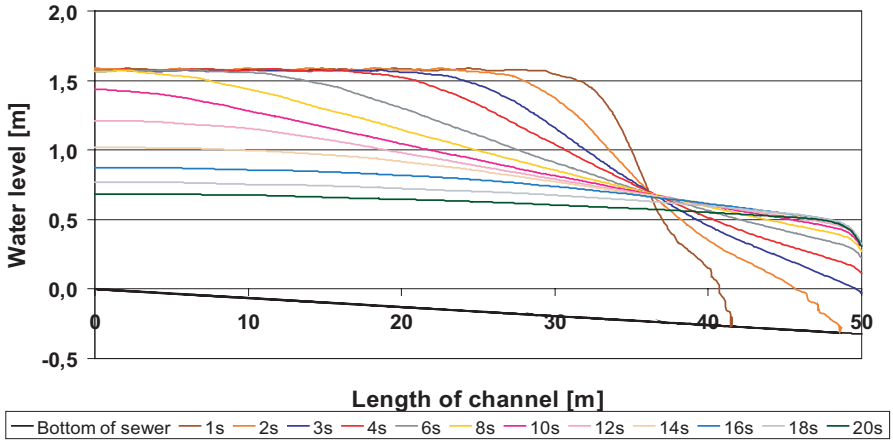

Figure 12.44: Water level propagation of the sunk wave, 3 s - 20 s

Figure 12.45 shows the three-dimensional distribution of the sunk wave after 1 second running time. The steep gradients in the flush and in the sunk wave are clearly visible.

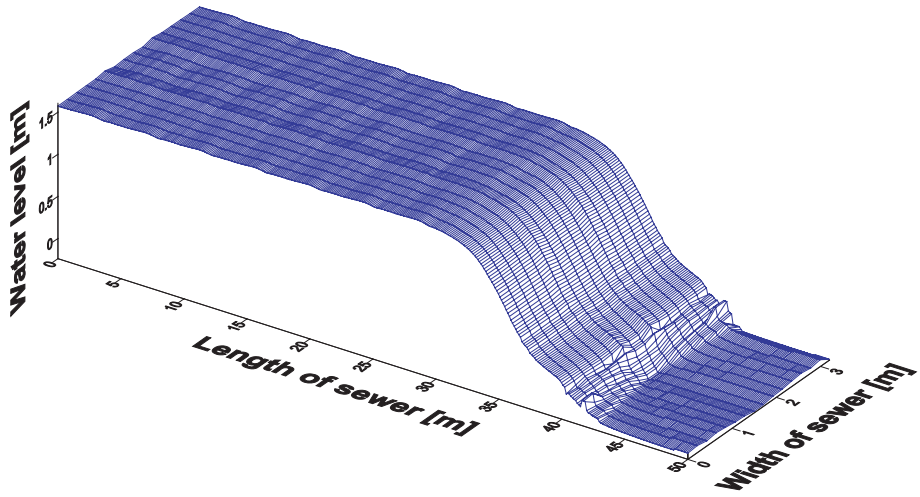

Figure 12.45: Three-dimensional water level propagation of the sunk wave, 1 s

12.7.2 Bottom shear stresses

Much more important for the cleaning results of the reservoir sewer are the bottom shear stresses of the sunk wave. An investigation of the shear stresses for the storage length of 35.5 m showed no significant difference for the dry-weather channel and the slopes. In figure 12.46 and 12.47 the progression of the shear stresses are displayed for the dry-weather channel and the slopes.

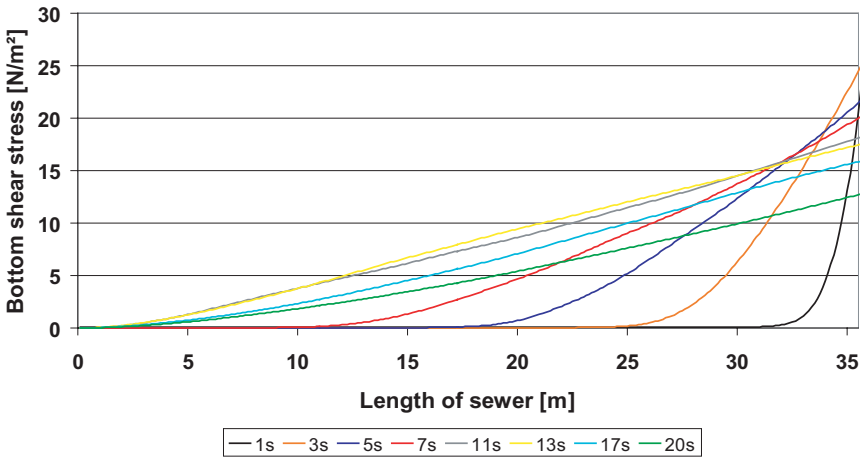

Figure 12.46: Propagation of the bottom shear stresses, DWC

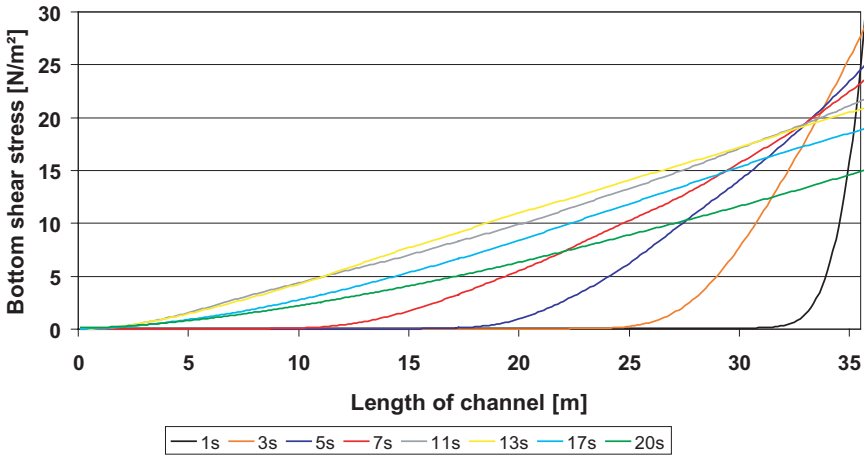

Figure 12.47: Propagation of the bottom shear stresses, Slopes

The shear stresses are moving backwards for 13 seconds then the sunk wave is reflected and is moving downstream. The critical value for the bottom shear stress of 5 N/m^2 is exceeded until z = 12 m, which means that the cleaning effect of the sunk wave covers 66 % of the initial storage length in this particular case.

12.8 Duration of critical shear stress

The previous chapters regarded the critical bottom shear stress as a momentary value at a certain location of the sewer. Once the critical shear stress $\tau_{crit} = 5$ N/m^2 was exceeded a good cleaning result was predicted. A look at the literature shows that a higher bottom shear stress is automatically connected with a better cleaning result. The duration was not taken into account for these considerations. What happens to consolidate deposits if a high peak of shear stress is reached for only a few seconds and then the shear stress drops down immediately? A behaviour like this can be found for the cleaning of storm water tanks with tipping buckets on short distances. The tipping buckets create high peaks of bottom shear stresses, which only last for a very short time. Sometimes one flush is not enough to erode all deposits and it is not uncommon to flush several times with tipping buckets.
It is now the question if it is not more successful to create a flush wave with a lower maximum shear stress value but with a longer duration above τ_{crit} regarding a certain location. The flush wave with a long lasting bottom shear stress clearly above τ_{crit} should have a better efficiency than a wave that has only one high peak of shear stress. Therefore the duration of the shear stress along the sewer bottom was investigated. In dependence of the initial storage level h_{store} and the initial storage volume V_{store} the duration of time was analysed when the bottom shear exceeded the value of τ_{crit} in the dry-weather channel and on the slopes.

12.8.1 Investigation of the initial storage level h_{store}

12.8.1.1 Approach

To describe the temporal distribution of the bottom shear stresses along the reservoir sewer several locations where chosen where the shear stresses were analysed for all storage levels (0.73 m - 2.20 m). The location of the probes were fixed and some further points were chosen to have equal distances between the probes. Table 12.10 displays the locations and the distances in-between the chosen points.

Location No.	Location z [m]	Distance to flushing gate [m]
1	35.5	0
2	53.22	17.7
3	75	21.8
4	100	25
5	139.5	39.5
6	179	39.5
7	231.3	52.3
8	283.6	52.3
9	336	52.3

Table 12.10: Locations for investigation of bottom shear stress

First the bottom shear stresses were analysed at the chosen location for the dry-weather channel and the slopes. Figure 12.48 shows the distribution of the bottom shear stresses at $z = 75$m at the slopes for the different storage levels.

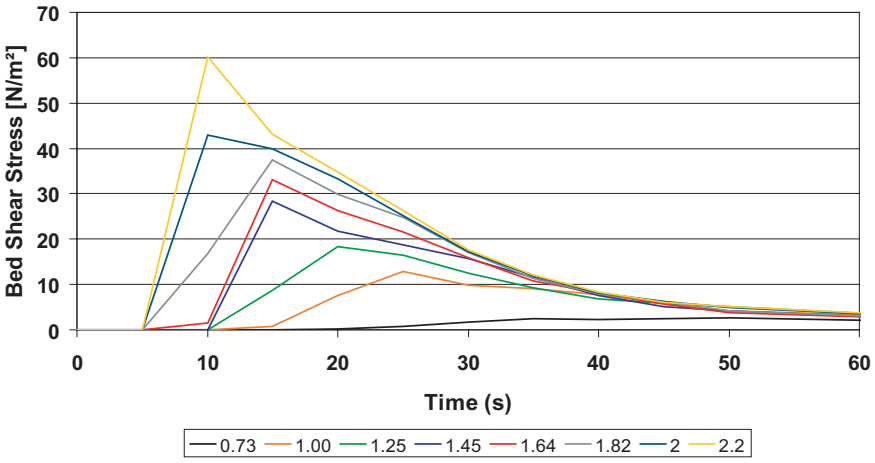

Figure 12.48: Propagation of the bottom shear stresses, z = 75m, Slopes

For each location the bottom shear stresses were examined this way. The duration when the bottom shear stresses exceeded the critical shear stress τ_{crit} was recorded for every storage level at each location. The results for the dry-weather channel and the slopes are shown in the next section in figure 12.49 and 12.50.

12.8.1.2 Results

Regarding the dry-weather channel there is no clear connection between the distribution of the duration of the bottom shear stress and the initial storage level at the flushing gate. The critical shear stress is exceeded for 40 seconds at the flushing gate for all storage levels. This duration is generally increasing for all storage levels up to 80 seconds for $h_{store} = 2.20$ m. Only the curves of 0.73 m, 1.0 m and 1.25 m storage level are decreasing and fall down to zero seconds which means the bottom shear stress is below the critical value. These storage levels are not suitable for a good cleaning result of the reservoir sewer on its complete length. (Figure 12.49)

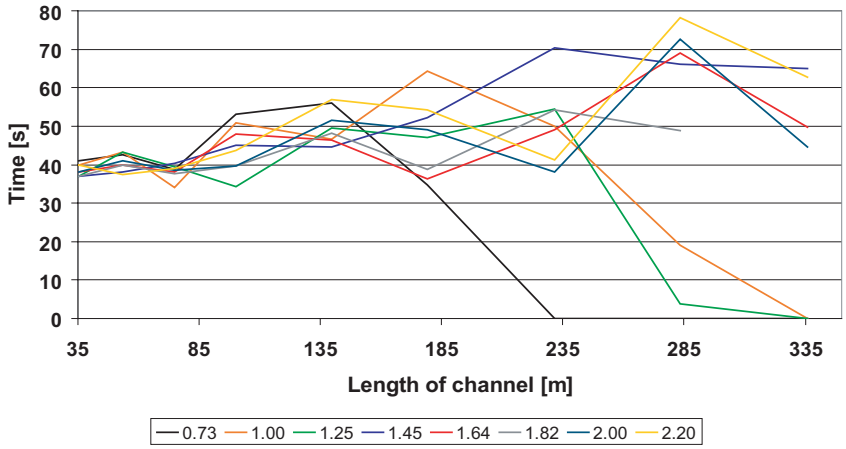

Figure 12.49: Duration of bottom shear stress exceeding τ_{crit}, DWC

Despite of the 1.82 m curve which is below the curves for 1.64 m and 1.45 m at $z = 283.5$ m the larger storage level leads to a longer duration of critical shear stress (2.20m $>$ 2.0m $>$ 1.64m $>$ 1.45m). The tendency of a growing duration can be explained with the reduced velocity of the flush wave after a longer running time. Compared to the start of the flush wave the peak of shear stress is of a more shallow nature which means it is rising and decreasing slower and this leads to a longer duration. At the location of $z = 283.5$ m all curves are decreasing. Only the curve of 1.45 m storage level seems to be constant. It grows until $z = 235$ m then it is decreasing slower than all other curves. In comparison to the storage levels of 1.65 m and 1.82 m the flush wave created by an initial storage level of 1.45 m seems to be well suited to clean the reservoir sewer efficiently on its whole length.

The relation of the duration and the initial storage level is clearer for the slopes. (Figure 12.50) In contrast to the dry-weather channel not all curves are rising. The curves for a storage level smaller or equal 1.45 m are all decreasing, only the curves for the a larger storage level are rising but only for a short time. At a distance of $z = 140$ m the remaining curves are decreasing. Even the flush wave of the largest storage level (2.20 m) is falling below the critical value of the bottom shear stress.
Generally it can be stated that a large initial storage level leads to a longer duration of critical shear stress. Storage levels below 1.45 m lead to a very slow flush wave and the duration decreases constantly. They are not suitable for a good cleaning result of the

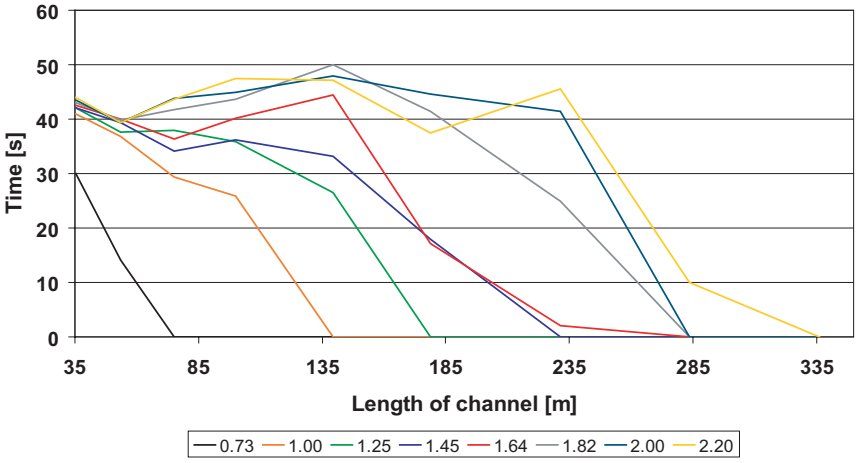

Figure 12.50: Duration of bottom shear stress exceeding τ_{crit}, Slopes

reservoir sewer. The larger storage levels create flush waves, which have a high velocity, which leads to a short duration of around 40 seconds. Then they slow down and this increases the duration until a point when the flush wave is too small and falls below the critical shear stress. To clean the sewer successfully along its whole length on the slopes only the initial storage level of 2.20 m would reach the necessary duration.

12.8.2 Investigation of the initial storage volume V_{store}

The influence of the storage volume on the duration of the critical bottom shear stress was investigated by analysing the shear stress created by flush waves with a constant storage level but varying storage volumes. The storage levels were chosen to 1.25 m and 1.82 m. The storage volume was changed by cutting down the storage length analogous to chapter 12.4. Table 12.11 shows the storage volumes in reference to the storage length and the storage level.

Storage level [m]	Storage length [m]	Storage volume [m^3]
1.25	35.5	100.25
1.25	30	84.71
1.25	20	56.47
1.25	10	28.24
1.82	35.5.5	164.99
1.82	30	139.43
1.82	20	92.96
1.82	10	46.48

Table 12.11: Storage volumes

The analysis of the duration of the bottom shear stresses was carried out equal to the previous section.

12.8.2.1 Storage level 1.25 m

The duration of the critical shear stress at the flushing gate is calculated to be between 10 and 40 seconds for the dry weather channel at an initial storage level of 1.25 m. (Figure 12.51) Then the duration is rising for each storage volume. The curve for the storage volume of 10 m is decreasing after $z = 135$ m, while the curves for 20 m and 30 m start to drop after $z = 185$ m. The curve for the highest flushing volume starts to decrease after $z = 235$ m. The curve for 30 m has the highest duration of shear stresses until the end of the reservoir sewer. The cleaning efficiency seems here to be the most constant.

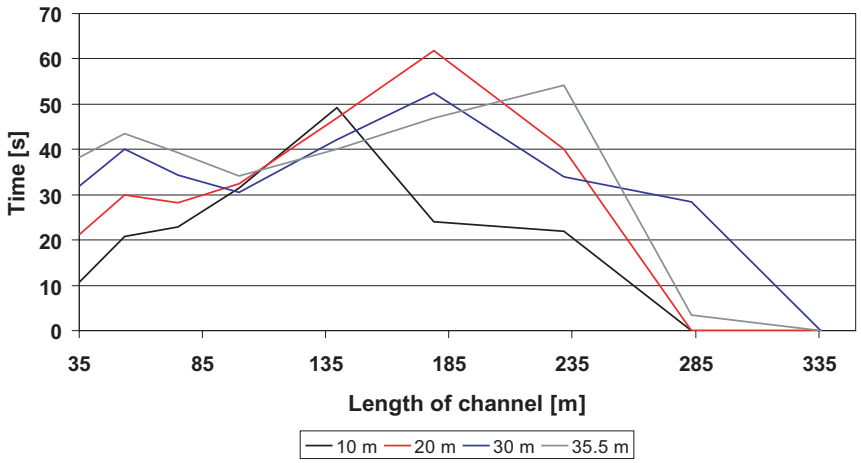

Figure 12.51: Duration of bottom shear stress exceeding τ_{crit} for different storage lengths, DWC

On the slopes the distribution of the duration of the critical shear stresses is very clear. The higher flushing volume creates a longer duration. The bottom shear stresses drop below the critical value after $z = 179$ m for all storage volumes. (Figure 12.52)

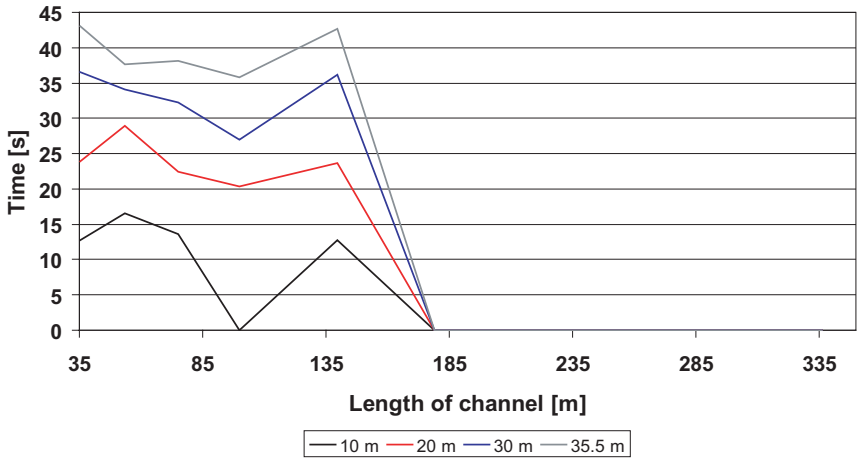

Figure 12.52: Duration of bottom shear stress exceeding τ_{crit} for different storage lengths, Slopes

12.8.2.2 Storage level 1.82 m

The distribution of the bottom shear stress duration in the dry-weather channel for an initial storage level of 1.82 m is different to the one at 1.25 m. Except of the 10 m curve all duration curves are rising along the sewer until its end. Only the 10 m curve decreases after $z = 179$ m and drops down below the critical shear stress. The other curves for the storage length of 20 m, 30 m and 35.5 m seems to be the suitable for the prediction of a very good cleaning result. (Figure 12.53)

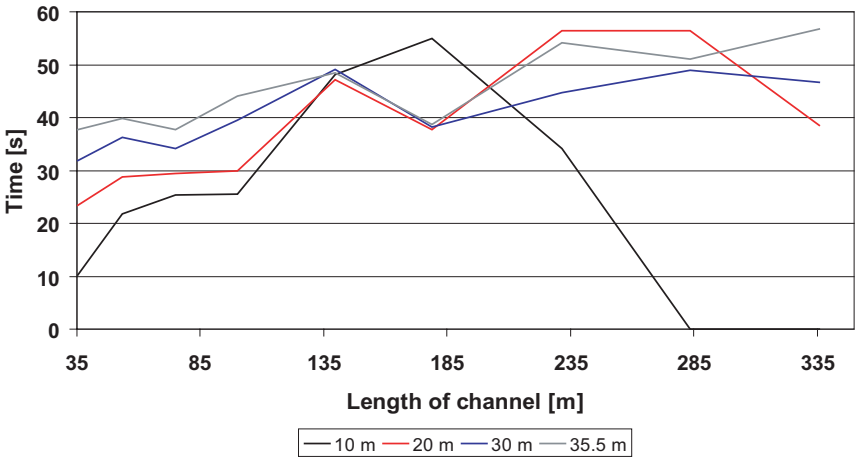

Figure 12.53: Duration of bottom shear stress exceeding τ_{crit} for different storage length, DWC

The results for the slopes show a clear distribution of the critical bottom shear duration. The higher storage volume leads to a longer duration. The values start at the flush gate between 12 and 44 seconds and then drop down after $z = 100$ m and 140 m. The critical shear stress stays above its critical value until $z = 285$ m only for two larger storage volumes. (Figure 12.54)

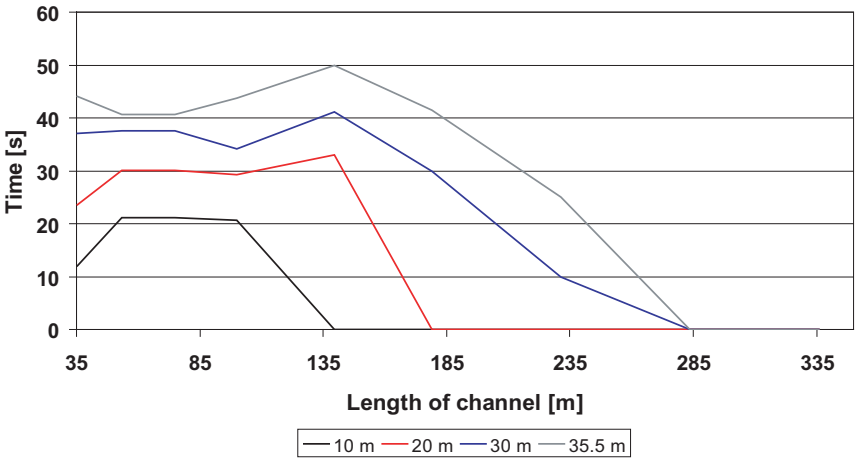

Figure 12.54: Duration of bottom shear stress exceeding τ_{crit} for different storage length, slopes

12.8.3 Conclusion

The results of the investigation of the duration of the critical bottom shear stress show that generally a higher storage level and a higher storage volume will lead to a better cleaning result. There is no obvious linear connection because especially for the dry-weather channel the result are not always obvious. Regarding the storage level it can be stated that a storage level below 1.45 m will result in a disappointing cleaning of the reservoir sewer. A fact that was also obvious in the previous sections of chapter 12.
For the slopes only the higher storage levels of 1.82 - 2.20 m will create a flush wave that cleans the reservoir sewer effectively. The results of the analysis for the storage volume showed that for the dry-weather channel a volume larger than 84 m^3 will be necessary to gain a clean sewer channel. To clean the slopes sustainable flushing volumes larger than 139 m^3 are needed.
To prove the before given suggestion the efficiency of a flush wave with a lower shear stress peak but with higher duration of critical bottom shear stresses should be tested on real sediments against a flush wave with a single high peak of shear stresses.

13 Summary and forecast

13.1 Summary

The intention of this thesis was to apply the approach of three-dimensional numerical modeling to investigate the hydrodynamic principles of flush waves in a reservoir sewer in a high temporal and spatial resolution. Boundary conditions like the flushing gate, the storage volume or numerical parameters such as the time step size were analyzed to understand their influence on the development and efficiency of the flush wave. A special focus had to been placed on the numerical modeling of the initial phase in contrast to historical analytical methods. The main investigation was focused on the potential cleaning efficiency of the flush wave. Therefore the calculation of the bottom shear stress under different boundary conditions was carried out to approximate the maximum flushing distance depending on the storage volume.

First an introduction to sewer deposits, flush cleaning and the methodical approach of this thesis is given. In the next chapter deposits in combined sewer systems are discussed. The formation of deposits in sewer channels leads to a cleaning demand, which can be fulfilled by flush cleaning approaches. The conditions, who lead to sedimentation are explained as well as the locations where the deposits occur. The knowledge of the content of deposits, for example the composition and the properties, is very important to develop efficient cleaning strategies. The height of deposits influences the hydraulic efficiency and the increased roughness reduces the runoff in the sewer channel.
The remobilisation and transport of sewer deposits is the main function of the flush cleaning. The mechanics of remobilisation are explained by the definition of the stability and the critical flow conditions. Different modeling approaches for sediment transport and the transport capacity of flows are presented.

In the following the basics of numerical modelling are given by the introduction of the three-dimensional Reynolds-averaged Navier-Stokes equations. The closure problem of these equations leads to the modeling of turbulence by using the $k - \epsilon$ turbulence model for example. The discretisation in space and time with the Finite Volume Method is displayed for a better understanding of the chosen three-dimensional fluid dynamic solver StarCD.
The determination of the free surface is a difficult issue and of great importance for the investigation of flush waves to visualise their movement. The Volume of Fluid Method is explained as it is used in StarCD. The boundary conditions define the behaviour of the flow at impervious walls for example and restrict the in- and outflow of the flow domain. Initial conditions like the storage height complete the numerical model. The wall shear stress is the major parameter for the evaluation of the cleaning success of a flush wave. Therefore the definition and calculation of the shear stress is explained in detail.
The analytical determination of the dam-break wave is another comparative way to

describe the behaviour of a flush wave in a sewer channel. The derivation of the three-dimensional Reynolds averaged Navier-Stokes equations leads to the two-dimensional depth-averaged classical shallow water equations. The next step is the derivation of the one-dimensional Saint-Venant equations with their general assumptions and possible solutions. In the following analytical solutions of Ritter and Dressler are derived from these one-dimensional equations. Both approaches have strong limitations, which restricts their suitability to describe dam-break or flush waves.

The next three chapters outline different literature reviews. The first shows convenient one-, two- and three-dimensional simulation modells to calculate flush waves. The differences are explained as well as the advantages and drawbacks of the single approaches. The model StarCD, which was chosen for the following investigations, is specified in detail. The second literature review covers numerous flushing devices. The historical background, the principle and the effects of flush waves are discussed. Then the flushing devices are separated into three group and presented in their applications. The last literature review resumes several investigations on flush cleaning. The main investigations and their results are described to give a comprehensive overview on the research carried out by universities, engineering consultants and companies.

The reservoir to be investigated subsequently is located in the August-Bebel Ring in Offenbach. The description of the reservoir sewer specifies the geometry of the sewer channel and the functionality of the rotary gate. To visualize the development of the flush waves and to receive data for the calibration and validation of the numerical model, three ultrasonic probes were installed along the reservoir sewer. Two further independent probes were installed for the control of the rotary gate. Six flush tests with different initial storage levels and corresponding flushing volumes were run to derive the necessary data for the numerical model. The measuring technique of the water level and the location of the ultrasonic probes are displayed to point out the chosen approach.

The geometry and the boundary condition of the reservoir sewer were reproduced in the three-dimensional numerical model StarCD. First a shortened model of 200 m length was set up to carry out the calibration of the model with short computational times according to the measured flush waves. A model of the complete reservoir sewer was built-on for the validation of the calibrated model and the following investigations of flush waves.
For the calibration of the numerical model the shortened geometry was set up with an initial storage level of h_s=1.03 m at the rotary gate. The calculated temporal water levels at the first two probes (no.1 and 4) downstream of the rotary gate were analyzed and compared with the measured wave possessing the same initial storage level. The roughness of the dry-weather channel and the slopes was then varied in three different scenarios to adjusted the modeled wave to the measured one. A roughness of $k = 0.15$ mm for the dry-weather channel and $k = 0.25$ mm for the slopes brought a good agreement of the calculated wave to the measured one. Further variations with different iteration time steps lead to no further improvement of the modelled results.
To validate the calibrated numerical model flush waves the geometry of the complete reservoir sewer was set up and calculated with the remaining five initial storage levels. The flush waves were evaluated at the probes no.1,4 and 5 for the temporal progression of the water level. The results were compared with the measured flush waves having the equal initial storage level at the rotary gate. At probe no.1 the waves showed a

good agreement. At the probes no.4 and 5 the modelled flush waves were slower then the measured one, having a lower maximum level and a faster declination. A reduction of the roughness would have led to a faster flush wave but it would have also meant a lower maximum and an increased declination. Therefore the chosen roughness for the dry-weather channel and the slopes offered a good compromise.

The numerical investigations of the behaviour, development and effect of flush waves were split up in eight different topics. Parts of these results presented in this thesis were already presented and published in Schaffner et al. (2006a,b).
First the initial phase of the flushing wave was analyzed using the analytical Ritter and Dressler solutions. A refined numerical model of the first 50 m of the reservoir sewer was set up to calculate the initial flow of the breaking wave. The analytical solutions were then compared with the modelled flush wave. Despite the limitations of the analytical approaches the waves showed a good agreement until a running time of 5 seconds. Then the modelled wave had a steeper front compare to the Ritter and Dressler solution due to influence of the bottom friction. The sunk wave upstream of the rotary gate displayed the most visible differences where the modelled wave declines faster then the analytical approaches. The determination of the wave development with the given bottom geometry using the Ritter or Dressler approach gave no meaningful results, especially when the wave is regarded for longer running times.

The analysis of the bottom shear stress was the main investigation in this thesis. It was the aim to study the effective flushing length for the dry-weather channel and the slopes against the storage level at the gate and the flushing volume.
Therefore the bottom shear stress was calculated for different running times of the flush wave. The maximum values at each time was then plot along the sewer to get the maximum bottom shear stress at different locations. Trend curves were then formed between these values to describe the progression of the maximum bottom shear stress for a given storage level. Using a critical bottom shear stress of 5 N/m^2 as the limiting value, the effective flushing length was calculated. The location where the bottom shear stress went below the critical value of the bottom shear stress the effective flushing distance was reached. The function of the trend curves varied with the number of time steps which were used for the analysis of the effective flushing distance. This way different effective flushing distances were determined for a certain storage volume. For these different flushing distances the mean value, the standard deviation and the 95 % confidence interval were calculated.
Regarding different storage levels and flushing volumes trend curves of the mean values and the confidence interval were formulated. The progression of these trend curves showed a different behaviour for the dry-weather channel and the slopes.

The maximum effective flushing distance was reached for the dry-weather channel between 360 - 370 m for a storage level of 1.82 m. Larger storage levels lead to shorter flushing distances. To clean the sewer along its complete length a storage level of at least 1.25 m was needed. In contrast to the dry-weather channel the effective flushing distance for the slopes showed a progression with an increasing storage level and flushing volume. The declination of the trend curve was not encountered as for the dry-weather channel. Maybe with higher storage levels than investigated in the present case this effect would become visible.
With the maximum storage level of the rotary gate of 1.82 m the critical bottom shear

stress of 5 N/m^2 could not be kept to the end of the sewer channel. Following the progression of the trend curve of the effective flushing distance a storage height of 2.55 m would have been necessary to clean the slopes along its whole length. Unfortunately this would not be possible in practice because the sewer channel has a total height of only 2.5 m.

The influence of the flushing gate on the effective flushing distance was the next investigation, which was carried out. Therefore a new numerical model was set up including the rotary gate in its horizontal position after the end of the opening. The calculated results of the bottom shear stresses were then compared with the results of the previous section.
The flush tests in Offenbach showed that the gate was not overflown in the initial phase for storage levels 1.25 m and below. For larger storage levels the overflow lasted only a few seconds before the flush wave was drained under the gate. The comparison between the two approaches shows that for a storage level of 1.64 m the gate does not affect the shear stresses in the dry-weather channel. The curve progression was nearly identical and the differences in the peak values were marginal. The analysis for the slopes showed that in the beginning the rotary gates influences the flush wave but after a running of 100 s the bottom shear stresses were again nearly equal. As a result it can be stated that for the flushing of long sewer stretches the hydraulical losses at the present type of flushing gate have a minor influence on the behaviour of the wave and on the cleaning effect.

The influence of the flushing volume on the effective flushing distance was the subject of further investigations. Therefore the flushing volume was varied by reducing the storage length whilst the gate was kept at the location of $z = 35.5$ m with a constant storage level. The numerical grid of the storage volume upstream of the gate was reduced to 10, 20 and 30 m for two different storage levels of $h_{store} = 1.25$ m and $h_{store} = 1.82$ m.
The calculations with $h_{store} = 1.25$ m showed that the increase of flushing volume lead only to a small improvement of the effective flushing distance for the dry-weather channel. The double flushing volume rised the effective flushing distance only about 20 %. For the slopes the progression of the mean values of the effective flushing distance was much more steeper than for the dry-weather channel. An increase of flushing volume had a greater influence on the cleaning success of the slopes. An increase of flushing volume of 100 % lead to a rise of the flushing distance of 35 %.
For a storage level of $h_{store} = 1.82$ m the distribution of the mean values of the effective flushing distance in dependence of the storage volume revealed a very shallow progression. It was apparent that an increase of the flushing volume of 355 % lead only to an increase in the flushing distance of 32 %. A different situation was found for the slopes with a steeper progression as for the dry-weather channel. The influence of the storage volume on the effective flushing distance was significantly greater for the slopes than for the dry-weather channel. For the chosen storage level of 1.82 m an increase of flushing volume of 355 % lead to an increase of the effective flushing length of 159 %.
The influence of the storage volume on the effective flushing length was strongly dependent on the position of the flush wave. A flush wave, which cleans successfully the dry-weather channel, does not necessarily cleans the slopes too. As shown in chapter 12.4 the regional distinctions of the shear stresses can be large and will determine the cleaning result. The dry-weather channel and the cleaning efficiency there is only weakly

influenced by the increase of flushing volume. The slopes must be threaded with caution, because the influence here is very strong.

The aim behind the following investigation was the analysis of the influence of the time step size used in the calculations on the bottom shear stress. Therefore the reduced numerical model of 200 m length, as used for the calibration, was chosen. The storage level was kept constant for all variants with $h_{store} = 1.03$ m. The roughness of the dry-weather channel was fixed with $k = 0.6$ mm and $k = 2$ mm for the slopes. The time step size was varied between 0.01 and 0.05 seconds.
The analysis of the bottom shear stresses for the dry-weather channel revealed, that the smallest time step had the highest maximum shear stress and the highest velocity for 1 to 5 seconds running time. After a wave running time of 10 seconds the bottom shear stresses were nearly equal for all time step sizes. Regarding the slopes of the sewer channel a similar behaviour of the bottom shear stresses was noticed. It can be stated that a higher temporal resolutions leads to higher shear stresses for the first 5 seconds of the flush wave running time. Usually the shear stresses in the initial phase are clearly above the critical values for the erosion of deposits. Because of this the initial phase is not really important for the cleaning success of a flush wave. Regarding longer running times and therefore longer flushing distances, which are more important, the shear stresses were similar for all variants. In the chosen range the time step size is negligible for the calculation of long distance flush waves and the determination of their cleaning success.

The calculation of the shear stress so far was carried out using the kinetic energy k of the $k - \epsilon$ turbulence model. This approach resulted in a mean value of τ for the bottom cell, but the $k - \epsilon$ turbulence model is not valid in the viscous sub-layer, where the flow is dominated by the viscosity. Above this zone the transition zone is placed and here the Reynolds stresses and the molecular viscosity are equal. In both zones the logarithmic law of the wall was used to describe the flow in the so-called boundary layer. The used modeling approach showed the problem that the grid cells at the walls were larger than the boundary layer, which led to an averaged value of the shear stresses at the walls. To calculate the shear stress at the walls more detailed it was necessary to refine the grid in such a way, that the sub-layer would be thicker than the wall cells. Because of highly transient flow of a flush wave it was not possible to use the a steady flow velocity to determine the thickness of the boundary layer x_2^+. Therefore it was necessary to use an iterative approach to determine the boundary layer depending on the development of the flush wave along the sewer channel.
First the thickness of the bottom gird cells was chosen, then x_2^+ was calculated by using τ_w and u_τ. If the value of x_2^+ exceeded the value 100 then the initially chosen grid thickness has to be refined until the dimension less wall distance fell below the limit and indicated the thickness of the boundary layer. A shortened model of 50 m length and an initial storage level of 1.82 m height was created to keep the calculation times in a realistic range. The results showed that a thickness of 0.625 cm was small enough to resolve the boundary layer for the initial phase of the flush wave with up to 3 seconds. The steep gradients of the breaking wave made it necessary to refine the grid to such a small size. To investigate the thickness of the boundary layer for a flush wave running for a longer time and longer distance a model with a length of 100 m was created. The results revealed that for a running flush wave, disregarding the initial phase, a thickness

of 2.5 cm was sufficient to resolve the boundary layer.
The last step of this investigation was to create a model to cover the complete length of the sewer channel. Therefore a numerical grid with a length of 340 m was modelled. The thickness of the bottom cell was chosen to 2.5 cm and the initial storage level to 1.82 m. The calculation time 2 months was very high with to model 200 seconds of wave running time.

To fulfill the original aim of a more detailed calculation of the bottom shear stresses the 50 m long numerical model was used for a comparison between the calculated bottom shear stresses according to models with a bottom cell thickness of 10 cm and 0.6 cm where the boundary layer is resolved. In the initial phase of the flush wave the differences for the maximum shear stresses were large. The values of the bottom shear stresses with the resolved boundary layer were up 300 % higher than for the 10 cm thickness model. With an increasing running time the difference decreased due to the reduced general flow velocity. It became also obvious that the flush wave modelled with the thinner grid cells was clearly faster that the second wave. The difference in the maximum values seemed to be minor especially for longer running times but the differences in flow velocity seemed to be increasing. Further investigations could be useful but they should be carried out on larger computational resources than the present one.

The determination of the behaviour of the sunk wave was modelled in a refined numerical grid. Only the first 50 m of the reservoir sewer were investigated. The chosen storage level at the flushing gate was 1.64 m. The modelling of the dropping water level in front of the gate and the sunk wave in its progression from 0.1 seconds until 3 seconds revealed that the gradients in the backward moving wave were steep until 2 seconds running time. Then the water level was dropping slowly. After 9 seconds the sunk wave reached the upstream boundary, the side weir. The numerical calculations showed no reflection of the sunk wave at the side weir. The water level was dropping slowly in the further progression. An investigation of the bottom shear stresses for the storage length of 35.5 m showed no significant difference for the dry-weather channel and the slopes. The shear stresses were moving backwards for 13 seconds then the sunk wave was reflected and moving downstream. The critical value for the bottom shear stress of 5 N/m^2 was exceeded until z = 12 m, which means that the cleaning effect of the sunk wave covers 66 % of the initial storage length in this particular case.

Usually the efficiency of a flush wave is measured on the absolute value of the achieved bottom shear stress. The duration of the exceeding of a certain critical value at a certain location is not taken into account. It was now the question if it is not more successful to create a flush wave with a lower maximum shear stress value but with a longer duration above τ_{crit} regarding a certain location. This wave should have a better efficiency than a wave that has only one high peak of shear stress. The investigation of the duration of the critical shear stress was split up in two parts. In the first part the influence of the initial storage level was analysed and in the second part the initial storage volume was regarded.
To describe the temporal distribution of the bottom shear stresses along the reservoir sewer several locations were chosen, where the shear stresses were analysed for all storage levels. Regarding the dry-weather channel there is no clear connection between the distribution of the duration of the bottom shear stress and the initial storage level at the flushing gate. For the slopes it can be stated that a large initial storage level leads to a

longer duration of critical shear stress. Storage levels below 1.45 m lead to a very slow flush wave and the duration decreased constantly. They were not suitable for a good cleaning result of the reservoir sewer in Offenbach. The larger storage levels created flush waves, which had a high flow velocity and a short duration of shear stresses of around 40 seconds. Then they slowed down and this increased the duration until a point when the flush wave was too small and fell below the critical shear stress.
The influence of the storage volume on the duration of the critical bottom shear stress was investigated by analysing the shear stress created by flush waves with a constant storage level but varying storage volumes. The storage levels were chosen to 1.25 m and 1.82 m. The storage volume was changed by cutting down the storage length analogous to chapter 12.4. The results of the analysis for the storage volume showed that for the dry-weather channel a volume larger than 84 m^3 will be necessary to gain a clean sewer channel. To clean the slopes sustainable flushing volumes larger than 139 m^3 were needed. To prove the before given suggestion the efficiency of a flush wave with a lower shear stress peak but with higher duration of critical bottom shear stresses should be tested on real sediments against a flush wave with a single high peak of shear stresses.

13.2 Forecast

The presented investigations and results in this thesis showed that three-dimensional numerical modelling can be a very good tool for fundamental analyses of flush waves. But these results are only valid for the reservoir sewer in Offenbach. The transfer of them on to other sewers with different hydraulic conditions and deposits must treated with great care. Further investigations of the hydraulic behaviour of flush waves at sewer channel singularities like strong curvatures, lateral inflows, siphons or constrictions can or should be carried out using three-dimensional models due to their high temporal and spatial resolution. Investigations of the effectiveness of flush waves in long distance sewers, long storage lengths or in sewer networks take three-dimensional models to the limit of computational resources. The very long calculation times will not be reasonable for engineering applications. In these cases good one-dimensional models with the ability to reproduce steep gradients would be the better choice. To model sewer networks with flushing devices it would sensible to combine well known existing models like SWMM [EPA, 2007] with adequate numerical schemes to reproduce the movement of flush waves. Especially for the daily engineering work one-dimensional models would offer short calculation times and therefore fast and reliable results.
Using one-dimensional model would allow to develop more universal design rules for the generation of flush waves for example in circular, egg-shaped or rectangular main sewer channels with different sizes and slopes. In contrast to the present investigation in an sub-main reservoir sewer the effective flushing distance in main sewers with all the hydraulic problems could be specified as a function of the flushing volume and the storage height. Especially the effective flushing of not totally drained main sewers due to lateral inflows and the effectiveness of sunk waves are practical problems which could be well investigated with appropriate one-dimensional models.
Long-term objectives can be the implementation of adequate sediment transport approaches, here particularly cohesive sediments, into the numerical modelling of flush

waves and the pollution load transport of flush waves due to the dispersion of sediments. In the case of sediment transport the actual transport models originating from river sediment transport seem not to be convenient for the use in sewer sediment transport calculations. The estimation of pollution load transport caused by flush waves is a completely new field where a large range investigations can be made.

14 References

Ab-Ghani, A. (1993): Sediment transport in sewers, *PhD thesis*, Universitaet of Newcastle, England.

Ackers, P. & White, W.R. (1973): Sediment transport: New approach and analysis, *Journal of the Hydraulics Division*, Proceedings of the American Society of Civil Engineers, **99**, (HY11), 2041-2060.

Ackers, P. (1991): Sediment aspects of drainage and outfall design, Environmental Hydraulics, *Proceedings International Symposium on Environmental Hydraulics*, Hong Kong.

Ahyerre, M. (1999): Bilans et mcanismes de mogration de la pollution organique en rseau d'assainissement unitaire, *PhD Thesis*, Ecole Nationale des Ponts et Chausses, France.

Arthur, S. (1996): Near bed solid transport in a combined sewer network, *PhD thesis*, University of Abertay Dundee, Scotland.

Arthur,S. & Ashley, R.M. (1997): Near bed solids transport rate predoction in a combined sewer network, *Water Science and Technology*, **36**,(8-9), 129-134.

Arthur, S., Ashley, R.M. & Nalluri, C. (1996): Near bed solids transport in sewers, *Water Science and Technology*, Pergamon Press, **33** (9), 69-76.

Arthur, S., Ashley, R., Tait, S. & Nalluri, C. (1999): Sediment transport in sewers - a step towards the design of a sewer to control sediment problems, *Proc. Inst. Civ. Engineers Water Marit & Energy*, **136**, 9-19.

Artires, O. (1988): Bildung und Remobilisierung von Ablagerungen in Mischwasserkanalisationen, *KA - Korrespondenz Abwasser*, (10), 1026 - 1033.

Ashley, R.M, Arthur, S., Coghlan, B.P. & McGregor, I. (1993): Fluid sediment movement and first flush in combined sewers, *Proceedings 6th International Conference on Urban Storm Drainage*, Canada, 875-883.

Ashley, R.M., Arthur, S. Coghlan, B.P. & McGregor, I. (1994): Fluid Sediment in combined sewers, *Water Science and Technology*, Pergamon Press, **29** (1-2), 113-123.

Ashley, R.M., Bertrand-Krajewski, J.-L., Hvitved-Jacobsen, T. & Verbanck, M. (Eds.) (2004): Solids in Sewers, *Scientific and Technical Report*, (14), IWA Publishing, London.

Ashley, R.M. & Dabrowski, W. (1995): Dry and storm weather transport of coliforms and faecal streptococci in combiened sewage ,*Water Sience and Technology*, **31**, (7), 311-320.

Ashley, R.M., Wotherspoon, D.J.J., Coghlan, B.P. & McGregor, I. (1992): The erosion and movement of sediments and associated pollutants in combined sewers, *Water Science and Technology*, Pergamon Press, **25** (8), 101-114.

ASA Technik GmbH, Bruckersche Strae 152 47839 Krefeld, www.asatechnik.de.

Bachoc, A. (1992): Location and general characteristics of sediment deposits into man-entry combined sewers, *Water Science & Technology*, Pergamon Press, **25** (8).

Barkhudarov, M.R. (2003): Semi-Lagrangian VOF Advection Method for *Flow-3D©*, *Flow Science Inc.*

Barth, M. (1996): Drehbogen - Pilotprojekt Dresden Leuben, *Institutsmitteilungen*, Institut fuer Wasserbau und Technische Hydromechanik, TU Dresden, **7**.

Barth, M., Cherubim, C., Gebhard, V. & Grothkopp, H. (1993): Einsatz des Drehbogens am Standort Dresden zur Kanalnetzbewirtschaftung und Kanalnetzreinigung, *Stuttgarter Berichte zur Siedlungswasserwirtschaft*, Institut fuer Wasserbau; Kommissionsverlag R. Oldenbourg, **123**.

Berlamont, J.E. & Torfs, H.M. (1996): Modelling (partly) cohesive sediment transport in sewer systems, *Water Science and Technology*, Pergamont Press, **33** (9) 171-178.

Bertrand-Krajewski, J.-L. (2003): Sewer sediment management: some historical aspects of egg-shaped sewers and flushing tanks, *Water Science and Technology*, Pergamon Press, **47**, (4), 109-122.

Bertrand-Krajewski, J.-L., Bardin, J.-P., Gibello, C. & Laplace, D. (2002): Hydraulics of a sewer flushing gate, *International Conference on Sewer Processes and Networks, Proceedings*, 137-I - 137-IX, Paris, France.

Bertrand-Krajewski, J.-L., Campisano, A., Creaco, E. & Modica, C. (2004): Experimental study and modelling of the hydraulic behaviour of a hydrass flushing gate, *Novatech, International Conference, Proceedings*, 557-564, Lyon, France.

Bertrand-Krajewski, J.-L. Campisano, A., Creaco, E. & Modica, C. (2005a): Experimental analysis of the Hydrass flusing gate and field validation of flush propagation modelling, *Water Science and Technology*, Pergamont Press, **51** (2) 129-137.

Bertrand-Krajewski, J.-L., Bardin, J. & Gibello, C. (2005b): Long term monitoring of sewer sediments accumulation and flushing experiments in a man-entry sewer, *10th International Conference on Urban Drainage, Proceedings*, 1-8, Copenhagen, Denmark.

Bertrand-Krajewski, J.-L. (2008): Flushing urban sewers until the beginning of the 20th century, *ICUD, International Conference on Urban Drainage, Proceedings*, Edinburgh, Scotland.

BIOGEST AG (2005), Siemensstrae 1,65232 Taunusstein, www.biogest.de.

Bland, C., Bayley, R. & Thomas, E. (1975): Some Observations on the Accumulation of Slime in Drainage Pipes and the Effect on the Accumulations on the Resistance to Flow, *The Public Health Engineer*, (13), 21-82.

Blumberg, D. & Bauer, W. (1994): Beseitigung von Ablagerungen in Abwasserkanaelen groer Durchmesser, *KA - Korrespondenz Abwasser*, **12**, 1063 - 1072.

Bollrich, G. (1989): *Technische Hydromechanik 2 - Spezielle Probleme*, Verlag fuer Bauwesen, Berlin.

Bollrich, G. (2000): *Technische Hydromechanik 1*, Verlag fuer Bauwesen, Berlin.

Borchardt, D. (1992): Wirkung stossartiger Belastungen auf ausgewaehlte Fliessgewaesserorganismen - Ein Beitrag zur Beurteilung oekologischer Schaeden durch Niederschlagseinleitungen aus Kanalisationen, Wasser-Abwasser-Abfall: *Schriftenreihe des Fachgebietes Siedlungswasserwirtschaft*, Verein zur Foerderung des Fachgebiets Siedlungswasserwirtschaft an der Universitaet - Gesamthochschule Kassel, **10**, 176f.

Bornschein, A. (2005): Die Ausbreitung von Schwallwellen auf trockener Sohle unter besonderer Beruecksichtigung der Wellenfront, *Dissertation am Institut fuer Wasserbau und Technische Hydromechanik*, TU Dresden.

Boussinesq, J. (1877): Thorie de lcoulement Tourbillant, M*em. Prsents par Divers Savants Acad. Sci. Inst. Fr.*, (23), 46-50.

Briechle, S. (2006): Die flaechenhafte Ausbreitung der Flutwelle nach Versagen von Hochwasserschutzeinrichtungen an Fliegewaessern, *Dissertation am Institut fuer Wasserbau und Wasserwirtschaft*, RWTH Aachen.

Brombach, H. (1982): Zwei Experimente zum Stofftransport im Mischwasserkanal, *KA - Korrespondenz Abwasser*, **5**, 284-291.

Brombach, H. (1995): Konstruktion und maschinelle Ausrstung von Regenberlaufbecken, *Dresdner Mitteilungen*, Institut fr Siedlungs- und Industriewasserwirtschaft, TU Dresden, (7), 71-88.

Brombach, H., Michelbach, St. & Woehrle, Chr. (1992): Sedimentations- und Remobilsisierungsvorgaenge im Abwasserkanal, *Universitaeres Verbundprojekt des Bundesministers fr Forschung und Technologie: Niederschlagsbedingte Schmutzbelastung der Gewsser aus staedtischen befestigten Flaechen - Teilprojekt 3*, Bad Mergentheim.

Brombach, H., Michelbach, S. & Woehrle, C. (1993): Feststoffe in der Mischwasserkanalisation, Sedimentation und Remobilisierung, *KA - Korrespondenz Abwasser*, **12**, 1910-1926.

Broeker, H.W. (1983): Auswirkungen der Kanalablagerungen auf den Kanalbetrieb, *Berichte aus Wasserguetewirtschaft und Gesundheitsingenieurwesen*, Technische Universitaet Muenchen, **44**.

Butler, D., Friedler, E. & Gatt, K.(1995): Characterising the quantity and quality of domestic wastewater inflows, *Water Science and Technology*, **31**, (7), 13-24.

Butler, D., Littlewood, K. & Orman, N.(2005a): Forces on sanitary solids in small sewers, *Water Science and Technology*, **52**, (3), 85-92.

Butler, D., Littlewood, K. & Orman, N.(2005b): A model for the movement of large solids in small sewers, *Water Science and Technology*, **52**, (5), 69-76.

Buergisser, M. (1998): Numerische Simulation der freien Wasseroberflaeche bei Ingenieurbauten, *Dissertation an der Versuchsanstalt fuer Wasserbau*, ETH Zuerich.

Campisano, A. & Modica, C. (2002): Flow velocities and shear stresses during flushing operations in sewer collectors, *International Conference on Sewer Processes and Networks*, Paris, France.

Campisano, A., Creaco, E. & Modica, C.(2004): Experimental and numerical analysis of the scouring effects of flushing waves on sediment deposit, *Journal of Hydrology*, **299**, (3-4), 324-334.

Campisano, A., Creaco, E. & Modica, C. (2005): Experimental analysis of the Hydrass flushing gate and laboratory validation of flush propagation modelling, *International Conference on Urban Drainage*, Copenhagen, Denmark.

Campisano, A., Creaco, E., Modica, C. & Retano, S. (2006): Flushing experiments with cohesive sediments, *International Conference on Sewer Operation and Maintenance*, 27-34, Vienna, Austria.

Chadwick, E. (1842): *Report on the sanitary condition of the labouring population of Great Britain*, University Press, edition 1965, Edinburgh.

Chebbo, G., Ashley, R. & Gromaire, M.C. (2003): The nature and pollutant role of solids of the water-sediment interface in combined sewer networks, Water, *Science and Technology*, **47**, (4), 1-10.

Clark, P., Payne, J.M, & May, R. (1993): Design of sewers to control sediment problems, *Proceedimgs of the 6th ICUSD, Niagara Falls*, Canada, **1**.

Chebbo, G., Laplace, D., Bachoc, A., Sanchez, Y. & Le Guennec, B. (1996): Technical solutions envisaged in managing solids in combined sewer networks, *Water Science and Technology*, Pergamon Press, **33** (9), 237-244.

Chow, V. T. (1959): *Open Channel Hydraulics*, McGraw Hill, Inc. New York.

Coghlan, B.P., Ashley, R.M. & Smith, G.M. (1996): Empirical equations for solids transport in combined sewers, *Water Science and Technology*, **33**, (9), 77-87.

Crabtree, R.W. (1988): *A classification of combined sewer sediment types and characteristics*, WRc Engineering, Swindon, England.

Creaco, E.F. (2005): Devices for the removal of solids from sewer channels. Experimental investigations and numerical models, *Dissertation at UNIVERSIT DI CATANIA*, Dipartimento di Ingegneria Civile e Ambientale.

Daubner, L. & Nowak, B. (1983): Quellen und Mengen der Schmutzstoffe in Regenabfluessen einer staedtischen Mischkanalisation, *Separatum Nr. 927*, Eidgenoessische Anstalt fuer Wasserversorgung, Abwasserreinigung und Gewaesserschutz, Technische Universitaet Zuerich.

Dette, H.-H., Macke, E., Vries, J.M.de & Schulz, O. (1996): Mischwasserschmutzfrachten in flachen Kanalnetzen, Stoffaustrag aus Kanalisation - *Hydrologie bebauter Gebiete (Forschungsbericht)*, VCH - Verlagsgesellschaft, 162-183.

Dettmar, J., Schueler, O. & Lorenzen, A. (2001): Anwendung selbstaetiger Schwallspuelklappen in der Mischwasserkanalisation, *KA - Korrespondenz Abwasser*, **11**, 1556-1564.

Dettmar, J. (2003): Optimierte Kanalreinigung durch Schwallspuelung, Darmstaedter Wasserbaulische Kolloquium 2001, *Veroeffentlichung in Mitteilungen Institut fuer Wasserbau*, Technische Universitaet Darmstadt, **130**.

Dettmar, J. & Stauffer, P. (2004): Modelling of Flushing Waves for Optimising Cleaning Operations, *Int. Conference on Urban Drainage Modelling,* , 241-249, Dresden, Germany.

Dettmar, J., & Stauffer, P. (2005a): Reduzierung von Schmutzfrachtstoessen durch optimierte Schwallspuelung von Stauraumkanaelen, *KA - Korrespondenz Abwasser*, **8**, 889-894.

Dettmar, J. & Stauffer, P. (2005b): Behavior of the activated storage-volume of flushing waves on cleaning performance, *Int. Conference on Urban Drainage*, Copenhagen, Denmark.

Dettmar, J. (2006): Beitrag zur Verbesserung der Reinigung von Abwasserkanaelen, *Dissertation am Institut fuer Siedlungswasserwirtschaft*, RWTH Aachen.

Dettmar, J. & Stauffer, P. (2006): Untersuchung eines neu entwickelten Reinigungssystems fuer den Einsatz in Stauraumkanaelen, *Schlussbericht zum Forschungsvorhaben*, Institut fuer Siedlungswasserwirtschaft, RWTH Aachen.

Dohmann, M. & Dettmar, J. (2003): Leitfaden zur Planung und Anwendung von Schwallspueleinrichtungen in Mischwasserkanalisationen, *Schlussbericht zum Forschungsvorhaben*, Institut fuer Siedlungswasserwirtschaft, RWTH Aachen.

Dressler, R.F. (1952): Hydraulic Resistance Effect upon the Dam-Break Function, *Journal of Research*, **49**, (3), 217-225.

Drews (1979): Schwallspuelungen zur Beseitigung von Ablagerungen im Mischwassersiel St. Pauli, Hafenstrae/Silbersackstollen, *Interner Verwaltungsbericht J3/E30 der Freien und Hansestadt Hamburg.*

Durbin, P.A. & Pettersson Reif, B.A. (2001); *Statistical theory and modelling for turbulent flows*, Wiley & Sons Ltd. , Chichester.

Einstein, H.A. (1942): Formulas for the transportation of bed load, *Transaction of the American Society of Civil Engineers*, **107**, 561-597.

Ehnert, M. (1980): Anforderungen an eine Kanalisation aus der Sicht eines Anwenders, *Tiefbau Ingenieurbau Straenbau (TIS)*, **7**, 596-600.

El-Zaemey, A.K. (1991): Sediment transport over deposited beds in sewers, *PhD thesis*, University upon Tyre, England.

Engelund, F. & Hansen, E. (1966): Investigation of flow in alluvial streams, *Acta Polytechnica Scandinavia*, Kopenhagen, Denmark.

EPA (2007): Strom Water Management Model SWMM, Urban Watershed Management Research, *U.S. Environmental Protection Agency*, http://www.epa.gov/ednnrmrl/models

/swmm/index.htm.

Fan, C.Y. et al. (2001): *Sewer and Tank flushing for corrosion and pollution control* Report 600/J-01/120, United States Environmental and Protective Agency, USA.

Fan, C.Y. (2004): *Sewer Sediment and Control* Report 600/R-04/059, United States Environmental and Protective Agency, Cincinnati, USA.

Ferziger, J.H. & Peric, M. (1996); *Computational Methods for Fluid Dynamics*, Springer Verlag.

Forkel, C. (1995): Die Grobstruktursimulation turbulenter Stroemungs- und Stoffausbreitungsprozesse in komplexen Geometrien , *Dissertation am Institut fuer Wasserbau und Wasserwirtschaft*, RWTH Aachen, **102**.

Frehmann, T. (2003): Untersuchung der Wirksamkeit von Stauraumkanaelen mit untenliegender Entlastung zur Regenwasserbehandlung, *Forum Siedlungswasserwirtschaft und Abfallwirtschaft*, Universitaet Essen, **21**, Shaker Verlag, Aachen.

Fruehling, A. (1910): *Handbuch der Ingenieurwissenschaften in fuenf Teilen, III. Teil: Der Wasserbau, 4.Band: Die Entwaesserung der Staedte*, Verlag von Wilhelm Engelmann.

Gathke, D. & Borchering, H. (1996): CSO-tunnel cleaning by a long-distancs flushing wave - Simulation and Experiments, *7th International Conference on Urban Storm Drainage Hannover 1996*, SuG Verlagsgesellschaft Hannover, **3**, 1539-1545

Gebhard, V. (2000): Sedimente in der Dresdner Kanalisation, *Dresdner Berichte*, Dresdner Kolloquium zur Siedlungswasserwirtschaft, P. Krebs (Hrsg.), Institut fuer Siedlungs- und Industriewasserwirtschaft, TU Dresden, **16**, 57-83.

Geiger, W.F. (1984): Mischwasserabflu und dessen Beschaffenheit - ein Beitrag zur Kanalnetzplanung, *Berichte aus Wasserguetewirtschaft und Gesundheitsingenieurwesen*, TU Muenchen, **50**.

Gendreau, N., Le Guennec, B. & Point-Chazel, J.P. (1993): Sediment motion under flood wave use of partial release of stored water by a weir, Proceedings 6th International Conference on Urban Strom Drainage, Canada.

Genzmer, E. (1924): *Handbuch der Ingenieurwissenschaften, 3. Teil: Wasserbau, 4. Band: Die Entwaesserung der Staedte*, 5. Auflage, Verlag von Wilhelm Engelmann.

Glazik, G. (1989): Geschiebe- und Schwebstoffbewegung in offenen Gerinnen, *Technische Hydromechanik 2 - Spezielle Probleme*, Hrgs.: Bollrich, G.,Verlag fuer Bauwesen, 439-480.

Griebel, M., Dornseifer, T. & Neunhoeffer, T. (1995): *Numerische Simulation in der Stroemungsmechanik*, Vieweg Verlag, Wiesbaden.

Grube, H., Kern, E. & Quintmann, H.D. (1990): Instandhaltungen von Betonbauwerken, *Beton-Kalender* ,Verlag Ernst & Sohn, (II), 681-805, Berlin.

Guerschner & Benzel (1921): *Der Staedtische Tiefbau.III.,Teil: Stadtuentwaesserung*, Verlag von G.B. Teubner, 4. Auflage.

Guo, Q., Fan, CY., Raghaven, R. & Field, R. (2004): Gate and Vacuum Flushing of Sewer Sediment: Laboratory Testing , *Journal of Hydraulic Engineering*, American Society of Civil Engineers, **130**, (5), 463-466.

Hager, W.H. (1998): Minimalgeschwindigkeiten und Sedimenttransport in Kanalisationen, *GWF-Gas/Wasser/Abwasser*, **5**, 346-350.

Hager, W. & Chervet, A. (1996): Geschichte der Dammbruchwelle, *wasser, energie, luft*, **88**, (3/4) 49-53.

Hager, W. & Lauber, G. (1996): Hydraulische Experimente zum Talsperrenbruchproblem, *Schweizer Ingenieur und Architekt*, **114**, (24), 515 524.

Hahn, H.H. & Xanthopoulos, C. (1990): Schadstoffe im Regenabflu aus staedtischen Gebieten - Praesentation eines BMFT-Verbundprojektes, *Schriftenreihe des Instituts fuer Siedlungswasserwirtschaft*, Technische Universitaet Karlsruhe, Oldenbourg Verlag, **58**.

Haumann, R. (1999): Kanalreinigung mit Hilfe der Schwallspuelung, *GWA - Gewaesserschutz, Wasser, Abwasser*, Schriftenreihe Lehrstuhl Siedlungswasserwirtschaft der RWTH-Aachen, **180**, 8/1-8/10.

Hey, R.D. (1979): Flow resistance in gravel-bed rivers, *Journal of the Hydraulics Division, ASCE*, **31**, 365-873.

Hirt, C.W. & Nichols, B.D. (1981): Volume of Fluid (VOF) Method for the Dynamics of Free Boundaries, *Journal of Computational Physics*, **3**, 201-225.

IKT (2004): Neue Methode zur Schwallspuelung "'Spuelsack"', *IKT - Institut fuer Unterirdische Infrastruktur*, Gelsenkirchen, www.ikt.de.

Jankowski, J.A. (1999): A non-hydrostatic model for free surface flows, *Bericht des Instituts fuer Stroemungsmechanik und Elektron. Rechnen im Bauwesen*, Universitaet Hannover, **56**.

Jaervenkylae, J.J. & Haavisto, K.T. (1993): The abrasion resistance of sewers. Part 1+2, *Pipes & Pipelines International*, 9/10 + 11/12.

Jefferies, S. & Ashley, R.M. (1994): Gross solids in sewer systems: temporal and catchment based relationships, *Water Science and Technology*, **30**, (1), 63-71.

Jones, W.P. & Launder, B.E. (1972); The prediction of laminarization with a two-equation model of turbulence, *International Journal of Heat and Mass Transfer* **15**, 301-314.

Kabir, M.R. & Torfs, H. (1992): Comparison of different methods to calculate bed shear stress, *Water Science and Technology*, Pergamon Press, **25** (8), 131-140.

Kamphuis, J. (1990): Influence of sand or gravel on the erosion of cohesive sediment, *Journal of Hydraulic Research*, **28** (1), 43-53.

Karakassonis, G.P. (1936): Die Bewegung der Schwerstoffe in flachgeneigten Rohren unter Beruecksichtigung von Steinzeugrohren mit praktischen Anwendungen, *Mitteilungen Institut fuer Wasserbau*, TH Berlin, **20**.

KEDING, M. (1990): Der Zustand der oeffentlichen Kanalisation in der BRD - Ergebnisse der ATV-Umfrage 1990, *KA - Korrespondenz Abwasser*, **10**, 1148-1154.

KINZELBACH, W. (2006): *Hydraulik 2*, Vorlesungsskript, Institut fuer Umweltingenieurwissenschaften, Professur fuer Grundwasser und Hydromechanik, ETH Zuerich.

KIRCHHEIM, N. (2003): Entstehung und Auswirkungen von Ablagerungen in der Mischwasserkanalisation, *Studienarbeit am FG Hydromechanik und Hydraulik*, TU Darmstadt.

KIRCHHEIM, N., SCHAFFNER, J. & OBERLACK, M. (2005): Parameter study of a flush wave using numerical modelling, *International Conference on Urban Drainage*, Copenhagen, Denmark.

KIRCHHEIM, N. (2005): *Kanalablagerungen in der Mischkanalisation*, Deutsche Vereinigung fuer Wasserwirtschaft, Abwasser und Abfall (DWA), Hennef.

KIVEKAES, N., RIIPINEN, I. & VUOLLEKOSKI, H. (2006): Near-Wall Treatments for Wall-Bounded Turbulent Flows, *Presentation at the Division of Atmospheric Science* , Department of Physical Science, Faculty of Science, University of Helsinki.

KOPPE, P. & STOZEK, A. (1999): *Kommunales Abwasser*, Vulkan-Verlag, 4. Auflage.

KRAUTH, K.H. (1971): Der Abfluss und die Verschmutzung des Abflusses in Mischkanalisationen bei Regen, Stuttgarter *Berichte zur Siedlungswasserwirtschaft*, Institut fuer Wasserbau, Universitaet Stuttgart, Kommissionsverlag R. Oldenbourg, **45**.

KRAUS, TH. (2002): Rauheitsaenderungen durch Biofilmbewuchs in Druckrohrleitungen, *Mitteilungen des Institutes fuer Wasserbau und Wasserwirtschaft*, Technische Universitaet Darmstadt, **123**.

KREBS, P., MERKEL, K. & KUEHN, V. (1999): Dynamic changes in wasteater compositions during rain runoff, *8th International Conference on Urban Storm Drainage Proceedings*, **2**, 920-927, Sydney, Australien.

KRUEGER, S. (2001): Computational Contribution to Highly Supercritical Flows, *Dissertation an der Versuchsanstalt fuer Wasserbau*, ETH Zuerich, **167**.

KUEHN, V. & GEBHARD, V. (1998): Auswirkungen des Kanalnetzes auf die Abwasserbeschaffenheit, in: Fortbildungskurs Biologische Abwasserreinigung, Wiener Mitteilungen Wasser, Abwasser, Gewaesser, H. Kroi (Hrsg.) *Institut fuer Wasserguete und Abfallwirtschaft*, Universitaet fuer Technische Universitaet Wien, **145**, 79-116.

LAPLACE, D., BACHOC, A., SANCHEZ, Y. & DARTUS, D. (1992): Trunk Sewer Clogging Development - Description and Solutions, *Water Science and Technology*, **25**, (8), 91-1000.

LAPLACE, D., OMS, C., AHYERRE, M, CHEBBO, G., LEMASSON, J. & FELOUZIS (2002): Removal of the organic surface layer in combined sewer systems using a flushing gate, *International Conference on Sewer Processes and Networks - Proceedings*, 121-128, Paris, France.

LAUBER, G. (1997): Experimente zur Talsperrenbruchwelle im glatten geneigten Rechteckkanal, *Dissertation an der Versuchsanstalt fuer Wasserbau*, ETH Zuerich, **152**.

Lauber G. & Hager W.H. (1998a): Experiments to dambreak wave: Horizontal channel , *Journal of Hydraulic Research*, **36** (3), 291-308.

Lauber G. & Hager W.H. (1998b): Experiments to dambreak wave: Sloping channel , *Journal of Hydraulic Research*, **36** (5), 761-773.

Launder, B.E. & Splading, D.B. (1972): *Mathematical Models of Turbulence*, Academic Press, London and New York.

Lenz, J. & Wielenberg, M. (1997): Sedimentation in Abwasserkanaelen und Kanalreinigung, *3R international*, **9**, 513-517.

Leo, G.H. (1969): *Wiliam Lindley, ein Pionier der technischen Hygiene*, Hamburgerische Bauwirtschaft, Hamburg.

Liem, R. (2003): Zur Verwendung der Flachwassertheorie bei der Simultation von Dammbruchwellen, *Dissertation am Institut fuer Wasserbau und Wasserwirtschaft*, RWTH Aachen, **128**.

Lindley, W. (1845): *Schlussbericht ueber die ausgefhrten Sielanlagen zur Entwaesserung der Stadt Hamburg*, Rath und Buerger Deputation, Hamburg.

Linehan, P. (2001): The design of flushing gates to transport sewer sediments, *Dissertation at the department of civil and structural engineering*, University of Sheffield, England.

Lorenzen, A., Ristenpart, E. & Pfuhl, W. (1996): Flush cleaning of sewers, *Water Science and Technology*, Pergamon Press, **33** (9), 221-228.

Lorenzen, A., Ristenpart, E. & Pfuhl, W. (1997): Reinigung von Abwasserkanaelen durch Schwallspuelung - Teil1: Feldversuche in einem Mischwasserkanal, *KA - Korrespondenz Abwasser*, **11**, 1194-2002.

Lorenzen, A. & Laplace, D. (1998): Reinigung von Abwasserkanaelen durch Schwallspuelung - Teil 2: Werkzeuge fuer die Schwallspuelung, *KA - Korrespondenz Abwasser*, **2**, 39-46.

Lysne (1969): Hydraulic design of self-cleaning sewage tunnels, *Jounal of the Sanitary Engineering*, Divivion, ASCE, **SA95**.

Macke, E. (1980): Vergleichende Betrachtungen zum Feststofftransport im Hinblick auf ablagerungsfreie Stroemungszustaende in Regen- und Schmutzwasserkanaelen, *Mitteilungen des Leichtweiss Institutes fuer Wasserbau*, Technischen Universitaet Braunschweig, **69**.

Macke, E. (1982): ber den Feststofftransport bei niedrigen Konzentartionen in teilgefuellten Rohrleitungen, *Mitteilungen des Leichtweiss Institutes fuer Wasserbau*, Technischen Universitaet Braunschweig, **76**.

Macke, E. (1983): Bemessung ablagerungsfreier Stroemungszustaende in Kanalisationensleitungen, *KA - Korrespondenz Abwasser*, **7**, 462-469.

Macke, E. & Froehlich, G. (1981): Eine Modellanlage zur Untersuchung der Gesetzmaessigkeiten bei der Feststoffbeseitigung und dem Feststofftransport in teilgefuellten

Kanaelen, *Mitteilungen, Leichtweiss-Institut fuer Wasserbau*, TU Braunschweig, **70**, 303-331.

Macke, E., Hartmann, A. & Koerber, N. von (2002): Zur Schmutzfracht von Regenwasser in groen, flach verlegten Mischwassernetzen, *KA - Wasserwirtschaft/Abwasser/Abfall*, **1**, 40-48.

Malcherek, A. (2001a): Numerische Methoden der Stroemungsmechanik, *Vorlesungsskript 5.0*, Bundesanstalt fuer Wasserbau, Hamburg.

Malcherek, A. (2001b): *Physik und Numerik der Oberflaechengewaesser*, Bundesanstalt fuer Wasserbau, Hamburg.

Mark, O. (1991); A sediment transport model for sewers, *First international Workshop on Sewer Sediments: Origin, occurence and behaviour of sediments in sewer systems*, Universtit Libre de Bruxelles.

Mark, O., Cerar, U. & Perrusgua, G. (1996): Prediction of locations with sediment deposits in sewers, *Water, Science and Technology*, **33**, (9), 147-155.

Martin, H. (1989): Ploetzlich veraenderliche instationaere Stroemungen in offenen Gerinnen, *Technische Hydromechanik 2 - Spezielle Probleme*, Hrgs.: Bollrich, G.,Verlag fuer Bauwesen, 565-635.

Martin, H. & Bollrich, G. (1983): Berechnungsgrundlagen fuer Schwall- und Sunkwellen sowie Dammbruchbroblemen, Symposium: Hydraulik offener Gerinne, *Wiener Mitteilungen Wasser*, Abwasser, Gewaesser, Technische Universitaet Wien, Institut fuer Hydraulik. Gewaesserkunde und Wasserwirtschaft, **79**, 139-164.

May, R.W.P. (1982): Sediment transport in sewers, *Hydraulic Research Station Report*, IT 222.

May, R.W.P., Brown, P.M., Hare, G.R & Jones K.D. et al. (1989): Self-cleansing conditions for sewer carrying sediments, *Hydraulic Research Report*, SR 211.

Mayerle, R. (1988): Sediment transport in rifid boundary channels, *PhD Thesis*, University of Newcastle upon Tyne, England.

Mayerle, R., Nalluri, C. & Novak, P. (1991): Sediment transport in rigid bed conveyances, *Journal of Hydraulic Research*, **29**, (3), 475-494.

Menk, H. (1998): Siedlungsentwaesserung wie sie frueher war - Streifzug durch die Zeitepochen, *Wasser & Boden*, **7**, 100-104.

Michelbach, St. & Woehrle, C. (1991): Settleable solids in a combined sewer system - measurment, quantity, characteristics, *First international Workshop on Sewer Sediments, Origin, occurence and behaviour of sediments in sewer systems*, Universtit Libre de Bruxelles.

Migniot, C. (1968): Etude des proprits physiques de diffrents sdiments trs fins et de leur compartement sous des actions hydrodynamiques, *La Houille Blanche*, **1**, 591-620.

Mittelstaedt, M. (1981): Sedimenttransport in offenen Gerinnen, *Fortbildungslehrgang in technische Hydraulik*, DVWK.

Moin P. & Kim J. (1982): Numerical inverstigation of turbulent channel flow, *J. Fluid Mech.*, **118**, 341-377.

Moine, O. & Madiec, H. (1994): Faut-il installer des dessableurs sur les roeaux d'assainissement, *Report Lyonnaise des Eaux-COSTA meetings*, Bordeaux, **11**.

Muzaferija, S., Peric, M., & Sames, P. et al (1998): A Two-Fluid Navier-Stokes Solver to Simulate Water Entry, *Procceedings 22th Symposium on Naval Hydrodynamics*, Washington, DC, 277-289.

Naef, D.R. (1997): Numerische Simulation von Stosswellen in Freispiegelstroemungen, *Dissertation an der Versuchsanstalt fuer Wasserbau*, ETH Zuerich, **148**.

Nalluri, C. (1991): The influence of cohesion on sediment behaviour in sewers, *First international Workshop on Sewer Sediments*, Origin, occurence and behaviour of sediments in sewers systems, Universtit Libre de Bruxelles, Bruessel.

Nalluri, C. & Alvarez, E.M. (1992): The influence of cohesion on sediment behaviour, *Water Science and Technology*, Pergamont Press, **25**, (8), 151-164.

Nalluri, C. & El-Zaemey, A.K.S. (1993): Sediment Transport over deposited beds in sewers, *Proceedings of the 6th International Conference of Urban Storm Drainage*, Niagara Falls, Canada, 631-637.

Nalluri, C., Ghani, A. & El-Zaemey, A.K.S. (1994): Sediment Transport over deposited beds in sewers, *Water Science and Technology*, **29**, (1-2), 125-133.

Nalluri, C. & Ab Ghani, A. (1993): Bed-load transport without deposition in channels of circular cross section, *Proceedings of the 6th International Conference on Urban storm drainage*, Niagara, 625-630.

Nikuradse J. (1932): Gesetzmaessigkeiten der turbulenten Stroemung in glatten Rohren, Forschung auf dem Gebiet des Ingenieurwesens, Ausgabe B, Band 3, **356**.

N.N. (1896): English Sewer Flushing Practice *Engineering News and American Railway Journal* ,**35**, (21), 343-344, in www.sewerhistory.org.

N.N. (2001): FBS-Innovationspreis 2000 - Zukunft wird aus Innovationen gemacht, *Tiefbau Ingenieurbau Straenbau (TIS)*, **12**, 42-45.

Novak, P. & Nalluri, C. (1975): Sediment transport in smooth fixed bed channels, *Journal of Hydraulic Division*, Proceedings ASCE, **HY9**, 1139-1154.

Oberlack, M. (1994); Herleitung und Loesung einer Laengenma- und Dissipations-Tensorgleichung fuer turbulente Stroemungen, *Dissertation am Institut fuer Technische Mechanik*, Rheinisch-Westfaelischen Technischen Hochschule Aachen.

Oberlack, M. (2003); *Hydromechanics B*, Course Material, Institut fuer Wasserbau und Wasserwirtschaft, Fachgebiet fuer Hydromechanik und Hydraulik, TU Darmstadt.

Oberlack, M., Schaffner, J., Kirchheim, N. (2005): Wirkungsweise und Anwendungsgrenzen eines Schwallspuelsystems zur Reinigung von Stauraumkanaelen, *Abschlussbericht Projekt Deutsche Bundesumweltstiftung*, Fachgebiet fuer Hydromechanik und Hydraulik, TU Darmstadt.

Oertel, H. jr. & Laurien, E. (2003): *Numerische Stroemungsmechanik*, 2.Auflage, Vieweg Verlag, Wiesbaden.

Ogden, H.N. (1899): *Sewer design*, 1th edition, 2th edition dated 1907, John Wiley and Sons, New York.

Olsen, N.R.B. (2002): *SSIIM, User Manual, Version 1.1 and 2.0*, Department of Hydraulic and Enviromental Engineering, NTNU Trondheim, Norwegen.

Oms, C., Gromaire, MC. & Chebbo, G. (2002): In situ observation of the water-bed interface in combined sewer systems using endoscopy, *International Conference on Sewer Processes and Networks - Proceedings*, Paris, France.

Paintal, A.S. (1972): Hydraullic design of self-cleaning circular sanitary sewers, *Water and Sewage works*, Scranton Gillet-Publication, USA.

Perrusquia, G. (1991): Bedload transport in storm sewers, *First international Workshop on Sewer Sediments, Origin, occurence and behaviour of sediments in sewer systems*, Universtit Libre de Bruxelles.

Perrusqua, G., Lyngfelt, S. & Sjoeberg, A. (1986): Floedeskapacifet hos avloppsleduingar delvis fyllda med sediment, *Report series B*, **48**, Chalmes Universitaee of Technology Goeteborg, Schweden.

Perrusquia, G. & Nalluri, C. (1995): Modelling of bedload trasport in pipe channels, *8th International Conference on Transport and Sedimentation of Solid Particles*, Prag.

Perrusquia, G., Petersen, O. & Larsen, T. (1995): Influence of sewer sediments on flow friction and shear stress distribution, *Water Science and Technology*, **31**, (7), 117-126.

Picologlou, B., Zelver, N. & Characklis, W. (1980): Biofilm growth and hydraulic performance, *Journal of Hydraulic Division*, ASCE, **106**, 733-746.

Pisano, W.C., Aronson, G. & Queiroz, C. (1979): *Dry-Weather Deposition and Flushing for Combined sewer overflow Control*, Report 600/2-79-133, United States Environmental and Protective Agency, Washington DC.

Pisano, W.C., Joyce, J., Sorensen, H. & Barsanti, J. (1998): *Sewer and Tank flushing: Case studies*, Report 600/R-98/157, United States Environmental and Protective Agency, Cincinnati, USA.

Pisano et al. (2003): Automated Sewer and Drainage Flushing Systems in Cambridge, Massachusetts, *Journal of Hydraulic Engineering*, ASCE, **129**, (4), 260-266.

Ploechinger, E. (1995): *Grundkurs hoehere Mathematik*, 1.Auflage, Verlag Harri Deutsch, Frankfurt/Main.

Pohle, F.V. (1952): Motion of water due to breaking of a dam and related problems, *Journal of Research / National bureau of standards*, 9.1952,**3**, 47-59.

Rastogi, A.K., Rodi, W. (1975): Three-dimensional calculation of heat and mass dispersion in open channel flows, *Proceedings 3th National Heat and Mass Transfer Conference*, Indian Institute of Technology, Bombay, India.

Reid, G. & Yang, T. (1959): Sewer Slimes cause Odors, *Wastes Engineering*, **30**, (9).

Reiff, H. (1992): Wachstum und Abtrag der Sielhaut in Mischwasserkanaelen, *Wasser-Abwasser Abfall: Schriftenreihe des Fachgebietes Siedlungswasserwirtschaft*, Verein zur Foerderung des Fachgebiets Siedlungswasserwirtschaft an der Universitaet - Gesamthochschule Kassel, **9**.

Reynolds, O. (1895): On the Dynamical Theory of Incompressible Viscous Fluids and the Determination of the Criterion, Royal Society Phil.Trans.,**A 186**,123.

Rhee, S.H., Makarov, B.P. & Krishan, H. et al. (2004): Assessment of Numerical Techniques in Volume of Fluid Method for Free Surface Flows, *9th Symposium on Practical Design of Ships and other Floating Structures*, Luebeck-Travemuende, Germany.

Ristenpart, E. (1995): Feststoffe in der Mischwasserkanalisation, *Stadtentwaesserung und Gewaesserschutz*, Institut fuer Wasserwirtschaft, Universitaet Hannover, **11**.

Ristenpart, E. (1995): Sediment Properties and their changes in a sewer, *Water Science and Technology*, Pergamont Press, **31**, (7), 77-83.

Ristenpart, E. (1998): Solids Tranport by Flushing of Combined sewers, *Water Science and Technology*, Pergamon Press, **37**, (1), 171-178.

Ritter, A. (1892): Die Fortpflanzung von Wasserwellen, *Zeitschrift Deutscher Ingenieure*, **36**, (33), 947-954.

Robinson, M.P. & Graf, W.H. (1972): Pipelining of low concentration sand-water mixture, *Journal of Hydraulic Divisions*, Proceedings ASCE , **98**, (HY7), 1221-1241.

Rodi, W. (1993) *Turbulence Models and Their Application in Hydraulics, A state-of-the-art review*, IAHR Monograph series. A.A. Balkema.

Rodi, W. (2004): *Turbulenzmodelle in der Stroemungsmechanik*, Institut fuer Hydromechanik, Universitaet Karlsruhe.

Roe, J. (1842): *On the causes of accumulation of deposits in sewers, and on the hithero generally prevalent mode of removing the same; with a description of a new flushing apparatus used for cleansing the sewers in the Holborn and Finsbury Divisions*, Proceedings of the Institution of Civil Engineers.

Rotta, J.C. (1972): *Turbulente Stroemungen*, Teubner Verlag, Stuttgart.

Rudman, M. (1997): Volume-Tracking Methods For Interfacial Flow Calculations, *International Journal for Numerical Methods in Fluids*, **24**, 671-691.

Ruettgers, E. (1987): Entwicklung neuer Reinigungsverfahren als Vorleistung fuer die Sanierung von Kanalnetzen, *Dokumentation 1. Internationaler Kongre Leitungsbau*, **I**, 245-255.

SAINT-VENANT, B. (1871): Thorie du Mouvement Non Permanent des Eaux, avec Application aux Crues des Rivires et lIntroduction des Mares dans leur *Comptes Rendus Hebdomadaires des Sances de lAcadmie des Sciences*, **73**, 147 154 and 237240.

Sakakibara, T. (1996): Sediments flushing experiment in a trunk sewer, *Water Science and Technology*, Pergamon Press, **33**, (9), 113-123.

Sander, Th. (1989): Ablagerungsprozess und Feststofftransport in Abwasserleitungen, *Mitteilungen des Leichtweis Institutes fuer Wasserbau*, Technischen Universitaet Braunschweig, **105**, 159-318.

Sauermann, H.B. (1983): Hydraulischer Transport von groben Feststoffen in Kreis- und Segmentrohren, *Mitteilungen des Leichtweis Institutes fuer Wasserbau*, Technischen Universitaet Braunschweig, **77**.

Saul, A. (1991): Sediments in storage tanks, *First international Workshop on Sewer Sediments, Origin, occurence and behaviour of sediments in sewer systems*, Universtit Libre de Bruxelles.

Schaffner, J. (2003a): Hydromechanische Grundlagen der Schwallspuelung, *41. Darmstaedter Wasserbauliches Kolloquium*, **130**, Institut fuer Wasserbau und Wasserwirtschaft, FG Hydromechanik und Hydraulik, TU Darmstadt.

Schaffner, J. (2003b): Numerical simulation of a flush cleaning wave in a reservoir sewer in Offenbach/Germany, *18th European Young Scientist Workshop on Sewer Processes and Networks*, Almograve, Portgual.

Schaffner, J., Oberlack, M. & Kirchheim, N. (2004): The application of numerical modelling (3-D) for the calculation of flush waves in sewer channels, *6th International Conference on Urban Drainage Modelling*, Institute for Urban Water Management, TU Dresden/Germany.

Schaffner, J., Oberlack, M. & Kirchheim, N. (2006a): Wirkungsweise und Anwendungsgrenzen eines Schwallspuelsystems zur Reinigung von Stauraumkanaelen, *Tagung Abflusssteuerung - Schwallspuelung - Gewaesserschutz*, Zentrum fuer Umweltkommunikation, DBU Osnabrueck.

Schaffner, J., Oberlack, M. & Kirchheim, N. (2006b): Numerical investigations on flush waves in sewer channels using computational fluid dynamics, *7th International Conference on Hydroinformatics*, Nice, France.

Schlichting, H., Gersten, K. (1997): *Grenzschicht-Theorie*, 9.Auflage, Springer Verlag, Berlin.

Schlueter, M. (2002): Kanalreinigung: Keine Alternativen zur HD-Spuelung, *IKT-eNewsletter*, www.ikt.de.

Schmitt, F. (1991): Zum Einflu von Kanalablagerungen auf die biogene Schwefelsaeure-Korrosion, *Umwelt Technologie*, **3**, 17f.

Schmitt, F. (1992): Einfluss von Ablagerungen auf den Betrieb von Abwasserkanaelen, *Veroeffentlichungen Institut fuer Siedlungswasserwirtschaft und Abfalltechnik*, Universitaet Hannover, **82**.

Schmitt, T.G. (1985): Der instationaere Kanalabfluss in der Schmutzfrachtmodellierung, Dissertation, *Schriftenreihe des Institus fuer Siedlungswasserwirtschaft*, Universitaet Karlsruhe, **42**.

Schoenung, B.E. (1990): *Numerische Stroemungsmechanik*, Springer Verlag, Berlin.

Schramm, J.M. (2003): Eindimensionale Berechnung instationaerer und diskontinuierlicher Stroemungen in abflussschwachen naturnahen Fliegewaessern, *Dissertation am Institut fuer Wasserbau und Wasserwirtschaft*, RWTH Aachen.

Schroeder, R.C.M. (1990): Hydraulische Methoden zur Erfassung von Rauheiten, *DVWK Schriften Nr.92*, Paul Parey Verlag.

Schultz (1960): ber die Berechnung der unterern Grenzgeschwindigkeiten in Kanalisationsnetzen, *Wasserwirtschat und Wassertechnik*, **7**.

Schuessler, O. (2002): Schwallspueleinrichtungen in Mischwasserkanalisationen, *Diplomarbeit am Lehrstuhl fuer Siedlungswasserwirtschaft*, Fakultaet fuer Bauingenieurwesen, RWTH Aachen.

Schween, W. (1936): Beitrag zum Ablaufen von Schwallwellen in nicht begehbaren Leitungen aufgrund von Messungen in Straenkanaelen, *Dissertation TH Dresden*, Fendingen: Buchdruck & Verlagsanstalt.

Seggelke, K. & Rosenwinkel, K.H. (2004): Manahmen zur Verbesserung der Leistungsfaehigkeit biologischer Klaeranlagen bei Mischwasserzufluessen, *GWF - Wasser/ Abwasser*, **12**, 856-866.

Seyfried, C.F. & Schmitt, F. (1989): Auswirkungen des Mischwasserzuflusses auf die Klaeranlage -Urbanhydrologie Teil 3, *Schriftenreihe des Instituts fuer Siedlungswasserwirtschaft*, Technische Universitaet Karlsruhe, Oldenbourg Verlag, **87**.

Shafai-Bajestan, M. & OstadAskari, M. (2000): Developing a computer model to predict the total load by modified Einstein method, *Journal of Science and Technology Agricultural and Natural Resources*, University of Isfahan Technology, **4**, (2), 29-41.

Sikora, B. (1989): Vanne cyclique autocurante dcantation, *Demande de Brevet d'Invention*, INPI, **2643971**.

Sperling, F. (1984): Die Belastung der Lippe bei Hamm durch Regenabfluss, *Stuttgarter Berichte zur Siedlungswasserwirtschaft*, Institut fuer Wasserbau, Universitaet Stuttgart, Kommissionsverlag R. Oldenbourg, **79**, 261-281.

Stansby, P., Chegini, A. & Barnes, C.D. (1998): The Initial Stages of a Dambreak Flow, *J. Fluid Mech.*, **370**, 203-222.

Star-CD Version 3.15 (2002): Methology, *Computational Dynamics Ltd*, CD adapco Group.

Stauffer, P., Dettmar, J. & Pinnekamp, J. (2006): Impact of the level of approximation on modeling flushing waves, *International Conference on Sewer, Operation and Maintenance*, Vienna, Austria.

Steffler, P.M.,& Jin, Yee-Chung (1993): Depth averaged and moment equations for moderately shallow free surface flow, *Journal of Hydraulic Research*, **31** (1), 5-17.

Stein, D. (1999): *Instandhaltung von Kanalisationen*, 3. Auflage, Ernst Sohn Verlag.

Steinhard, J. & Schaffner, J. (2006): Numerical investigation of the self-acting flushing system HydroFlush GS in Frankenberg/Germany, *International Conference on Sewer, Operation and Maintenance*, Vienna, Austria.

Steinhardt Wassertechnik GmbH (2005), Roederweg 10, 65232 Taunusstein, www.steinhardt.de.

Stoker, J. J. (1957): *Water Waves The Mathematical Theory with Applications*, Interscience Publisher, New York.

Stotz, G. & Krauth, K.H. (1986): Deposition in combined sewers and their flushing behavior, *Proceedings International Symposium on comparison of urban drainage models with real catchment data*, USM, edited by Maksimivic, Dubrovnik.

Sulzer, S.C. (2001): Flood Discharge Estimation for Complex River Geometries by Inverse Numerical Modelling, *Dissertation am Institut fuer Hydromechanik*, ETH Zuerich.

Taylor, R.H. & Brooks, N.H. (1962): Discussion to "Resistance to flow in alluvial channels", *Transactions of the American Society of Civil Engineers*, **127**, 982-992.

Uphoff, C. & Toews, R. (2004): Untersuchung ueber die Beseitigung von Kanalablagerungen mit einem Spuelschacht, *Tiefbau Ingenieurbau Straenbau, tis*, **46** (11), 18-21.

Van Rijn, L.C. (1982): Equivalent roughness of alluvial bed, *Journal of the Hydraulics Divisions, ASCE*, **108** (HY10), 1215-1218.

Valentin, F. & Rinaldi, P. (2001): Skript Hydraulik III , *Lehrstuhl fuer Hydraulik und Gewaesserkunde*, Technische Universitaet Muenchen.

Verbanck, M. A. (1992): Origin, Accurrence and behaviour of sediment in sewers systems, *Water Science and Technology*, **25**, (8).

Verbanck, M.A. (1995): Capturing and releasing settleable solids - The significance of dense undercurrents in combined sewer flows, *Water Science and Technology*, Pergamont Press, **31**, (7), 85-93.

Verbanck, M. A. (2000): Computing and releasing near-bed solids - the significance of dense undercurrents in combined sewer flows, *Urban Water*, **2**, (4), 277-284.

Verbanck, M.A. & Ashley, R.M. (1992): International Workshop on Origin, Occurrence and Behavoir of Sediments in Sewer Systems: Outline of Technical Conclusions, *Water Science and Technology*, **27**, (12), 173-176.

Verbanck, M.A., Ashley, R.M. & Bachoc, A. (1994): International workshop on origin, occurrence and behaviour of sediments in sewer systems: Summary of conclusions, *Water Resources*, **28**, (1), 187-194.

Versteeg, H., Malalasekra, W. (1995): *An Introduction to Computational Fluid Dynamics, The Finite Volume Method Approach*, Addison-Wesley International.

Vollmers, H. & Pernecke, L. (1976): Beginn des Feststofftransportes fuer feinkoernige Materialien in einer richtungskonstanten Stroemung, *Zeitschrift des Vereins Deutscher Ingenieure*, **6**, 236-261.

Vreugdenhil, C.B. (1994): *Numerical Methods for shallow-water flow*, Kluwer Academic Publishers, Dordrecht, Netherlands.

Wang, M.-H. & Han, Y. (1996): Study of sediment trapping by detention basins, *7th International Conference on Urban Storm Drainage*, Hannover, Germany, 743 f.

Westrich, B. (1984): Hydraulische Bedingungen fuer Ablagerung und Abtrag von Feststoffen bei Freispiegelabfluss, *Stuttgarter Berichte zur Siedlungswasserwirtschaft*, Institut fuer Wasserbau, Universitaet Stuttgart, Kommissionsverlag R. Oldenbourg, **79**, 3-30.

Whitham, G.B. (1955): The Effects of Hydraulic Resistance in the Dam-Break Problems, *Proceedings of the Royal society*, London, **227**, (1), 399-407.

Wilcox, D.C. (1998): *Turbulence Modeling for CDF*, 2. Edition, DCW Industries, Inc.

Williams, D.J.A., Williams, P.R. & Crabtree, R.W. (1989): Preliminary investigations into the rheological properties of sewer sediment deposits and the development of a synthetic material for laboratory studies, *FWR Report*, **0016**, Swindon.

Wotherspoon, D.J.J. (1994): The Movement of cohesive sediments in a large combined sewer, *Dissertation Dundee Institute of Technology.*

Xanthopoulos, C. & Augustin, A. (1991): Input and Characterisation of Sediments in Urban Sewer Systems, *First International Workshop on Sewer Sediments, origin, occurence and behaviour of sediments in sewer systems*, Universit Libre de Bruxelles.

Youngs, D.L. (1982): Time-Dependent Multi-Material Flow with Large Fluid Distortion, in Morton K.W. und Baines, M.J.(Editoren), *Numerical Methods for Fluid Dynamics*, Acdemic, New York, 273-285.

Yao, K.M. (1974): Sewer line design based on critical shear stress, *Journal of the Environmental Engineering Division*, ASCE, **100**, 507-520.

Yu, G. & Tan, S.K. (2006): Performances of Hydraulics and Bedload Sediment Flushing in Rigid Channel using Surge Flows, *Journal of Irrigation and Drainage Engineering*, **132** (2), 171-179.

Zanke,U.C.E. (2004): Zum Einfluss der Turbulenz auf den Bewegungsbeginn - On the Influence of Turbulence on the Initiation of Sediment Motion, *BAW-Workshop: Boden- und Sohl-Stabilitaet Betrachtungen an der Schnittstelle zwischen Geotechnik und Wasserbau*, Bundesanstalt fuer Wasserbau, Karlsruhe.

A Inclination of the reservoir sewer August-Bebel Ring / Offenbach

Section no.	Inclination [‰]	Length [m]
1	5,18	55
2	1	60
3	1,9	62,4
4	0,8	57,2
5	1,08	63,15
6	1,36	44

Source: Official plans by Eigenbetrieb Stadt Offenbach (ESO)

B Flush Tests

Temporal development of the flush waves at different storage levels

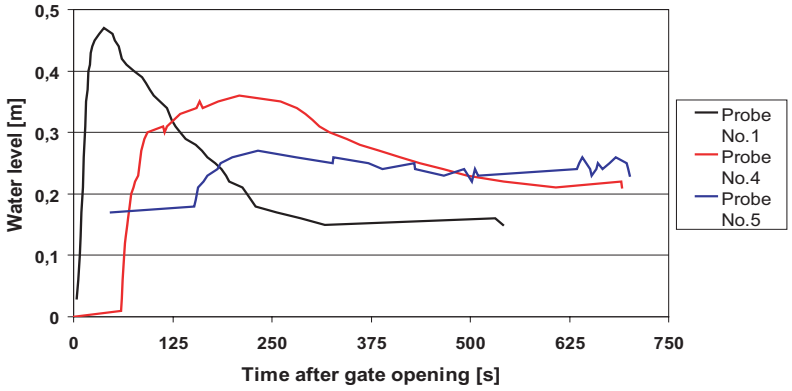

Figure B.1: Storage level 0.73 m

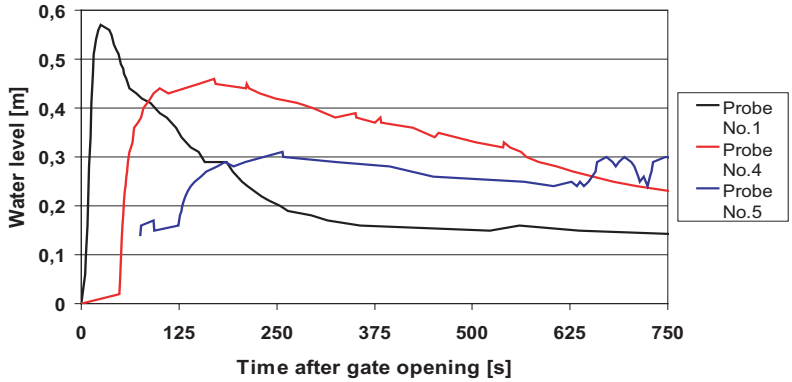

Figure B.2: Storage level 1.03 m

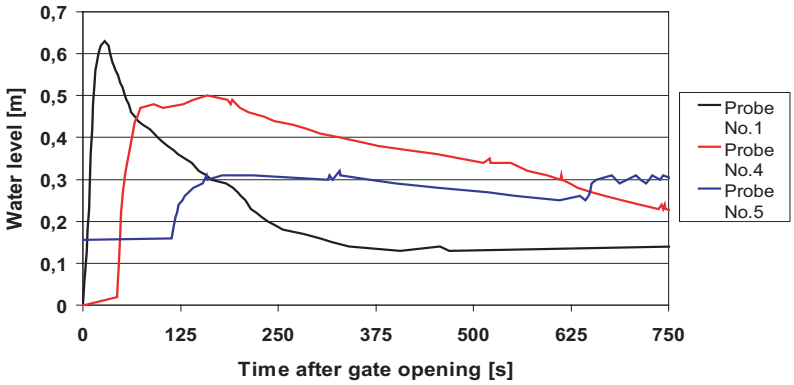

Figure B.3: Storage level 1.25 m

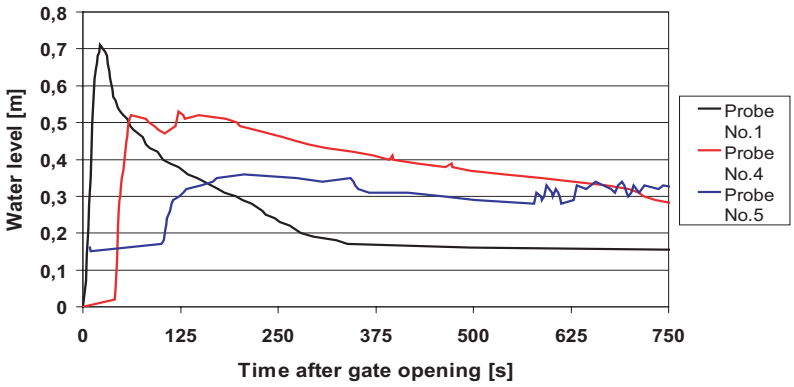

Figure B.4: Storage level 1.45 m

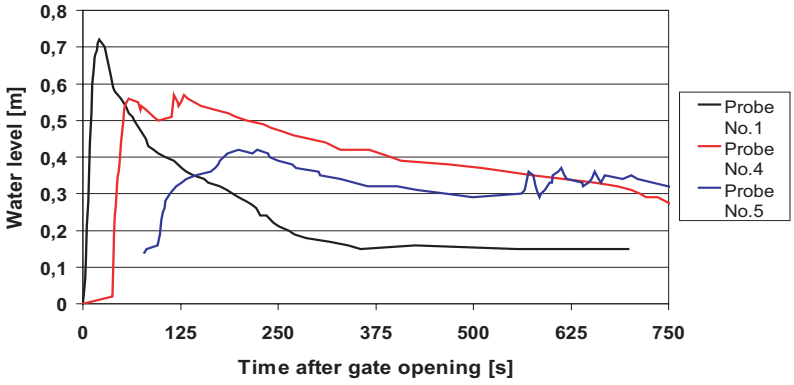

Figure B.5: Storage level 1.64 m

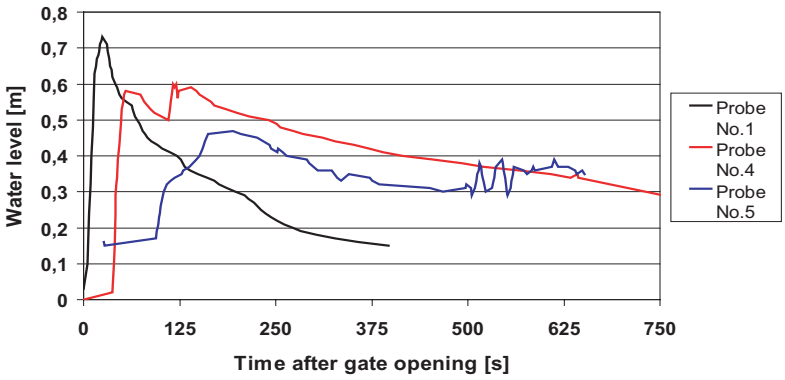

Figure B.6: Storage level 1.82 m

C Cross-section no. 1

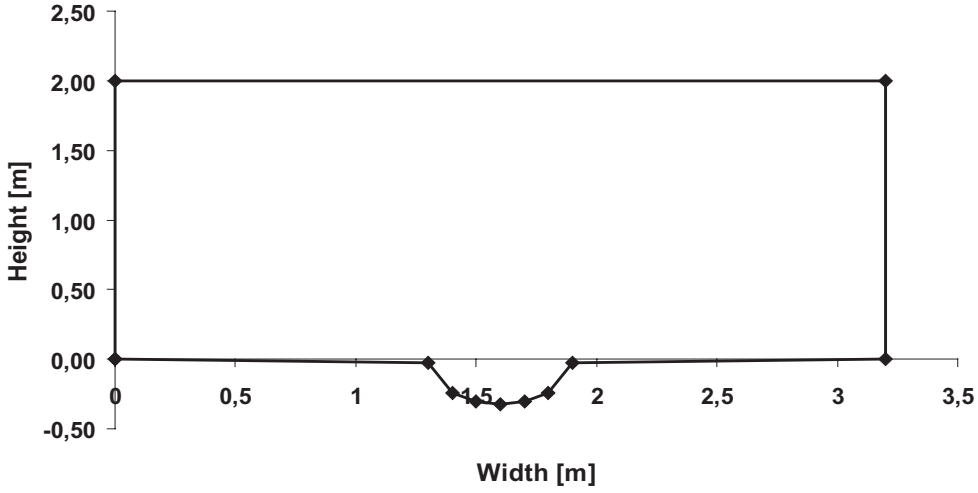

Figure C.1: Cross-section no.1 for $z = 0$ m

D Comparison of measured and modelled flush waves

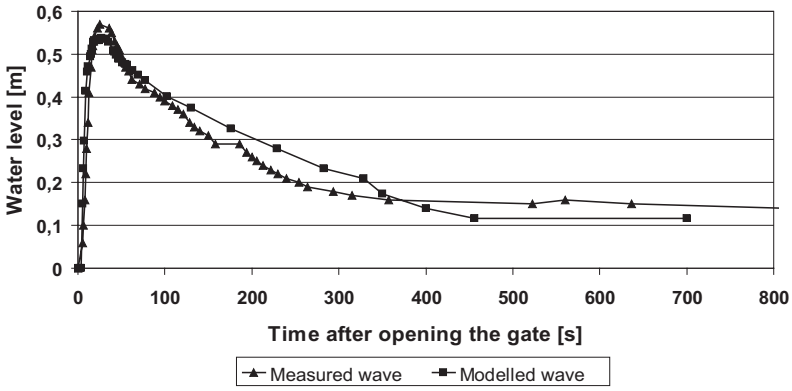

Figure D.1: Comparison of flush waves, probe no. 1, storage level 1.03 m

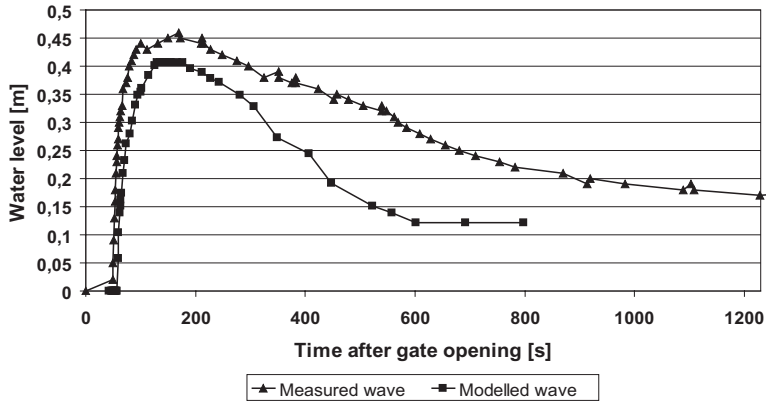

Figure D.2: Comparison of flush waves, probe no. 4, storage level 1.03 m

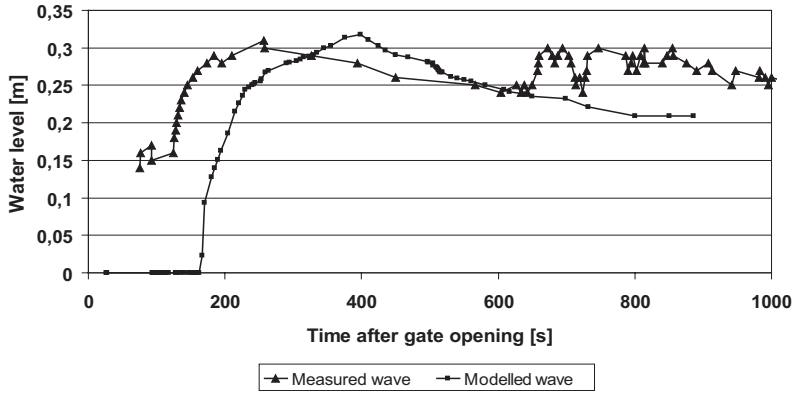

Figure D.3: Comparison of flush waves, probe no. 5, storage level 1.03 m

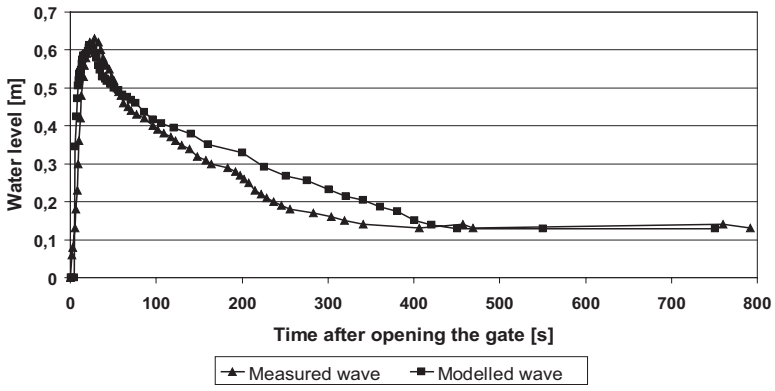

Figure D.4: Comparison of flush waves, probe no. 1, storage level 1.25 m

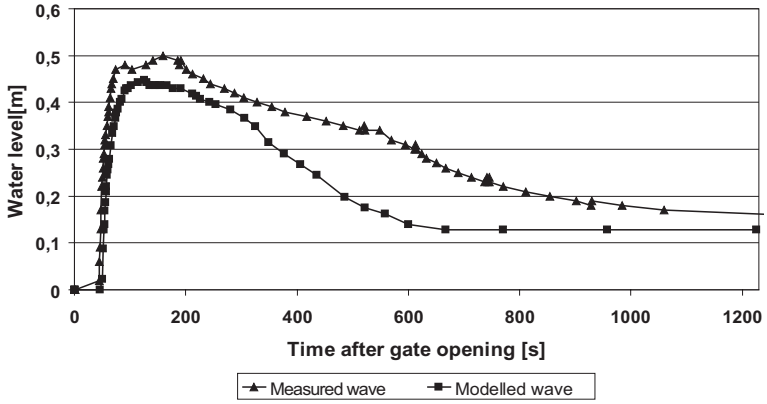

Figure D.5: Comparison of flush waves, probe no. 4, storage level 1.25 m

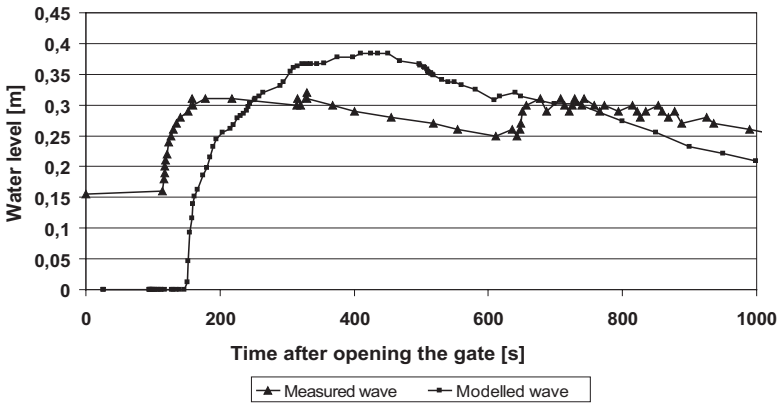

Figure D.6: Comparison of flush waves, probe no. 5, storage level 1.25 m

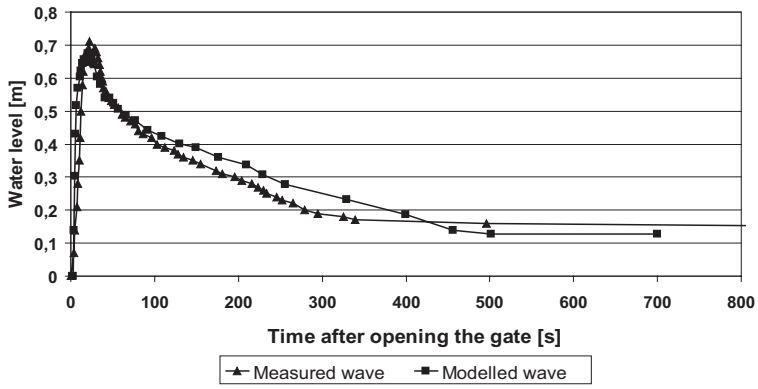

Figure D.7: Comparison of flush waves, probe no. 1, storage level 1.45 m

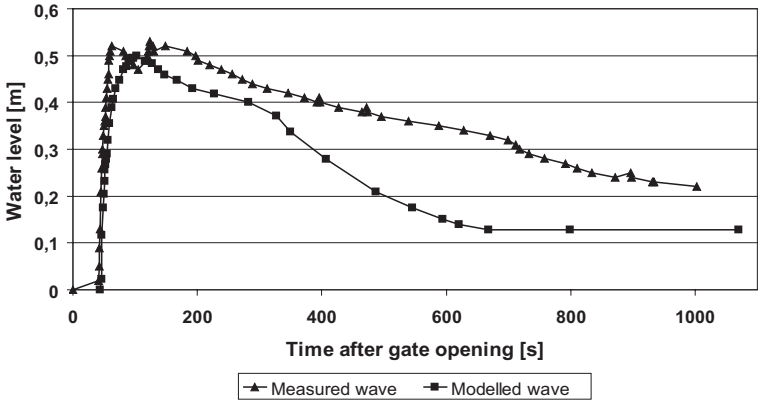

Figure D.8: Comparison of flush waves, probe no. 4, storage level 1.45 m

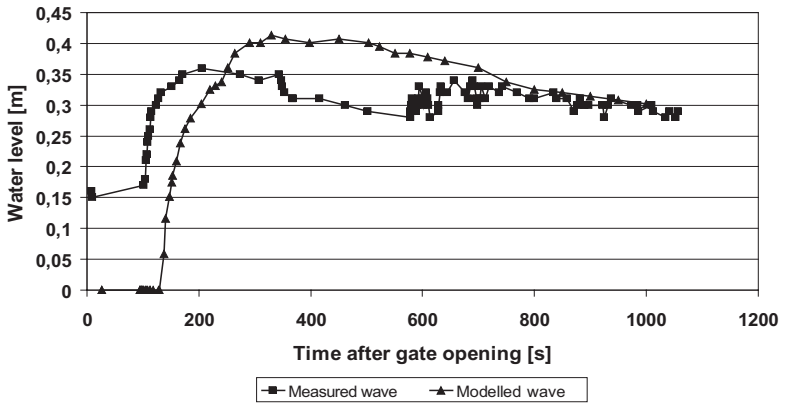

Figure D.9: Comparison of flush waves, probe no. 5, storage level 1.45 m

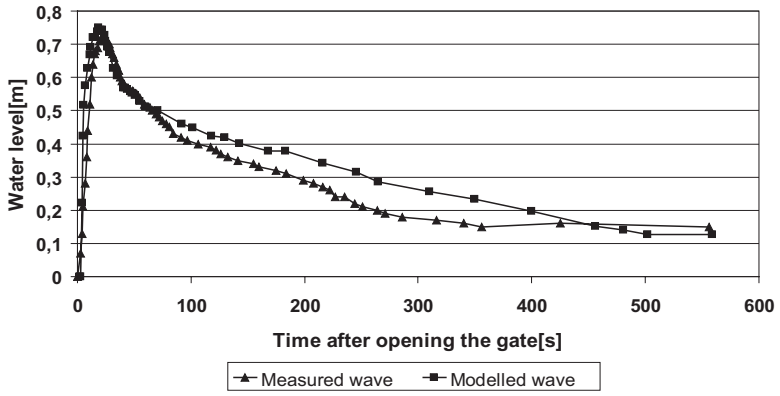

Figure D.10: Comparison of flush waves, probe no. 1, storage level 1.64 m

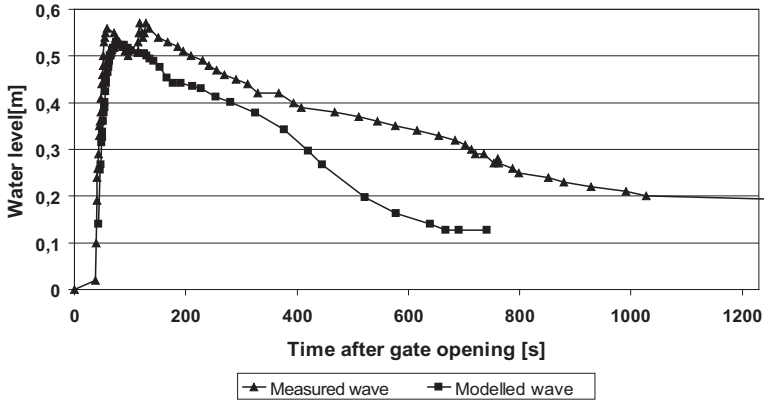

Figure D.11: Comparison of flush waves, probe no. 4, storage level 1.64 m

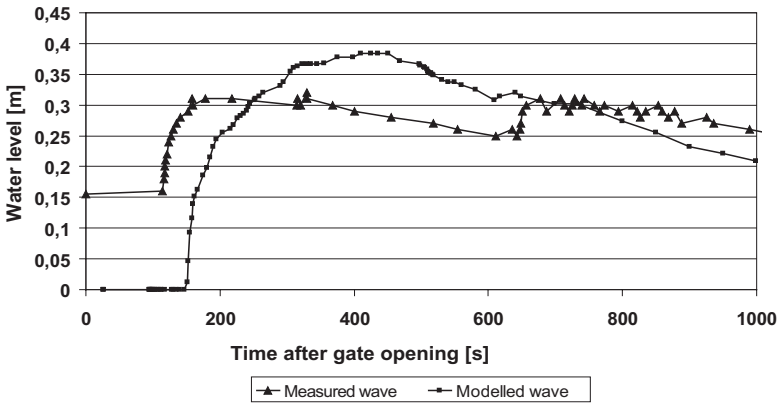

Figure D.12: Comparison of flush waves, probe no. 5, storage level 1.64 m

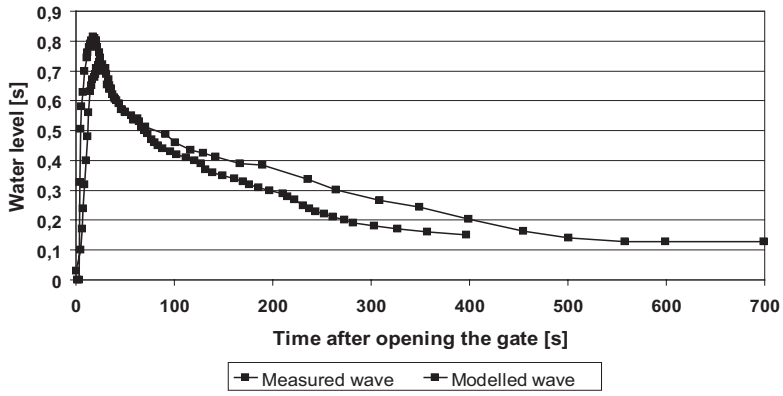

Figure D.13: Comparison of flush waves, probe no. 1, storage level 1.82 m

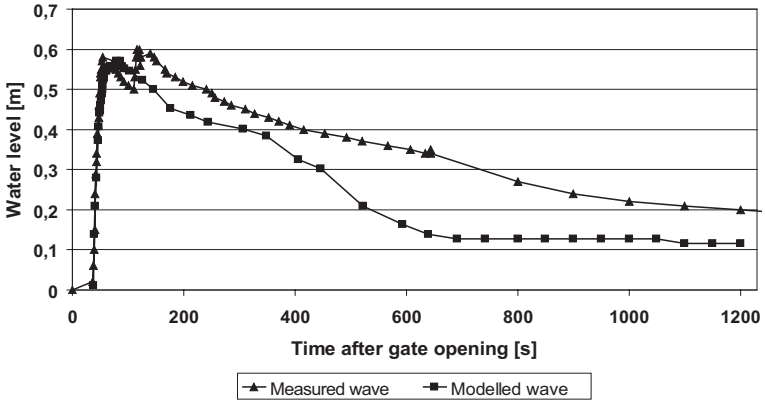

Figure D.14: Comparison of flush waves, probe no. 4, storage level 1.82 m

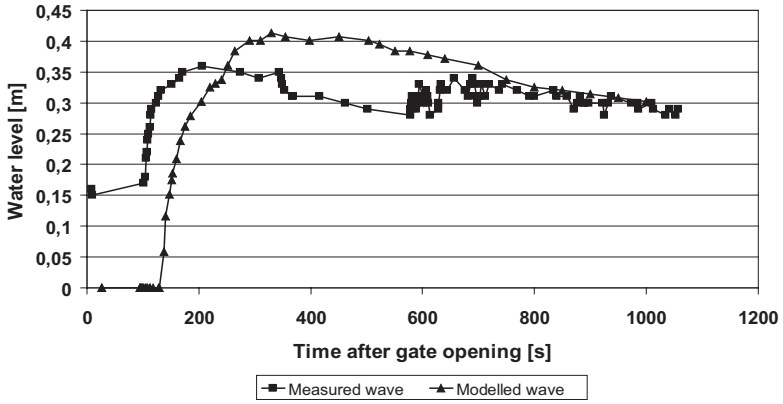

Figure D.15: Comparison of flush waves, probe no. 5, storage level 1.82 m

E Comparison of analytical and numerical solutions

Dressler solution, Ritter wave and numerical solution

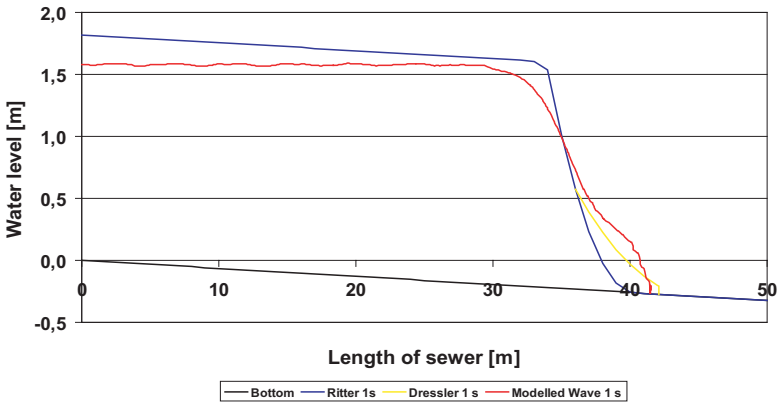

Figure E.1: Comparison of analytical and numerical solutions, 1s

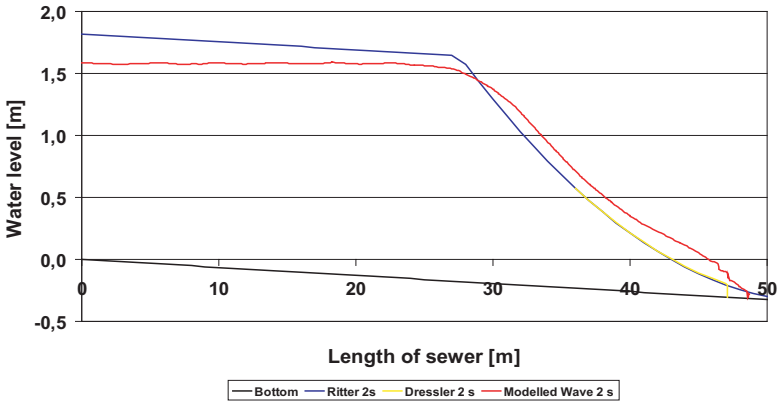

Figure E.2: Comparison of analytical and numerical solutions, 2s

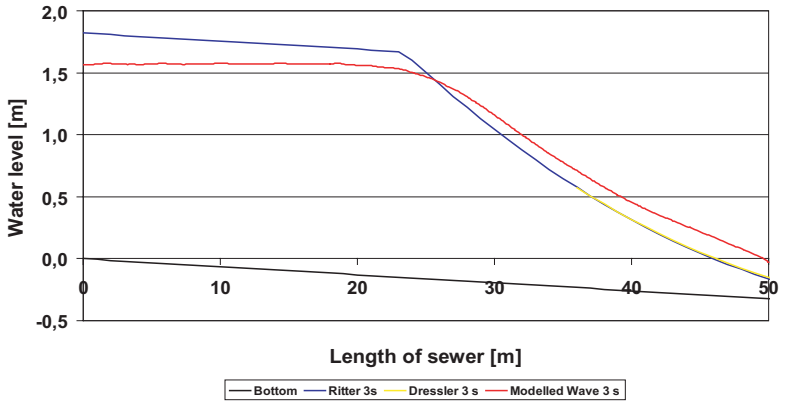

Figure E.3: Comparison of analytical and numerical solutions, 3s

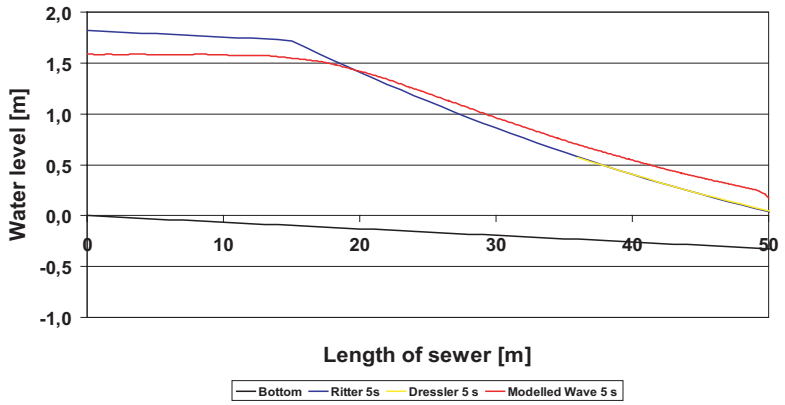

Figure E.4: Comparison of analytical and numerical solutions, 5s

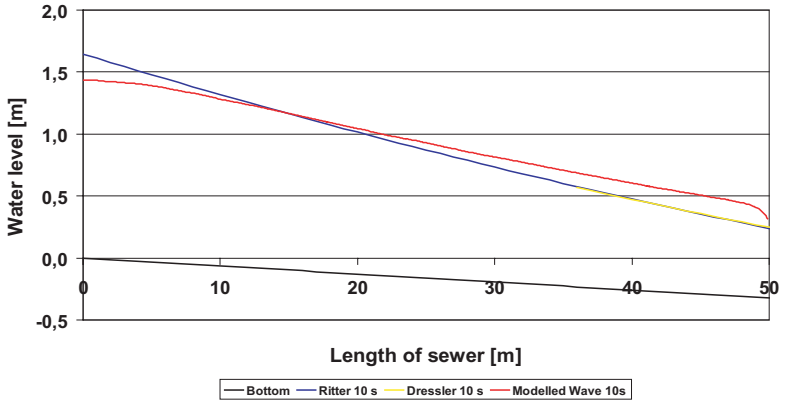

Figure E.5: Comparison of analytical and numerical solutions, 10s

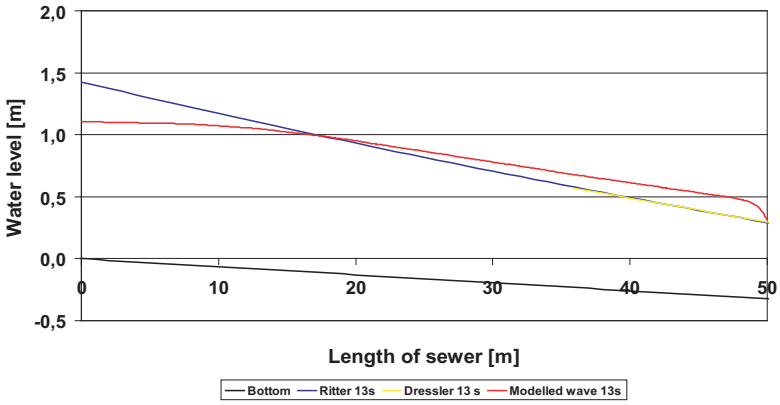

Figure E.6: Comparison of analytical and numerical solutions, 13s

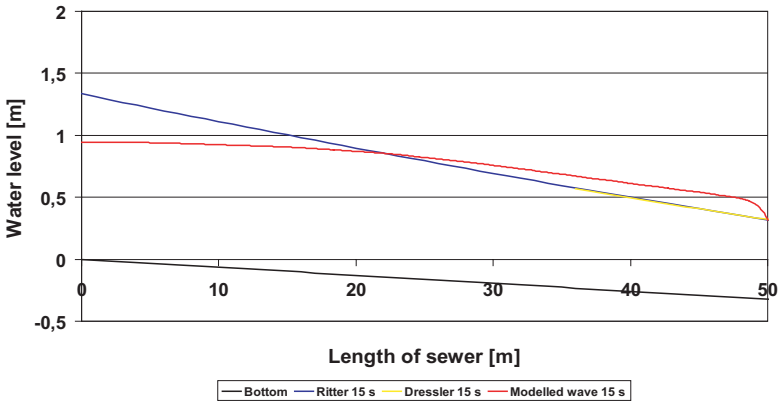

Figure E.7: Comparison of analytical and numerical solutions, 15s

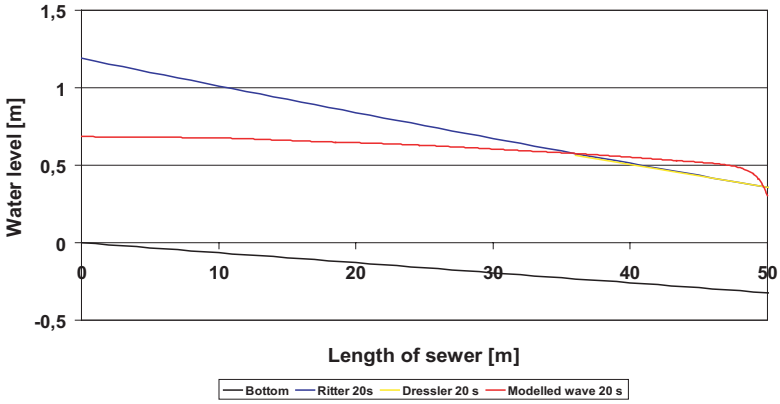

Figure E.8: Comparison of analytical and numerical solutions, 20s

F Analysis of bottom shear stress

Progression of bottom shear stress
Dry-weather channel

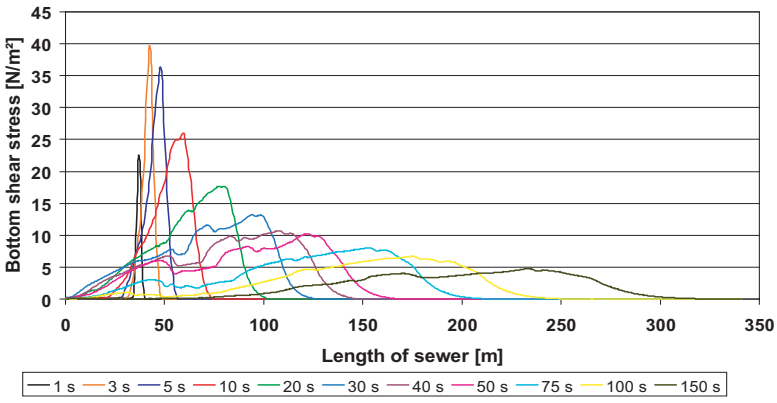

Figure F.1: Progression of the bottom shear stress, h_{store}=0.73 m, Dry-weather channel

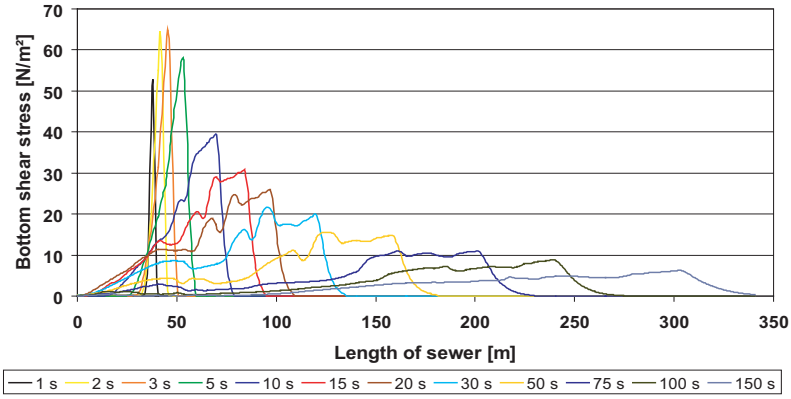

Figure F.2: Progression of the bottom shear stress, h_{store}=1.03 m, Dry-weather channel

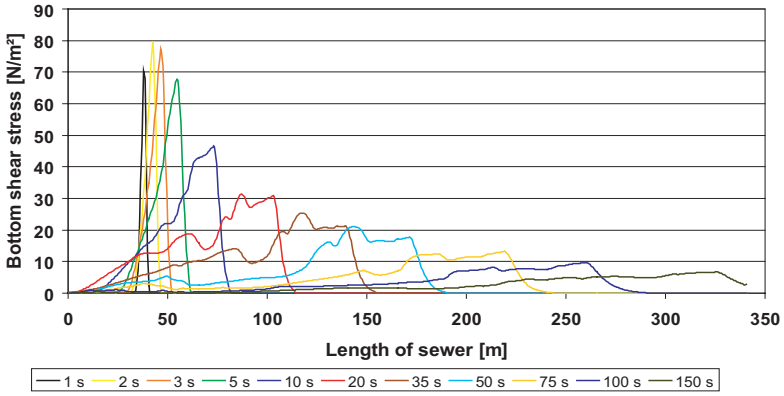

Figure F.3: Progression of the bottom shear stress, h_{store}=1.25 m, Dry-weather channel

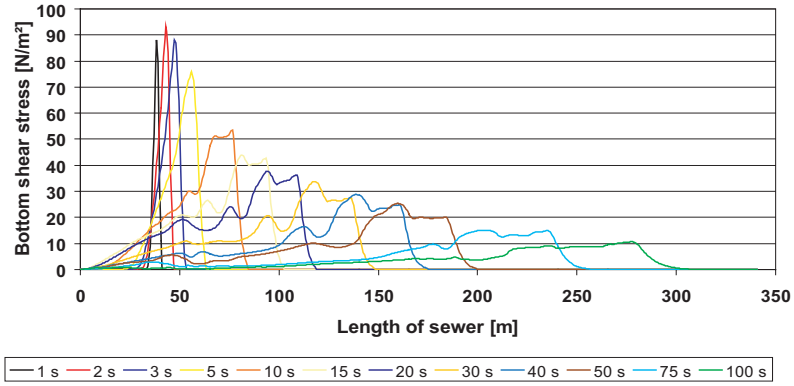

Figure F.4: Progression of the bottom shear stress, h_{store}=1.45 m, Dry-weather channel

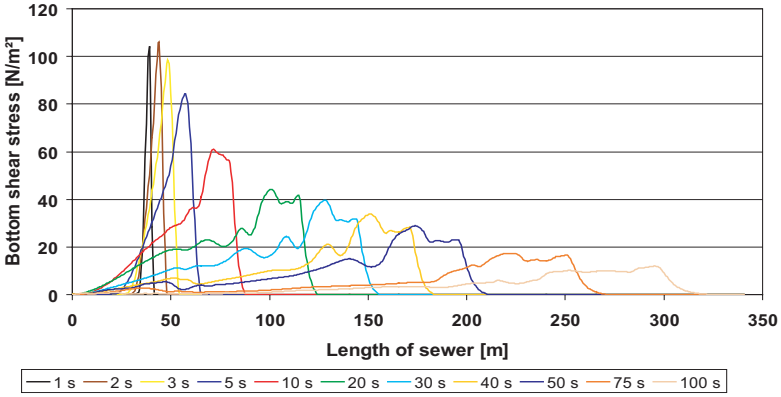

Figure F.5: Progression of the bottom shear stress, h_{store}=1.64 m, Dry-weather channel

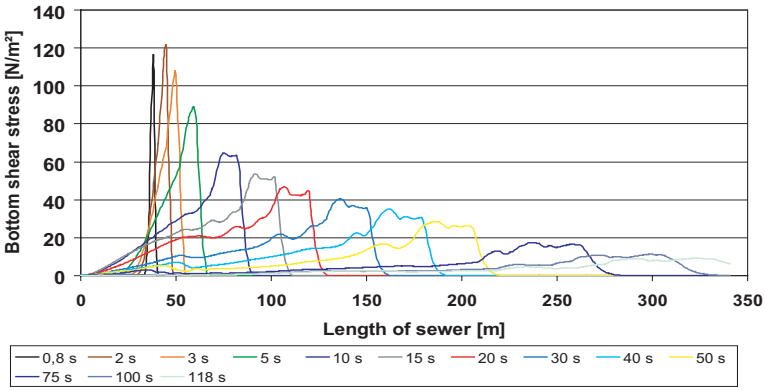

Figure F.6: Progression of the bottom shear stress, h_{store}=1.82 m, Dry-weather channel

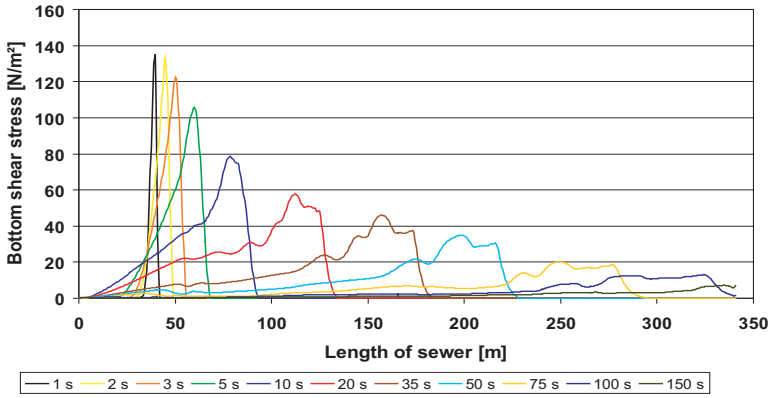

Figure F.7: Progression of the bottom shear stress, h_{store}=2.02 m, Dry-weather channel

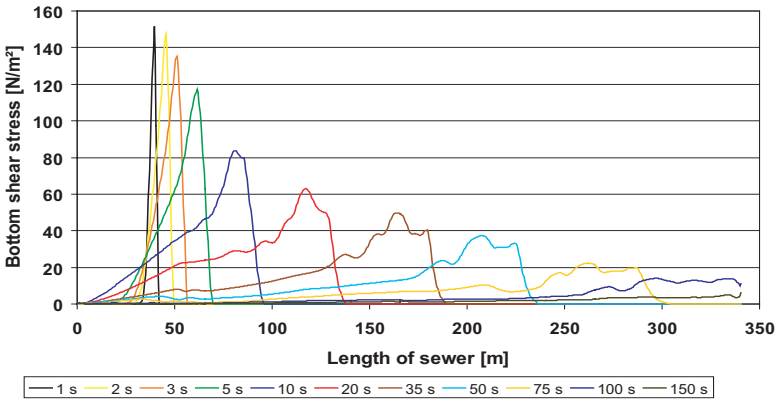

Figure F.8: Progression of the bottom shear stress, h_{store}=2.20 m, Dry-weather channel

Slopes

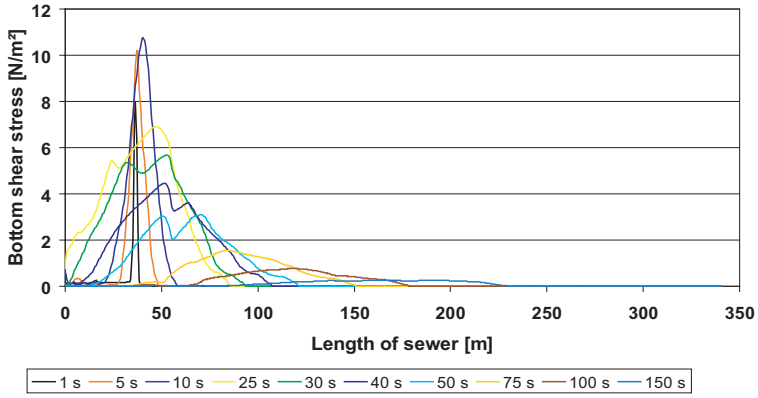

Figure F.9: Progression of the bottom shear stress, h_{store}=0.73 m, Slopes

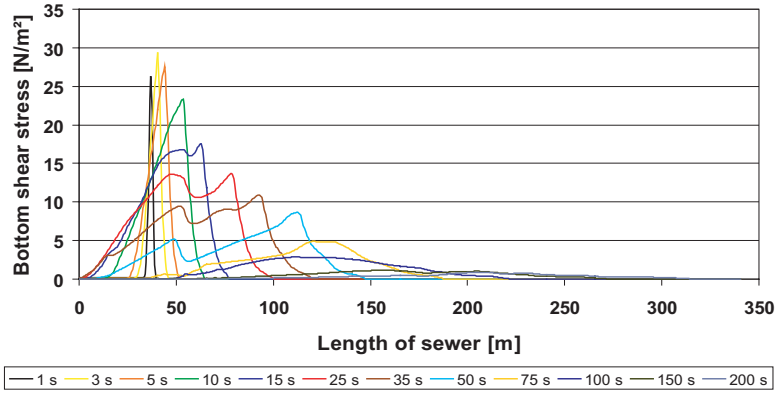

Figure F.10: Progression of the bottom shear stress, h_{store}=1.03 m, Slopes

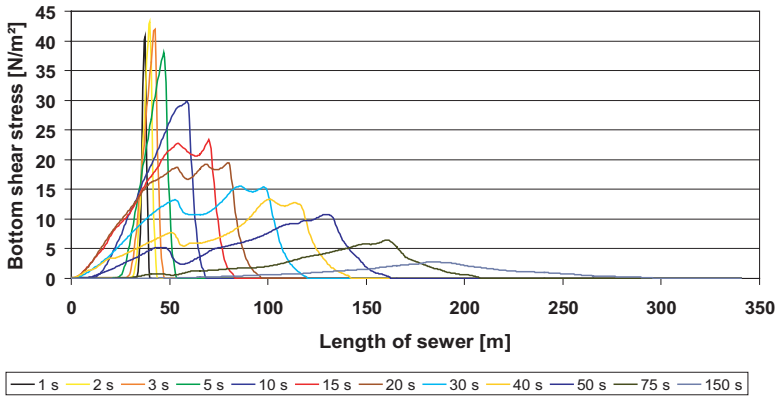

Figure F.11: Progression of the bottom shear stress, h_{store}=1.25 m, Slopes

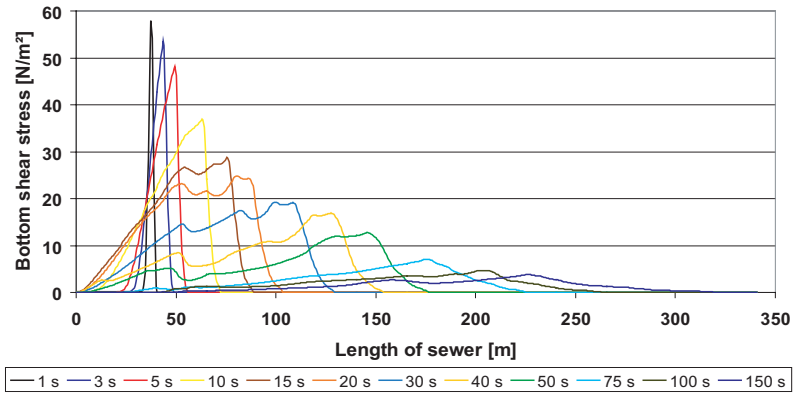

Figure F.12: Progression of the bottom shear stress, h_{store}=1.45 m, Slopes

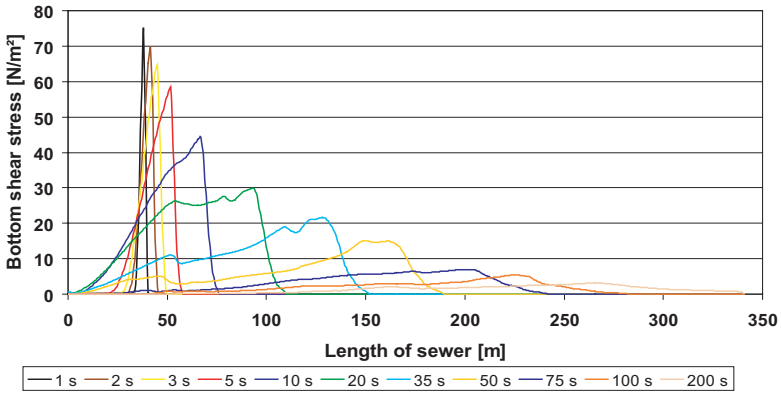

Figure F.13: Progression of the bottom shear stress, h_{store}=1.64 m, Slopes

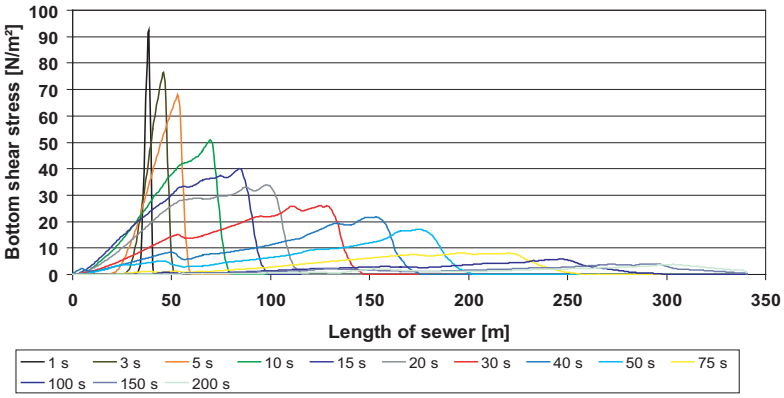

Figure F.14: Progression of the bottom shear stress, h_{store}=1.82 m, Slopes

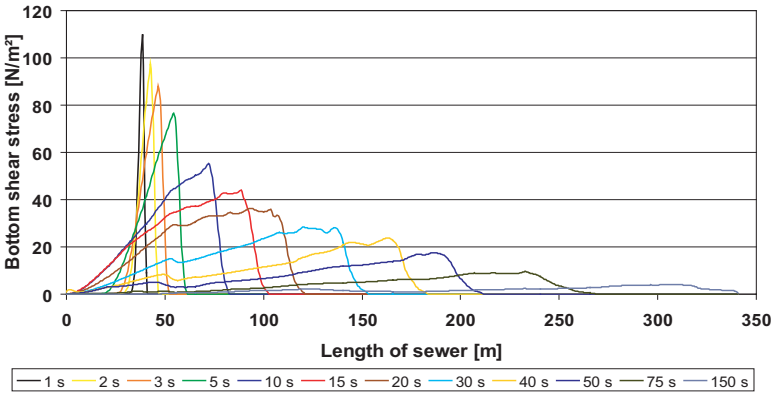

Figure F.15: Progression of the bottom shear stress, h_{store}=2.02 m, Slopes

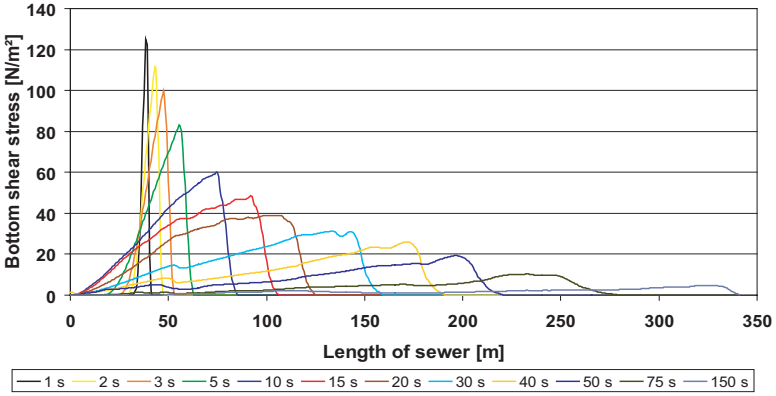

Figure F.16: Progression of the bottom shear stress, h_{store}=2.20 m, Slopes

Maximum bottom shear stress

Dry-weather channel

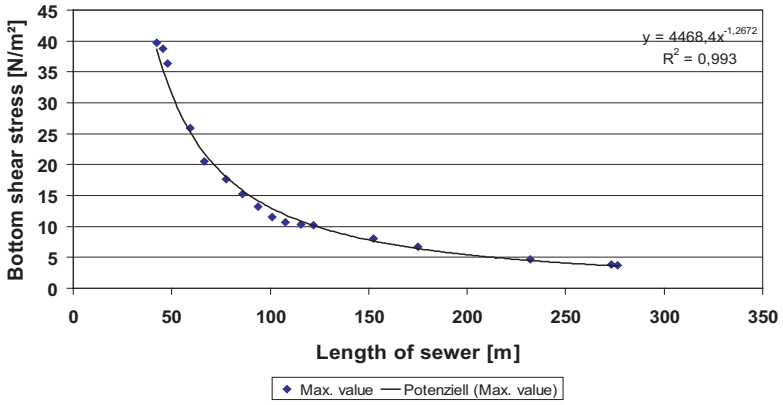

Figure F.17: Maximum bottom shear stress, h_{store}=0.73 m, Dry-weather channel

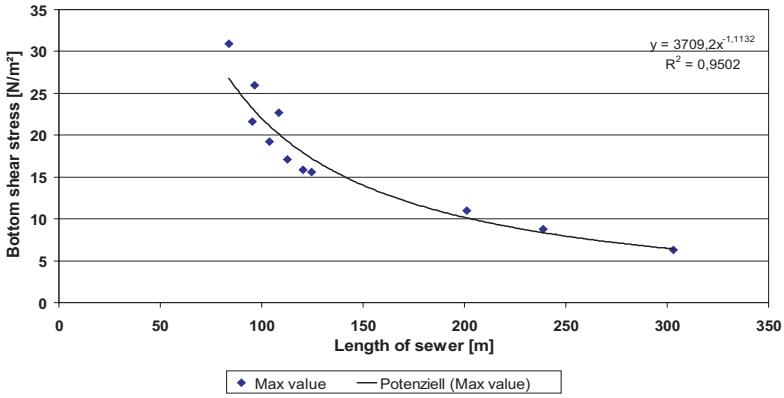

Figure F.18: Maximum bottom shear stress, h_{store}=1.03 m, Dry-weather channel

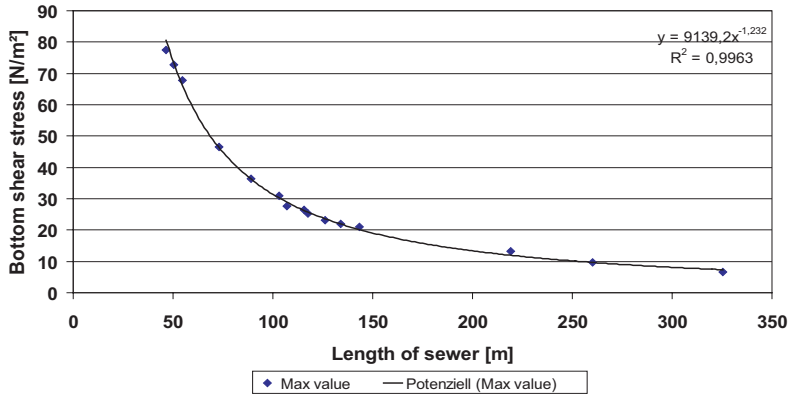

Figure F.19: Maximum bottom shear stress, h_{store}=1.25 m, Dry-weather channel

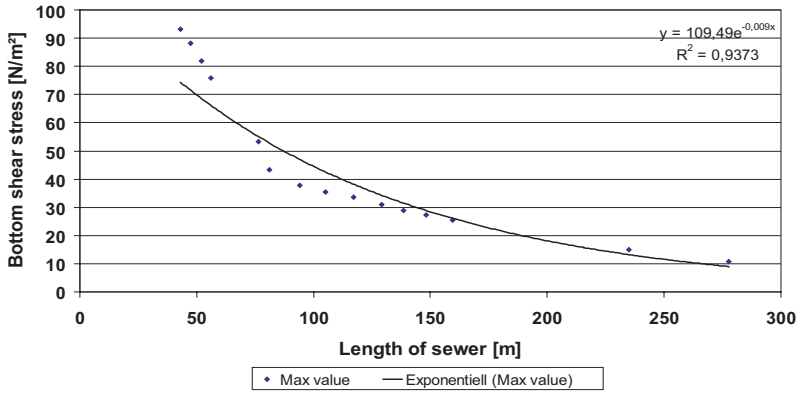

Figure F.20: Maximum bottom shear stress, h_{store}=1.45 m, Dry-weather channel

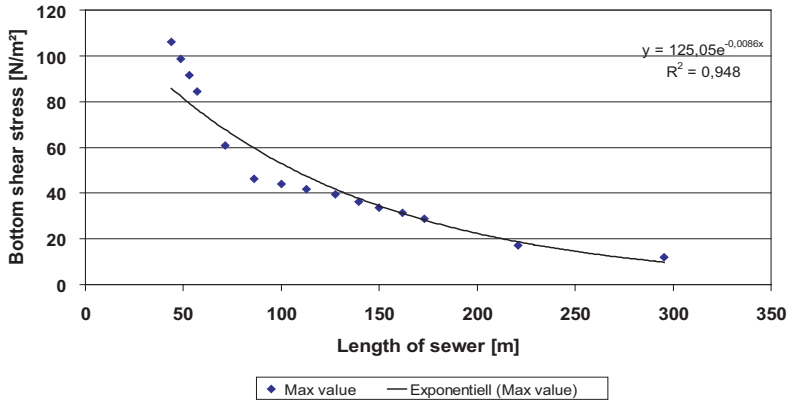

Figure F.21: Maximum bottom shear stress, h_{store}=1.64 m, Dry-weather channel

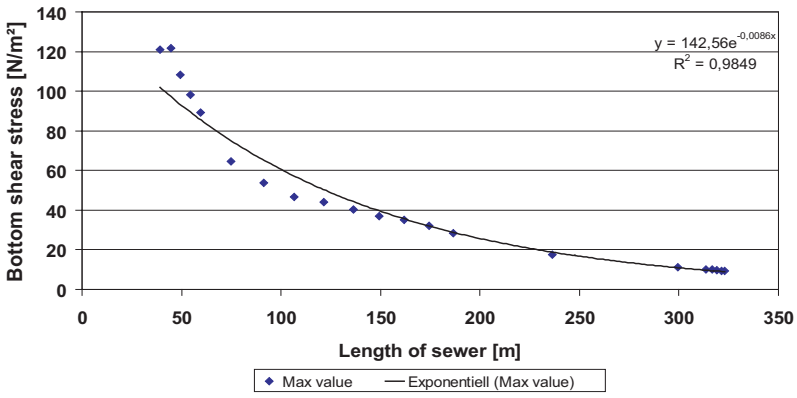

Figure F.22: Maximum bottom shear stress, h_{store}=1.82 m, Dry-weather channel

Slopes

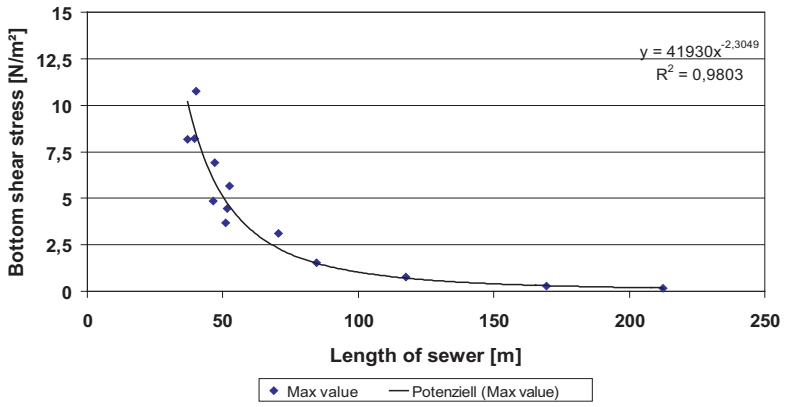

Figure F.23: Maximum bottom shear stress, h_{store}=0.73 m, Slopes

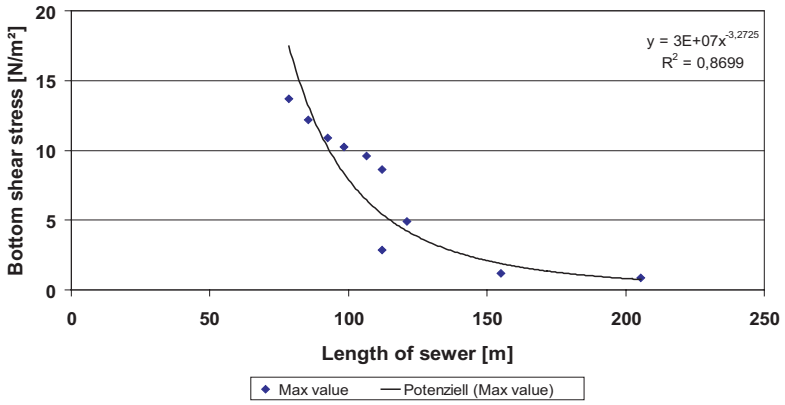

Figure F.24: Maximum bottom shear stress, h_{store}=1.03 m, Slopes

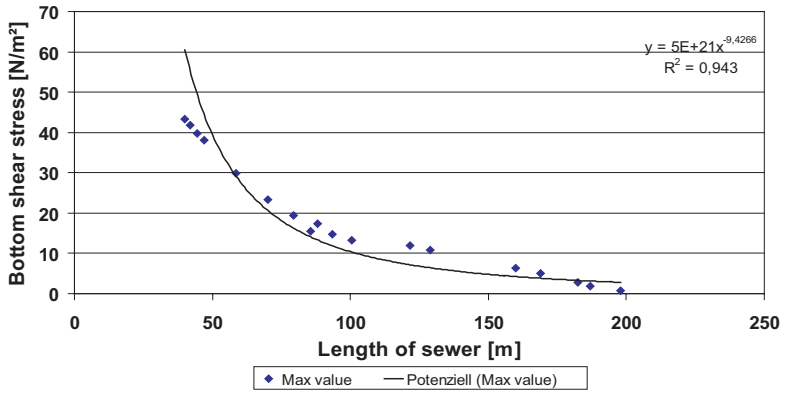

Figure F.25: Maximum bottom shear stress, h_{store}=1.25 m, Slopes

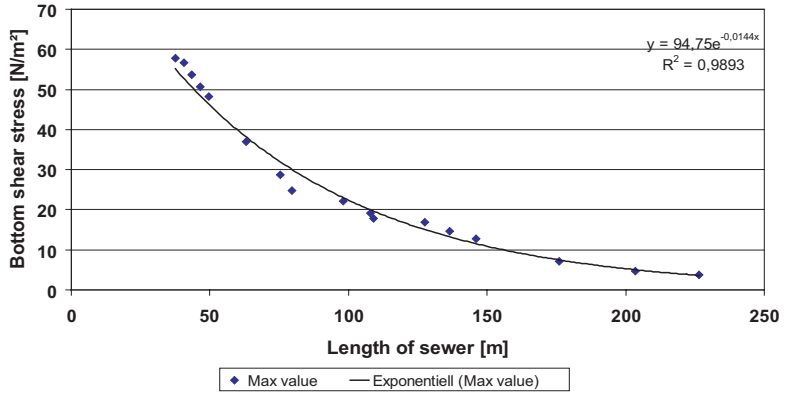

Figure F.26: Maximum bottom shear stress, h_{store}=1.45 m, Slopes

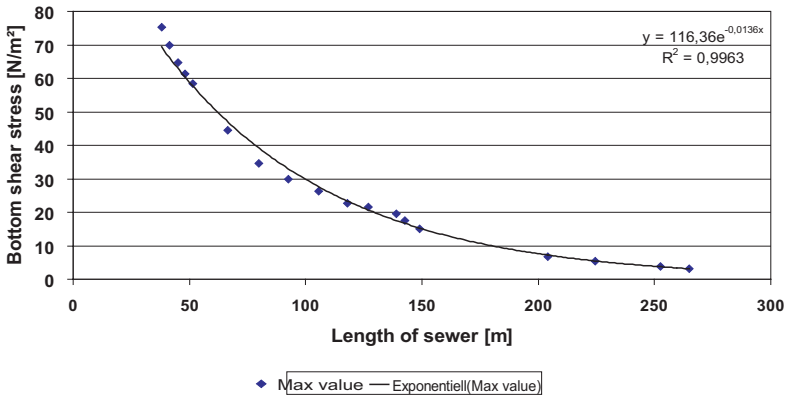

Figure F.27: Maximum bottom shear stress, h_{store}=1.64 m, Slopes

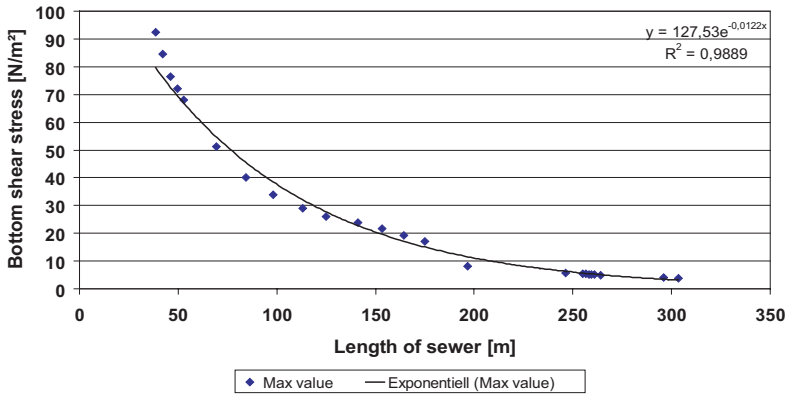

Figure F.28: Maximum bottom shear stress, h_{store}=1.82 m, Slopes

Effective flushing distance

Dry-weather channel

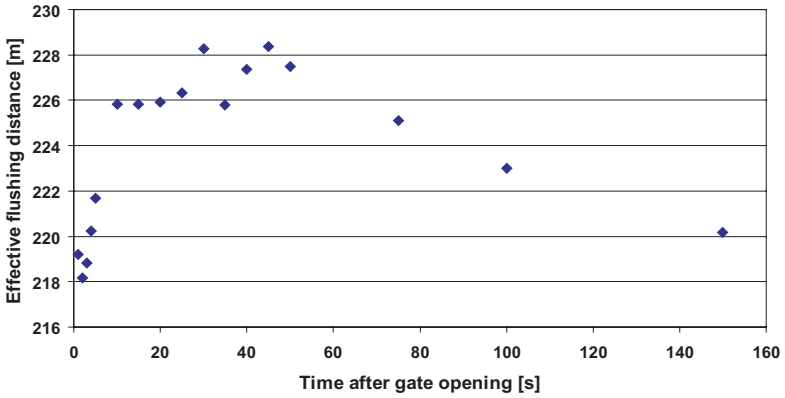

Figure F.29: Effective flushing distance, h_{store}=0.73 m, Dry-weather channel

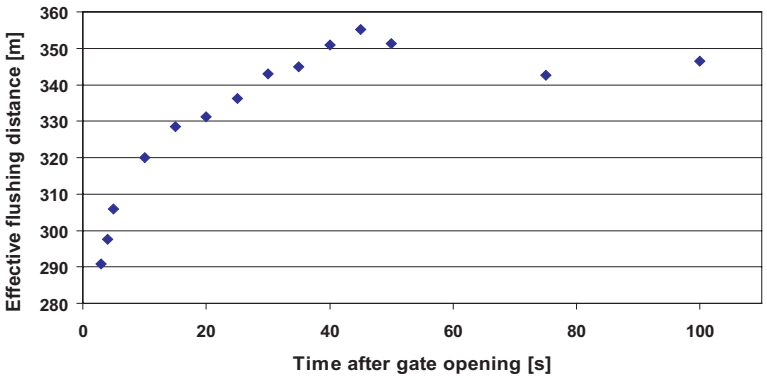

Figure F.30: Effective flushing distance, h_{store}=1.03 m, Dry-weather channel

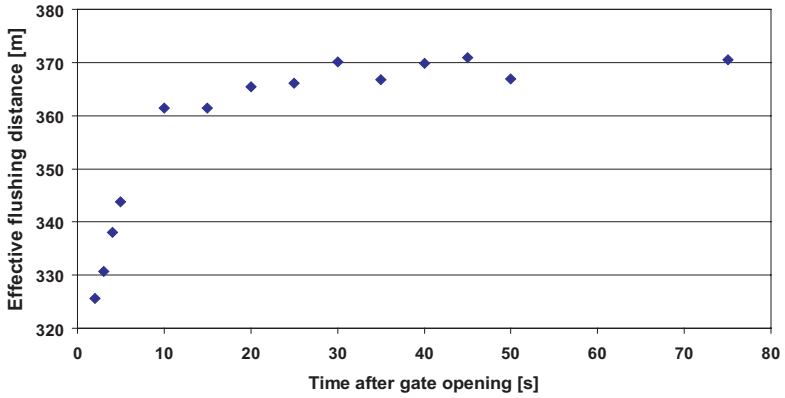

Figure F.31: Effective flushing distance, h_{store}=1.25 m, Dry-weather channel

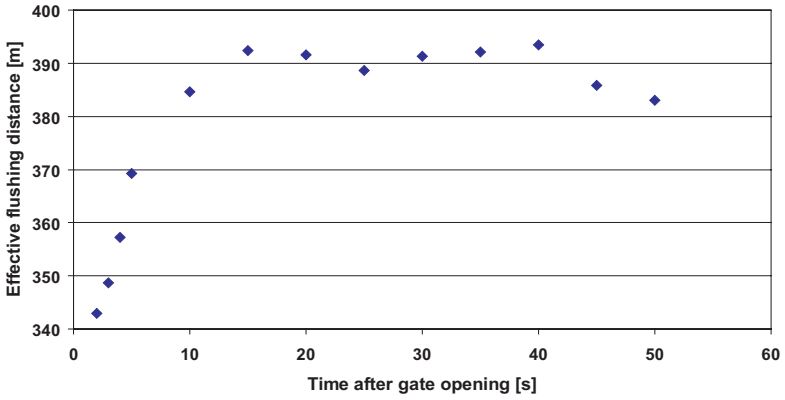

Figure F.32: Effective flushing distance, h_{store}=1.45 m, Dry-weather channel

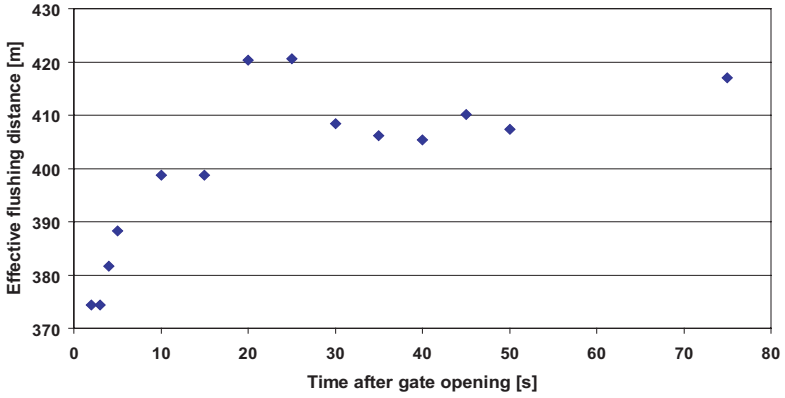

Figure F.33: Effective flushing distance, h_{store}=1.64 m, Dry-weather channel

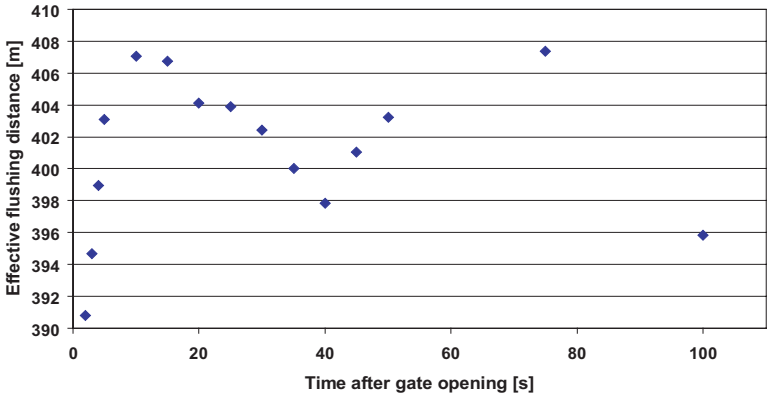

Figure F.34: Effective flushing distance, h_{store}=1.82 m, Dry-weather channel

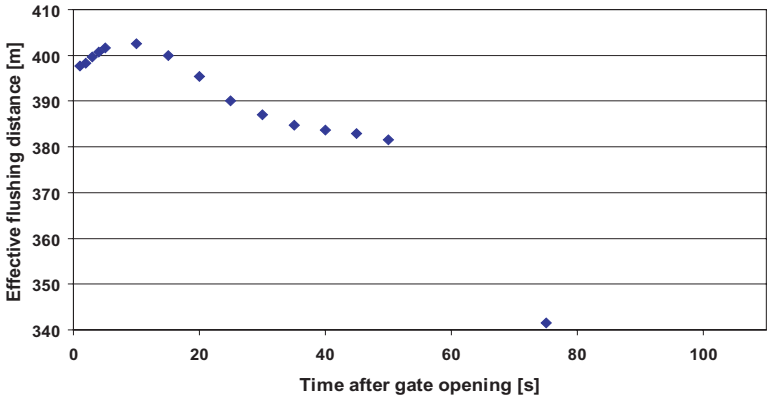

Figure F.35: Effective flushing distance, h_{store}=2.02 m, Dry-weather channel

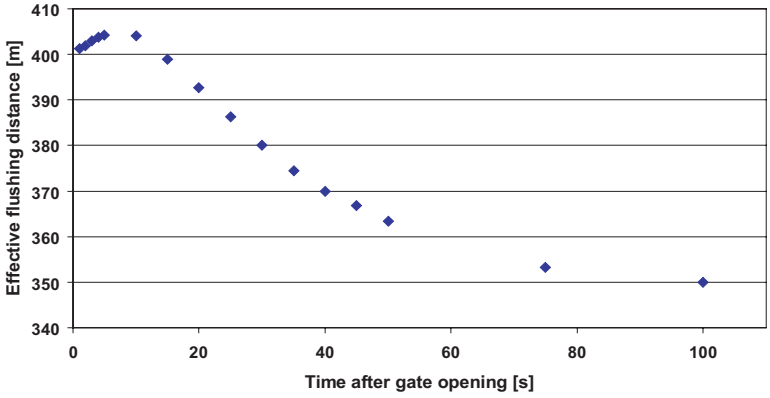

Figure F.36: Effective flushing distance, h_{store}=2.20 m, Dry-weather channel

Slopes

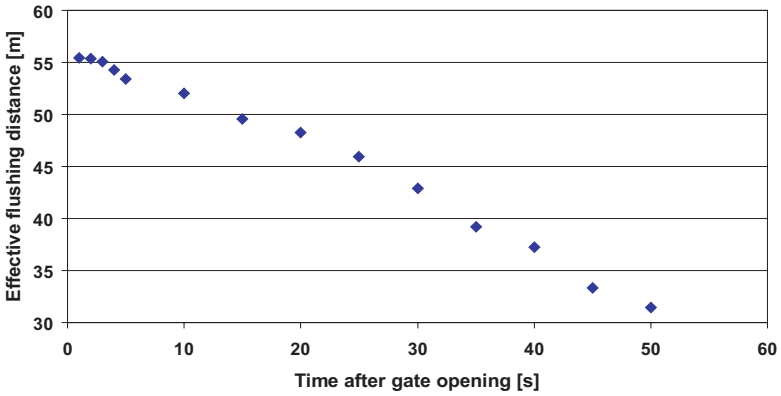

Figure F.37: Effective flushing distance, h_{store}=0.73 m, Slopes

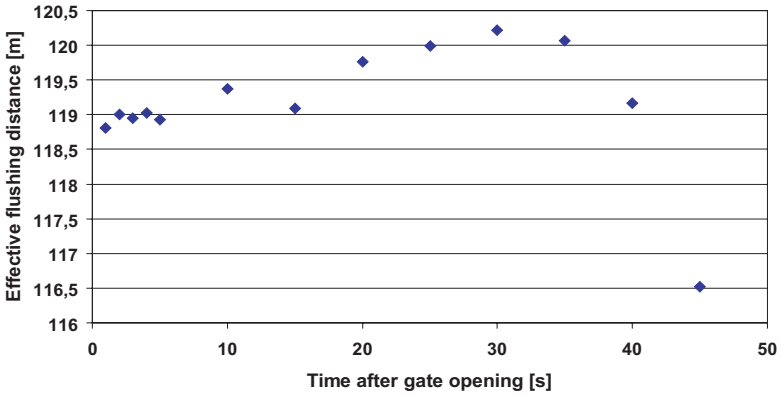

Figure F.38: Effective flushing distance, h_{store}=1.03 m, Slopes

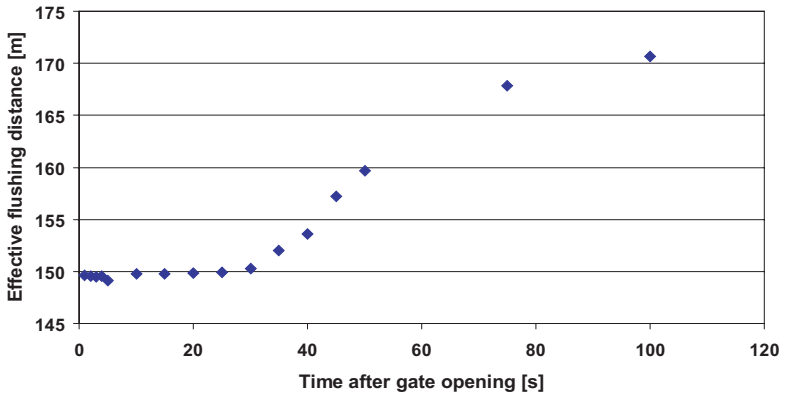

Figure F.39: Effective flushing distance, h_{store}=1.25 m, Slopes

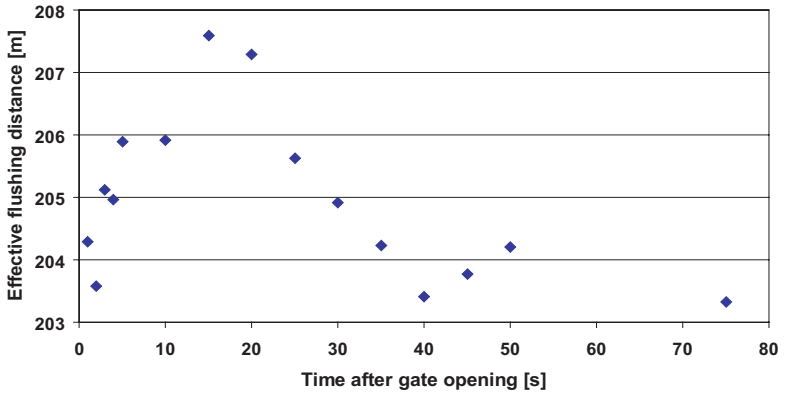

Figure F.40: Effective flushing distance, h_{store}=1.45 m, Slopes

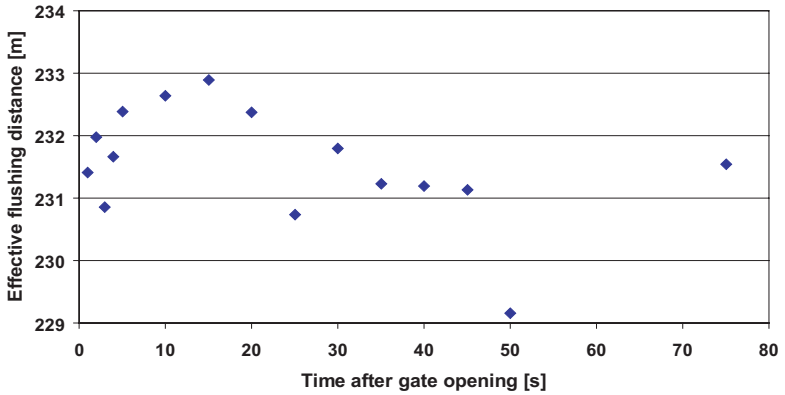

Figure F.41: Effective flushing distance, h_{store}=1.64 m, Slopes

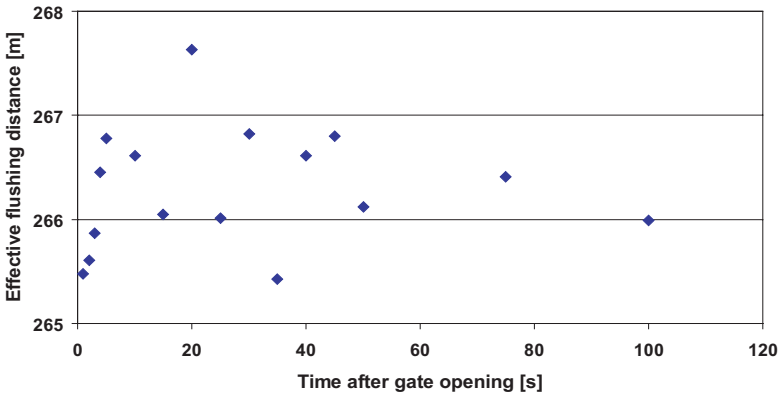

Figure F.42: Effective flushing distance, h_{store}=1.82 m, Slopes

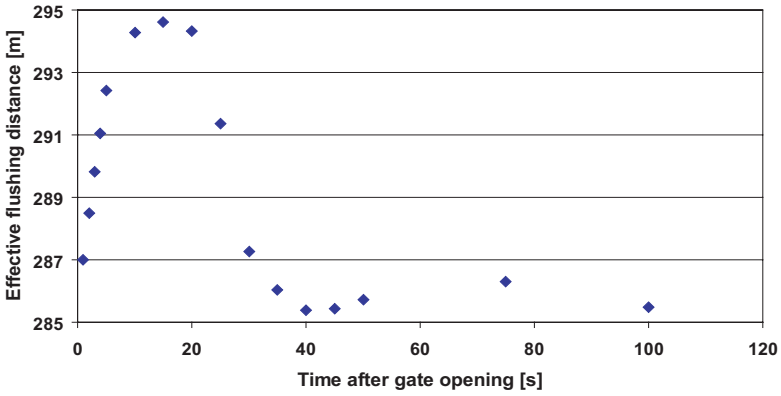

Figure F.43: Effective flushing distance, h_{store}=2.02 m, Slopes

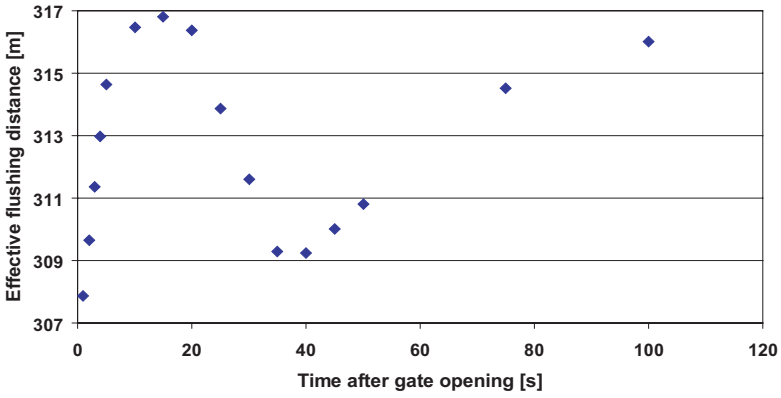

Figure F.44: Effective flushing distance, h_{store}=2.20 m, Slopes

G Investigation of the gate influence

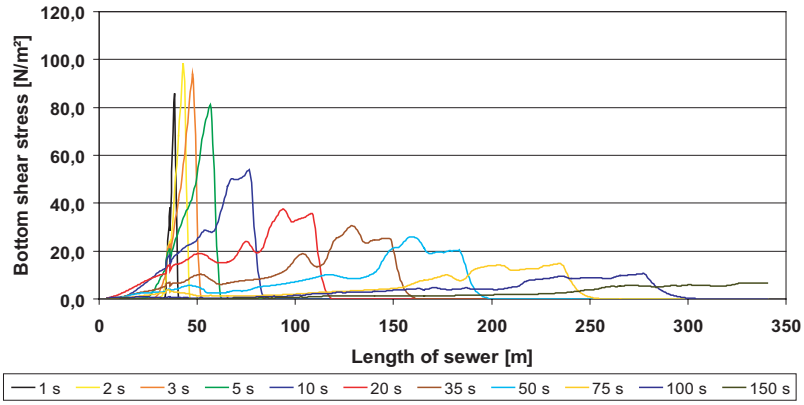

Figure G.1: Bottom shear stress, Storage level 1.45 m, Dry-weather channel

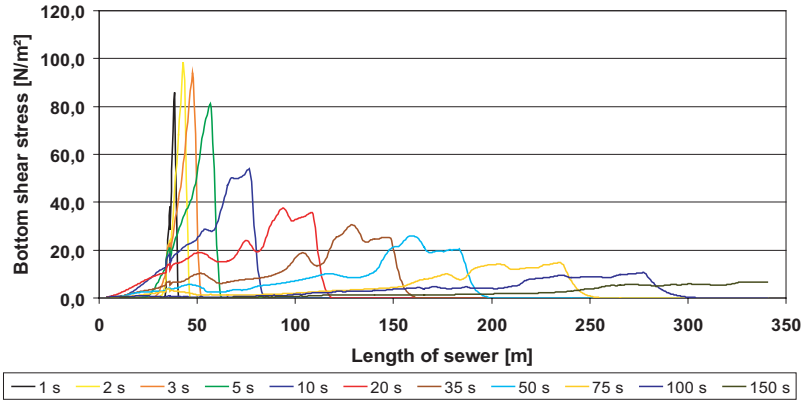

Figure G.2: Bottom shear stress, Storage level 1.45 m, Dry-weather channel

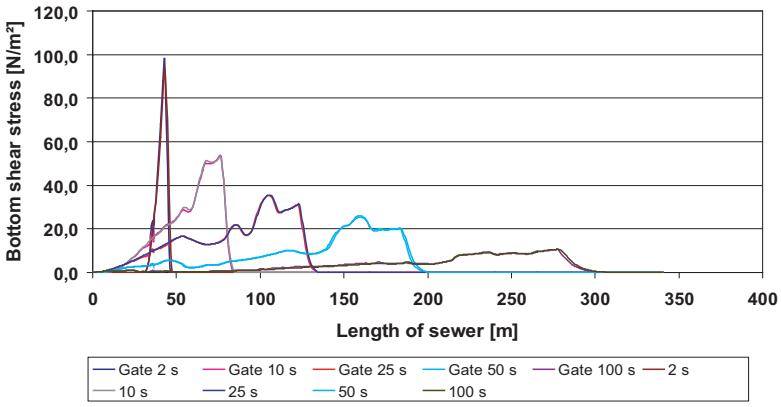

Figure G.3: Influence of the flushing gate for the dry-weather channel, storage level of 1.45 m.

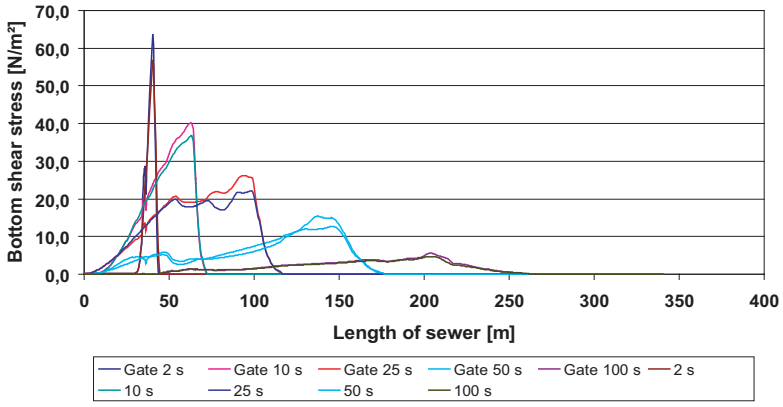

Figure G.4: Influence of the flushing gate at the slopes, storage level of 1.45 m.

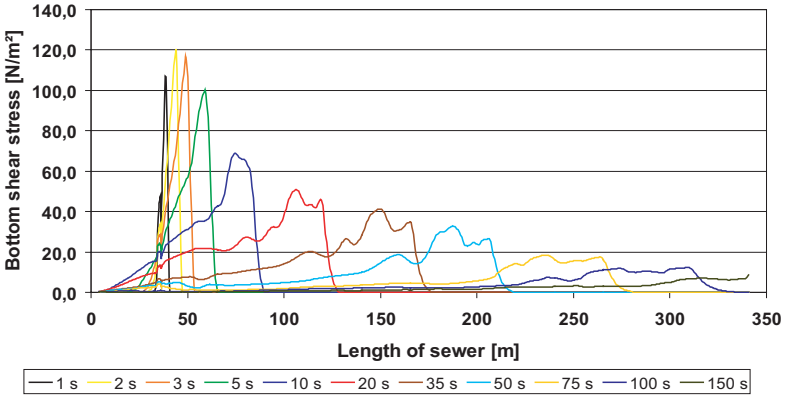

Figure G.5: Bottom shear stress, Storage level 1.82 m, Dry-weather channel

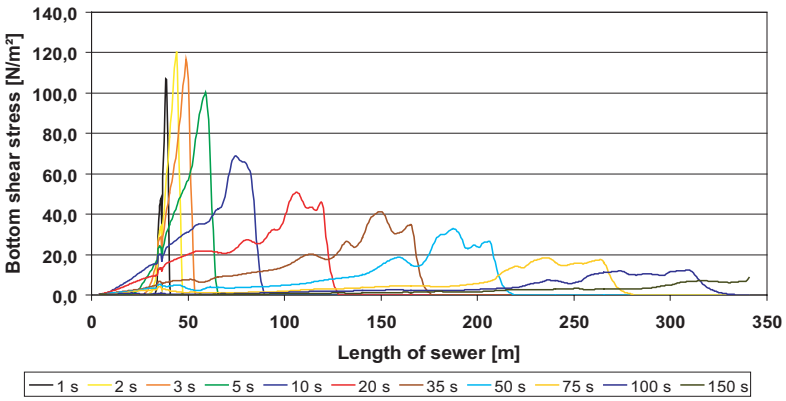

Figure G.6: Bottom shear stress, Storage level 1.82 m, Dry-weather channel

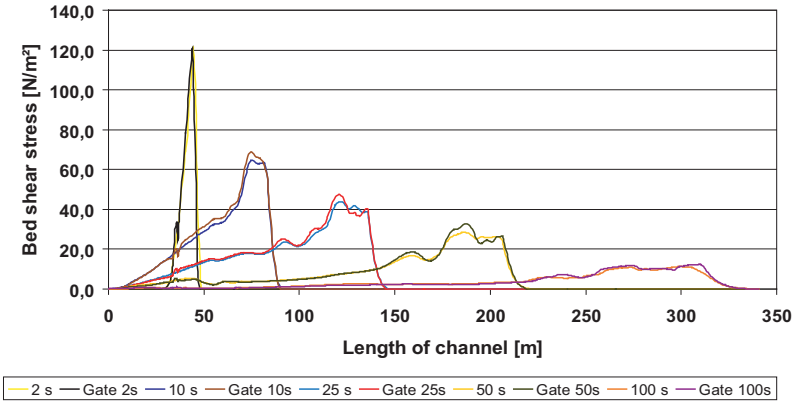

Figure G.7: Influence of the flushing gate for the dry-weather channel, storage level of 1.82 m.

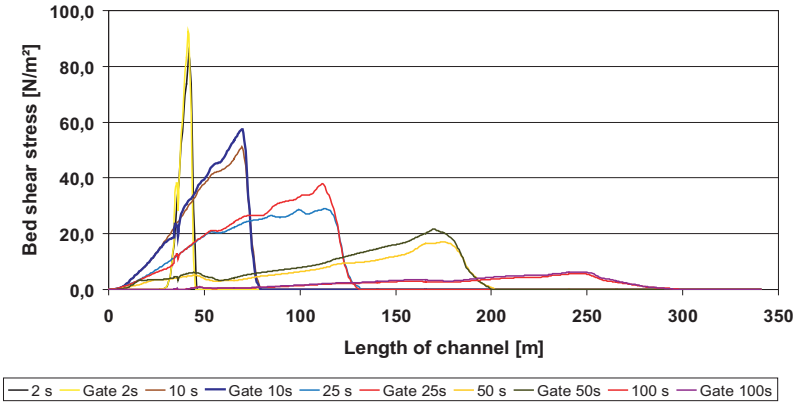

Figure G.8: Influence of the flushing gate at the slopes, storage level of 1.82 m.

H Influence of storage volume

Storage level 1.25 m
Dry-weather channel

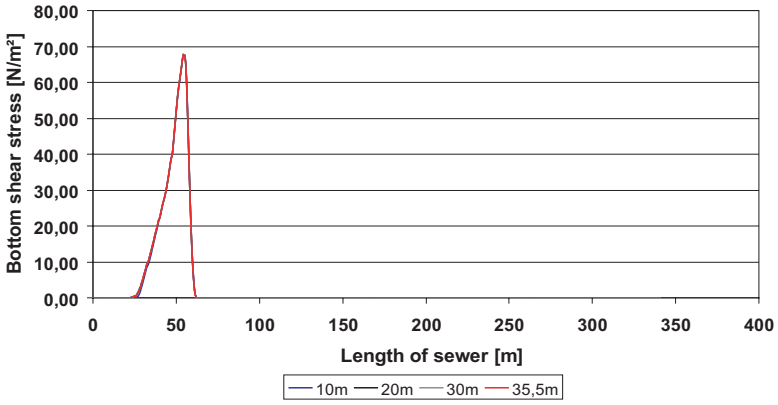

Figure H.1: Distribution of bottom shear stresses, 5 s

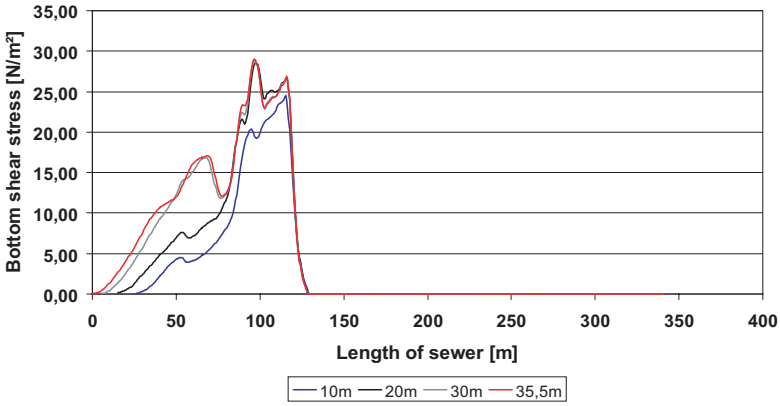

Figure H.2: Distribution of bottom shear stresses, 25 s

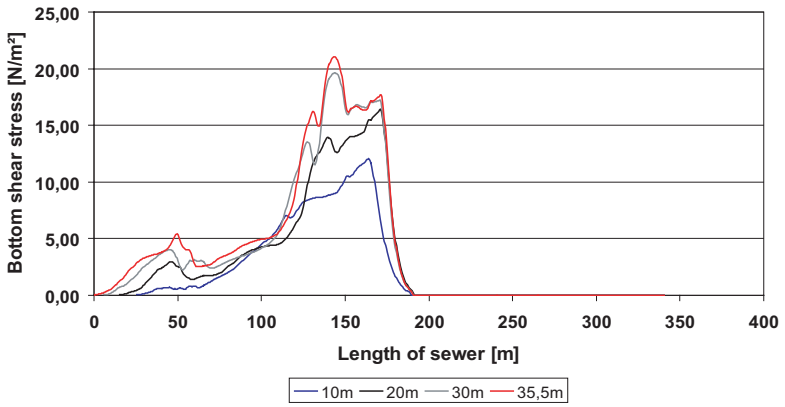

Figure H.3: Distribution of bottom shear stresses, 50 s

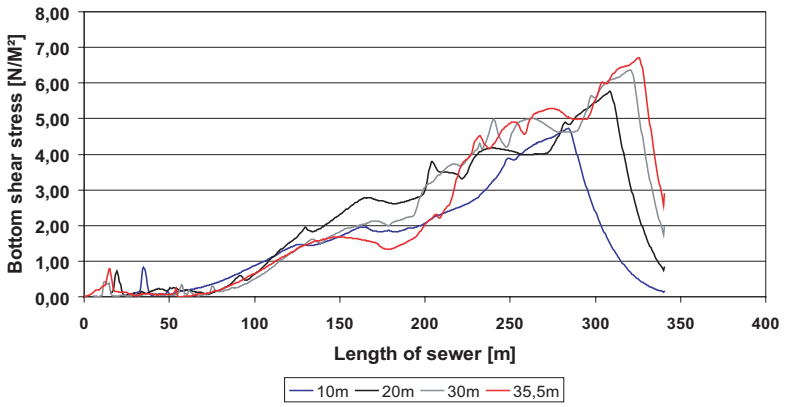

Figure H.4: Distribution of bottom shear stresses, 150 s

Slopes

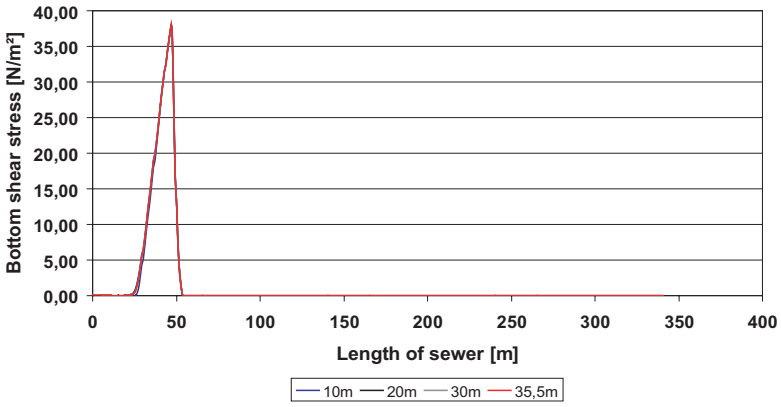

Figure H.5: Distribution of bottom shear stresses, 5 s

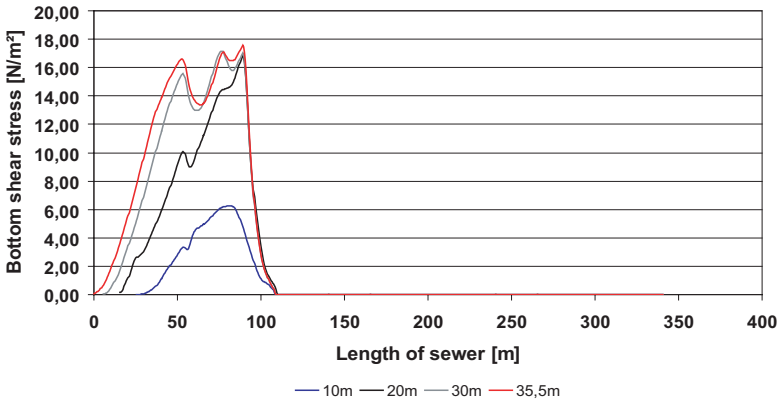

Figure H.6: Distribution of bottom shear stresses, 25 s

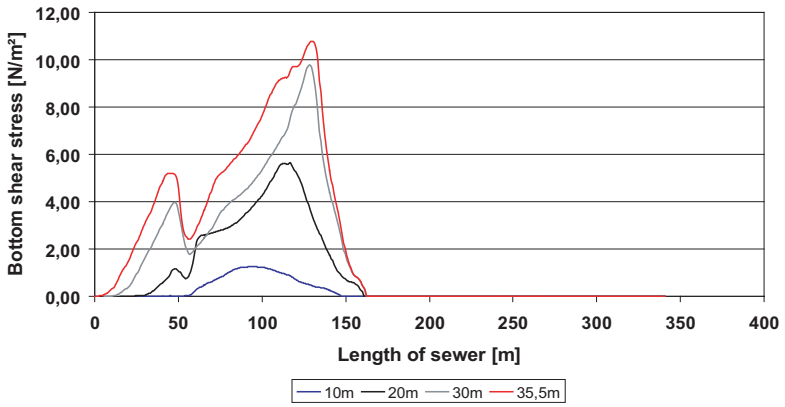

Figure H.7: Distribution of bottom shear stresses, 50 s

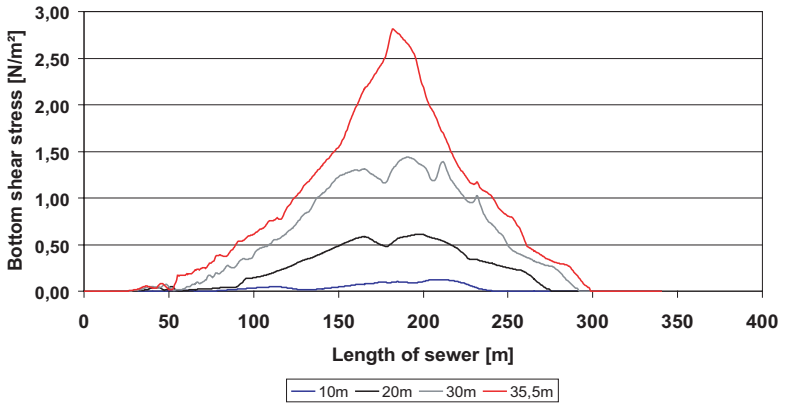

Figure H.8: Distribution of bottom shear stresses, 150 s

Storage level 1.82 m

Dry-weather channel

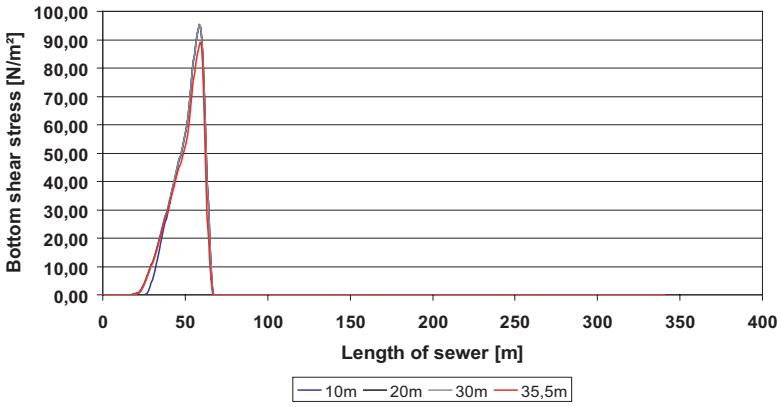

Figure H.9: Distribution of bottom shear stresses, 5 s

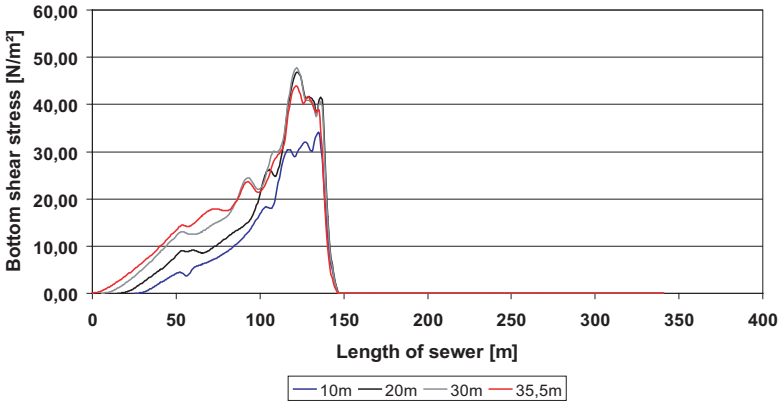

Figure H.10: Distribution of bottom shear stresses, 25 s

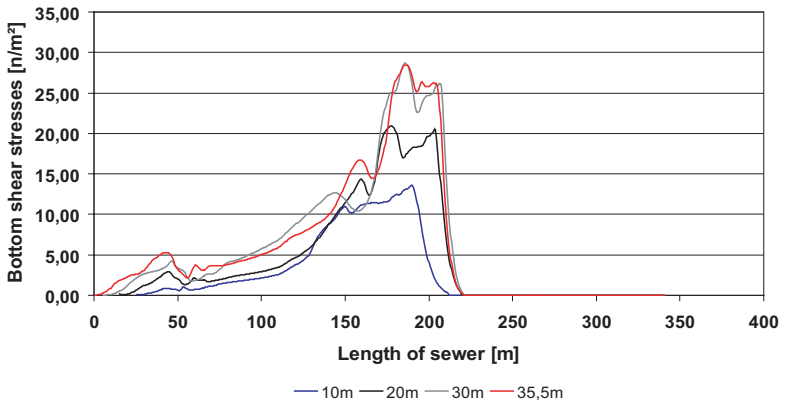

Figure H.11: Distribution of bottom shear stresses, 50 s

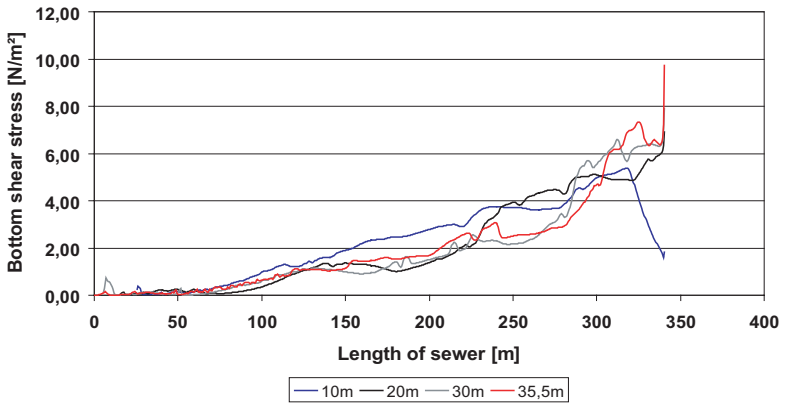

Figure H.12: Distribution of bottom shear stresses, 150 s

Slopes

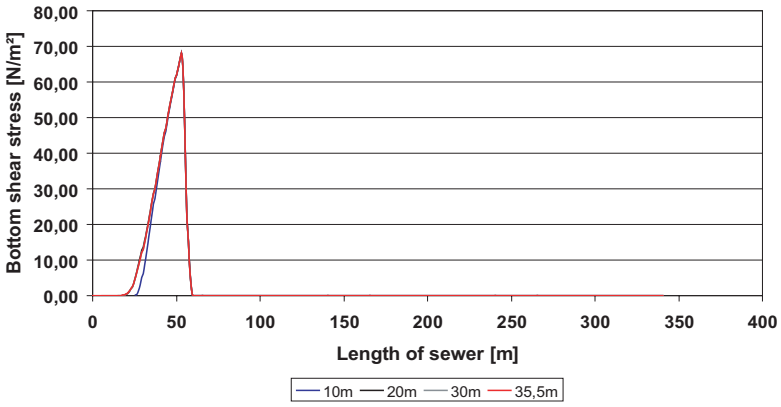

Figure H.13: Distribution of bottom shear stresses, 5 s

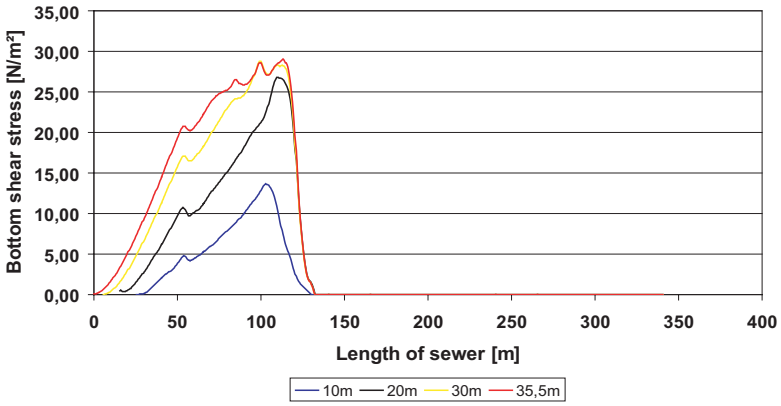

Figure H.14: Distribution of bottom shear stresses, 25 s

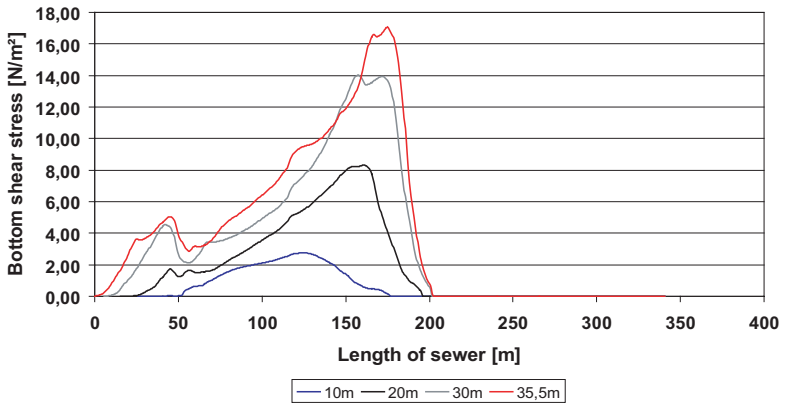

Figure H.15: Distribution of bottom shear stresses, 50 s

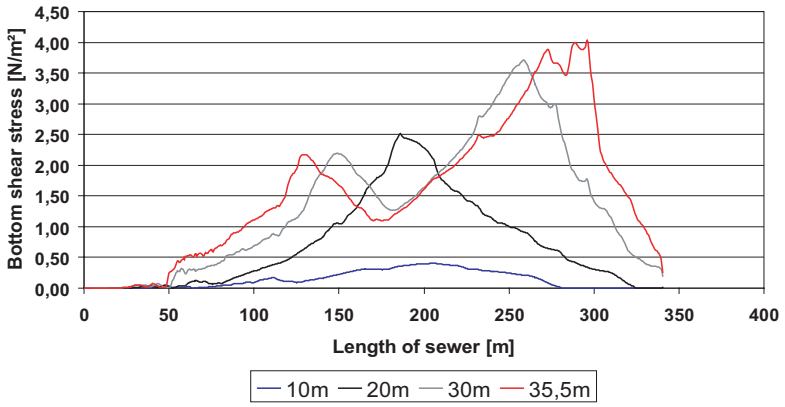

Figure H.16: Distribution of bottom shear stresses, 150 s

Curriculum Vitae

Jörg Schaffner

Personal data:

Date of birth:	13. August 1970
Place of birth:	Rüsselsheim
Nationality:	German
Family status:	Single

Education:

07/77 - 06/81	Elementary school in Klein-Gerau
07/81 - 06/83	Comprehensive school in Gross-Gerau
07/83 - 06/90	Grammar school in Gross-Gerau Degree: Final secondary-school examinations - General qualification for university entrance

Military service:

07/90 - 06/91	Military service in Neustadt/Hessen

Studies:

10/91 - 09/93	Electrical engineering at the Technische Universität Darmstadt
10/93 - 11/99	Civil engineering at the Technischen Universität Darmstadt Intermediate examination: Intermediate diploma Degree: Diploma

Occupational activity:

12/99 - 06/05	Research assistant and PhD student at the Technische Universität Darmstadt Department of Civil Engineering Section of Engineering Hydromechanics and Hydraulics
09/05 - present	Department manager Steinhardt Wassertechnik Company in Taunusstein Department of Construction and Sales